DENDRITIC SPINES: FROM BIOPHYSICS TO NEUROPATHOLOGY

EDITED BY: Menahem Segal, Martine Ammassari-Teule and Carlo Sala
PUBLISHED IN: Frontiers in Synaptic Neuroscience

frontiers Research Topics

frontiers

ISSN 1664-8714
ISBN 978-2-88966-633-1
DOI 10.3389/978-2-88966-633-1

About Frontiers

Frontiers is more than just an open-access publisher of scholarly articles: it is a pioneering approach to the world of academia, radically improving the way scholarly research is managed. The grand vision of Frontiers is a world where all people have an equal opportunity to seek, share and generate knowledge. Frontiers provides immediate and permanent online open access to all its publications, but this alone is not enough to realize our grand goals.

Frontiers Journal Series

The Frontiers Journal Series is a multi-tier and interdisciplinary set of open-access, online journals, promising a paradigm shift from the current review, selection and dissemination processes in academic publishing. All Frontiers journals are driven by researchers for researchers; therefore, they constitute a service to the scholarly community. At the same time, the Frontiers Journal Series operates on a revolutionary invention, the tiered publishing system, initially addressing specific communities of scholars, and gradually climbing up to broader public understanding, thus serving the interests of the lay society, too.

Dedication to Quality

Each Frontiers article is a landmark of the highest quality, thanks to genuinely collaborative interactions between authors and review editors, who include some of the world's best academicians. Research must be certified by peers before entering a stream of knowledge that may eventually reach the public - and shape society; therefore, Frontiers only applies the most rigorous and unbiased reviews.
Frontiers revolutionizes research publishing by freely delivering the most outstanding research, evaluated with no bias from both the academic and social point of view. By applying the most advanced information technologies, Frontiers is catapulting scholarly publishing into a new generation.

What are Frontiers Research Topics?

Frontiers Research Topics are very popular trademarks of the Frontiers Journals Series: they are collections of at least ten articles, all centered on a particular subject. With their unique mix of varied contributions from Original Research to Review Articles, Frontiers Research Topics unify the most influential researchers, the latest key findings and historical advances in a hot research area! Find out more on how to host your own Frontiers Research Topic or contribute to one as an author by contacting the Frontiers Editorial Office: frontiersin.org/about/contact

DENDRITIC SPINES: FROM BIOPHYSICS TO NEUROPATHOLOGY

Topic Editors:
Menahem Segal, Weizmann Institute of Science, Israel
Martine Ammassari-Teule, National Research Council (CNR), Italy
Carlo Sala, National Research Council (CNR), Italy

Citation: Segal, M., Ammassari-Teule, M., Sala, C., eds. (2021). Dendritic Spines: from Biophysics to Neuropathology. Lausanne: Frontiers Media SA. doi: 10.3389/978-2-88966-633-1

Table of Contents

frontiers in Synaptic Neuroscience

EDITORIAL
published: 18 February 2021
doi: 10.3389/fnsyn.2021.652117

Editorial: Dendritic Spines: From Biophysics to Neuropathology

Martine Ammassari-Teule[1], *Carlo Sala*[2] *and Menahem Segal*[3]*

[1] Istituto di Biochimica e Biologia Cellulare, National Research Council (CNR) and Fondazione Santa Lucia, Rome, Italy, [2] Neurobiology Department, National Research Council (CNR) Neuroscience Institute, Milan, Italy, [3] Neurobiology Department, Weizmann Institute, Rehovot, Israel

Keywords: dendritic spine, calcium, Alzheimer's disease, plasticity, hippocampus

Editorial on the Research Topic

Dendritic Spines: From Biophysics to Neuropathology

The molecular and cellular mechanisms that govern dendritic spine formation, modification, and elimination have been the focus of tremendous interest in recent years. Using an advanced arsenal of molecular and high-resolution imaging methodologies, the analysis of dendritic spine functions becomes more complex and detailed. The striking morphological heterogeneity of adjacent spines on the same dendritic branch and their minute size prohibits the structure/function analysis of spines. Despite the growing number of publications (more than 10,000 to date), major issues concerning the molecular, cellular, and functional attributes of spines remain unsettled. Are there different molecular pathways for different spines? Are there structural correlates of different classes of memories (e.g., episodic, semantic, short, and long term)? What happens to the structural change when a memory is forgotten? Can we improve memory by changing the structure? These and many other issues are still open. Every so often one needs to pause and review the literature to see how far we have advanced and how far away we are from understanding spines in relation to growth, maintenance, and deterioration of brain functions.

This Research Topic on *Dendritic Spines From biophysics to Neuropathology* addresses these issues. It includes four extensive review articles and five original research articles written by leading groups in the field cover subjects ranging from biophysics and molecular biology to functional and network attributes of spine functions. The reviews address standing issues in the study of spines. For example, Pchitskaya and Bezprozvanny propose to replace the standard classification of spine categories into mushroom, stubby, long, and filopods to a continuum of spine shapes. This new proposal is logical in view of the current inability to associate distinctly separate functions to different shapes of spines, but it requires more analytical tools to characterize the exact shape of a given spine.

Another review, by Runge et al., attempts to link spine dynamics with circuit rewiring in relation to external signals that generate these network changes found in neuropsychiatric disorders. They list two-photon microscopy (TPM) as a leading tool in the attempt to track changes in spines in the living brain. Studies using TPM have made a great contribution to the analysis of spine function, including the assertion that spines are transient and do not last throughout the life of the organism, but that their turnover time is different for different structures. This brings back the question of whether the individual spine is the locus of memory.

Ammassari-Teule takes us to the pathological end of spine functions. Therapeutic attempts to cure Alzheimer's disease (AD) have failed in the past decade, suggesting that when behavioral symptoms appear, the brain is already affected by the disease in an irreversible manner. Thus, the idea is to detect early signs of neuropathology and continue from there. It has been suggested in mouse models of AD that the early changes are physiological—a reduction in ability to express long term potentiation (LTP). Ammassari-Teule then reviews studies that examine whether such

OPEN ACCESS

Edited and reviewed by:
P. Jesper Sjöström, McGill University, Canada

***Correspondence:**
Menahem Segal
menahem.segal@weizmann.ac.il

Received: *11 January 2021*
Accepted: *27 January 2021*
Published: *18 February 2021*

Citation:
Ammassari-Teule M, Sala C and Segal M (2021) Editorial: Dendritic Spines: From Biophysics to Neuropathology. Front. Synaptic Neurosci. 13:652117. doi: 10.3389/fnsyn.2021.652117

changes can be detected in dendritic spines at the early stage of AD. The review focuses on changes in postsynaptic density as an early sign of AD, suggesting that synaptic dysfunction is a cause rather than a consequence of the cognitive decline associated with AD.

Finally, Costa et al. review the role of Rac GTPase in spine plasticity. They link the molecular, morphological, and functional aspects of GTPs in the brain. Rac GTPase is one of many chemicals associated with spine functions. They are able to show that altered Rac activity is associated with abnormal spine morphology and brain functions, including neurodegeneration. This is an elegant link between a single small GTPase and an array of brain functions from the single memory to complex networks of the human brain.

The original research reports span the whole spectrum of methods and levels of analysis. Regulation of intracellular calcium ion concentration ($[Ca^{2+}]i$), which has been known to regulate different forms of synaptic plasticity, is addressed by Jodar et al., studying olfactory bulb granular cell spines, and Kushnireva et al., studying calcium stores in cultured hippocampal neurons. SK channels, activated by calcium influx, regulate the excitability of dendritic spines and are shown to control spine plasticity via modulation of CaMKII (Shrestha et al.). These three studies illustrate the wide spectrum of calcium regulation of dendritic spine plasticity. One interesting diversion from the traditional focus on intra-spine constituents is illustrated by the work of Nguyen et al., who analyzed the effects of variation in ephrinB1, a resident molecule in astrocytes, on dendritic spine structure and function in relation to learning and memory. Finally, de Schultz et al., expanded on their ongoing work on parent/offspring association in relation to long term effects of parental deprivation on dendritic spines in the medial prefrontal cortex. This work illuminates the role of parents and the long-lasting male/female difference in the effects of stress on the juvenile brain.

All in all, these studies highlight the current status of the major effort across the world on trying to understand the roles of dendritic spines, the minute but extremely important neuronal organelle, in the regulation of brain function. Over the years, this tiny structure turned out to be an extremely complex organelle, where over 500 different types of molecules coordinate to regulate its structure and function. Many issues remain, including the tremendous heterogeneity of adjacent spines on the same dendrite, the fast turnover rate of spines in different behavioral states, and the cardinal issue of whether a given spine is the locus of memory. These and many more issues should be addressed in future studies using more advanced molecular tools.

AUTHOR CONTRIBUTIONS

All authors listed have made a substantial, direct and intellectual contribution to the writing of this Editorial, and approved it for publication.

Conflict of Interest: The authors declare that the research was conducted in the absence of any commercial or financial relationships that could be construed as a potential conflict of interest.

frontiers in Synaptic Neuroscience

ORIGINAL RESEARCH
published: 31 October 2019
doi: 10.3389/fnsyn.2019.00018

SK Channel Modulates Synaptic Plasticity by Tuning CaMKIIα/β Dynamics

*Amita Shrestha, Razia Sultana, Charles C. Lee and Olalekan M. Ogundele**

Department of Comparative Biomedical Sciences, Louisiana State University School of Veterinary Medicine, Baton Rouge, LA, United States

N-Methyl-D-Aspartate Receptor 1 (NMDAR)-linked Ca^{++} current represents a significant percentage of post-synaptic transient that modulates synaptic strength and is pertinent to dendritic spine plasticity. In the hippocampus, Ca^{++} transient produced by glutamatergic ionotropic neurotransmission facilitates Ca^{++}-Calmodulin-dependent kinase 2 (CaMKII) Thr286 phosphorylation and promote long-term potentiation (LTP) expression. At CA1 post-synaptic densities, Ca^{++} transients equally activate small conductance (SK2) channel which regulates excitability by suppressing Ca^{++} movement. Here, we demonstrate that upstream attenuation of GluN1 function in the hippocampus led to a decrease in Thr286 CaMKIIα phosphorylation, and increased SK2 expression. Consistent with the loss of GluN1 function, potentiation of SK channel in wild type hippocampus reduced CaMKIIα expression and abrogate synaptic localization of T286 pCaMKIIα. Our results demonstrate that positive modulation of SK channel at hippocampal synapses likely refine GluN1-linked plasticity by tuning dendritic localization of CaMKIIα.

Keywords: NMDAR-GluN1, SK2/3, CaMKIIα, hippocampus, ISI, firing rate

OPEN ACCESS

Edited by:
Martine Ammassari-Teule, Italian National Research Council (CNR), Italy

Reviewed by:
Veronica Ghiglieri, University of Perugia, Italy
A. J. Baucum, Indiana University, Purdue University Indianapolis, United States

****Correspondence:***
Olalekan M. Ogundele
ogundele@lsu.edu

Received: *21 January 2019*
Accepted: *20 May 2019*
Published: *31 October 2019*

Citation:
Shrestha A, Sultana R, Lee CC and Ogundele OM (2019) SK Channel Modulates Synaptic Plasticity by Tuning CaMKIIα/β Dynamics. Front. Synaptic Neurosci. 11:18. doi: 10.3389/fnsyn.2019.00018

INTRODUCTION

The hippocampus is the center for processing of spatial working memory. At hippocampal synapses, synaptic long-term potentiation (LTP) is dependent on glutamatergic neurotransmission (Cacucci et al., 2007; Allen et al., 2016). Specifically, ionotropic neurotransmission mediated by N-Methyl-D-Aspartate Receptor 1 (NMDAR) underlie the functional basis of synaptic structural plasticity that determines the pattern of neural encoding (Gustin et al., 2011; Tovar et al., 2013; Coultrap et al., 2014; Huang and Gibb, 2014; Ratnadurai-Giridharan et al., 2014; Yao and Zhou, 2017; Yi et al., 2017; Rebollo et al., 2018). The loss of NMDAR function has been implicated in several developmental neurocognitive disorders and may represent a convergence for disease progression. Notably, NMDAR hypofunction has been reported in patients and experimental animals exhibiting behavioral symptoms of autism spectrum disorder, bipolar depression, and schizophrenia (Seillier and Giuffrida, 2009; Uchino et al., 2010; Gustin et al., 2011; Namba et al., 2011; Ramsey et al., 2011; Anticevic et al., 2012; Duffney et al., 2013; Snyder and Gao, 2013; Aow et al., 2015; Stein et al., 2015; Ogundele and Lee, 2018). Owing to its role in synaptic plasticity, loss of NMDAR function often leads to a change in synaptic morphology

(González Burgos et al., 2012; Bosch et al., 2014; Chazeau and Giannone, 2016; Bustos et al., 2017; Frangeul et al., 2017; Forrest et al., 2018). To this effect, synaptic perturbations in the cognitive centers translate into impairment of neural encoding of instantaneous (working) memory.

In synaptic potentiation, high-frequency spiking events involve the transient surge of postsynaptic Ca^{++} current that is mediated by NMDAR-linked ionotropic neurotransmission (Xia et al., 1996; Coultrap and Bayer, 2012). In addition to the modulation of synaptic plasticity, the transient Ca^{++} current also couples LTP to cellular regulation and gene expression (Xia et al., 1996; Li et al., 2001; Yao and Wu, 2001; Salter and Kalia, 2004; Yoshii and Constantine-Paton, 2007; Coultrap and Bayer, 2012; Stein et al., 2015; Takei et al., 2015; Sanderson et al., 2016; Wang et al., 2016; Swiatkowski et al., 2017). Ca^{++} surge produced by NMDAR activates synaptic Ca^{++}-Calmodulin-dependent kinase 2 (CaMKII) by facilitating autophosphorylation at T286/287 sites of the 9α/3β components of the holoenzyme. Consequently, T286 phosphorylated CaMKIIα targets other synaptic substrates (S831 site of GluA1) and promotes fast-spiking activity that is characteristic of LTP (Lisman et al., 2012; Lai and Ip, 2013; Coultrap et al., 2014; Hell, 2014; Hlushchenko et al., 2016; Khan et al., 2016; Nakahata and Yasuda, 2018). On the other hand, the transient Ca^{++} currents produced by NMDAR ionotropic neurotransmission also activate small conductance channels that are co-localized with NMDAR at postsynaptic densities. Repetitive activation of SK2 attenuates post-synaptic transient Ca^{++} current, and leads to a decline in the frequency of neuronal firing (Lee et al., 2003; Hammond et al., 2006; Lin et al., 2008; Ohtsuki et al., 2012; Ballesteros-Merino et al., 2014; Lee and MacKinnon, 2018).

Activation of NMDAR, and accompanying calcium release, are not isolated events in LTP. Modulation of synaptic potentiation events that underlie LTP involves the movement of monovalent K^+ ions through the SK2, and constitutes an ion channel gating mechanism (Xia et al., 1998; Stackman et al., 2002; Ngo-Anh et al., 2005; Hammond et al., 2006; Lin et al., 2008). Together, LTP embodies the movement of ions in an organized process of oscillation between Ca^{++} and K^+ currents. The efflux of K^+ ions through SK2 decreases synaptic strength by attenuating neuronal firing while creating a state of refractoriness. Positive modulation of SK2 has also been shown to alter frequency-dependent LTP and neural encoding in the hippocampus (Maylie et al., 2004; Lin et al., 2008). Previous studies suggest that SK2 modulate LTP by producing afterhyperpolarization current (I_{AHP}) that determines the interspike interval for evoked potentials (Hammond et al., 2006; Lin et al., 2008; Maingret et al., 2008). Additionally, by suppressing transient Ca^{++} current associated with NMDAR, SK2 refine synaptic strength through an activity-linked feedback loop (Ngo-Anh et al., 2005; Kuiper et al., 2012; García-Negredo et al., 2014; Lee and MacKinnon, 2018).

Elsewhere, we reported that the pharmacologically-induced NMDAR hypofunction suppressed CaMKII expression, and increased SK2 expression in the hippocampus of WT mice (Ogundele and Lee, 2018). This outcome suggests that T286 phosphorylation of CaMKIIα and expression of SK2 may be inversely related in NMDAR hypofunction. Here, we tested the hypothesis that SK2 regulation of synaptic excitability may impact CaMKII synaptic localization. We assessed the structural and physiological properties of hippocampal synapses after genetic ablation of GluN1 sub-unit of NMDAR. In addition to dendritic spine perturbations, an upregulated SK2 expression was accompanied by a loss T286/T287 phosphorylation of CaMKII in the hippocampus. Likewise, positive modulation of SK channel in a wild type (WT) hippocampus (normal GluN1) dysregulates T286/T287 phosphorylation, and synaptic localization of CaMKII. Together, our results suggest that SK2 regulate hippocampal excitability—in part—by modulating dendritic localization of CaMKII.

MATERIALS AND METHODS

Animals

Adult male and female animals were acquired from the Jackson's Lab (Bar Harbor, ME, USA). The animals were bred to generate F_1 offspring which were later inbred for two generations. All experimental animals were housed under standard laboratory conditions of 12 h alternating light and dark cycle. Food and water were provided *ad libitum*. All animal handling procedures were approved by the Institutional Animal Care and Use Committee of the Louisiana State University School of Veterinary Medicine. The animals used for this study weighed ∼24 gm.

Adeno-Associated Virus (AAV) Injection

Mice were anesthetized by intraperitoneal Ketamine/Xylazine (100 mg/Kg:10 mg/Kg) injection and assessed for pain sensation by toe pinching. The head of the mouse was gently fixed in a multi-rail stereotaxic apparatus (Köpf Instruments, Tujunga, CA, USA) for a craniotomy procedure. The Adeno-associated virus (AAV) cocktail was injected into the anterior hippocampus at coordinates (AP: −1.94 mm, ML: 1.0 mm, DV: 1.5 mm) relative to the Bregma. Approximately 800 nl of AAV cocktail was delivered at the rate of 60 nl per min (3 min interval) using a manual Hamilton's syringe holder (World Precision Instruments Inc., Sarasota, FL, USA). After the last injection, the syringe was allowed to stay in place for 15 min before it was gradually withdrawn.

Hypomorphic Mutation of GluN1

Serotype 5 AAVs were used in this study. AAV-CMV-Cre-eGFP ($\Delta GluN1^{Hypomorph}$) or control AAV-CMV-eGFP ($GluN1^{flx/flx}$) was injected into the hippocampus of GluN1 floxed mice (Jax: 005246; B6.129S4-Grin1tm2Stl/J). The expression of the reporter protein (eGFP) was verified by fluorescence imaging after 21 days. AAV-CMV-eGFP and AAV-CMV-Cre-eGFP were procured from the University of North Carolina Vector Core.

Hippocampal Expression of ChR2

Double floxed AAV-EF-1a-ChR2-eYFP-WPRE (University of North Carolina Vector Core) was injected bilaterally into the hippocampus of CaMKII-Cre mice (Jax: 005359;

B6.Cg-Tg(Camk2a-cre)T29-1Stl/J) to express light controlled channelrhodopsin (ChR2; n = 4). The expression of the ChR2 in dendritic spines was verified by fluorescence expansion microscopy after 21 days (Tillberg et al., 2016; Chang J. B. et al., 2017). In a separate set of n = 5 mice, we crossed Ai27D mouse (Jax: 012567; RCL-hChR2(H134R)/tdT-D) with the CaMKII-Cre line. The F1 offspring were inbred to create homozygous Ai27D:CaMKII-Cre mice expressing ChR2 in the hippocampus. Both CaMKII-Cre:ChR2 and Ai27D:ChR2 mice were used for photostimulation experiments (blue light; 470 nm).

Adult Hippocampal SK Channel Positive Modulation (48 h)

An ICV cannula guide was positioned in the CA1 of a GluN1$^{flx/flx}$ mouse by stereotaxic surgery (AP: −1.94 mm, ML: 1.0 mm), and affixed with a dental cement. The cannula guide was covered with a dummy cannula. Seven days after the implant, the dummy cannula was replaced with an ICV cannula for a single dose (10 μM CyPPA) drug delivery [SK2/3(+)]. The drug solution was delivered at the rate of 10 μL/min using a manual Hamilton's syringe holder (World Precision Instruments Inc., Sarasota, FL, USA).

Specimen Preparation

Deeply anesthetized mice were euthanized in an isoflurane chamber. The animals were transcardially perfused with 10 mM PBS (pH 7.4) and the whole brain was harvested. The brain was rapidly placed in cold artificial cerebrospinal fluid (ACSF) maintained on ice, and saturated with 95% O_2/5%CO_2. A clean razor blade was used to cut the brain along the sagittal plane. The hippocampus was microdissected and extracted from the right and left hemispheres.

Immunoblotting

The harvested hippocampal tissue was kept in tubes and stored at −80°C until further processing. Frozen hippocampal tissue was incubated on ice with RIPA lysis buffer containing protease and phosphatase inhibitor cocktail. After 30 min, the incubated tissue was rapidly homogenized to obtain tissue lysate. The homogenate was centrifuged to obtain supernatants containing cytoplasmic, membrane, and synaptic fragments. Hippocampal lysate (10 μl) containing 10 μg of protein was processed for SDS-PAGE electrophoresis. After western blotting (wet transfer), Polyvinylidene fluoride membrane (PVDF) was incubated in Tris-buffered saline with 0.01% Tween 20 (TBST) for 15 min (TBST) at room temperature. Afterward, the membrane was blocked in 3% bovine serum albumin (prepared in TBST) for 50 min at room temperature. The protein of interest and housekeeping protein were detected using the following primary antibodies; Rabbit anti KCNN2 Antibody (ThermoFisher Scientific #PA5-41071); Mouse anti CaMKIIα Antibody (ThermoFisher Scientific #MA1-048), Rabbit anti Phospho-CaMKIIα/β:T286/T287 (Cell Signaling #12716), Rabbit anti Phospho-CaMKII T305/306 (ThermoFisher Scientific #702357), Rabbit anti-Phospho-CaMKIIβ/δ/γ:T287(ThermoFisher Scientific #PA5-37833), and Rabbit anti NMDAR1:NR1 Polyclonal Antibody (ThermoFisher Scientific #PA3-102). All primary antibodies were diluted in the blocking solution at 1:1,000. Subsequently, the primary antibodies were detected using Chicken anti-Rabbit-HRP (ThermoFisher Scientific #A15987; 1:5,000) or Donkey anti-Mouse-HRP (ThermoFisher Scientific #A16017; 1:5,000) secondary antibody. The reaction was developed using a chemiluminescence substrate (ThermoFisher-#34579). In order to normalize protein expression, the membranes were treated with Restore PLUS Western Blot Stripping Buffer (ThermoFisher Scientific #46430), and re-probed with β-Actin (8H10D10) Mouse mAb HRP Conjugate (Cell Signaling #12262S). Protein expression (SK2, GluN1, CaMKII) was normalized per lane using the corresponding β-Actin expression. However, for phosphorylated CaMKII (T286, T287, and T305/306 pCaMKII), normalization was done with the base protein expression (CaMKII).

Slice Preparation and Acute Brain Slice Treatment

For *ex vivo* acute treatment, the hippocampus was microdissected (bilateral) and incubated in oxygenated ACSF with 95% O_2/5%CO_2 constantly being bubbled through the ACSF (ACSF; in mM 125 NaCl, 25 $NaHCO_3$, 3 KCl, 1.25 NaH_2PO_4, 1 $MgCl_2$, 2 $CaCl_2$ and 25 Glucose). The set up was maintained on a water bath at 37°C. At the onset of the experiment, 10 μM L-Glutamate was added to the ACSF to induce synaptic activation. After 10 min, 10 μM autocamtide-related inhibitory peptide (A2RIP; a CaMKII inhibitor; Li et al., 2017) and 10 μM CyPPA (concentration-dependent SK2 potentiator; Kasumu et al., 2012) was added to the incubation bath. The set up was maintained for 1 h and the hippocampus was processed to isolate synaptosomal and shaft-cytosol extract using the sucrose gradient method (**Supplementary Figure S1**), followed by immunoblot validation (**Supplementary Figure S2**). Gel electrophoresis and western blotting were performed as described above for whole lysates. Here, we used the following primary antibodies—Rabbit anti CaMKIIα Antibody (Cell Signaling #11945S), Rabbit anti Phospho-CaMKIIα/β:T286/T287 (Cell Signaling #12716), Rabbit anti phospho-CaMKII T305/306 (ThermoFisher Scientific #702357), and Rabbit anti-Phospho-CaMKIIβ:T287(ThermoFisher Scientific #PA5-37833)-to detect CaMKII and phosphorylated isoforms (T286, T287 and T395/306) in synaptosomal and shaft-cytosol extracts. Effective separation of cellular component was verified by GluN1 (ThermoFisher Scientific #PA3-102), PSD-95 (Cell Signaling #3450S), ErK1/2 (ThermoFisher Scientific #PA1-4703) and pErK1/2 (ThermoFisher Scientific ABfinity™ Antibody #700012) localization in synaptosomal and shaft-cytosol extracts. A reciprocal test for an effective separation was done by verifying the absence of PSD-95/GluN1 and ErK1/2/pErK1/2 in cytosolic and synaptosomal extracts, respectively.

Immunofluorescence

After transcardial perfusion with PBS, the animal was perfused with 4% phosphate-buffered paraformaldehyde (PB-PFA). The whole brain was removed and fixed overnight in 4% PB-PFA. Subsequently, the whole brain was transferred

into freshly prepared 4% PB-PFA containing 30% sucrose for cryopreservation for at least 72 h. Free-floating cryostat sections (40 μm) were obtained and preserved in 48-well plates containing 10 mM PBS at 4°C. The sections were washed three times (5 min each) in 10 mM PBS (pH 7.4) on a slow orbital shaker (35 rpm). Blocking was performed in 5% Normal Goat serum (Vector Labs #S-1000), prepared in 10 mM PBS + 0.03% Triton-X 100, for 1 h at room temperature. The sections were incubated overnight at 4°C in Rabbit anti SK2 Antibody (ThermoFisher Scientific #PA5-41071) and Rabbit anti α-actinin Antibody (ThermoFisher #701914). The primary antibodies were diluted in blocking solution (10 mM PBS + 0.03% Triton-X 100 and 5% normal goat serum). After primary antibody incubation, the sections were washed twice in 10 mM PBS (5 min each), and labeled with a secondary antibody—Goat anti-Rabbit Alexa 568 (ThermoFisher Scientific #A-11036)—diluted in the blocking solution. Secondary antibody incubation was done for 1 h at room temperature, with gentle shaking. Immunolabeled sections were washed and mounted on gelatin-coated slides using ProLong^{TM} Diamond Antifade Mountant (ThermoFisher Scientific #P36970).

Microscopy and Quantification

Fluorescence images were acquired in a Nikon-*NiU* fluorescence upright microscope that is configured for 3D imaging. Z-stacks were obtained across a depth of 15 μm and rendered as 3D (eGFP) or converted into 2D images through the "extended depth of focus" option in Nikon Element Advanced Research software. Normalized fluorescence intensity for immunolabeled proteins in the hippocampus was determined in optical slices for serial section images (n = 5 per mouse brain). Cell counting and fluorescence intensity quantification were done using Nikon Element AR and ImageJ software. Average count and intensity were determined per field for n = 12 fields of view.

Spine Morphology

Fluorescence

Vibrotome sliced 100 μm thick sections containing the hippocampus were prepared in oxygenated aCSF and rapidly fixed in 4% PFA. DIL Neurotracer paste (ThermoFisher scientific #N22880) was applied to the hippocampus with the tip of a pulled capillary glass tube. After DIL treatment, the sections were incubated in a PBS humidified chamber overnight at room temperature. Subsequently, the sections were washed in PBS and blocked with 5% normal goat serum prepared in PBST. After blocking, sections were incubated overnight in Rabbit anti-Mouse Synaptophysin antibody (ThermoFisher Scientific #MA5-14532) prepared in the blocking serum solution. The morphology of dendritic spines with synaptophysin expression was imaged in an Olympus FluoView10i Confocal laser scanner. Subsequent quantification of dendritic spines was done in ImageJ.

Transmission Electron Microscopy (TEM)

Microdissected hippocampal tissue was fixed in primary EM fixative composed of 1.6% paraformaldehyde, 2.5% glutaraldehyde, and 0.03% $CaCl_2$ in 0.05M cacodylate buffer (pH 7.4). The hippocampus was trimmed into ∼1 mm sections using a sharp razor and transferred into a fresh fixative for 2 h at room temperature. In subsequent steps, the samples were washed in 0.1 M cacodylate buffer supplemented with 5% sucrose and fixed in 2% osmium tetroxide for 1 h at RT. The sections were washed in water, then in-block stained with 2% uranyl acetate prepared in 0.2 M sodium acetate buffer (pH 3.5), for 2 h. Stained sections were dehydrated in ascending grades of alcohol and propylene oxide. The processed sections were embedded in Epon-Araldite mixture and polymerized for 24 h at 60°C. Tissue blocks were sectioned using a Leica Ultratome (Leica EM UC7). Thin (80 nm) sections were recovered and stained with lead citrate for 5 min. Transmission electron photomicrographs were obtained in a JEOL 1400 Transmission Electron Microscopy (TEM) microscope, equipped with a GATAN digital camera. All reagents for electron microscopy were from EMS (Hatfield, PA, USA). A typical synapse was identified by the presence of synaptic vesicles, postsynaptic mitochondria, and post-synaptic density. The length of dendritic spines was determined in TEM photomicrographs. As such, we estimated the distance between the post-synaptic density, and the stalk of the dendritic spine.

Acute Extracellular Recording

In vivo recording was carried out in the hippocampus of anesthetized mice. Animals were deeply anesthetized with Urethane (0.2 mg/Kg i.p.), then the head was affixed on a stereotaxic frame. For combined recording and photostimulation, CaMKII-Cre::ChR2 mice were anesthetized with ketamine/xylazine. Mice were tested for toe pinch response to ensure the absence of sensation before the commencement of the procedure. A craniotomy was done in order to expose the dura. Drops of ACSF was applied to this area to prevent dryness. Under a digital dissection microscope, the dura over the exposed brain area was carefully excised using a bent needle tip. An acute neural probe, with a 10 mm long and 50 μm thick shank was used for this procedure (Neuronexus, Ann Arbor, MI, USA). The probe shank carried four electrodes arranged as a tetrode, with an inter-electrode distance of 25 μm. The electrodes were connected to a pre-amplifier head stage (Intantech, Los Angeles, CA, USA), tethered to a recording controller and amplifier system (Intantech, Los Angeles, CA, USA). The electrode was gently lowered into the brain tissue using an ultrafine (μm range) hydraulic micromanipulator (Narishige, Japan) to reach the CA1 dendritic field (radiatum/molecular layer) at stereotaxic coordinates (AP: 1.94 mm, ML: 1.0 mm, DV: 1.5 mm) relative to the Bregma. Stainless steel ground wires soldered onto the head stage-electrode adapter (Neuronexus; A4 to Omnetics CM32 adapter) were tied to a ground screw that was fixed in the occipital bone. For recording procedure involving optogenetics, the recording electrode shank, optic fiber and Hamilton's syringe were stereotactically positioned in the CA1. TTL (Prizmatix, Southfield, MI, USA) driven 470 nm LED source (Thorlabs, Newton, NJ, USA) was triggered to generate 50 ms pulses over a 789 s duration (at 1 Hz). In three separate groups, we applied: (1) photostimulation (470 nm); (2) photostimulation with 100 nM Apamin (SK2 blocker; Kasumu et al., 2012)

infusion; and (3) photostimulation combined with 10 μM CyPPA (SK2 positive modulation) infusion.

The stereotaxic apparatus, micromanipulator, electrode and subject mouse were kept in a Faraday cage and connected to the amplifier ground. At the onset of each recording procedure, the impedance of the electrodes was determined at 1 KHz. For all recording sessions in this study, impedance measurement for the silicon tetrodes ranged between 0.6 and 3.1 Ω. Single unit activity was recorded by setting the cut-off frequency as 250 Hz and 7.5 KHz, respectively for lower and upper limits, sampled at 20 KHz/s. Neural activity was monitored for 20 min to ensure the stability of the animal's vitals before the commencement of recordings. Continuously recorded spike trains from the CA1 dendritic field was processed in an Offline Spike Sorting software (*OFSS*; Version 4; Plexon Inc., Dallas, TX, USA). Further analysis of the sorted spikes was done in Neuroexplorer Version 5 (Nex Technologies, Colorado Springs, CO, USA).

Neural Spike Processing and Analysis

Neural spikes were extracted from the continuous data through threshold crossing in the OFSS. The extracted spikes were sorted into clusters using a combination of Valley seeking and K-means clustering methods. Spikes were assigned to single unit clusters through a 3-dimensional space principal component analysis (PCA) projection. Where necessary, unsorted spikes were assigned to clustered units, or invalidated if outlying. Sorted neural spike waveforms, clustered units, and up-sampled continuous data were exported into the Neuroexplorer software for analysis of spike properties.

Social Interaction Test

Mice were habituated in the testing area for 24 h before the commencement of the behavioral test (Kaidanovich-Beilin et al., 2011). At each phase of the test, the compartment was wiped with 70% isopropyl alcohol to prevent odor-specific cues and bias in the subsequent steps. Two smaller holding compartments in the testing area were designated "E (Empty)" during the habituation trial (5 min). For the sociability test, a stranger mouse ($S1_0$; stranger 1) was introduced into one of the compartments while the subject animal was re-introduced into the chamber (5 min). After an inter-trial time of 30 min, we introduced a second stranger mouse (S2), along with the first stranger (now $S1_n$) into two separate holdings (social novelty test). The contact with (E or $S1_0$), and ($S1_n$, S2) were estimated to determine sociability [$S1_0$/(E+$S1_0$)] and social novelty [S2/(S2+$S1_n$)] indices respectively. While "0" represents the first encounter with S1 during sociability test, "*n*" represents the second encounter with S1 in a novel position during the social novelty test. Therefore, different time measurements were done at $S1_0$ and $S1_n$. The time spent in contact with E, S2, $S1_0$, and $S1_n$ in the sociability and social novelty tests were estimated blindly by an independent investigator using a software—Ethovision (Noldus, Leesburg, VA, USA).

Statistics and Sample Size

Outcomes for WT ($n = 4$), $GluN1^{flx/flx}$ ($n = 4$), ΔGluN1 ($n = 7$) were compared in One-Way analysis of variance (ANOVA) with Tukey *post hoc* test. Statistical comparison for $GluN1^{flx/flx}$ ($n = 4$) vs. ΔGluN1 ($n = 4$) or Control ($n = 4$) vs. SK2/3(+; $n = 4$) were done in *T*-test analysis. For ACSF ($n = 4$), L-Glut ($n = 4$), L-Glut+A2RIP ($n = 4$), and L-Glut+CyPPA ($n = 4$), outcomes were compared in One-Way ANOVA with Tukey *post hoc* test. For photostimulation electrophysiological recording experiments involving CaMKII-Cre::ChR2, $n = 3$ mice were used per group (light OFF, light ON, light ON+Apamin, and light ON+CyPPA). Statistical analysis was performed in One-Way ANOVA with Tukey *post hoc* test. All statistical analysis was done in GraphPad Prism Version 8. Results are presented as bar graphs with error bar depicting the mean and standard error of mean, respectively. Also, as pie charts where applicable.

RESULTS

Hypomorphic Attenuation of GluN1 Function

In order to create GluN1 hypomorphic mutation ($\Delta GluN1^{hypomorph}$; ΔGluN1 used interchangeably), AAV (**Figure 1A**) that expresses *Cre* recombinase (AAV-CMV-Cre-eGFP) or a control AAV (AAV-CMV-eGFP) was stereotactically injected into the anterior hippocampus of GluN1 (Grin1) floxed mice. Three weeks after hippocampal AAV injection, transfection was verified by fluorescence imaging of the reporter (gene) protein harbored by the AAV constructs (eGFP). As shown in **Figure 1B**, hippocampus transfected with AAV produced eGFP fluorescence after 3 weeks.

Dendritic Spine Morphology and Synaptic Structure

The general outline of dendritic spines was demonstrated using a combination of DIL Neurotracer, and synaptophysin immunofluorescence labeling (**Figures 2A,B**). Low magnification images demonstrate a significant increase in the distribution of DIL positive cytoskeletal aggregates in the CA1 of the ΔGluN1 hippocampus when compared with the WT and $GluN1^{flx/flx}$. At higher magnification, this translates into a significant loss of dendritic spines in the ΔGluN1 hippocampus (**Figure 2B**; $p < 0.01$). To verify this outcome, dendritic spine morphology was further examined by ultrastructural imaging (TEM) of hippocampal synapses. As illustrated in **Figures 2C,D**, transmission electron photomicrographs revealed a prominent loss of cytoskeletal filament assembly (yellow arrowheads) in ΔGluN1 hippocampal synapse when compared with WT and $GluN1^{flx/flx}$. In addition to the loss of dendritic spines and synaptic cytoskeletal perturbation, TEM images of the ΔGluN1 hippocampus also revealed a prominent decrease in the thickness of post-synaptic densities (**Figures 2E,F**; $p < 0.001$).

Morphology of Dendrites

The expression of membrane-bound eGFP conveyed by the AAV vectors was used to assess the morphology of the dendrites. Given that the expression of eGFP in the neuropil outlines dendrite branching, we used 3D-fluorescence imaging to demonstrate and measure the length of ΔGluN1 CA1 dendrites (μm). However, in order to assess the length of dendritic spines,

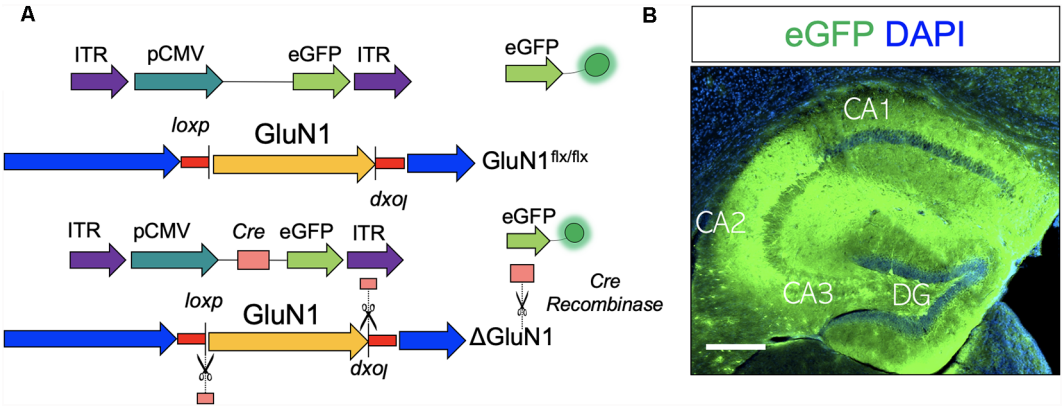

FIGURE 1 | Adeno-associated virus (AAV)-mediated ablation of GluN1 in the hippocampus. **(A)** Schematic illustration of AAV-CMV-eGFP and AAV-CMV-Cre-eGFP construct. **(B)** AAV expression is verified by eGFP (reporter) fluorescence in the hippocampus. Scale bar = 100 μm.

we used ultrastructural synapse images acquired in TEM. **Figure 3A** illustrates the general outline of CA1 pyramidal neurons where DL and Ds.L represent the dendrite length and dendritic spine length, respectively. ΔGluN1 CA1 pyramidal neurons exhibits a significant decrease in dendrite length when compared with the GluN1$^{flx/flx}$ ($p < 0.001$; **Figures 3B,C**). In assessing dendritic spine length (TEM), the distance between the dendrite shaft and the tip of the spine was determined (**Figure 3A**; Ds.L). The synapse (sy) in **Figure 3D** illustrates the tip of the dendritic spine where postsynaptic densities are present. Yellow arrowheads connote the dendritic spine shaft and synaptic expansion. In addition to a decrease in dendrite length (DL), the ΔGluN1 hippocampal neurons were also characterized by a decrease in dendritic spine length (Ds.L: $p < 0.001$; **Figures 3D,E**).

Burst Activity in the CA1 Neural Network

The relationship between the observed synaptic perturbations and neural encoding in the ΔGluN1 hippocampus was assessed by *in vivo* extracellular neural recording. Spontaneously evoked neural spikes in the CA1 dendritic field was analyzed to determine the impact of GluN1 loss of function on multi-synaptic burst encoding *in vivo*. Continuously recorded spike trains for $n = 4$ mice per group (**Figure 4A**) were sorted offline to isolate single units (GluN1$^{flx/flx}$: $n = 77$ and ΔGluN1: $n = 54$) across six sessions. Spike train properties were assessed using the interspike interval (ISI) parameters which represent neural refractoriness over a time window. The firing property of each cell was determined with the ISI histogram (ISIH). Based on the ISIH properties, we grouped the neuron units as bursty, tonic, or irregular firing (**Figure 4B**). For the GluN1$^{flx/flx}$ hippocampus, about 48% of the neurons exhibited distinct burst firing patterns while 38% are irregular firing neurons ($p < 0.01$). Conversely, in the ΔGluN1 hippocampus, 20% of the neurons showed characteristic burst firing pattern while ∼60% were irregular firing neurons ($p < 0.01$; **Figures 4B,C**). Consistent with the suppression of burst firing, ΔGluN1 CA1 neurons exhibit a prolonged ISI peak duration ($p < 0.001$; **Figure 4D**), and an increased mean ISI duration ($p < 0.05$; **Figure 4E**).

In addition to a decreased burst firing, structural changes in ΔGluN1 hippocampal synapses was accompanied by an increased firing irregularity. Here, we determined the regularity of firing as the coefficient of variation (CV_2) of the ISI in a fixed time window. A score of $CV_2 < 1$ or $CV_2 = 1$ depicts a regular firing pattern, while $CV_2 > 1$ represents irregular firing between two fixed time points (τ_n to τ_{n+1}). Regularity of firing based on the CV_2 illustrates a time window computation of the ISI and is not affected by slight changes in firing frequency (spikes/s). Consistent with the percentage of irregular firing neurons, an average score of $CV_2 = 1.2$ was recorded for the ΔGluN1 neurons when compared with the GluN1$^{flx/flx}$ which showed significant firing regularity ($CV_2 = 0.5$; **Figure 4F**). A prolonged ISI and increased irregularity of firing in the ΔGluN1 CA1 spike train was also associated with a decrease in burst count per unit time when compared with the GluN1$^{flx/flx}$ spike train ($p < 0.001$; **Figure 4G**).

$$CV_2 = \frac{2\,[ISIn - ISIn + 1]}{ISIn + ISIn + 1} \quad (1)$$

ΔGluN1-Linked Synaptic Perturbations Led to a Reduced Neuronal Firing Rate

In addition to ISIH characterization of spike train properties (bursty, tonic and irregular), we further examined the neuron population dynamics based on the percentage of *fast* or *slow* spiking neurons determined by autocorrelogram plots (**Figures 5A,B**). This was further verified by the peri-event raster plots which demonstrates number of events (ticks) per trial (**Figure 5C**) when the activity of all neurons (per session) was compared with a neuron with the highest raster count. By combining the autocorrelogram and peri-event raster plots, the neurons were further grouped based on their firing rate *r(t)* over a fixed time window (τ ms).

$$r\,(t) = n/t \quad (2)$$

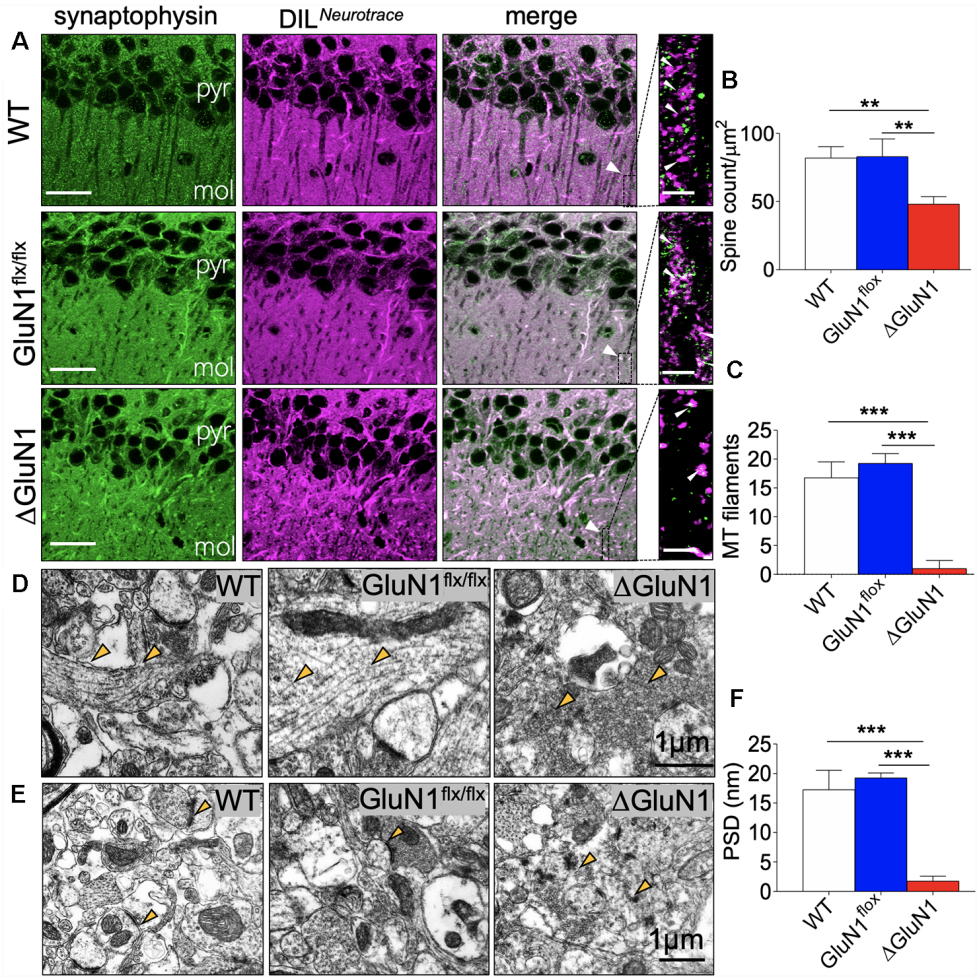

FIGURE 2 | ΔGluN1 induced loss of dendritic spines in CA1 neurons. **(A)** Representative confocal images demonstrating co-localization of synaptophysin and DIL neurotracer in the CA1 (pyr, pyramidal layer; mol, molecular layer). Scale bar = 20 μm and 5 μm. **(B)** Bar graph [One-Way analysis of variance (ANOVA)] illustrating statistical comparison of CA1 dendritic spine count (DIL/synaptophysin). **(C)** Bar graph (One-Way ANOVA) comparing cytoskeletal filament count in hippocampal dendritic spines. **(D)** Transmission electron microscopy (TEM) photomicrographs illustrating hippocampal synapses. Yellow arrowheads indicate the synaptic cytoskeleton. Scale bar = 1 μm. **(E)** TEM photomicrographs demonstrating post-synaptic densities (PSD) in the hippocampus. Scale bar = 1 μm. **(F)** Bar graph illustrating the comparative thickness of PSDs (**B,C,F**; $^{**}p < 0.01$, $^{***}p < 0.001$).

Together with ISIH characterization of neuron firing pattern, it was noted that the fast-spiking neurons were also bursty in their firing properties. On the other hand, irregular firing neurons exhibited a skewed autocorrelogram plot that connotes slow or desynchronized firing. As illustrated by the pie charts, the ΔGluN1 spike train exhibited a significant increase in the percentage of slow and irregularly firing neurons when compared with the GluN1$^{flx/flx}$ spike train ($p < 0.001$; **Figure 5D**). Consequently, the mean firing rate *r(t)* for the ΔGluN1 CA1 network reduced significantly vs. the GluN1$^{flx/flx}$ ($p < 0.01$; **Figure 5E**). In order to ascertain the impact of the highlighted synaptic changes on neural function, ΔGluN1 mice were assessed for sociability and social novelty. Heat maps in **Figure 5F** illustrates a significant decrease in sociability and social novelty performance index for ΔGluN1 mice when compared with the GluN1$^{flx/flx}$. Together with the observed synaptic perturbations the ΔGluN1 mice also exhibited a decline in cognitive function ($p < 0.001$; **Figure 5G**).

Cellular Basis of Firing Rate and ISI Dynamics in ΔGluN1 CA1

Synaptic potentiation in the hippocampus is mediated by several factors. However, it has been established that T286 phosphorylation of CaMKIIα and activation of SK2 can respectively enhance and attenuate synaptic activity (**Figure 6A**). Here, we showed that an increased ISI duration for the ΔGluN1 spike train was linked with a significant upregulation of hippocampal SK2 expression when compared with the controls (WT and GluN1$^{flx/flx}$). Double labeling immunofluorescence in (**Figures 6B,C**) demonstrates a significant increase in SK2 expression for eGFP positive neurons in the ΔGluN1 CA1 ($p < 0.01$).

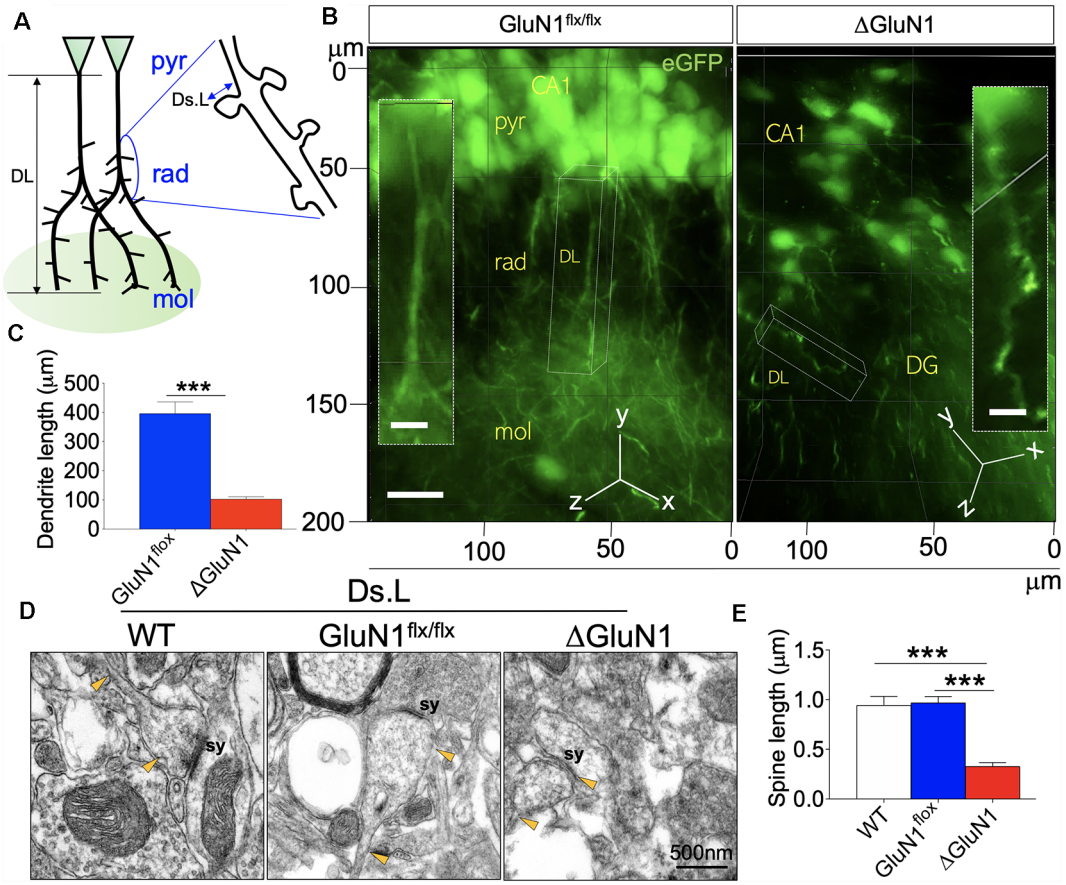

FIGURE 3 | Length of dendrites and dendritic spine in the ΔGluN1 hippocampus. **(A)** Schematic illustration of dendrite length (DL) and dendritic spine length (Ds.L) for CA1 neurons (pyr, pyramidal layer; rad, radiatum layer; mol, molecular layer). **(B)** 3D-fluorescence images (eGFP) showing the outline of CA1 dendrites (pyr, pyramidal layer; rad, radiatum layer; mol, molecular layer). Scale bar = 20 μm, (inset) 5 μm. **(C)** Bar graph illustrating statistical comparison (*T*-test) of dendrite length. **(D)** TEM photomicrographs demonstrating dendritic spine morphology. Scale bar = 0.5 μm. **(E)** Bar graph (One-Way ANOVA) showing statistical comparison of dendritic spine length (TEM; **C,E**; $^{***}p < 0.001$).

Since SK2 activity determines the ISI, it is logical to speculate that the increased peak and mean of ISI duration (**Figures 4D,E**) were—in part—as a result of upregulated CA1 SK2 expression.

T286 pCaMKIIα synaptic localization and substrate targeting is required for LTP expression that is pertinent to long-term synaptic plasticity. As such, we determined the firing *r(t)* and burst discharge rate as indirect measures of synaptic T286 pCaMKIIα translocation efficiency in the CA1 neural network *in vivo*. In the ΔGluN1 hippocampus, the expression of CaMKIIα did not change significantly when compared with the control level (WT and GluN1$^{flx/flx}$; **Figures 6D–F**). However, reduced firing (**Figure 5E**) and burst rates (**Figure 4G**) in the ΔGluN1 CA1 dendritic network was accompanied by a prominent decrease in T286 pCaMKIIα and T287 pCaMKIIβ ($p < 0.01$; **Figures 6D–G**; also **Supplementary Figure S3**). Together, ΔGluN1-induced dendritic spine perturbations and loss of neural plasticity involved the loss CaMKII activity and increased SK2 expression (**Figure 6H**).

Activity-Coupled Regulation of SK2 and GluN1 Expression

While assessing synaptic function in the ΔGluN1 hippocampus, a notable change in spike train properties was an increase in the mean ISI duration (**Figure 4E**), and a reduced firing rate (**Figure 5E**). A possibility is that ΔGluN1 caused a decrease in transient Ca^{++} current that is necessary for SK2 activation and may cause SK2 overexpression through an activity coupled feedback mechanism. To test this hypothesis, we pharmacologically activated SK2 and determined the expression of GluN1 and SK2 by western blotting. Previously, we demonstrated that ablation of GluN1 (upstream) led to an increase in SK2 expression (**Figure 6B**). Here, we noted that positive modulation of SK2 caused a moderate increase in GluN1 expression ($p < 0.05$; **Figures 7A,B**), and significantly downregulate hippocampal SK2 expression ($p < 0.01$; **Figures 7C,D**; **Supplementary Figure S4**). These outcomes suggest that the expression of GluN1 and SK2 is inversely linked to their activity. Consequently, in the ΔGluN1 hippocampus, reduced Ca^{++} current required for the activation of SK2 may

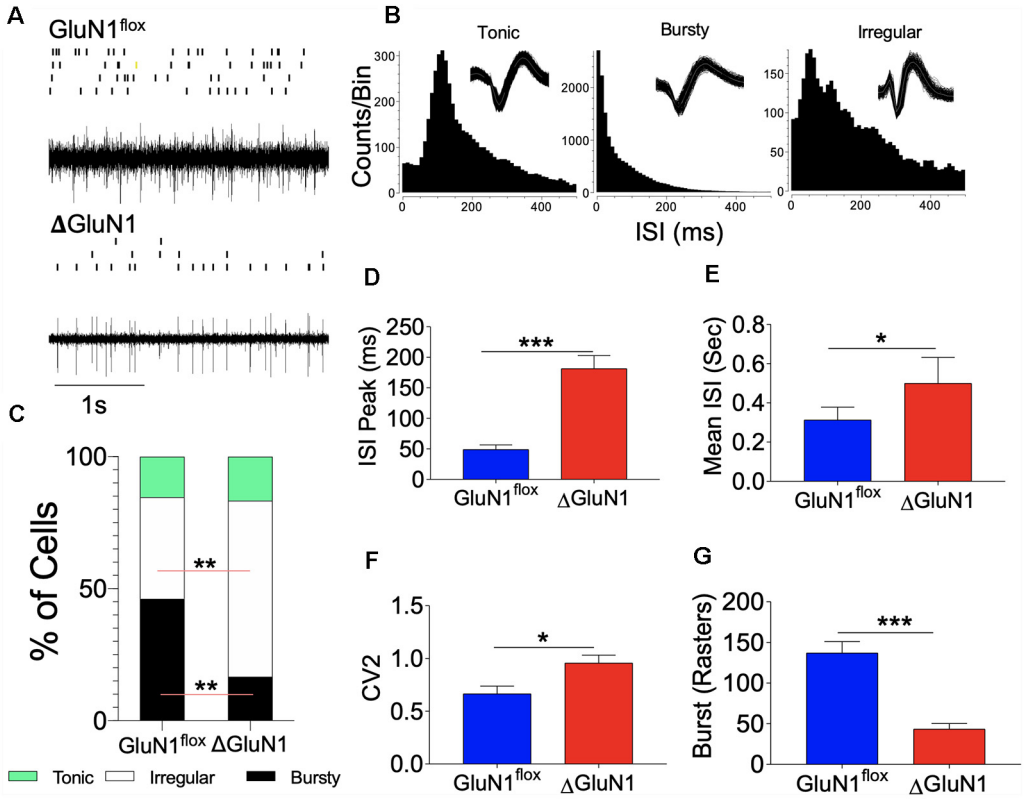

FIGURE 4 | Interspike interval (ISI) characterization of CA1 spike train. **(A)** Single unit spike train and rasters recorded form the CA1 dendritic field. **(B)** Representative Interspike ISI histograms and waveform for tonic, bursty and irregular firing CA1 trains neuron units. **(C)** Composite bar graph depicting the percentage of CA1 neuron units based on ISI characterization of firing pattern. **(D–F)** Bar graphs illustrating ISI peak duration (ms), Mean ISI (ms), and CV_2 of ISI for CA1 spike trains. **(G)** Bar graph illustrating the number of bursts recorded in the spike train per unit time (**D–G**; $^*p < 0.05$, $^{**}p < 0.01$, $^{***}p < 0.001$).

drive an increase in SK2 expression to compensate for the initial reduction in its activation. Likewise, repetitive activation of SK2-downstream of NMDAR—attenuates synaptic potentiation, and lead to an increase in GluN1 expression through a similar feedback mechanism. **Figure 7E** illustrates the site for stereotaxic implant of the cannula guide and drug delivery through the cannula.

SK2-NMDAR Cross-Talk in the Regulation of CaMKIIα Activity

Given that the expression and activity of GluN1 and SK2 are tightly linked, an important question yet to be addressed is whether downstream positive modulation of SK channel can impact CaMKII activity and if such interaction might be dependent on NMDAR. In the ΔGluN1 hippocampus, T286/T287 phosphorylation of CaMKII decreased significantly. Although GluN1 expression was upregulated after a positive modulation of SK channel, the expression and T286 phosphorylation of CaMKIIα was significantly suppressed in the SK2/3(+) hippocampus (**Figures 8A–C**; $p < 0.001$; **Supplementary Figure S5**). Likewise, SK channel potentiation caused a significant decrease in T287 pCaMKIIβ (**Figure 8D**; $p < 0.001$). Ultimately, SK channel potentiation led to a decrease in percentage T286/T287 phosphorylated CaMKII in the hippocampus (**Figure 8E**; $p < 0.001$). These results are indicative of the role of SK2 in the tuning synaptic plasticity by CaMKII modulation.

Positive SK Channel Modulation Impairs Synaptic Localization of CaMKII

CaMKIIβ anchors the CaMKII (9α/3β) to dendritic spine F-actin by binding to α-actinin. There is substantial evidence to suggest that α-actinin—a F-actin binding protein—is pertinent to CaMKII (9α/3β) localization on synaptic cytoskeleton (Shen et al., 1998; Robison et al., 2005; Gustin et al., 2011; Jalan-Sakrikar et al., 2012; Lisman et al., 2012; Bosch et al., 2014; Hell, 2014; Khan et al., 2016). Consequent of the interaction between the CaMKIIα/β and α-actinin, the anchored CaMKII (9α/3β) determines the shape of the F-actin assembly, and structural plasticity of dendritic spines (Shen et al., 1998; Jalan-Sakrikar et al., 2012; Bosch et al., 2014; Hell, 2014). In acute slice preparation, perfusion with Ca^{++}-ACSF containing L-Glutamate caused no significant change in hippocampal α-actinin expression when compared with ACSF only (**Figures 9A–C**). However, when a CaMKII inhibitor (A2RIP) or SK channel positive modulator (CyPPA) is paired with L-Glutamate, there

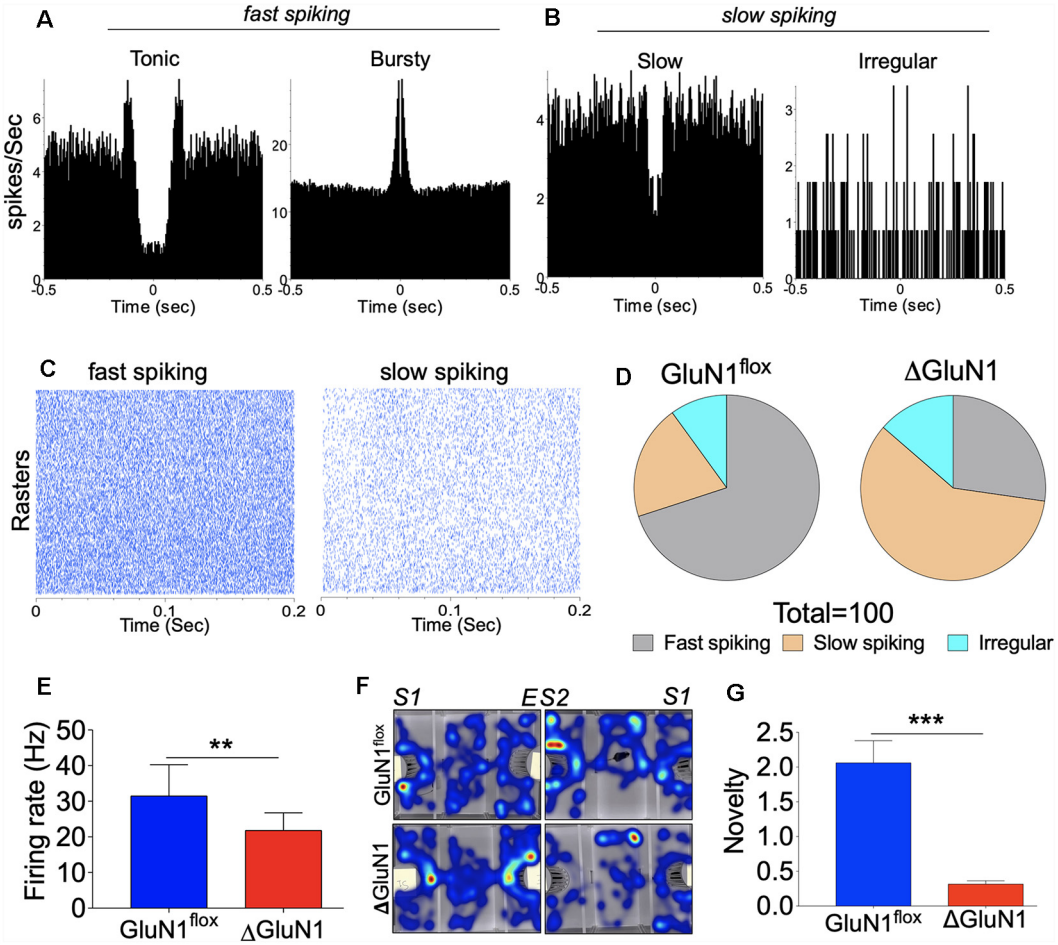

FIGURE 5 | Firing rate (spikes/sec) characterization of the CA1 spike train. **(A,B)** Representative autocorrelogram for typical fast and slow spiking CA1 neuron units. **(C)** Perievent raster representation of fast and slow spiking CA1 units. **(D)** Pie chart depicting the percentage of fast, slow and irregularly firing CA1 neuron units. **(E)** Bar graph showing statistical comparison of mean firing rates (Hz). **(F)** Heat map demonstrating sociability and social novelty exploration pattern. **(G)** Bar graph illustrating social novelty memory index (**E,G**; $^{**}p < 0.01$, $^{***}p < 0.001$).

was a significant loss of α-actinin in the hippocampus ($p < 0.01$; **Figure 9C**). Based on these outcomes, we propose that SK2 may suppress long-term synaptic plasticity by attenuating synaptic localization of T286 pCaMKIIα (**Figures 9D,E**).

Compartmental Localization of CaMKII in the Hippocampus

We processed microdissected whole hippocampus to isolate synaptosomal extracts containing post-synaptic densities (PSD), and cytosolic extracts containing dendritic shaft. We validated the tissue extracts by western blotting to detect PSD proteins—PSD-95 and GluN1—in the synaptosomal extract. Likewise, the shaft-cytosol extract was validated by immunoblot detection of ErK1/2 and pErK1/2. The validation protocol was set up as a reciprocal detection experiment where synaptic proteins are also assessed in shaft-cytosol extracts, and vice versa. For all samples, PSD-95 (S2.1,S2.2) and GluN1 (S2.3,S2.4) were enriched in the synaptosomal extract, and not in the shaft-cytosol domain. Similarly, ErK1/2 (S2.5,S2.6) and pErK1/2 (S2.7,S2.8) were enriched in the shaft-cytosol domain only. In order to determine compartmental localization of CaMKIIα, we performed immunoblot detection of CaMKIIα, and T286α/T287β phosphorylated isoforms in the synaptosome and shaft-cytosol extracts. Our results revealed that CaMKIIα is predominantly localized in the synaptic compartment when compared with the shaft-cytosol (**Figures 10A,B**; $p < 0.001$). Likewise, T286 pCaMKIIα and T287 pCaMKIIβ were also enriched in the synaptic compartment when compared with the shaft-cytosol extract (**Figures 10C,D**; $p < 0.001$).

In subsequent experiments, we incubated the microdissected hippocampus in glucose-rich oxygenated Ca^{++}-ACSF to determine how an *ex vivo* treatment might affect the compartmental localization of CaMKII (**Figures 10A–D**). After 1 h of incubation in ACSF, CaMKIIα and T286α/T287β were predominantly localized in the shaft-cytosol domain (**Figure 10E**). However, when 10 μM L-Glutamate is included the ACSF, CaMKIIα was predominantly localized in the

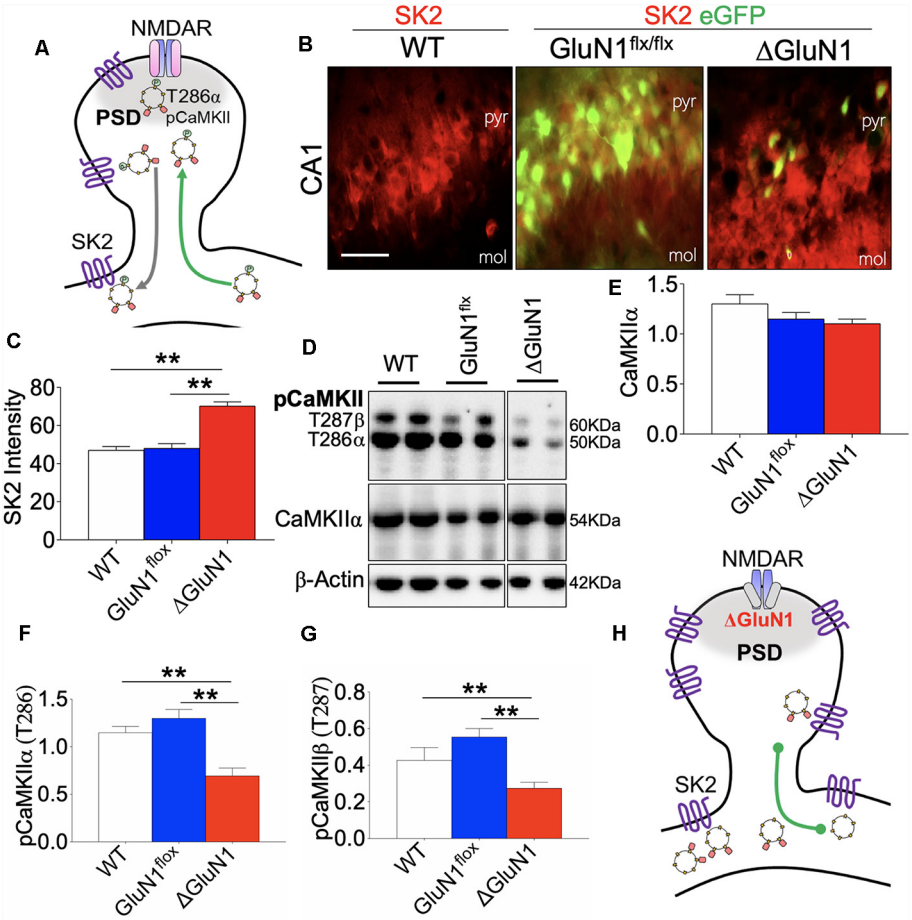

FIGURE 6 | Co-dysregulation of SK2 and CaMKII in the ΔGluN1 hippocampus. **(A)** Schematic illustration of N-Methyl-D-Aspartate Receptor 1 (NMDAR), T286 pCaMKIIα, and SK2 co-localization at postsynaptic densities. **(B,C)** Representative fluorescence images and bar graph (One-Way ANOVA) demonstrating SK2 expression in the CA1 (pyr, pyramidal layer; mol, molecular layer). Scale bar = 20 μm **(B)**. **(D)** Representative immunoblots showing the expression of CaMKIIα, T286 pCaMKIIα and T287 pCaMKIIβ in whole hippocampal lysate. **(E–G)** Bar graphs showing statistical comparison of CaMKIIα (normalized with β-Actin), T286 pCaMKIIα, and T287 pCaMKIIβ (normalized with CaMKII). **(H)** Schematic representation of the ΔGluN1 hippocampal dendritic spine. T286 pCaMKIIα reduced significantly while SK2 expression is upregulated (**C,E,F,G**; $^{**}p < 0.01$).

synaptic compartment, and was accompanied by a near total T286α/T287β synaptic translocation (**Figures 10E,F**; $p < 0.001$). These results suggest that L-Glutamate-driven synaptic potentiation is required for spine recruitment of CaMKIIα and T286α/T287β (**Figure 10G**).

SK Channel Potentiation Reduced the Efficiency of CaMKII Translocation

Figure 8 demonstrates a significant loss of neural CaMKII, T286α and T287β after SK channel potentiation *in vivo* (48 h). In order to determine the short-term (1 h) effect of SK channel on synaptic localization of CaMKII, we paired L-Glutamate treatment with SK channel potentiation in acute preparations (**Figure 11A**). L-Glutamate treatment significantly increased synaptic localization of CaMKIIα ($p = 0.0031$; **Figure 11B**). Normalized synaptic expression of CaMKIIα also increased when L-Glutamate was paired with CaMKII inhibitor (A2RIP; $p = 0.0024$) or SK channel potentiator ($p = 0.0010$; **Figure 11B**). Similar to L-Glutamate treatment, a combination of L-Glutamate with A2RIP or CyPPA did not impact the shaft-cytosol localization of CaMKIIα (**Figure 11C**). L-Glutamate treatment increased synaptic localization of CaMKIIβ when compared with ACSF only ($p = 0.0216$; **Figure 11D**). However, when combined with CyPPA, the synaptic translocation of CaMKIIβ was significantly upregulated ($p = 0.0015$). L-Glutamate treatment caused a significant decrease in shaft-cytosol localization of CaMKIIβ when compared with ACSF ($p = 0.0453$). This was attenuated by SK channel potentiation and CaMKII inhibition. For these treatment combinations, there was no significance vs. ACSF (baseline; A2RIP and CyPPA; **Figure 11E**).

In order to ascertain the effect of SK channel potentiation (CyPPA) on CaMKII translocation efficiency, we normalized synaptosomal pCaMKII (T286, T287, T305/306) with shaft-cytosolic expression level. While L-Glutamate significantly increased synaptosomal translocation of T305/306 pCaMKII

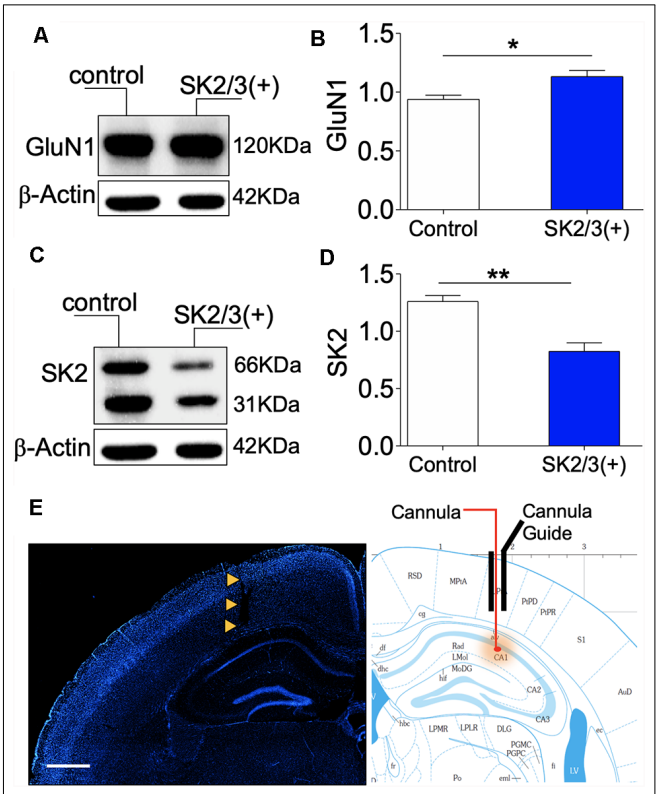

FIGURE 7 | Activity-dependent expression of SK2 and GluN1. **(A,B)** Western blot and bar graph demonstrating hippocampal NMDAR-GluN1 expression. **(C,D)** Representative immunoblot and bar graph illustrating hippocampal SK2 expression. **(E)** Fluorescence image (DAPI) showing the track of the cannula guide and cannula for intrahippocampal injections. Scale bar = 0.5 mm (**E**; **B,D**; $*p < 0.05$, $**p < 0.01$).

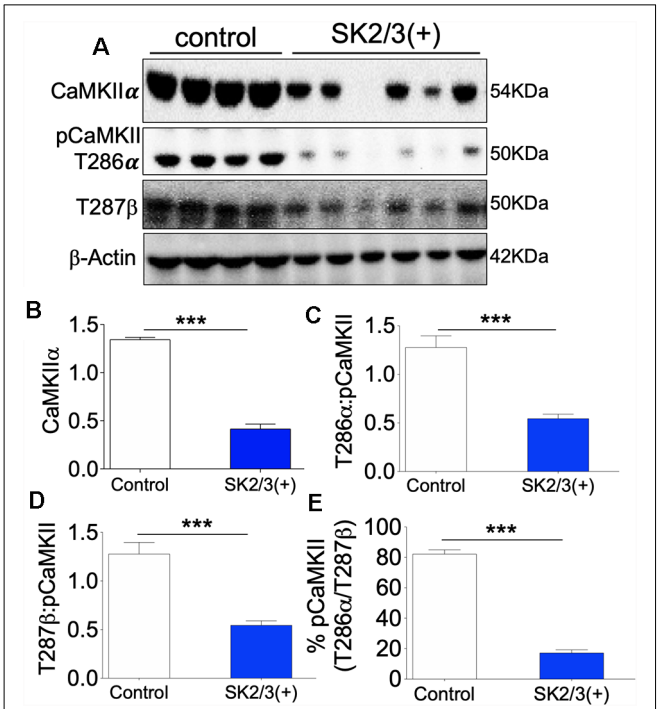

FIGURE 8 | SK channel potentiation reduced hippocampal CaMKII expression (48 h after treatment *in vivo*). **(A)** Western blots demonstrating detected level of CaMKII, T286 pCaMKIIα, and T287 pCaMKIIβ in whole hippocampal lysate. **(B)** Bar graph representing comparative β-actin-normalized CaMKII expression (*T*-test). **(C,D)** Bar graph representing comparative CaMKII-normalized T286 pCaMKIIα and T287 pCaMKIIβ expression (*T*-test). **(E)** Bar graph demonstrating percentage T286/T287 (total) pCaMKII in the hippocampus (**B,C,D,E**; $***p < 0.001$).

(p = 0.0158), pairing L-Glutamate with either CaMKII inhibition or SK channel potentiation suppressed synaptic translocation of T305/306 (**Figure 11F**). Accordingly, when L-Glutamate is paired with A2RIP or CyPPA, there is no significant change in synaptic T305/306 expression vs. ACSF (**Figure 11F**). L-Glutamate treatment increased the synaptic localization of T286 pCaMKIIα when compared with ACSF (p = 0.0016). Similar to T305/306, pairing L-Glutamate with SK channel potentiation reduced synaptic T286 pCaMKIIα localization (**Figure 11G**). Here, the significance recorded for L-Glutamate—vs. ACSF only—was abolished when L-Glutamate is paired with CyPPA (ns). L-Glutamate treatment also increased the synaptic localization of T287 pCaMKIIβ when compared with ACSF only (p = 0.0170; **Figure 11H**). As shown in **Figure 11D**, CyPPA treatment induced a more prominent increase in synaptic CaMKIIβ expression (p = 0.0015) when compared with L-Glutamate (p = 0.0216); vs. ACSF. To this effect, pairing L-Glutamate with CyPPA also caused a prominent increase in synaptic T287 pCaMKIIβ ($p < 0.0001$) when compared with L-Glutamate (p = 0.0170); vs. ACSF (**Figure 11H**). Together, our results suggest that SK channel potentiation suppressed synaptic translocation of T286 pCaMKIIα while increasing T287β pCaMKII phosphorylation in acute experiments.

SK Channel Potentiation Modulates CA1 Burst Encoding

The physiological implication of a suppressed T286/T287 phosphorylation and imbalanced translocation to the synapse is that LTP may be abrogated. In addition, long-term synaptic plasticity modulated by CaMKII may become significantly dysregulated. In a separate experiment, we examined the effect of SK channel positive modulation (10 μM CyPPA) or inhibition (100 nM Apamin) on CA1 dendritic neural network burst encoding *in vivo*. In anesthetized mice, SK channel agonist (CyPPA) was infused, and spontaneously evoked spikes were recorded with a tetrode. Subsequently, Apamin (SK2 blocker) was infused to attenuate the activity of SK2 in the CA1 dendritic field. As illustrated in **Figure 12A**, positive modulation of SK channel function significantly reduced spontaneous CA1 firing while Apamin treatment rescued CA1 firing and burst activity (**Figures 12A,B**). Based on ISI characterization of firing pattern (**Figures 4B,C**), there was a significant increase in the percentage of irregular firing neurons and a decrease in bursty neurons for SK2/3(+) CA1 spike train ($p < 0.001$; **Figure 12C**). Subsequent Apamin treatment increased the percentage of cells with characteristic bursty

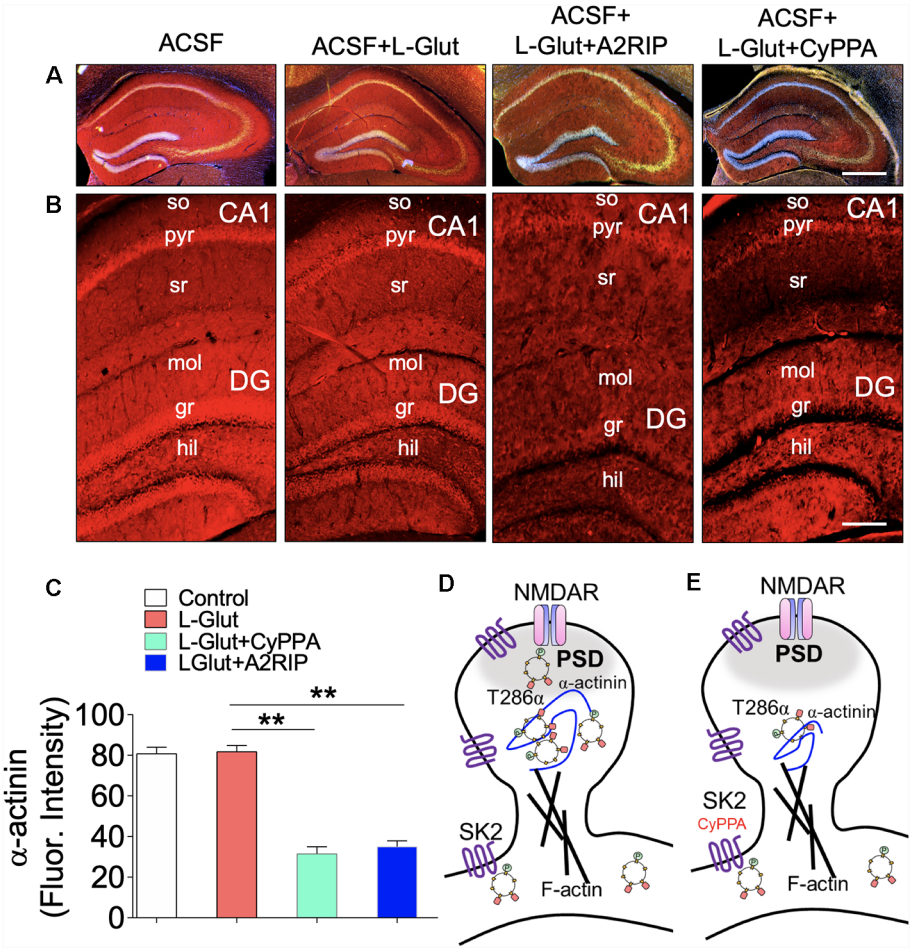

FIGURE 9 | SK channel potentiation impacts hippocampal α-actinin expression. **(A–B)** Fluorescence images illustrating α-actinin expression in the hippocampus (so, stratum oriens; pyr, pyramidal layer; sr, stratum radiatum; mol, molecular layer; gr, granule cell layer, and hil, hilus). Scale bar = 0.4 mm **(A)**, 100 μm **(B)**. **(C)** Bar graph representation of α-actinin fluorescence intensity in the hippocampus (One-Way ANOVA). Schematic illustration of SK2 modulation of CaMKII spine anchorage: **(D)** synaptic pCaMKII is structurally linked with to the GluN2B sub-unit of NMDAR and is anchored to the dendritic spine cytoskeleton (F-actin) by α-actinin. In NMDAR-mediated synaptic potentiation, synaptic accumulation of pCaMKIIα/β is facilitated by α-actinin. **(E)** SK channel potentiation induced a loss CaMKII and α-actinin expression (**C**; $^{**}p < 0.01$).

firing pattern, while also reducing the percentage of irregular firing neurons (**Figure 12C**; $p < 0.001$). Further evaluation of the ISI revealed that SK2 blockade by Apamin reduced the mean ISI duration ($p < 0.01$; **Figure 12D**) and increased the regularity of firing (**Figure 12E**) of CA1 neurons. This was seen as a decrease in CV_2 score for the ISI ($p < 0.01$) following Apamin infusion.

SK Channel Modulation of Firing Rate

Here, we measured CA1 network firing rate (Hz) when pyramidal cell dendritic field photostimulation is paired with pharmacological modulation of SK2 *in vivo*. **Figures 13A,B** illustrates the expression of ChR2 in the hippocampus and dendritic spine. Dotted lines represent the electrode/optic fiber track in the hippocampus (**Figure 13B**). The experimental set up for placement of the recording electrode, optic fiber, and needle for drug infusion is schematically illustrated in **Figure 13C**. Blue light pulse (470 nm) was delivered by a square wave (TTL) generator at 1 Hz (50 ms) to potentiate the spines. The effect of the photostimulation regime is demonstrated by the 470 nm light ON phase (**Figures 13D–F**). When the ISI histogram was used for the characterization of the firing pattern, ChR2 photostimulation increased burst firing as indicated by the percentage of bursty neurons (**Figure 13G**; $p < 0.001$). Interestingly, when SK2 inhibition (Apamin) is paired with photostimulation, the threshold of bursting activity increased drastically with ∼100% of neurons showing burst activity. However, when photostimulation is paired with SK channel potentiation, a significant decrease in burst activity was recorded ($p < 0.001$). This is further evident in perievent histogram plots that depict response strength and synchrony of CA1 synaptic units. A paired photostimulation and SK2 inhibition regime increased the firing rate and synchrony when compared with photostimulation

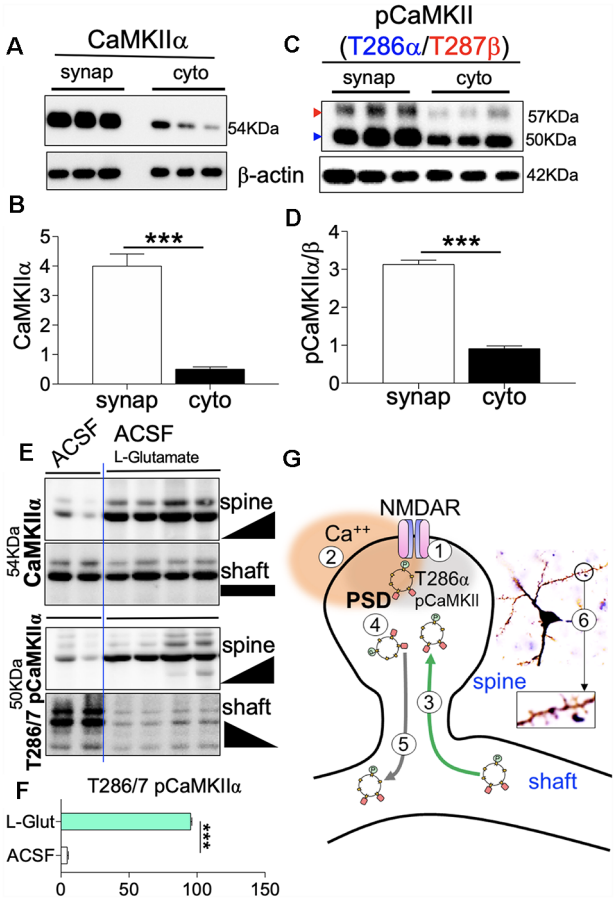

FIGURE 10 | Synaptic potentiation increase spine (synaptic) translocation of CaMKII. **(A–D)** Representative western blots and bar graphs demonstrating the distribution of CaMKII and T286 pCaMKIIα/T287 pCaMKIIβ in synaptosomal and shaft-cytosol tissue extracts derived from WT hippocampus. **(E)** Representative immunoblots illustrating the comparative synaptic (spine) and shaft-cytosol expression of CaMKII and T286/T287 pCaMKIIα/β. **(F)** Bar graph (*T*-test) illustrating the synaptic translocation of T286/T287 pCaMKIIα/β post L-Glutamate treatment. **(G)** Schematic illustration of synaptic translocation of T286/T287 pCaMKIIα/β. (1) NMDAR potentiation; (2) post-synaptic Ca^{++} transient activates SK2; (3) Ca^{++} transient facilitates T286/T287 CaMKII phosphorylation, and synaptic translocation; (4) increased SK2 activity facilitates removal of synaptic T286/T287 pCaMKIIα/β; and (5) translocation of CaMKII from dendritic spine to shaft-cytosol. (**B,D,F**; ***$p < 0.001$).

only. Conversely, SK channel activation by CyPPA scrambled the synchrony and response strength of the CA1 units (**Figures 13H–K**).

The significance of this outcome is further evident in the analysis of the ISI histogram plot. For paired photostimulation and SK channel inhibition, the ISI histogram shows strong burst activity that is characterized by a decreased ISI, and rapid onset for ISI decay (red arrow head; **Figures 14A,B**). On the other hand, pairing SK channel potentiation with photostimulation prolonged the ISI duration, and delayed the onset of ISI decay (>400 ms; **Figure 14C**). This outcome is further supported by analysis of autocorrelogram which revealed a prominent increase in firing strength as a result photostimulation (**Figure 14D**; red arrow heads); compared with spontaneously firing bursty neuron (inset). Pairing photostimulation and SK2 inhibition further enhanced burst strength of CA1 network as illustrated by a further depression of the edge of autocorrelogram plot (**Figure 14E**). However, when photostimulation is coupled with SK channel potentiation, synaptic response strength and synchrony decreased significantly as shown by a decrease in autocorrelogram peak strength (**Figure 14F**). This is consistent with an increased ISI duration (ms; **Figure 14C**), and reduced synchrony of firing shown by the perievent raster plot (**Figure 13K**). Suppression of SK2 activity by Apamin during photostimulation increased the firing rate and the number of spikes in a burst when compared with photostimulation only (**Figures 14G,H**, $p < 0.0001$). As expected, pairing SK channel potentiation with photostimulation abolished the firing rate increase recorded in photostimulation only (**Figures 14G,H**). Interestingly, our results revealed that the mean burst duration was not altered irrespective of the paired SK2 modulation event. Based on these outcomes, we deduced that the dendritic SK channel modulates burst encoding by directing the firing rate and number of spikes in a burst. While these parameters are linked to the probability of burst firing, we noted that SK channel modulation did not alter the duration of burst events in the CA1 neural network.

DISCUSSION

NMDAR is a glutamate type ionotropic receptor that is relatively abundant in the hippocampus and mediates LTP (Hatton and Paoletti, 2005; Coultrap and Bayer, 2012; Lisman et al., 2012; Babiec et al., 2017). A change in the expression of NMDAR or loss of function of its sub-units (GluN1 and GluN2A and 2B) have been identified in the etiology and progression of neuropsychiatric disorders (Hansen et al., 2014; Huang and Gibb, 2014; Wesseling et al., 2014; Bustos et al., 2017). Neurocognitive disorders such as autism, schizophrenia, and depression exhibit various forms of NMDAR hypofunction (Duffney et al., 2013; Snyder and Gao, 2013; Cohen et al., 2015; Zhou et al., 2016; Gulchina et al., 2017; Nakazawa et al., 2017; Ogundele and Lee, 2018; Rebollo et al., 2018). Although the causes of developmental neuropsychiatric defects are wide and varied, recent evidence suggests that loss of NMDAR function is a determinant of the synaptic and behavioral defects.

In LTP, synaptic potentiation by NMDAR-linked ionotropic neurotransmission is regulated through various mechanisms. Notably, positive modulation of synaptic strength which is pertinent to memory encoding is facilitated by CaMKIIα T286 phosphorylation (Gustin et al., 2011; Coultrap and Bayer, 2012; Lisman et al., 2012; Coultrap et al., 2014). On the other hand, negative modulation of synaptic strength could be driven by small conductance (SK2) ion channel (Ngo-Anh et al., 2005; Hammond et al., 2006; Maingret et al., 2008). The NMDAR-mediated Ca^{++} current constitutes 75% of post-synaptic transient that is central to synaptic potentiation and LTP. The mechanism involves activation (T286 autophosphorylation) of a closed CaMKII structure (T305/T306) to promotes kinase

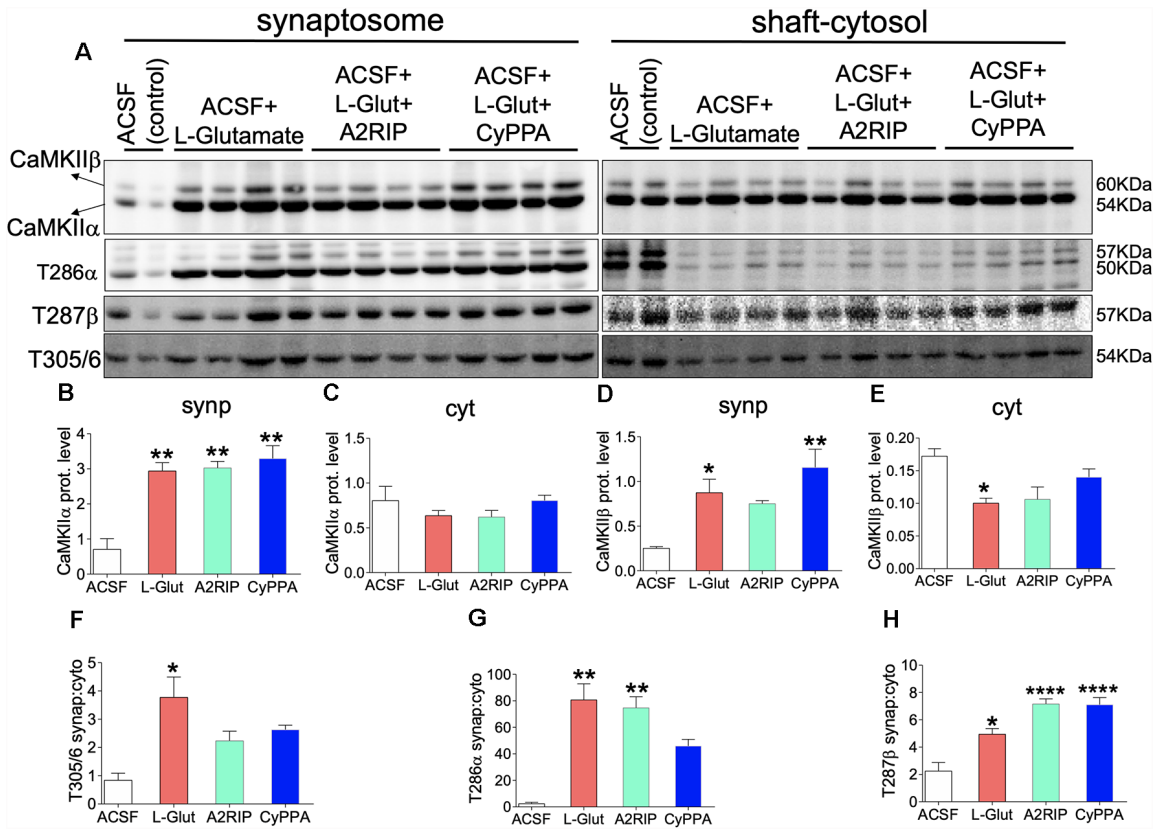

FIGURE 11 | SK channel potentiation impacts hippocampal synaptic translocation of T286/T287 pCaMKIIα/β. **(A)** Representative western blots illustrating synaptosomal and shaft-cytosol level of CaMKIIα, CaMKIIβ, T286 pCaMKIIα, T287 pCaMKIIβ, and T305/306 pCaMKII. Bar graphs illustrating; **(B)** synaptosomal expression of CaMKIIα. **(C)** Shaft-cytosol expressions of CaMKIIα. **(D)** Synaptosomal expression of CaMKIIβ. **(E)** Shaft-cytosol expressions of CaMKIIβ. **(F)** Level of normalized synaptic T305/306 pCaMKII relative to shaft-cytosol expression. **(G)** Level of normalized synaptic T286 pCaMKIIα relative to shaft-cytosol expression. **(H)** Level of normalized synaptic T287 pCaMKIIβ relative to shaft-cytosol expression (**B–H**; $^{*}p < 0.05$, $^{**}p < 0.01$, $^{****}p < 0.0001$).

activity and substrate targeting (Lisman et al., 2002, 2012). In the T286 autophosphorylated state, CaMKII holds an increased (10-folds) affinity for Ca^{++}-calmodulin binding, and promotes high-frequency firing that leads to LTP expression (Gustin et al., 2011; Coultrap and Bayer, 2012; Hell, 2014; Ma et al., 2015). On the other hand, activation of SK2 by the Ca^{++} surge suppresses neuronal firing by spike frequency adaptation that is pertinent to intrinsic excitability regulation (Ngo-Anh et al., 2005; Hammond et al., 2006; Lin et al., 2008; Lee and MacKinnon, 2018). Mechanistically, the activity of SK2 constitutes the after-hyperpolarization phase, that depicts the interspike interval, during which a synaptic unit is least expected to fire (Stackman et al., 2002, 2008; Ngo-Anh, 2006; Kim and Hoffman, 2008; Lin et al., 2008; Maingret et al., 2008; Prescott and Sejnowski, 2008; Toporikova and Chacron, 2009; Kuiper et al., 2012; Trimmer, 2015). Based on these concepts, NMDAR hypofunction may also imply—to an extent—the suppression of CaMKIIα T286 phosphorylation and (or) a positive modulation of SK2 function. Consistent with this idea, genetic ablation of NMDAR or pharmacological potentiation of SK2 suppressed T286 phosphorylation of CaMKIIα and reduced the firing rate of CA1 neurons *in vivo*.

The frequency of NMDAR Ca^{++} transients represents a significant aspect of synaptic potentiation that impacts dendritic spine plasticity in the hippocampus. As such, the structure of dendritic spines, distribution of dendritic spines, and CA1 network firing pattern are directly related to LTP expression and structural plasticity (Jauregui et al., 2017; Nakahata and Yasuda, 2018). While an increased CaMKII T286 phosphorylation is characteristic of high-frequency neuronal firing, an increased SK2 function attenuates neuronal firing. Given that NMDAR activation produces the transient Ca^{++} current that activates CaMKII and SK2 for synaptic potentiation and depression respectively, a significant aspect of this interaction that is yet to be considered is whether SK2 refine synaptic plasticity by modulating the spine dynamics of CaMKII. Taken together, our results demonstrate that genetic ablation of GluN1 in the hippocampus significantly perturbed dendritic spine morphology, and attenuate CA1 burst firing *in vivo*. This is attributable—in part—to the activity-coupled upregulation of SK2 expression, and a suppression of T286 CaMKIIα phosphorylation. Interestingly, in the presence of normal GluN1 function, positive modulation of SK channel equally reduced hippocampal synaptic T286 pCaMKIIα localization.

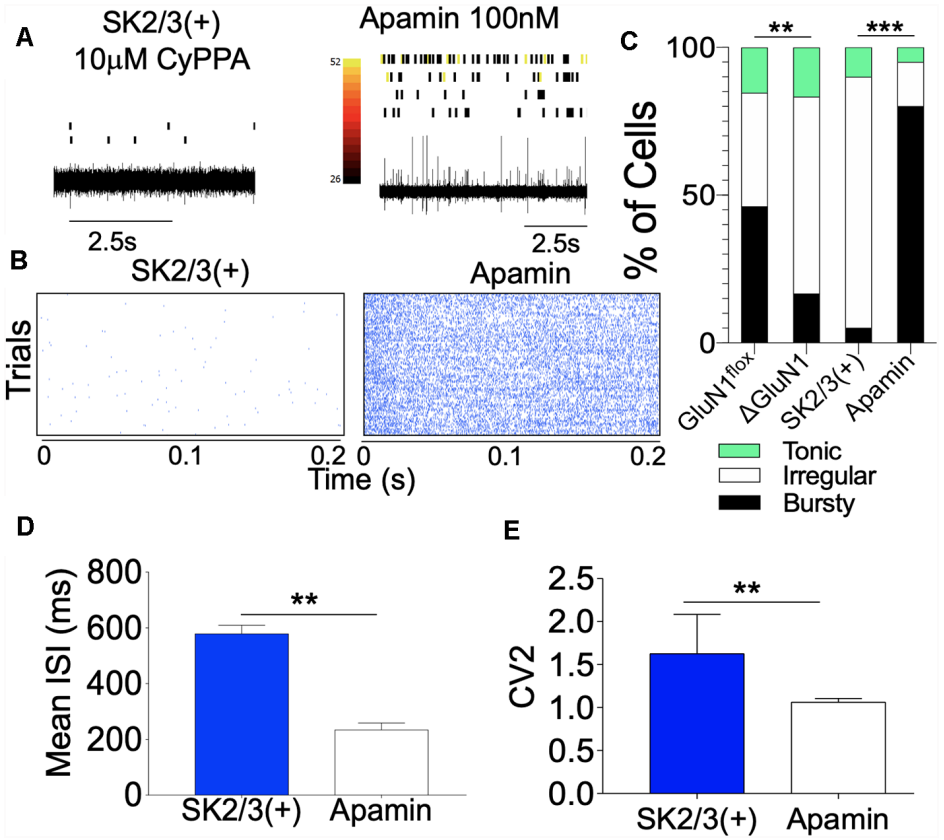

FIGURE 12 | SK channel potentiation attenuates spontaneous CA1 firing. **(A)** Spike train with aligned rasters demonstrating CA1 dendritic field neural activity. **(B)** Perievent rasters demonstrating a change in neural activity following SK channel potentiation and inhibition. **(C)** Composite bar graph demonstrating percentage distribution of neuron units characterized by ISI properties. **(D)** Bar graph demonstrating Mean ISI (ms) duration. **(E)** Bar graph demonstrating regularity of firing (CV_2 of ISI). (**C–E**; $^{**}p < 0.01$, $^{***}p < 0.001$).

Cytoskeletal Anchorage of CaMKII

Our results demonstrate that SK channel potentiation *in vivo* caused prominent loss of CaMKII, and suppressed T286/287 phosphorylation after 48 h. However, in acute treatment (1 h) performed with *ex vivo* slices, we found that SK channel potentiation disrupts T286 pCaMKIIα and T287 pCaMKIIβ synaptic homeostasis. It follows that the CaMKII heteromeric dodecamer (9α/3β) is anchored to dendritic spine cytoskeleton by an F-actin binding protein—α-actinin (Shen et al., 1998; Robison et al., 2005; Jalan-Sakrikar et al., 2012; Khan et al., 2016). However, it has been previously established that CaMKIIβ holds a stronger affinity, and is primarily involved in anchoring the holoenzyme α-actinin/F-actin (Coultrap and Bayer, 2012). T287β phosphorylation allows the holoenzyme to detach from the cytoskeletal anchor and facilitates substrate targeting (kinase activity) of the T286 pCaMKIIα component. Here, our results demonstrate that SK channel potentiation suppresses synaptic localization of T286 pCaMKIIα while promoting T287β phosphorylation (**Figures 11G,H**). The physiological implication is that the synaptic substrate activity (T286 pCaMKIIα) and cytoskeletal anchorage (CaMKIIβ) are significantly reduced following SK channel potentiation. The latter is further evident by the prominent loss of α-actinin in the hippocampus after SK channel potentiation (**Figure 9**).

SK2 in CA1 Burst Encoding

Spontaneously evoked synaptic potentials are necessary for hippocampal neural plasticity and are representative of the state of CA1 neural network (Winnubst et al., 2015). Here, neurons were characterized using the shape of the ISIH which is mostly dependent on SK2 function and represents a distinct firing signature based on repetitive patterns of refractoriness (Maylie et al., 2004; Ngo-Anh et al., 2005; Hammond et al., 2006). Additionally, we assessed burst and firing rate events that are dependent on the threshold of T286 pCaMKIIα synaptic localization (Coultrap and Bayer, 2012; Hell, 2014; Penny and Gold, 2018). Together with the structural perturbations of dendritic spine, our results suggest that loss of GluN1 function may also connote the suppression of CaMKII T286 phosphorylation and upregulation of SK2 function (**Figure 6H**). Here, we showed that the suppression of CaMKII function in the ΔGluN1 hippocampus was associated with a reduced burst firing (**Figure 4**). Likewise,

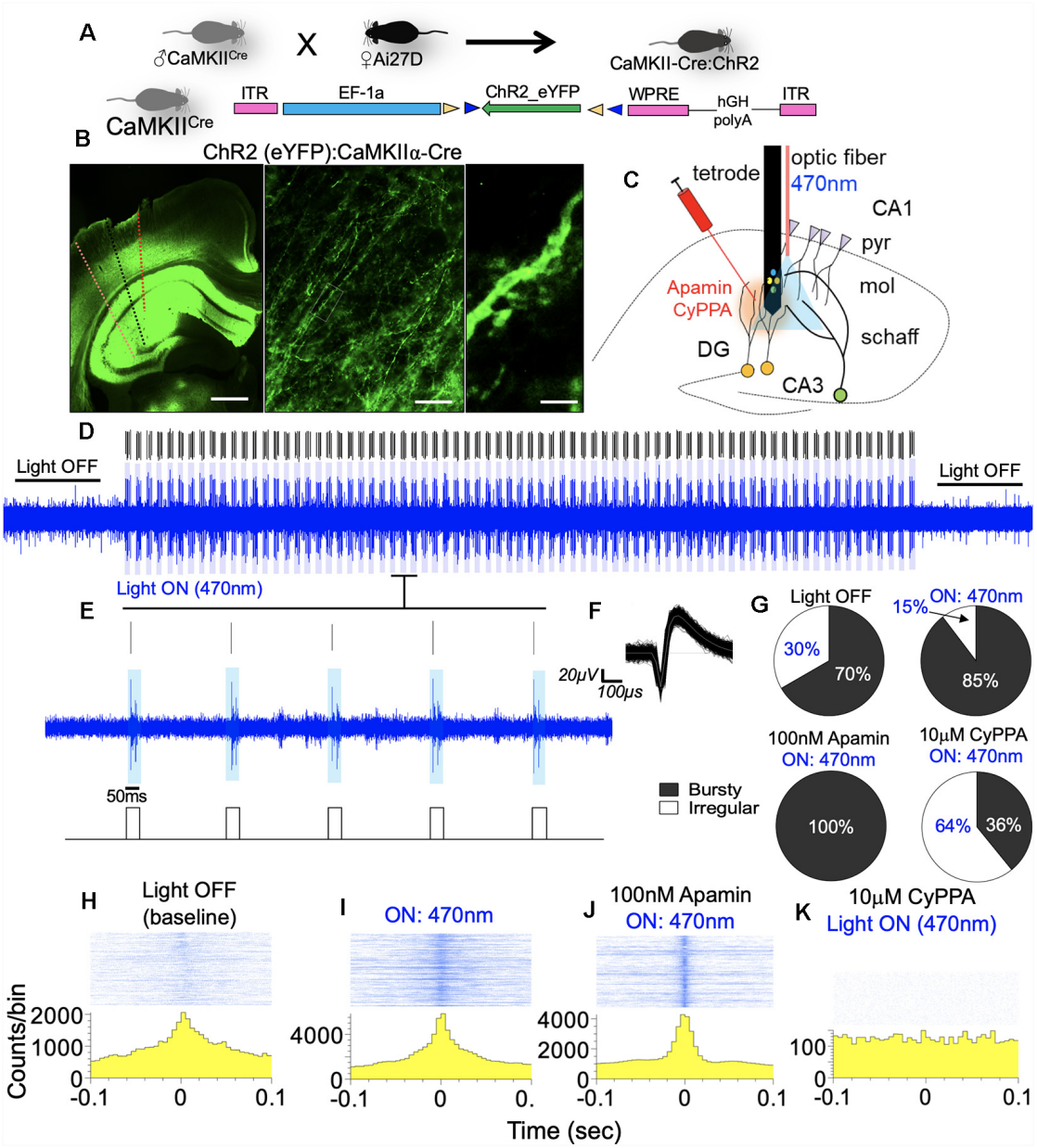

FIGURE 13 | SK channel modulation of CA1 burst discharge. **(A)** Schematic illustration of a double floxed AAV-ChR2-eYFP expression in CaMKIIα-Cre hippocampus. **(B)** Reporter eYFP—fluorescence in the hippocampus of CaMKII-Cre:ChR2 mouse. **(C)** Schematic illustration of an experimental set up depicting the relative position of the optic fiber, drug injection, and recording electrode shank (pyr, pyramidal layer; mol, molecular layer; schaff, schaffer collateral). Scale bar = 0.5 mm, 50 μm, 5 μm. **(D,E)** Spike train with adjoining rasters demonstrating 470 nm LED light pulse (50 ms) at 1 Hz. **(F)** Sample waveform for spikes generated by optogenetic stimulation of CA1 neuron units. **(G)** Pie chart representing ISI histogram characterization of neurons based on firing properties. **(H–K)** Sample perievent histogram demonstrating rhythmicity of neuronal population during photostimulation, and when paired with SK channel modulation *in vivo*.

upregulated SK2 expression may underlie an increase in the ISI duration within the CA1 neural network (**Figures 4**, **12**).

Spontaneously evoked neural spikes recorded from the CA1 dendritic field were characterized by mean a firing rate of 30 spikes/s (**Figure 5**). As a result of GluN1 loss of function (ΔGluN1), there was a significant decrease in firing rate. This is further supported by an increased percentage of irregularly firing neurons, and a decrease in the count of bursty neuron units. To this effect, loss of GluN1 function in the hippocampus was associated with an increased irregularity of firing which was determined by the coefficient of variation (CV_2) of the ISI. Determining the regularity of firing based on CV_2 is solely dependent on the ISI and is not affected by a slight change in firing frequency. Since SK2 function impacts the ISI, the CV_2 over a time window may be representative of the effect of SK2 on firing regularity. To support this outcome, in normal

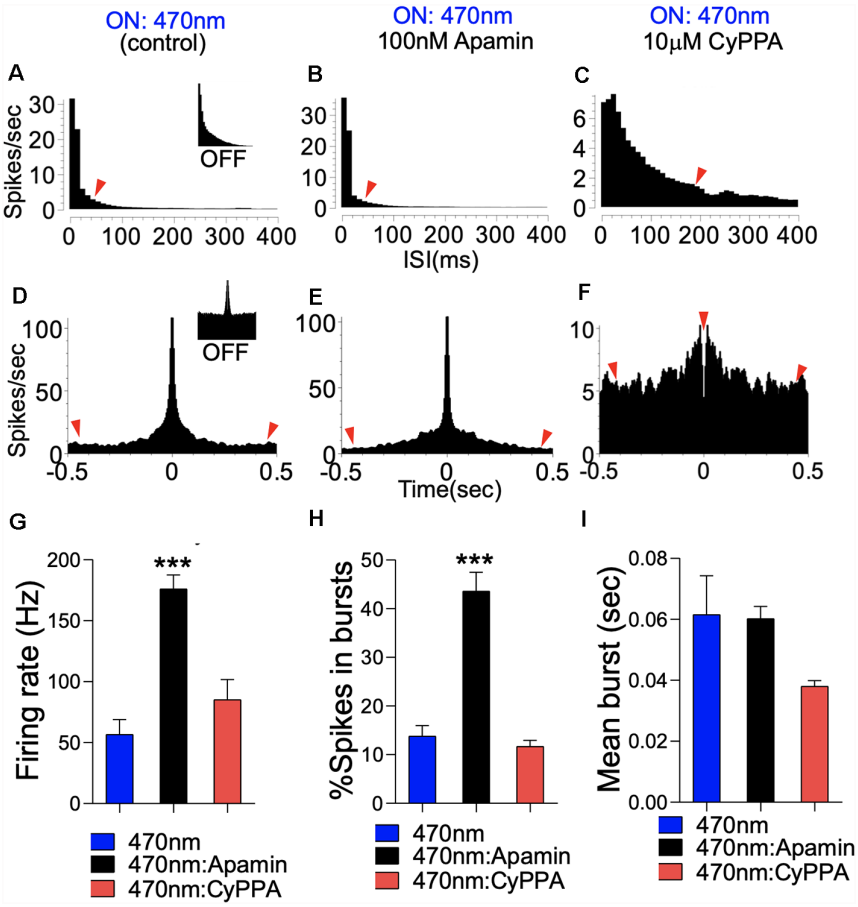

FIGURE 14 | SK modulation of burst firing in CA1 dendritic neural network. **(A)** Representative ISI histogram for a bursty CA1 neuron unit following optogenetic stimulation. Inset (Light Off). **(B)** ISI histogram illustrating a prominent increase in burst firing when photostimulation is paired with SK2 inhibition (Apamin). **(C)** ISI histogram illustrating scrambled firing pattern when photostimulation is paired with SK channel potentiation (CyPPA). **(D–F)** Autocorrelogram demonstrating a monosynaptic/pyramidal firing pattern in the CA1 neural network, and the effect of SK channel modulation. Inset (**D**; Light OFF). **(G)** Bar graph illustrating a change in firing rate. **(H)** Bar graph illustrating a change in percentage spikes in a burst. **(I)** Bar graph demonstrating the mean burst duration (**G–I**; ***$p < 0.001$).

GluN1 function (**Figure 12**), potentiation of SK2 reduced the regularity of firing while suppressing the firing rate.

In addition to an increased ISI, positive modulation of SK2 also suppressed burst and firing rates in the CA1 neural network (**Figures 12A,B**). In a typical synaptic potentiation event, high-frequency firing is dependent on NMDAR Ca^{++} transient, and CaMKIIα T286 phosphorylation at postsynaptic densities. Here, we noted that SK channel potentiation reduced the fringing rate—number of spikes per unit time (n/t)—by suppressing synaptic localization of T286 pCaMKIIα (**Figures 8**, **11**). Although GluN1 ablation led to a loss of T286 pCaMKIIα (**Figures 6D,E**), the associated upregulation of SK2 likely enhanced the suppression of T286 pCaMKIIα synaptic localization.

SK2 Regulation of Synaptic Plasticity Involves CaMKII Modulation

Our results suggest that GluN1 regulation of synaptic plasticity is dependent on a balanced activity of SK2 and CaMKII in hippocampal dendritic spines. Activation (T286 phosphorylation) of CaMKIIα promotes synaptic potentiation, and is a determinant of neuronal firing rate (n/t), and burst activity (Giese et al., 1998; Coultrap and Bayer, 2012; Coultrap et al., 2014). A coupled activation of SK2 by Ca^{++} transient determines the pattern of neural refractoriness and duration between successive spikes (ISI). Since SK2 modulate the ISI duration, it is also directly involved in the regulation of burst rates (Stackman et al., 2002, 2008; Lin et al., 2008; Maingret et al., 2008). As a result, there is a possibility of an overlap in CaMKII activity and SK2 function in LTP. Consistent with the previously described changes in dendritic spine morphology, we noted that an increase in ISI inversely correlated with both regularity of firing (**Figure 4F**) and the firing rate in the ΔGluN1 CA1 network (**Figure 5E**). Likewise, when SK2 was activated in the WT hippocampus (normal GluN1 function), both the firing rate and regularity of firing reduced significantly (**Figure 12**); similar to ΔGluN1. In addition to a decreased firing rate,

positive modulation of SK channel function led to an abrupt suppression of CaMKIIα and its T286 phosphorylation in the hippocampus (**Figure 8**). To this effect, a subsequent infusion of SK2 blocker—Apamin—increased neuronal firing rate and percentage bursty neurons when compared with the SK channel potentiation.

SK2 Modulation of Firing Rate and Neural Burst Discharge

Synaptic translocation of T286 pCaMKIIα is dependent on the stimulation frequency. Accordingly, high-frequency stimulation events facilitate a rapid synaptic T286pCaMKIIα recruitment (LTP) compared to low-frequency stimulation (Håvik et al., 2003; Coultrap and Bayer, 2012; Coultrap et al., 2014; Chang J. Y. et al., 2017). Since positive modulation of SK channel activity attenuate hippocampal T286 pCaMKIIα localization (**Figure 8**) and burst discharge rate (**Figure 12**), we ask whether SK modulation of CA1 firing properties is dependent on the stimulation state. Photostimulation of genetically encoded ChR2 in the hippocampus of mice increased burst activity and synaptic strength when the ISI histogram and autocorrelogram plots were evaluated (**Figures 13H**, **14**). Interestingly, Apamin-induced SK2 blockage further enhanced burst firing and the firing rate of CA1 neurons when compared with photostimulation only. In the absence of an external stimulus *in vivo*, spontaneously evoked CA1 firing rate and burst rate were significantly attenuated during SK channel potentiation (**Figure 12**). Likewise, when we paired photostimulation with SK channel potentiation, it significantly abolished the burst and firing rate increase associated with the photostimulation event (**Figures 14G–I**).

SUMMARY

Together, our results suggest that GluN1 modulation of spine plasticity and neuronal firing involves the co-regulation of SK2 and CaMKII. Additionally, SK2 can tune long-term synaptic plasticity by refining spine-specific localization and activity of CaMKII.

ETHICS STATEMENT

All animal handling procedures were approved by the Institutional Animal Care and Use Committee (IACUC) of the Louisiana State University (LSU) School of Veterinary Medicine (SVM).

AUTHOR CONTRIBUTIONS

OO and CL designed the experiments and prepared the manuscript. OO, AS and RS conducted the experiments and analyzed the results. OO, CL, RS and AS checked the manuscript.

FUNDING

This study was supported by Louisiana State University School of Veterinary Medicine (LSU-SVM) Corp. grant, CBS Bridging grant awarded to OO; also, NIH Grant R03 MH 104851 awarded to CL.

ACKNOWLEDGMENTS

We would like to acknowledge Dr. Karl Disseroth (Stanford University) for making the double floxed AAV-ChR2 available for our use. Dr. Susumu Tonegawa (MIT) for making the Grin1 floxed and CaMKII-Cre mice; also, Dr. Hongkui Zeng (Allen Institute for Brain Science) for making the Ai27D mouse line.

SUPPLEMENTARY MATERIAL

The Supplementary Material for this article can be found online at: https://www.frontiersin.org/articles/10.3389/fnsyn.2019.00018/full#supplementary-material.

REFERENCES

Allen, T. A., Salz, D. M., McKenzie, S., and Fortin, N. J. (2016). Nonspatial sequence coding in CA1 neurons. *J. Neurosci.* 36, 1547–1563. doi: 10.1523/JNEUROSCI.2874-15.2016

Anticevic, A., Gancsos, M., Murray, J. D., Repovs, G., Driesen, N. R., Ennis, D. J., et al. (2012). NMDA receptor function in large-scale anticorrelated neural systems with implications for cognition and schizophrenia. *Proc. Natl. Acad. Sci. U S A* 109, 16720–16725. doi: 10.1073/pnas.1208494109

Aow, J., Dore, K., and Malinow, R. (2015). Conformational signaling required for synaptic plasticity by the NMDA receptor complex. *Proc. Natl. Acad. Sci. U S A* 112, 14711–14716. doi: 10.1073/pnas.1520029112

Babiec, W. E., Jami, S. A., Guglietta, R., Chen, P. B., and O'Dell, T. J. (2017). Differential regulation of NMDA receptor-mediated transmission by SK channels underlies dorsal-ventral differences in dynamics of schaffer collateral synaptic function. *J. Neurosci.* 37, 1950–1964. doi: 10.1523/JNEUROSCI.3196-16.2017

Ballesteros-Merino, C., Martínez-Hernandez, J., Aguado, C., Watanabe, M., Adelman, J. P., and Lujan, R. (2014). Localization of SK2 channels relative to excitatory synaptic sites in the mouse developing Purkinje cells. *Front. Neuroanat.* 8:154. doi: 10.3389/fnana.2014.00154

Bosch, M., Castro, J., Saneyoshi, T., Matsuno, H., Sur, M., and Hayashi, Y. (2014). Structural and molecular remodeling of dendritic spine substructures during long-term potentiation. *Neuron* 82, 444–459. doi: 10.1016/j.neuron.2014.03.021

Bustos, F. J., Jury, N., Martinez, P., Ampuero, E., Campos, M., Abarzua, S., et al. (2017). NMDA receptor subunit composition controls dendritogenesis of hippocampal neurons through CAMKII, CREB-P, and H3K27ac. *J. Cell. Physiol.* 232, 3677–3692. doi: 10.1002/jcp.25843

Cacucci, F., Wills, T. J., Lever, C., Giese, K. P., and O'Keefe, J. (2007). Experience-dependent increase in CA1 place cell spatial information, but not spatial reproducibility, is dependent on the autophosphorylation of the α-isoform of the calcium/calmodulin-dependent protein kinase II. *J. Neurosci.* 27, 7854–7859. doi: 10.1523/JNEUROSCI.1704-07.2007

Chang, J. B., Chen, F., Yoon, Y. G., Jung, E. E., Babcock, H., Kang, J. S., et al. (2017). Iterative expansion microscopy. *Nat. Methods* 14, 593–599. doi: 10.1038/nmeth.4261

Chang, J. Y., Parra-Bueno, P., Laviv, T., Szatmari, E. M., Lee, S. R., and Yasuda, R. (2017). CaMKII autophosphorylation is necessary for optimal integration of Ca^{2+} signals during LTP induction, but not maintenance. *Neuron* 94, 800.e4–808.e4. doi: 10.1016/j.neuron.2017.04.041

Chazeau, A., and Giannone, G. (2016). Organization and dynamics of the actin cytoskeleton during dendritic spine morphological remodeling. *Cell. Mol. Life Sci.* 73, 3053–3073. doi: 10.1007/s00018-016-2214-1

Cohen, S. M., Tsien, R. W., Goff, D. C., and Halassa, M. M. (2015). The impact of NMDA receptor hypofunction on GABAergic neurons in the pathophysiology of schizophrenia. *Schizophr. Res.* 167, 98–107. doi: 10.1016/j.schres.2014.12.026

Coultrap, S. J., and Bayer, K. U. (2012). CaMKII regulation in information processing and storage. *Trends Neurosci.* 35, 607–618. doi: 10.1016/j.tins.2012.05.003

Coultrap, S. J., Freund, R. K., O'Leary, H., Sanderson, J. L., Roche, K. W., Dell'Acqua, M. L., et al. (2014). Autonomous CaMKII mediates both LTP and LTD using a mechanism for differential substrate site selection. *Cell Rep.* 6, 431–437. doi: 10.1016/j.celrep.2014.01.005

Duffney, L. J., Wei, J., Cheng, J., Liu, W., Smith, K. R., Kittler, J. T., et al. (2013). Shank3 deficiency induces NMDA receptor hypofunction via an actin-dependent mechanism. *J. Neurosci.* 33, 15767–15778. doi: 10.1523/JNEUROSCI.1175-13.2013

Forrest, M. P., Parnell, E., and Penzes, P. (2018). Dendritic structural plasticity and neuropsychiatric disease. *Nat. Rev. Neurosci.* 19, 215–234. doi: 10.1038/nrn.2018.16

Frangeul, L., Kehayas, V., Sanchez-Mut, J. V., Fièvre, S., Krishna, K. K., Pouchelon, G., et al. (2017). Input-dependent regulation of excitability controls dendritic maturation in somatosensory thalamocortical neurons. *Nat. Commun.* 8:2015. doi: 10.1038/s41467-017-02172-1

García-Negredo, G., Soto, D., Llorente, J., Morató, X., Galenkamp, K. M., Gómez-Soler, M., et al. (2014). Coassembly and coupling of SK2 channels and mGlu5 receptors. *J. Neurosci.* 34, 14793–14802. doi: 10.1523/JNEUROSCI.2038-14.2014

Giese, K. P., Fedorov, N. B., Filipkowski, R. K., and Silva, A. J. (1998). Autophosphorylation at Thr286 of the α calcium-calmodulin kinase II in LTP and learning. *Science* 279, 870–873. doi: 10.1126/science.279.5352.870

González Burgos, I., Nikonenko, I., and Korz, V. (2012). Dendritic spine plasticity and cognition. *Neural Plast.* 2012:875156. doi: 10.1155/2012/875156

Gulchina, Y., Xu, S. J., Snyder, M. A., Elefant, F., and Gao, W. J. (2017). Epigenetic mechanisms underlying NMDA receptor hypofunction in the prefrontal cortex of juvenile animals in the MAM model for schizophrenia. *J. Neurochem.* 143, 320–333. doi: 10.1111/jnc.14101

Gustin, R. M., Shonesy, B. C., Robinson, S. L., Rentz, T. J., Baucum, A. J. II., Jalan-Sakrikar, N., et al. (2011). Loss of Thr286 phosphorylation disrupts synaptic CaMKIIα targeting, NMDAR activity and behavior in pre-adolescent mice. *Mol. Cell. Neurosci.* 47, 286–292. doi: 10.1016/j.mcn.2011.05.006

Hammond, R. S., Bond, C. T., Strassmaier, T., Ngo-Anh, T. J., Adelman, J. P., Maylie, J., et al. (2006). Small-conductance Ca^{2+}-activated K^+ channel type 2 (SK2) modulates hippocampal learning, memory, and synaptic plasticity. *J. Neurosci.* 26, 1844–1853. doi: 10.1523/JNEUROSCI.4106-05.2006

Hansen, K. B., Ogden, K. K., Yuan, H., and Traynelis, S. F. (2014). Distinct functional and pharmacological properties of Triheteromeric GluN1/GluN2A/GluN2B NMDA receptors. *Neuron* 81, 1084–1096. doi: 10.1016/j.neuron.2014.01.035

Hatton, C. J., and Paoletti, P. (2005). Modulation of triheteromeric NMDA receptors by N-terminal domain ligands. *Neuron* 46, 261–274. doi: 10.1016/j.neuron.2005.03.005

Håvik, B., Røkke, H., Bårdsen, K., Davanger, S., and Bramham, C. R. (2003). Bursts of high-frequency stimulation trigger rapid delivery of pre-existing alpha-CaMKII mRNA to synapses: a mechanism in dendritic protein synthesis during long-term potentiation in adult awake rats. *Eur. J. Neurosci.* 17, 2679–2689.doi: 10.1046/j.1460-9568.2003.02712.x

Hell, J. W. (2014). CaMKII: claiming center stage in postsynaptic function and organization. *Neuron* 81, 249–265. doi: 10.1016/j.neuron.2013.12.024

Hlushchenko, I., Koskinen, M., and Hotulainen, P. (2016). Dendritic spine actin dynamics in neuronal maturation and synaptic plasticity. *Cytoskeleton* 73, 435–441. doi: 10.1002/cm.21280

Huang, Z., and Gibb, A. J. (2014). Mg^{2+} block properties of triheteromeric GluN1-GluN2B-GluN2D NMDA receptors on neonatal rat substantia nigra pars compacta dopaminergic neurones. *J. Physiol.* 592, 2059–2078. doi: 10.1113/jphysiol.2013.267864

Jalan-Sakrikar, N., Bartlett, R. K., Baucum, A. J. II., and Colbran, R. J. (2012). Substrate-selective and calcium-independent activation of CaMKII by α-actinin. *J. Biol. Chem.* 287, 15275–15283. doi: 10.1074/jbc.m112.351817

Jauregui, E., Du, L., Gleason, C., and Poovaiah, B. W. (2017). Autophosphorylation of calcium/calmodulin-dependent protein kinase (CCaMK) at S343 or S344 generates an intramolecular interaction blocking the CaM-binding. *Plant Signal. Behav.* 12:e1343779. doi: 10.1080/15592324.2017.1343779

Kaidanovich-Beilin, O., Lipina, T., Vukobradovic, I., Roder, J., and Woodgett, J. R. (2011). Assessment of social interaction behaviors. *J. Vis. Exp.* 48:2473. doi: 10.3791/2473

Kasumu, A. W., Hougaard, C., Rode, F., Jacobsen, T. A., Sabatier, J. M., Eriksen, B. L., et al. (2012). Selective positive modulator of calcium-activated potassium channels exerts beneficial effects in a mouse model of spinocerebellar ataxia type 2. *Chem. Biol.* 19, 1340–1353. doi: 10.1016/j.chembiol.2012.07.013

Khan, S., Conte, I., Carter, T., Bayer, K. U., and Molloy, J. E. (2016). Multiple CaMKII binding modes to the actin cytoskeleton revealed by single-molecule imaging. *Biophys. J.* 111, 395–408. doi: 10.1016/j.bpj.2016.06.007

Kim, J., and Hoffman, D. A. (2008). Potassium channels: newly found players in synaptic plasticity. *Neuroscientist* 14, 276–286.doi: 10.1177/1073858408315041

Kuiper, E. F., Nelemans, A., Luiten, P., Nijholt, I., Dolga, A., and Eisel, U. (2012). $K_{Ca}2$ and $k_{ca}3$ channels in learning and memory processes and neurodegeneration. *Front. Pharmacol.* 3:107. doi: 10.3389/fphar.2012.00107

Lai, K. O., and Ip, N. Y. (2013). Structural plasticity of dendritic spines: the underlying mechanisms and its dysregulation in brain disorders. *Biochim. Biophys. Acta* 1832, 2257–2263. doi: 10.1016/j.bbadis.2013.08.012

Lee, C. H., and MacKinnon, R. (2018). Activation mechanism of a human SK-calmodulin channel complex elucidated by cryo-EM structures. *Science* 360, 508–513. doi: 10.1126/science.aas9466

Lee, W. S., Ngo-Anh, T. J., Bruening-Wright, A., Maylie, J., and Adelman, J. P. (2003). Small conductance Ca^{2+}-activated K^+ channels and calmodulin: cell surface expression and gating. *J. Biol. Chem.* 278, 25940–25946. doi: 10.1074/jbc.M302091200

Li, B. S., Sun, M. K., Zhang, L., Takahashi, S., Ma, W., Vinade, L., et al. (2001). Regulation of NMDA receptors by cyclin-dependent kinase-5. *Proc. Natl. Acad. Sci. U S A* 98, 12742–12747. doi: 10.1073/pnas.211428098

Li, D. P., Zhou, J. J., Zhang, J., and Pan, H. L. (2017). CaMKII regulates synaptic NMDA receptor activity of hypothalamic presympathetic neurons and sympathetic outflow in hypertension. *J. Neurosci.* 37, 10690–10699. doi: 10.1523/JNEUROSCI.2141-17.2017

Lin, M. T., Lujan, R., Watanabe, M., Adelman, J. P., and Maylie, J. (2008). SK2 channel plasticity contributes to LTP at Schaffer collateral-CA1 synapses. *Nat. Neurosci.* 11, 170–177. doi: 10.1038/nn2041

Lisman, J., Schulman, H., and Cline, H. (2002). The molecular basis of CaMKII function in synaptic and behavioural memory. *Nat. Rev. Neurosci.* 3, 175–190. doi: 10.1038/nrn753

Lisman, J., Yasuda, R., and Raghavachari, S. (2012). Mechanisms of CaMKII action in long-term potentiation. *Nat. Rev. Neurosci.* 13, 169–182. doi: 10.1038/nrn3192

Ma, J., Duan, Y., Qin, Z., Wang, J., Liu, W., Xu, M., et al. (2015). Overexpression of αCaMKII impairs behavioral flexibility and NMDAR-dependent long-term depression in the medial prefrontal cortex. *Neuroscience* 310, 528–540. doi: 10.1016/j.neuroscience.2015.09.051

Maingret, F., Coste, B., Hao, J., Giamarchi, A., Allen, D., Crest, M., et al. (2008). Neurotransmitter modulation of small-conductance Ca^{2+}-activated K^+ channels by regulation of Ca^{2+} gating. *Neuron* 59, 439–449. doi: 10.1016/j.neuron.2008.05.026

Maylie, J., Bond, C. T., Herson, P. S., Lee, W. S., and Adelman, J. P. (2004). Small conductance Ca^{2+}-activated K^+ channels and calmodulin. *J. Physiol.* 554, 255–261. doi: 10.1113/jphysiol.2003.049072

Lee, C. H., and MacKinnon, R. (2018). Activation mechanism of a human SK-calmodulin channel complex elucidated by cryo-EM structures. *Science* 360, 508–513. doi: 10.1126/science.aas9466

Nakahata, Y., and Yasuda, R. (2018). Plasticity of spine structure: local signaling, translation and cytoskeletal reorganization. *Front. Synaptic Neurosci.* 10:29. doi: 10.3389/fnsyn.2018.00029

Nakazawa, K., Jeevakumar, V., and Nakao, K. (2017). Spatial and temporal boundaries of NMDA receptor hypofunction leading to schizophrenia. *NPJ Schizophr.* 3:7. doi: 10.1038/s41537-016-0003-3

Namba, T., Ming, G. L., Song, H., Waga, C., Enomoto, A., Kaibuchi, K., et al. (2011). NMDA receptor regulates migration of newly generated neurons in the adult hippocampus via Disrupted-In-Schizophrenia 1 (DISC1). *J. Neurochem.* 118, 34–44. doi: 10.1111/j.1471-4159.2011.07282.x

Ngo-Anh, T. J. (2006). *Functional Roles of SK2 Channels in Area CA1 of the Hippocampus.* Ph.D. Thesis, Oregon State University.

Ngo-Anh, T. J., Bloodgood, B. L., Lin, M., Sabatini, B. L., Maylie, J., and Adelman, J. P. (2005). SK channels and NMDA receptors form a Ca^{2+}-mediated feedback loop in dendritic spines. *Nat. Neurosci.* 8, 642–649. doi: 10.1038/nn1449

Ogundele, O. M., and Lee, C. C. (2018). CaMKIIα expression in a mouse model of NMDAR hypofunction schizophrenia: putative roles for IGF-1R and TLR4. *Brain Res. Bull.* 137, 53–70. doi: 10.1016/j.brainresbull.2017.11.007

Ohtsuki, G., Piochon, C., Adelman, J. P., and Hansel, C. (2012). SK2 channel modulation contributes to compartment-specific dendritic plasticity in cerebellar Purkinje cells. *Neuron* 75, 108–120. doi: 10.1016/j.neuron.2012.05.025

Penny, C. J., and Gold, M. G. (2018). Mechanisms for localising calcineurin and CaMKII in dendritic spines. *Cell. Signal.* 49, 46–58. doi: 10.1016/j.cellsig.2018.05.010

Prescott, S. A., and Sejnowski, T. J. (2008). Spike-rate coding and spike-time coding are affected oppositely by different adaptation mechanisms. *J. Neurosci.* 28, 13649–13661. doi: 10.1523/JNEUROSCI.1792-08.2008

Ramsey, A. J., Milenkovic, M., Oliveira, A. F., Escobedo-Lozoya, Y., Seshadri, S., Salahpour, A., et al. (2011). Impaired NMDA receptor transmission alters striatal synapses and DISC1 protein in an age-dependent manner. *Proc. Natl. Acad. Sci. U S A* 108, 5795–5800. doi: 10.1073/pnas.1012621108

Ratnadurai-Giridharan, S., Stefanescu, R. A., Khargonekar, P. P., Carney, P. R., and Talathi, S. S. (2014). Genesis of interictal spikes in the CA1: a computational investigation. *Front. Neural Circuits* 8:2. doi: 10.3389/fncir.2014.00002

Rebollo, B., Perez-Zabalza, M., Ruiz-Mejias, M., Perez-Mendez, L., and Sanchez-Vives, M. V. (2018). β and γ oscillations in prefrontal cortex during NMDA hypofunction: an *in vitro* model of schizophrenia features. *Neuroscience* 383, 138–149. doi: 10.1016/j.neuroscience.2018.04.035

Robison, A. J., Bass, M. A., Jiao, Y., MacMillan, L. B., Carmody, L. C., Bartlett, R. K., et al. (2005). Multivalent interactions of calcium/calmodulin-dependent protein kinase II with the postsynaptic density proteins NR2B, densin-180 and α-actinin-2. *J. Biol. Chem.* 280, 35329–35336. doi: 10.1074/jbc.M502191200

Salter, M. W., and Kalia, L. V. (2004). Src kinases: a hub for NMDA receptor regulation. *Nat. Rev. Neurosci.* 5, 317–328. doi: 10.1038/nrn1368

Sanderson, J. L., Gorski, J. A., and Dell'Acqua, M. L. (2016). NMDA receptor-dependent LTD requires transient synaptic incorporation of Ca^{2+}-permeable AMPARs mediated by AKAP150-anchored PKA and calcineurin. *Neuron* 89, 1000–1015. doi: 10.1016/j.neuron.2016.01.043

Seillier, A., and Giuffrida, A. (2009). Evaluation of NMDA receptor models of schizophrenia: divergences in the behavioral effects of sub-chronic PCP and MK-801. *Behav. Brain Res.* 204, 410–415. doi: 10.1016/j.bbr.2009.02.007

Shen, K., Teruel, M. N., Subramanian, K., and Meyer, T. (1998). CaMKIIβ functions as an F-actin targeting module that localizes CaMKIIα/β heterooligomers to dendritic spines. *Neuron* 21, 593–606. doi: 10.1016/s0896-6273(00)80569-3

Snyder, M. A., and Gao, W. J. (2013). NMDA hypofunction as a convergence point for progression and symptoms of schizophrenia. *Front. Cell. Neurosci.* 7:31. doi: 10.3389/fncel.2013.00031

Stackman, R. W. Jr., Bond, C. T., and Adelman, J. P. (2008). Contextual memory deficits observed in mice overexpressing small conductance Ca^{2+}-activated K^+ type 2 (KCa2.2, SK2) channels are caused by an encoding deficit. *Learn. Mem.* 15, 208–213. doi: 10.1101/lm.906808

Stackman, R. W., Hammond, R. S., Linardatos, E., Gerlach, A., Maylie, J., Adelman, J. P., et al. (2002). Small conductance Ca^{2+}-activated K^+ channels modulate synaptic plasticity and memory encoding. *J. Neurosci.* 22, 10163–10171. doi: 10.1523/jneurosci.22-23-10163.2002

Stein, I. S., Gray, J. A., and Zito, K. (2015). Non-ionotropic NMDA receptor signaling drives activity-induced dendritic spine shrinkage. *J. Neurosci.* 35, 12303–12308. doi: 10.1523/jneurosci.4289-14.2015

Swiatkowski, P., Nikolaeva, I., Kumar, G., Zucco, A., Akum, B. F., Patel, M. V., et al. (2017). Role of Akt-independent mTORC1 and GSK3β signaling in sublethal NMDA-induced injury and the recovery of neuronal electrophysiology and survival. *Sci. Rep.* 7:1539. doi: 10.1038/s41598-017-01826-w

Takei, Y., Kikkawa, Y. S., Atapour, N., Hensch, T. K., and Hirokawa, N. (2015). Defects in synaptic plasticity, reduced NMDA-receptor transport and instability of postsynaptic density proteins in mice lacking microtubule-associated protein 1A. *J. Neurosci.* 35, 15539–15554. doi: 10.1523/jneurosci.2671-15.2015

Tillberg, P. W., Chen, F., Piatkevich, K. D., Zhao, Y., Yu, C. C., English, B. P., et al. (2016). Protein-retention expansion microscopy of cells and tissues labeled using standard fluorescent proteins and antibodies. *Nat. Biotechnol.* 34, 987–992. doi: 10.1038/nbt.3625

Toporikova, N., and Chacron, M. J. (2009). SK channels gate information processing *in vivo* by regulating an intrinsic bursting mechanism seen *in vitro*. *J. Neurophysiol.* 102, 2273–2287. doi: 10.1152/jn.00282.2009

Tovar, K. R., McGinley, M. J., and Westbrook, G. L. (2013). Triheteromeric NMDA receptors at hippocampal synapses. *J. Neurosci.* 33, 9150–9160. doi: 10.1523/jneurosci.0829-13.2013

Trimmer, J. S. (2015). Subcellular localization of K^+ channels in mammalian brain neurons: remarkable precision in the midst of extraordinary complexity. *Neuron* 85, 238–256. doi: 10.1016/j.neuron.2014.12.042

Uchino, S., Hirasawa, T., Tabata, H., Gonda, Y., Waga, C., Ondo, Y., et al. (2010). Inhibition of N-methyl-D-aspartate receptor activity resulted in aberrant neuronal migration caused by delayed morphological development in the mouse neocortex. *Neuroscience* 169, 609–618. doi: 10.1016/j.neuroscience.2010.05.024

Wang, J., Lu, W., Chen, L., Zhang, P., Qian, T., Cao, W., et al. (2016). Serine 707 of APPL1 is critical for the synaptic NMDA receptor-mediated Akt phosphorylation signaling pathway. *Neurosci. Bull.* 32, 323–330. doi: 10.1007/s12264-016-0042-9

Wesseling, H., Guest, P. C., Lee, C. M., Wong, E. H., Rahmoune, H., and Bahn, S. (2014). Integrative proteomic analysis of the NMDA NR1 knockdown mouse model reveals effects on central and peripheral pathways associated with schizophrenia and autism spectrum disorders. *Mol. Autism* 5:38. doi: 10.1186/2040-2392-5-38

Winnubst, J., Cheyne, J. E., Niculescu, D., and Lohmann, C. (2015). Spontaneous activity drives local synaptic plasticity *in vivo*. *Neuron* 87, 399–410. doi: 10.1016/j.neuron.2015.06.029

Xia, Z., Dudek, H., Miranti, C. K., and Greenberg, M. E. (1996). Calcium influx via the NMDA receptor induces immediate early gene transcription by a MAP kinase/ERK-dependent mechanism. *J. Neurosci.* 16, 5425–5436. doi: 10.1523/jneurosci.16-17-05425.1996

Xia, X. M., Fakler, B., Rivard, A., Wayman, G., Johnson-Pais, T., Keen, J. E., et al. (1998). Mechanism of calcium gating in small-conductance calcium-activated potassium channels. *Nature* 395, 503–507. doi: 10.1038/26758

Yao, W. D., and Wu, C. F. (2001). Distinct roles of CaMKII and PKA in regulation of firing patterns and K^+ currents in Drosophila neurons. *J. Neurophysiol.* 85, 1384–1394. doi: 10.1152/jn.2001.85.4.1384

Yao, L., and Zhou, Q. (2017). Enhancing NMDA receptor function: recent progress on allosteric modulators. *Neural Plast.* 2017:2875904. doi: 10.1155/2017/2875904

Yi, F., Traynelis, S. F., and Hansen, K. B. (2017). Selective cell-surface expression of triheteromeric NMDA receptors. *Methods Mol. Biol.* 1677, 145–162. doi: 10.1007/978-1-4939-7321-7_7

Yoshii, A., and Constantine-Paton, M. (2007). BDNF induces transport of PSD-95 to dendrites through PI3K-AKT signaling after NMDA receptor activation. *Nat. Neurosci.* 10, 702–711. doi: 10.1038/nn1903

Zhou, Y., Kaiser, T., Monteiro, P., Zhang, X., Van der Goes, M. S., Wang, D., et al. (2016). Mice with Shank3 mutations associated with ASD and schizophrenia display both shared and distinct defects. *Neuron* 89, 147–162. doi: 10.1016/j.neuron.2015.11.023

Conflict of Interest: The authors declare that the research was conducted in the absence of any commercial or financial relationships that could be construed as a potential conflict of interest.

frontiers in Synaptic Neuroscience

ORIGINAL RESEARCH
published: 17 March 2020
doi: 10.3389/fnsyn.2020.00010

Astrocytic Ephrin-B1 Controls Synapse Formation in the Hippocampus During Learning and Memory

Amanda Q. Nguyen[1,2†], Jordan Koeppen[1,3†], Simone Woodruff[1], Karen Mina[1], Zoe Figueroa[1] and Iryna M. Ethell[1,2,3]*

[1] Division of Biomedical Sciences, University of California Riverside School of Medicine, Riverside, CA, United States, [2] Neuroscience Graduate Program, University of California, Riverside, Riverside, CA, United States, [3] Cell, Molecular, and Developmental Biology Graduate Program, University of California, Riverside, Riverside, CA, United States

Astrocytes play a fundamental role in synapse formation, pruning, and plasticity, which are associated with learning and memory. However, the role of astrocytes in learning and memory is still largely unknown. Our previous study showed that astrocyte-specific ephrin-B1 knock-out (KO) enhanced but ephrin-B1 overexpression (OE) in hippocampal astrocytes impaired contextual memory recall following fear conditioning. The goal of this study was to understand the mechanism by which astrocytic ephrin-B1 influences learning; specifically, learning-induced remodeling of synapses and dendritic spines in CA1 hippocampus using fear-conditioning paradigm. While we found a higher dendritic spine density and clustering on c-Fos-positive (+) neurons activated during contextual memory recall in both wild-type (WT) and KO mice, overall spine density and mEPSC amplitude were increased in CA1 neurons of KO compared to WT. In contrast, ephrin-B1 OE in hippocampal astrocytes impaired dendritic spine formation and clustering, specifically on c-Fos(+) neurons, coinciding with an overall decrease in vGlut1/PSD95 co-localization. Although astrocytic ephrin-B1 influenced learning-induced spine formation, the changes in astrocytic ephrin-B1 levels did not affect spine enlargement as no genotype differences in spine volume were observed between trained WT, KO, and OE groups. Our results suggest that a reduced formation of new spines rather than spine maturation in activated CA1 hippocampal neurons is most likely responsible for impaired contextual learning in OE mice due to abundantly high ephrin-B1 levels in astrocytes. The ability of astrocytic ephrin-B1 to negatively influence new spine formation during learning can potentially regulate new synapse formation at specific dendritic domains and underlie memory encoding.

Keywords: astrocyte, ephrin-B1, contextual memory, hippocampus, synapse, dendritic spine

OPEN ACCESS

Edited by:
Carlo Sala,
Institute of Neuroscience (CNR), Italy

Reviewed by:
Silvia Bassani,
Institute of Neuroscience (CNR), Italy
Michael J. Schmeisser,
Johannes Gutenberg University Mainz, Germany

****Correspondence:***
Iryna M. Ethell
iryna.ethell@medsch.ucr.edu;
iryna.ethell@ucr.edu

† These authors have contributed equally to this work

Received: *11 December 2019*
Accepted: *24 February 2020*
Published: *17 March 2020*

Citation:
Nguyen AQ, Koeppen J, Woodruff S, Mina K, Figueroa Z and Ethell IM (2020) Astrocytic Ephrin-B1 Controls Synapse Formation in the Hippocampus During Learning and Memory. Front. Synaptic Neurosci. 12:10. doi: 10.3389/fnsyn.2020.00010

INTRODUCTION

Hippocampal circuits are known for their plastic nature and play an important role in the formation of new memories and life-long learning (Milner et al., 1998; Neves et al., 2008). Contextual fear learning and retrieval relies on the hippocampus, particularly the CA1 region. This hippocampal-dependent learning requires activation of CA1 pyramidal neurons (Strekalova et al., 2003; Goshen et al., 2011), and promotes the growth and maturation of hippocampal synapses. Indeed,

maturation of dendritic spines has been shown to be activity dependent, allowing for the recruitment of AMPARs and an increase in spine volume (Matsuo et al., 2008). In addition to promoting synapse maturation, experience has also been shown to modify hippocampal circuits through selective formation or removal of synapses (Lichtman and Colman, 2000; Draft and Lichtman, 2009; Holtmaat and Svoboda, 2009; Sala and Segal, 2014; Segal, 2017). Therefore, experience and learning can profoundly impact spine turnover rates (Yang et al., 2008; Holtmaat and Svoboda, 2009; Fu et al., 2012; Lai et al., 2012; Sala and Segal, 2014; Segal, 2017). Additionally, learning-induced spine changes are associated with selective spine clustering and formation of "hot spots" on dendrites (Fu et al., 2012; Frank et al., 2018; Lai et al., 2018), which are suggested to allow for efficient storage of information (Hayashi-Takagi et al., 2015; Frank et al., 2018). Most research has focused on neuron–neuron interactions; however, little is known about astrocyte-derived signals that regulate the synaptic remodeling during learning and memory.

Astrocytes play a critical role in maintaining, supporting, and directly modulating neuronal activity and function. Astrocytic processes encapsulate synapses allowing for astrocytes to communicate with neurons. The interactions between astrocytes and synapses can regulate synaptogenesis and pruning, synaptic transmission, and plasticity (Araque et al., 1999; Clarke and Barres, 2013; Chung et al., 2015; Allen and Eroglu, 2017). As these synaptic changes underlie the acquisition, retention, and retrieval of memory, astrocytes are well positioned to influence learning and memory (Nishiyama et al., 2002; Newman et al., 2011; Suzuki et al., 2011; Tadi et al., 2015; Gao et al., 2016; Adamsky et al., 2018). Activation of hippocampal astrocytes was recently suggested to enhance synaptic potentiation and acquisition of contextual fear memory (Adamsky et al., 2018). Astrocytes are also shown to regulate synapse formation, recruitment of AMPARs, and modulating synaptic functions through the release of gliotransmitters, such as glutamate (Fellin et al., 2004), thrombospondin (Christopherson et al., 2005), glypican (Allen et al., 2012), D-serine (Henneberger et al., 2010), and lactate (Alberini et al., 2018). Besides gliotransmission, astrocytes can communicate and affect synaptic functions through contact-mediated factors. Astrocytic contacts with neurons can direct synaptogenesis (Hama et al., 2004; Garrett and Weiner, 2009) and synapse elimination (Chung et al., 2013), which may allow for the refinement of memories.

Trans-synaptic Eph/ephrin-B interactions promote postsynaptic dendritic spine formation and maturation during development (Henderson et al., 2001; Henkemeyer et al., 2003; Kayser et al., 2006) and high levels of EphB receptors and ephrins are retained in the adult hippocampus (Grunwald et al., 2001; Liebl et al., 2003). Furthermore, the loss of EphA4 and EphB2 receptors are reported to affect associative memory in mice (Gerlai et al., 1999; Halladay et al., 2004; Willi et al., 2012; Dines et al., 2015). Interestingly, EphB2 loss affects both short and long-term contextual fear conditioning memory formation, but only long-term memory depends on EphB2 forward signaling (Dines et al., 2015). Disruption of ephrin-B reverse signaling in neurons was also implicated in impaired hippocampal-dependent learning and memory in EphB2 KO mice (Grunwald et al., 2001). In addition, ephrin-B2 expression is upregulated in CA1 neurons but not the cortex or amygdala following fear conditioning without changes in levels of EphA4 receptor (Trabalza et al., 2012). While ephrin-B2 can activate both EphA4 and EphB receptors, ephrin-B1 is known for its high affinity for EphB but not EphA4 receptors. Deletion of neuronal ephrin-B1 was also responsible for impaired contextual recall in ephrin-B1 KO mice following fear conditioning (Arvanitis et al., 2014). Mutations in the *efnb1 gene* that encodes ephrin-B1 are associated with CranioFrontalNasal Syndrome, characterized by hypertelorism, frontonasal dysplasia, coronal craniosynostosis, and mild learning disability (Twigg et al., 2004; Wieland et al., 2004). However, little is known about the role of astrocytic ephrin-B1. We previously reported that deletion and overexpression (OE) of astrocytic ephrin-B1 in the adult CA1 hippocampus affects contextual memory (Koeppen et al., 2018), but the mechanism is still not clear.

Our new findings suggest that astrocytic ephrin-B1 influences hippocampal-dependent contextual memory by regulating new dendritic spine formation and clustering on hippocampal neurons activated during memory recall, without affecting spine maturation. While we found that both wild-type (WT) and astrocytic ephrin-B1 knock-out (KO) mice showed a significant increase in dendritic spine density and clustering on activated c-Fos(+) neurons compared to c-Fos(-) neurons following contextual recall, dendritic spine density remained higher in trained KO compared to WT, which coincided with a greater vGlut1/PSD95 co-localization and enhanced excitatory postsynaptic currents (EPSCs) in CA1 neurons of KO mice. In contrast, astrocytic ephrin-B1 overexpressing (OE) mice showed no increase in dendritic spine density and clustering on c-Fos(+) neurons compared to c-Fos(-) neurons, which coincided with an overall decrease in vGlut1/PSD95 co-localization. However, changes of ephrin-B1 levels in astrocytes did not affect spine enlargement, as no genotype differences in spine volume were observed between trained WT, KO, and OE groups. Our results suggest that the deficits in dendritic spine formation and clustering, but not spine maturation, may underlie impaired contextual memory recall in OE mice. These studies implicate astrocytic ephrin-B1 as a negative regulator of synapse formation in the activated hippocampal neurons during learning, which can influence contextual memory. Future studies will determine whether activity-dependent up-regulation or down-regulation of ephrin-B1 levels in selective astrocytes controls addition or removal of synapses on specific neurons or dendrites, which may potentially underlie memory encoding.

MATERIALS AND METHODS

Mice

All animal care protocols and procedures were approved by the UC Riverside Animal Care & Use Program and done according to NIH and Institutional Animal Care and Use Committee guidelines; animal welfare assurance number A3439-01 is on file with the Office of Laboratory Animal

Welfare (OLAW). Mice were maintained in an AAALAC accredited facility under 12-h light/dark cycle and fed standard mouse chow. ERT2-Cre^{GFAP} male mice (B6.Cg-Tg(*GFAP*-cre/ERT2)505Fmv/J, RRID: IMSR_JAX:012849) were crossed with *ephrin-B1*$^{flox/+}$ female mice (129S-*Efnb1*^{tm1Sor}/J, RRID: IMSR_JAX:007664) to obtain ERT2-Cre^{GFAP}*ephrin-B1*$^{flox/y}$ (KO) or ERT2-Cre^{GFAP}*ephrin-B1*$^{+/y}$ (WT) male mice. Postnatal day (P) 70–90 adult WT and KO littermates received intraperitoneal (IP) injection of tamoxifen (TAM) (1 mg in 5 mg/ml of 1:9 ethanol/sunflower seed oil solution) once a day for 7 consecutive days. There were no detectable changes in ephrin-B1 levels in astrocytes or neurons of TAM-injected WT mice (not shown). In TAM-treated KO mice, ephrin-B1 immunoreactivity was observed only in neuronal cell bodies and dendrites of the CA1 hippocampus, but was significantly reduced in hippocampal astrocytes as previously reported (Nikolakopoulou et al., 2016; Koeppen et al., 2018). Genotypes were confirmed by PCR analysis of genomic DNA isolated from mouse tails.

Stereotaxic Microinjections

Expression of ephrin-B1 and tdTomato was induced in hippocampal astrocytes via adeno-associated viruses (AAV7) containing *AAV7.GfaABC1D.ephrin-B1.SV40* [AAV-ephrin-B1; viral titer at 7.56×10^{12} viral particles (VP)/ml] or *AAV7.GfaABC1D.tdTomato.SV40* (AAV-tdTomato; viral titer at 4.46×10^{12} VP/ml), respectively (both obtained from UPenn Vector Core[1]). VP were concentrated with Amicon ultra-0.5 centrifugal filter (UFC505024, Sigma-Aldrich), which was pretreated with 0.1% Pluronic F-68 non-ionic surfactant (24040032, Thermo Fisher). Mice were anesthetized with IP injections of ketamine/xylazine mix (80 mg/kg ketamine and 10 mg/kg xylazine). To ensure for adequate anesthesia, paw pad pinch test, respiratory rhythm, righting reflex, and/or loss of corneal reflex were assessed. Adult P70-90 Thy1-EGFP mice (RRID: IMSR_JAX: 007788) received craniotomies (1 mm in diameter) and VPs were stereotaxic injected into the dorsal hippocampus (2.5 mm posterior to bregma, 1.0 mm lateral to midline, and 1.2 mm from the pial surface). Control mice were bilaterally injected with 2 µl of 1.16×10^{13} VP/ml AAV-tdTomato, and experimental animals received bilateral injection of 1 µl of 3.78×10^{13} VP/ml AAV-ephrin-B1 + 1 µl of 2.32×10^{13} VP/ml AAV-tdTomato. Post-surgery, mice received 0.3 ml of buprenorphine by subcutaneous injection every 8 h for 48 h, as needed for pain. Animals were allowed to recover for 14 days prior to fear conditioning tests and/or immunohistochemistry. There was a significant four-fold increase in ephrin-B1 immunoreactivity in CA1 hippocampal astrocytes of mice injected with AAV-ephrin-B1 + tdTomato (OE) compared to AAV-tdTomato (WT) as previously reported (Koeppen et al., 2018). Mice showing bilateral hippocampal tdTomato expression were used for the analysis.

Fear Conditioning Test

A fear-conditioning paradigm was used to assess hippocampal dependent contextual learning as previously described (Anagnostaras et al., 2001; Koeppen et al., 2018). Two contexts were used to test contextual memory. Context A was an 18 × 18 cm rectangular clear plexiglass box with 16-grated steel bar flooring; trials in context A were in white light and the scent of Quatricide TB. Context B was in a cylinder with a diameter of 15 cm and a height of 20 cm and checkered black and white walls; trials in context B were in altered light with fresh litter and the scent of Windex. Animals were allowed to acclimate in the behavioral room for 30 min before each testing day and handled for 2 min for 5 days prior to testing. On day 1, the test mouse was placed in context A and habituated to the chamber for 10 min, 1 h after context A mice were habituated to context B for 10 min. The mouse was removed and separated from its home cage until all mice in that cage were habituated to both contexts. On day 2, test mice were trained to associate an unconditioned stimulus (US; 0.6 mA scrambled foot shock) with a conditioned stimulus (CS; 9 kHz, 70 dB tone) in context A. Initially, test mice were placed in context A and given 3 min for habituation, then followed by a 30 s tone (CS), which co-terminated with a 2 s foot shock (US). The CS–US pairing occurred five times, with a pseudorandom interval between pairings. The test mouse, again, was removed and separated from its home cage until all mice in that cage were trained. On day 3, animals were tested for their associated memory of the context (in context A) and of the CS tone (in context B). For contextual recall, mice were placed in context A for 5 min with no sound and returned to home cage for 1 h before testing context B. For tone recall test, mice were placed in context B for a total of 6 min, with the CS tone playing for the final 3 min. Control mice were taken directly from their home cage in the vivarium and immediately perfused and did not undergo the fear conditioning paradigm. For dendritic spine analysis and immunohistochemistry, three to four animals were euthanized and perfused 1 h after context A contextual recall only. Animals undergoing both context A and context B recall were euthanized and perfused 1 h after context B tone recall. Freezing behavior was measured as a percentage of time freezing using TopScan Software. GraphPad Prism 6 software (RRID: SCR_002798) was used to perform a one-way ANOVA followed by Tukey's *post hoc* analysis or *t*-test when appropriate, data represent mean ± SEM.

Immunohistochemistry

Animals were anesthetized with isoflurane and transcardially perfused first with 0.9% NaCl, followed by fixation with 4% paraformaldehyde (PFA) in 0.1 M phosphate-buffered saline (PBS), pH 7.4. Brains were post-fixed overnight with 4% PFA in 0.1 M PBS and sectioned into 100 µm coronal slices with a vibratome. Excitatory presynaptic boutons were labeled by immunostaining against vesicular glutamate transporter 1 (vGlut1) using rabbit anti-vGlut1 antibody (0.25 mg/ml, Invitrogen Cat# 482400, RRID: AB_2533843), postsynaptic sites were identified with mouse anti-postsynaptic density-95 (PSD95) antibody (1.65 µg/ml, Invitrogen Cat# MA1-045, RRID: AB_325399). Inhibitory sites were detected with mouse anti-glutamic acid decarboxylase 65 (GAD65) antibody (10 µg/ml, BD Pharmingen Cat# 559931, RRID:

[1]http://www.med.upenn.edu/gtp/vectorcore

AB_397380). Parvalbumin (PV)-positive cells were identified with mouse anti-PV antibody (6 μg/ml, Sigma-Aldrich Cat# P3088, RRID: AB 477329). Activated neurons were detected with anti-c-Fos antibodies (40 μg/ml, Invitrogen Cat# PA1-37437, RRID: AB_1073599). The secondary antibodies used were Alexa Fluor 594-conjugated donkey anti-mouse IgG (4 mg/ml, Molecular Probes Cat# A-21203, RRID: AB_141633), Alexa Fluor 647-conjugated donkey anti-rabbit IgG (4 mg/ml, Molecular Probes Cat# A-31573, RRID: AB_2536183), Alexa Fluor 647-conjugated donkey anti-goat IgG (4 mg/ml, Molecular Probes Cat# A-21447, RRID: AB_141844), or Alexa Fluor 488-conjugated donkey anti-goat IgG (4 mg/ml, Molecular Probes Cat# A-11055, RRID: AB_2534102). Sections were mounted on slides with Vectashield mounting medium containing DAPI (Vector Laboratories Inc. Cat# H-1200, RRID: AB_2336790).

Confocal Imaging and Analysis

Confocal images of the stratum radiatum (SR) and stratum lacunosum-moleculare (SLM) layers of dorsal CA1 hippocampus were taken with a Leica SP2 and LSM 880 Airyscan Carl Zeiss confocal laser-scanning microscope. A series of high-resolution optical sections (1,024 × 1,024-pixel format) were captured with a 20× or 63× water-immersion objective (1.2 numerical aperture) and 1× zoom at 1-μm step intervals (*z*-stack of 10 optical sections). All images were acquired under identical conditions. For the analysis of vGlut1, GAD65, PSD95, and PV immunolabeling, at least six sequential images were captured for a selected area at 1-μm step intervals; each image in the series was threshold-adjusted to identical levels (0–160 intensity), and puncta (0.5–10 μm^2) were measured using ImageJ software (RRID: nif-0000-30467). Three adjacent areas from SR and SLM were imaged and analyzed per each hippocampus from at least three animals/group. Colocalization of vGlut1/PSD95 and vGlut1/PV was analyzed using ImageJ plugin for colocalization.[2] Statistical analysis was performed with one-way ANOVA followed by Tukey's *post hoc* analysis or *t*-test when appropriate using GraphPad Prism 6 software (RRID: SCR_002798), data represent mean ± standard error of the mean (SEM).

Dendritic Spine Analysis

Dendritic spines were analyzed in dorsal CA1 hippocampus with GFP using transgenic Thy1-GFP-M mice [Tg(Thy1-EGFP)MJrs/J, RRID: IMSR_JAX:007788] for ephrin-B1 OE condition and Diolistic approach (Henkemeyer et al., 2003) in ephrin-B1 KO mice. Animals were anesthetized with isoflurane and transcardially perfused initially with 0.9% NaCl, followed by fixation with 4% PFA in 0.1 M PBS, pH 7.4. Brains were post-fixed for 2 h in 4% PFA in 0.1 M PBS, and 100 μm coronal sections were cut with a vibratome. Dendritic spines were labeled in ephrin-B1 KO mice and their WT counterparts using a DiOlistic approach (Henkemeyer et al., 2003) using fluorescent lipophilic dye 1,1′-dioctadecyl-3,3,3′,3′-tetramethyl-indocarbocyanine perchlorate (DiO, D3898, Molecular Probes) coating tungsten particles. DiO was delivered by helium-powered ejection (Bio-Rad Helios Gene Gun System) into hippocampal slices and incubated in 0.1 M PBS for 72 h. CA1 hippocampal neurons were imaged using LSM 880 Airyscan Carl Zeiss confocal microscope. Ten to fifteen DiO-labeled or GFP-expressing neurons were randomly selected per group, and dendrites were imaged using a 63× objective (1.2 NA), 1× zoom. Three-dimensional fluorescent images were created by the projection of each *z*-stack containing 50–100 high-resolution optical serial sections (1,024 × 1,024-pixel format) taken at 0.5 μm intervals in the *X*–*Y* plane. Quantifications of the spine density (spines per 10 μm dendrite), lengths (μm), volumes (μm^3), and inter-spine intervals (μm) were carried out using Neurolucida 360 software (MicroBrightField RRID: SCR_001775). We observed an overall higher density of spines in DiO-labeled WT neurons compared to GFP-expressing WT neurons, which was most likely due to a better detection of smaller spines with membrane dye DiO than GFP. There were about 60–70% of smaller spines in DiO labeled WT neurons compared to 50–55% of smaller spines in GFP-expressing WT neurons (**Table 1**). Therefore, comparisons were made only between DiO-expressing WT and KO groups or GFP-expressing WT and OE groups. Statistical analysis was performed with two-way ANOVA followed by Bonferroni's *post hoc* analysis using GraphPad Prism 6 software (GraphPad Prism, RRID: SCR_002798), data represent mean ± SEM.

Synaptosome Purification

Synaptosome purification was performed as previously described (Hollingsworth et al., 1985). Briefly, hippocampal tissues were homogenized in 1 ml synaptosome buffer (124 mM NaCl, 3.2 mM KCl, 1.06 mM KH_2PO_4, 26 mM $NaHCO_3$, 1.3 mM $MgCl_2$, 2.5 mM $CaCl_2$, 10 mM Glucose, 20 mM HEPES), then filtered through a 100 μm nylon net filter (NY1H02500, Millipore) and 5 μm nylon syringe filter (SF15156, Tisch International). Homogenate flow through was collected, and synaptosomes were spun down at 10,000 × *g*, at 4°C, for 30 min. Synaptosomes were resuspended in 800 μl synaptosome buffer and processed for western blot analysis.

Western Blot Analysis

Tissue homogenate or purified synaptosome samples were centrifuged at 10,000 × *g*, 4°C, for 30 min. Pellets were re-suspended in lysis buffer (50 mM Tris, 100 mM NaCl, 2% TritonX-100, 10 mM EDTA) containing 2% protease inhibitor cocktail (P8340, Sigma-Aldrich) and incubated for 2 h at 4°C. Samples were added to 2× Laemmli Buffer (S3401, Sigma-Aldrich) and run on an 8–16% Tris-Glycine Gel (EC6045BOX, Invitrogen). Protein samples were transferred onto a nitrocellulose blotting membrane (10600007, GE Healthcare). Blots were blocked with 5% milk in TBS (10 mM Tris, 150 mM NaCl, pH 8.0), followed by immunostaining with mouse anti-PSD95 (1.65 μg/ml, Invitrogen Cat# MA1-045, RRID: AB_325399), rabbit anti-GluA1 (1:100, Millipore Cat# AB1504, RRID: AB_2113602), rabbit anti-GluA2/3 (0.1 μg/ml, Millipore Cat# AB1506,

[2]https://imagej.nih.gov/ij/plugins/colocalization.html

TABLE 1 | (Extended data table supporting **Figures 1C–E**.) Average dendritic spine density, length and volume in Fos(−) and c-Fos(+) CA1 neurons of WT and KO mice.

			Spine distribution (%)		
	Spine density (spines/10 μm)	Spine length (μm)	0–0.5 μm^3	0.5–1.0 μm^3	>1.0 μm^3
WT					
c-Fos(−) (*n* = 10)	10.42 ± 0.68	2.31 ± 0.20	69.35 ± 1.86	24.73 ± 2.12	5.92 ± 0.58
c-Fos(+) (*n* = 12)	13.27 ± 0.57*	2.74 ± 0.08*	59.62 ± 3.49*	29.23 ± 2.20	11.15 ± 1.80*
KO					
c-Fos(−) (*n* = 11)	12.37 ± 0.99	2.36 ± 0.03	71.06 ± 2.32	24.12 ± 1.86	4.80 ± 0.78
c-Fos(+) (*n* = 11)	15.98 ± 0.78**	2.47 ± 0.04	60.03 ± 2.04**	29.87 ± 1.17	10.15 ± 1.42*

*Statistical analysis was performed using two-way ANOVA (genotype and c-Fos as factors) with Bonferroni's post hoc test; c-Fos(−) versus c-Fos(+): *P < 0.05, **P < 0.01.*

RRID: AB_90710), or mouse anti-GAPDH (0.2 μg/ml, Thermo Fisher Scientific Cat# 39-8600, RRID: AB_2533438) antibodies in 0.1% tween 20/TBS at 4°C for 16 h. The secondary antibodies used were HRP conjugated donkey anti-mouse IgG (Jackson ImmunoResearch Cat#715-035-150, RRID: AB_2340770) or HRP conjugated goat anti-rabbit IgG (Jackson ImmunoResearch Cat# 111-035-003, RRID: AB_2313567). Blots were incubated in ECL 2 Western Blotting Substrate (Pierce Cat# 80196) and a signal was collected with CL-XPosure film (34090, Pierce). Band density was analyzed by measuring band and background intensity using Adobe Photoshop CS5.1 software (RRID: SCR_014199). Statistical analysis was performed with a one-way ANOVA followed by Tukey's *post hoc* analysis or *t*-test when appropriate using GraphPad Prism 6 software (RRID: SCR_002798), data represent mean ± SEM.

Electrophysiology

Brain slices were obtained from naïve or trained adult mice (P90-110) 1 h after recall test. Animals were deeply anesthetized with isoflurane and decapitated. Mouse brains were rapidly removed and immersed in ice-cold "slushy buffer" with high Mg^{2+} and sucrose concentration containing the following (in mM): 87 NaCl, 75 sucrose, 2.5 KCl, 0.5 $CaCl_2$, 7 $MgCl_2$, 1.25 NaH_2PO_4, 25 $NaHCO_3$, 10 glucose, 1.3 ascorbic, acid, 0.1 kynurenic acid, 2.0 pyruvate, and 3.5 MOPS with a pH of 7.4 and saturated with 95% O_2/5% CO_2. Transverse hippocampal slices (350 μm) were prepared by using a vibrating blade microtome (Campden 5100mz-Plus, Campden Instruments Ltd.) and transferred into a holding chamber containing oxygenated ACSF (in mM; 125 NaCl, 2.5 KCl, 2.5 $CaCl_2$, 1.3 $MgCl_2$, 1.25 NaH_2PO_4, 26 $NaHCO_3$, 15 glucose, 3.5 MOPS with a pH of 7.4) for 1 h at 33°C. Slices were then transferred to a submersion recording chamber continually perfused with oxygenated ACSF at a flow rate of 1 ml/min. Slices were allowed to equilibrate for approximately 10 min to reach a stable baseline response prior to running experimental protocols.

Blind whole-cell patch experiments were performed as described (Castaneda-Castellanos et al., 2006). Tight-seal whole-cell voltage clamp recordings were obtained using pipettes made from borosilicate glass capillaries pulled on a Narishige PC-10 vertical micropipette puller (Narishige, Tokyo, Japan). Pipette resistance ranged from 3 to 4 MΩ, filled with an internal solution containing (in mM) 130 CsOH, 130 D-gluconic acid, 0.2 EGTA, 2 $MgCl_2$, 6 CsCl, 10 HEPES, 2.5 ATP-Na, 0.5 GTP-Na, 10 phosphocreatine, and 0.1% biocytin for cellular post labeling, pH adjusted to 7.2–7.3 with CsOH, osmolarity adjusted to 300–305 mOsm with ATP-Na. The series resistance was <25 MΩ and was compensated, if the series resistance changed >20% during the course of an experiment, the data were discarded. For evoked EPSCs and IPSCs, electrical stimuli (0.1 Hz) were delivered through a bipolar, Teflon®-coated tungsten electrode placed in the SR region and close proximity to the recording electrode. Neurons were voltage-clamped at either −70 mV to measure AMPAR evoked responses or +40 mV to measure NMDA receptor evoked responses. All EPSCs were recorded in the presence of 50 μM picrotoxin, a $GABA_A$ receptor antagonist, to block $GABA_A$-mediated currents at 33°C. To measure inhibitory postsynaptic currents (IPSCs), neurons were voltage-clamped at 0 mV with 10 μM NBQX, an AMPA receptor antagonist, and 50 μM D-AP5, a NMDA receptor antagonist at 33°C. 1 μM tetrodotoxin was added to isolate mEPSC and mIPSC responses. EPSCs and IPSCs were recorded using an EPC-9 amplifier (HEKA Elektronik, Lambrecht, Germany), filtered at 1 kHz, digitized at 10 kHz, and stored on a personal computer using pClamp 10.7 software (Molecular Device) to run analysis. AMPA, NMDA-mediated EPSCs, IPSCs evoked responses, mEPSCs, and mIPSCs were analyzed by Clampfit 10.7 software (Molecular Device). All averaged data were presented as means ± SEM. Statistical significance was determined by Student's *t*-test using Prism 7.0 software (GraphPad Software, Avenida, CA, United States).

RESULTS

We previously reported that the loss of astrocytic ephrin-B1 in adult mice resulted in enhanced contextual recall, while OE of ephrin-B1 in the adult hippocampal astrocytes impaired contextual memory recall (Koeppen et al., 2018). The goal of this study was to understand the mechanism by which astrocytic ephrin-B1 affects contextual fear conditioning memory, in particular how the deletion or OE of astrocytic ephrin-B1 affects remodeling of synapses and dendritic spines in the CA1 hippocampus following contextual learning. To accomplish this, astrocyte-specific ephrin-B1 KO and ephrin-B1 OE mice,

with corresponding WT counterparts, were trained in a fear condition paradigm to associate a context with an electric shock. Next day, the mice were placed in context A, in which they were trained, and their freezing was evaluated as a measure of contextual memory (**Supplementary Figure 1**). Dendritic spine density, morphology, and clustering were analyzed in the CA1 hippocampus of these mice 1 h after contextual memory recall. As specific memories are encoded in a subset of hippocampal neurons (Liu et al., 2012; Tonegawa et al., 2015), we further analyzed dendritic spine changes in CA1 hippocampal pyramidal neurons that were activated (c-Fos+) or not activated (c-Fos−) during contextual memory recall. Additionally, changes in the excitatory synaptic sites were analyzed by co-labeling of vGlut1 with PSD-95 puncta in CA1 hippocampus.

Dendritic Spine Density Is Higher on CA1 Hippocampal Neurons of Ephrin-B1 KO Mice, Specifically on cFos(+) Neurons That Are Activated During Contextual Recall

To examine the effects of ephrin-B1 deletion in adult hippocampal astrocytes on remodeling of dendritic spines following contextual learning, coronal hippocampal sections were collected from WT and KO mice 1 h following contextual recall. We used immunostaining against early immediate *gene c-fos* to identify CA1 neurons that were activated during memory recall (red; **Figures 1A,B**). Dendritic spines were labeled with DiO (green; **Figure 1A**) to visualize dendritic spines in both c-Fos(+) and c-Fos(−) neurons (**Figures 1A,B**).

Spine density was significantly higher in trained KO compared to WT (**Supplementary Figure 2A** and **Supplementary Table 1**; *t*-test; $t_{(43)} = 2.414$, $p = 0.0201$); however, spine volume and length were not different between trained KO and WT animals (**Supplementary Figures 2B,C**; spine volume: $t_{(44)} = 1.581$, $p = 0.1210$; spine length: $t_{(42)} = 0.920$, $p = 0.3626$; *t*-test). Interestingly, in addition to the effect of genotype further analysis showed a significant increase in the spine density on c-Fos(+) neurons compared to c-Fos(−) neurons in KO mice [**Figure 1C** and **Table 1**; two-way ANOVA, c-Fos $F(1,48) = 19.91$, $p < 0.0001$; genotype $F(1,48) = 11.55$, $p = 0.0014$; interaction $F(1,48) = 0.4134$, $p = 0.5233$; Bonferroni's *post hoc* test, $^{**}p < 0.0066$ c-Fos(+) KO vs. c-Fos(−) KO; $^{*}p = 0.0422$ c-Fos(+) WT vs. c-Fos(−) WT]. We also observed higher spine density in c-Fos(+) neurons of KO mice compared to c-Fos(+) WT (**Figure 1C**; Bonferroni's *post hoc* test, $^{*}p = 0.0446$), but no significant differences were observed between c-Fos(−) WT and c-Fos(−) KO groups. When we analyzed spine volume, c-Fos(+) neurons in both WT and KO mice showed a significant decrease in smaller spines and an increase in larger spines ($>1.0\ \mu m^3$) with no effect of genotype [**Figure 1E** and **Table 1**; two-way ANOVA c-Fos $F(2,123) = 946.1$, $p < 0.0001$; genotype $F(3,123) = 9.739e{-}005$, $p > 0.9999$; Bonferroni's *post hoc* test, $^{**}p < 0.01$, $^{*}p < 0.05$].

The results suggest that increased number of dendritic spines may underlie enhanced contextual memory in astrocyte-specific ephrin-B1 KO mice. While the increase in spine volume is observed on c-Fos(+) neurons in both WT and KO mice, dendritic spine density remains higher in KO compared to WT mice.

Excitatory Responses Were Enhanced in CA1 Hippocampal Neurons of Trained Ephrin-B1 KO Compared to Trained WT and Naïve KO Mice

Changes in dendritic spine density may affect neuronal functionality; specifically, an increase in dendritic spine numbers in trained KO compared to WT may indicate an increase in excitatory responses. Whole-cell patch clamp experiments were conducted to determine if CA1 hippocampal pyramidal neurons in trained KO mice also show increased excitatory responses compared to trained WT mice. Indeed, increased evoked excitatory responses were observed in CA1 hippocampal neurons of trained KO mice compared to WT mice by measuring both NMDAR and AMPAR currents (**Figures 2A,B**; WT AMPAR: 527.65 ± 30.30 vs. KO AMPAR: 713.52 ± 43.33, $t_{(398)} = 3.568$, $p = 0.0004$, *t*-test; WT NMDAR: 186.36 ± 13.12; KO NMDAR: 307.43 ± 23.59, $t_{(373)} = 4.610$ $p < 0.0001$, *t*-test). Interestingly, AMPAR/NMDAR ratio was not significantly different between trained WT and KO mice (**Figure 2C**; WT: 2.40 ± 0.60; KO: 2.51 ± 0.48, $t_{(17)} = 0.149$, $p = 0.8829$, *t*-test). Increased excitatory post-synaptic strength in trained KO mice was further confirmed by increased mEPSC amplitude (**Figures 2D,G,H**; WT: 7.74 ± 0.73; KO: 15.06 ± 2.76, $t_{(12)} = 2.927$, $p = 0.0127$, *t*-test), whereas no differences were observed in mEPSC frequencies between WT and KO trained mice (**Figures 2D–F**; WT: 0.79 ± 0.12; KO: 0.81 ± 0.30; $t_{(12)} = 0.07389$, $p = 0.9422$, *t*-test). In addition, we analyzed mEPSCs in naïve WT and KO mice. We found that mEPSC frequency was reduced in naïve KO compared to naïve WT (**Figures 2I–K**; WT: 0.44 ± 0.06; KO 0.25 ± 0.044, $t_{(10)} = 2.561$, $p = 0.0283$, *t*-test), but no significant differences in mEPSC amplitude (**Figures 2L,M**; WT: 7.47 ± 0.75; KO: 7.01 ± 0.92, $t_{(10)} = 0.3833$, $p = 0.7095$, *t*-test). Moreover, two-way ANOVA analysis shows a significant increase of both mEPSC amplitude [two-way ANOVA, training $F(1,22) = 8.115$, $p = 0.0093$; genotype $F(1,22) = 5.536$, $p = 0.0280$, Bonferroni's *post hoc* test, $^{**}p < 0.01$] and mEPSC frequency in trained KO compared to naïve KO group [two-way ANOVA, training $F(1,22) = 0.13.99$, $p = 0.0011$; genotype $F(1,22) = 0.4598$, $p = 0.5048$, Bonferroni's *post hoc* test, $^{*}p < 0.05$]; and supports previously reported biochemical results showing similar increase in synaptic AMPAR levels in trained KO compared to naïve KO group (Koeppen et al., 2018).

It is important to note that inhibitory evoked responses as well as mIPSC amplitude and frequency were not significantly different between WT and KO mice (**Supplementary Figure 3**), indicating loss of astrocytic ephrin-B1 affects mainly excitatory but not inhibitory function in the adult CA1 hippocampus. Together these results show increased excitability in trained KO mice compared to naïve KO mice, most likely due to increase

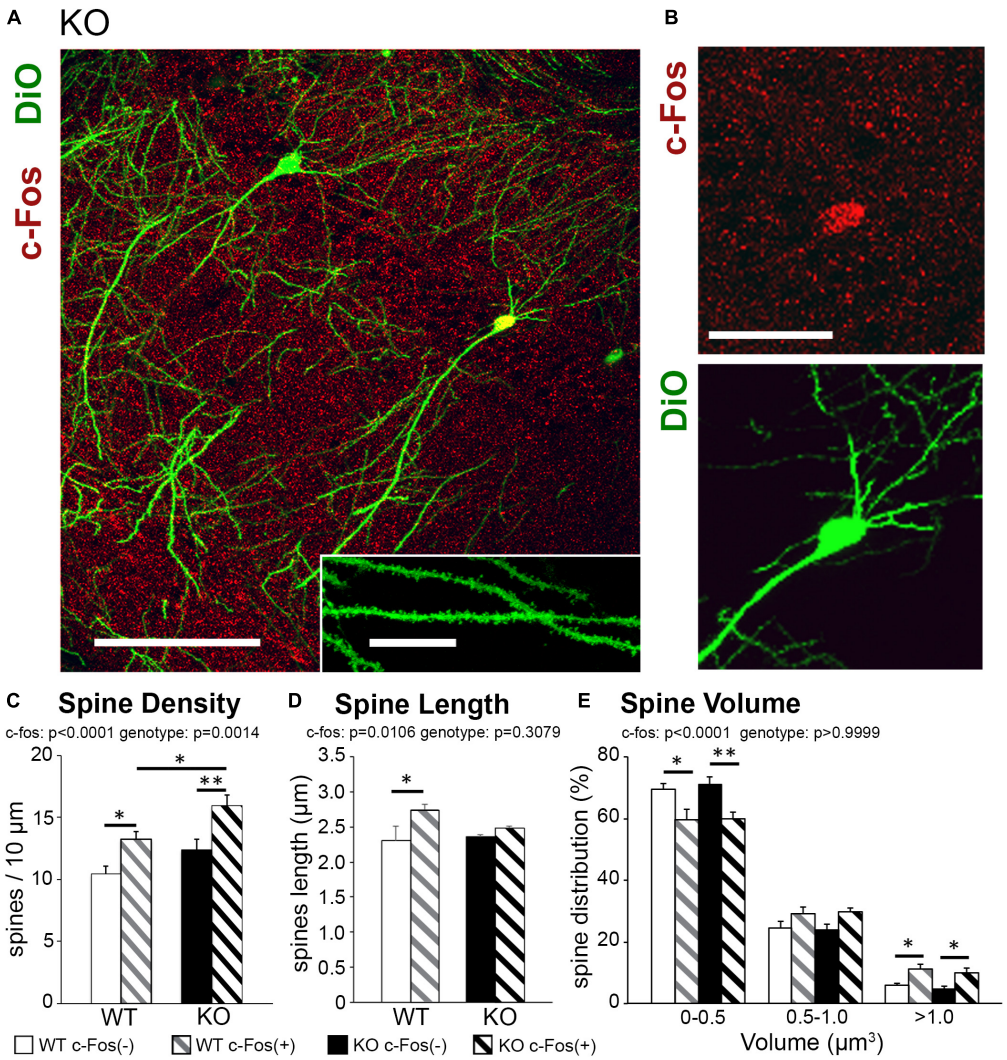

FIGURE 1 | Learning-induced spine formation is observed on CA1 neurons in astrocyte-specific ephrin-B1 KO mice, specifically on cFos(+) neurons that are activated during contextual recall. **(A)** Confocal image showing DiO (green) and c-Fos (red) labeled neurons in CA1 hippocampus of adult KO mice, scale bar is 150 µm. High magnification shows examples of dendritic spines, scale bar is 20 µm (insert). **(B)** High magnification image of CA1 pyramidal neuron showing c-Fos(+) immunoreactivity (red) and DiO labeling (green). **(C–E)** Graphs show the average number of dendritic spines per 10 µm dendrite **(C)**, spine length **(D)**, and spine volume **(E)** in c-Fos(+) and c-Fos(–) CA1 neurons from WT and KO mice. **(C)** There is a significant increase in average dendritic spine density in c-Fos(+) neurons compared to c-Fos(–) neurons in KO mice [two-way ANOVA, c-Fos $F(1,48) = 19.91$, $p < 0.0001$; genotype $F(1,48) = 11.55$, $p = 0.0014$; Bonferroni's *post hoc* test, $^{**}p < 0.0066$ c-Fos(+) KO vs. c-Fos(–) KO; $^{*}p = 0.0422$ c-Fos(+) WT vs. c-Fos(–) WT]. We also observed higher spine density in c-Fos(+) neurons of KO mice compared to c-Fos(+) WT (Bonferroni's *post hoc* test, $^{*}p = 0.0446$), but no significant differences were observed between c-Fos(–) WT and c-Fos(–) KO groups. **(D)** Spine length was slightly increased in WT c-Fos(+) neurons compared to WT c-Fos(–) neurons [two-way ANOVA c-Fos $F(1,40) = 7.183$, $p = 0.0106$; genotype $F(1,40) = 1.067$, $p = 0.3079$; Bonferroni's *post hoc* test, $^{*}p < 0.05$]. **(E)** A significant increase in the percentage of larger spines (>1.0 µm^3) was seen in c-Fos(+) neurons compared c-Fos(–) in both WT and KO [two-way ANOVA, c-Fos $F(2,123) = 946.1$, $p < 0.0001$; genotype $F(3,123) = 9.739e{-}005$, $p > 0.9999$; Bonferroni's *post hoc* test, $^{**}p < 0.01$, $^{*}p < 0.05$).

in the number of excitatory synapses and the recruitment of AMPAR to postsynaptic sites.

Overexpression of Astrocytic Ephrin-B1 Inhibits New Dendritic Spine Formation on CA1 Neurons Following Learning

To determine the effects of ephrin-B1 OE in adult hippocampal astrocytes on dendritic spine formation following contextual learning, coronal hippocampal sections were collected 1 h following contextual recall from Thy1-GFP mice containing hippocampal astrocytes expressing tdTomato (WT) or tdTomato with ephrin-B1 (ephrin-B1 OE). We used immunostaining against early immediate *c-fos gene* to identify CA1 neurons that were activated during memory recall [c-Fos(+), blue; **Figures 3A,B**]. Dendritic spines were visualized with GFP (green, **Figure 3A**) in both c-Fos(+) and c-Fos(−) neurons and astrocytes expressed td-Tomato (red, **Figure 3A**).

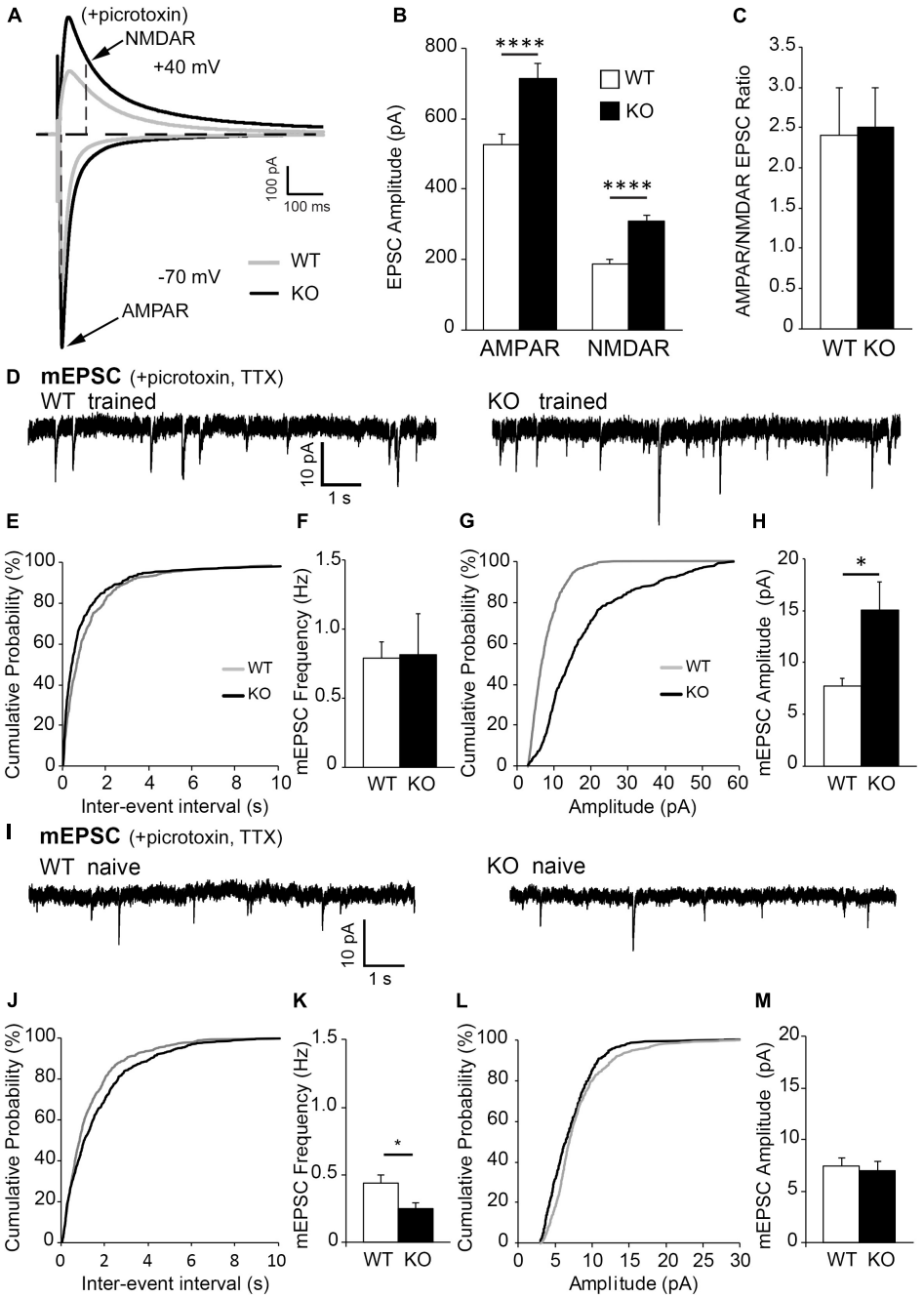

FIGURE 2 | Excitatory post-synaptic responses are enhanced in CA1 hippocampal neurons from astrocytic ephrin-B1 KO mice compared to WT mice. **(A)** Representative traces of excitatory postsynaptic responses in CA1 hippocampal neurons in hippocampal slices from WT (gray) and KO (black) trained mice evoked by stimulating CA3 Schaffer collaterals in the presence of 50 μM picrotoxin, a $GABA_A$ receptor antagonist. Neurons were voltage-clamped at either –70 mV to measure AMPAR-mediated EPSCs or +40 mV to measure NMDAR-mediated EPSCs. **(B,C)** Graphs show average EPSC amplitude **(B)** and corresponding ratio of AMPAR- and NMDAR-mediated EPSCs **(C)** (n = 12–13 cells, six mice). Evoked AMPAR and NMDAR-mediated currents were significantly increased (AMPAR: $t_{(398)} = 3.568$, $^{***}p = 0.0004$; NMDAR: $t_{(373)} = 4.61$, $p < 0.0001$, t-test, $^{****}p < 0.0001$); however, AMPAR/NMDAR EPSC ratio was unchanged ($t_{(17)} = 0.1495$, $p = 0.8829$, t-test). **(D)** Sample recordings of mEPSCs from CA1 neurons in hippocampal slices from trained WT and KO mice; recorded in the presence of TTX and picrotoxin (n = 6 mice). **(E)** Cumulative probability curve of inter-event intervals between spikes in WT (gray) and KO (black). **(F)** Total average frequency of mEPSCs in WT and KO. **(G)** Cumulative probability curve of mEPSC amplitude in WT and KO. **(H)** Average amplitude of mEPSCs was significantly higher in KO compared to WT ($t_{(12)} = 2.927$, $^{*}p = 0.0127$, t-test). **(I)** Sample recordings of mEPSCs from CA1 neurons in hippocampal slices from naïve WT and KO mice; recorded in the presence of TTX and picrotoxin (n = 6 mice). **(J)** Cumulative probability curve of inter-event intervals between spikes in naïve WT (gray) and KO (black). **(K)** Total average frequency of mEPSCs in naïve WT and KO. Average frequency of mEPSCs was significantly lower in naïve KO than WT mice ($t_{(10)} = 2.561$, $^{*}p = 0.0283$). **(L)** Cumulative probability curve of mEPSC amplitude in naïve WT and KO. **(M)** Average amplitude of mEPSCs between naïve WT and KO. Error bars represent SEM; $^{*}p < 0.05$, $^{****}p < 0.0001$.

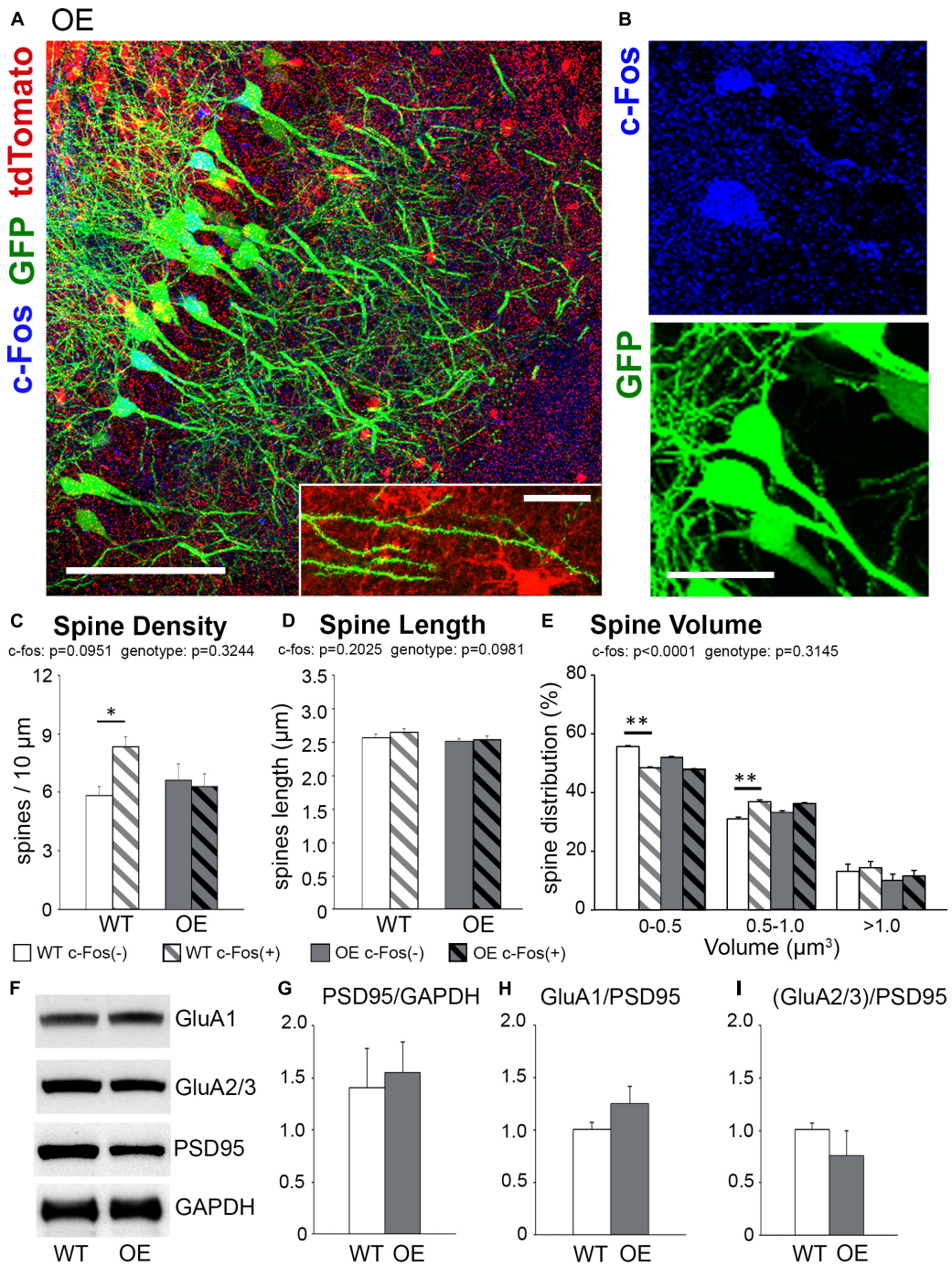

FIGURE 3 | The increase in spine density on c-Fos(+) neurons compared to c-Fos(–) neurons is impaired in OE mice. **(A)** Confocal images of the CA1 neurons expressing GFP (green) and astrocytes expressing tdTomato (red). Some neurons show c-Fos immunoreactivity (blue), scale bar is 100 µm. High magnification image shows example of dendritic spines located in a close proximity to tdTomato-expressing astrocytes, scale bar is 20 µm (insert). **(B)** High magnification images of c-Fos(+) (blue) and GFP-expressing (green) CA1 pyramidal neurons. **(C–E)** Graphs show the average number of dendritic spines per 10 µm dendrite **(C)**, spine length **(D)**, and spine volume **(E)** in c-Fos(+) and c-Fos(–) neurons from WT and OE mice. **(C)** There was an increased dendritic spine density in WT c-Fos(+) neurons compared with WT c-Fos(–) neurons [two-way ANOVA, c-Fos $F(1,41) = 2.920$, $p = 0.0951$; genotype $F(1,41) = 0.995$, $p = 0.3244$; interaction $F(1,41) = 4.787$, $p = 0.0344$; Bonferroni's *post hoc* $^{*}p < 0.05$ c-Fos(+) WT vs. c-Fos(–) WT]. **(D)** Spine length was no different between c-Fos(–) and c-Fos(+) neurons in both WT and OE mice. **(E)** A significant decrease in the percentage of smaller spines (<0.5 µm^3) and an increase in the percentage of larger spines (0.5–1.0 µm^3) were seen in c-Fos(+) neurons compared c-Fos(–) neurons with no effect of genotype [two-way ANOVA, c-fos $F(2,141) = 837.4$, $p < 0.0001$; genotype $F(3,141) = 1.194$, $p = 0.3145$ Bonferroni's *post hoc* $^{**}p < 0.01$ c-Fos(–) WT vs. c-Fos(+) WT]. **(F)** Western blots show levels of AMPAR subunits (GluA1 and GluA2/3), PSD95, and GAPDH in synaptosomes isolated from the hippocampus of WT and OE mice 1 h after context A recall. **(G–I)** Graphs show ratios of synaptic PSD95 to GAPDH **(G)**, GluA1 to PSD95 **(H)**, or GluA2/3 to PSD95 **(I)**. Graphs show mean values and error bars represent SEM; $^{*}p < 0.05$, $^{**}p < 0.01$.

TABLE 2 | (Extended data table supporting **Figures 3C–E**.) Average dendritic spine density, length and volume in Fos(-) and c-Fos(+) CA1 neurons of WT and OE mice.

			Spine distribution (%)		
	Spine sensity (spines/10 μm)	Spine length (μm)	0–0.5 μm^3	0.5–1.0 μm^3	>1.0 μm^3
WT					
c-Fos(−) (*n* = 10)	5.83 ± 0.47	2.56 ± 0.05	55.65 ± 0.25	31.00 ± 0.52	13.35 ± 0.02
c-Fos(+) (*n* = 13)	8.35 ± 0.51*	2.65 ± 0.05	48.58 ± 0.27**	37.03 ± 0.49**	14.43 ± 0.02
OE					
c-Fos(−) (*n* = 11)	6.60 ± 0.86	2.50 ± 0.05	51.96 ± 0.26	33.36 ± 0.49	10.09 ± 0.93
c-Fos(+) (*n* = 11)	6.29 ± 0.67	2.54 ± 0.05	48.05 ± 0.27	36.25 ± 0.46	11.55 ± 0.80

*Statistical analysis was performed using two-way ANOVA (genotype and c-Fos as factors) with Bonferroni's post hoc test: c-Fos(−) versus c-Fos(+): *P < 0.05, **P < 0.01.*

We observed no significant differences in overall spine density, volume or length between trained OE and WT mice (**Supplementary Figures 2D–F**; density, *t*-test, $t_{(42)}$ = 1.463, p = 0.1509). However, further analysis showed a significantly higher spine density on c-Fos(+) neurons compared to c-Fos(−) neurons in trained WT but not OE mice [**Figure 3C** and **Table 2**; two-way ANOVA, c-Fos $F(1,41)$ = 2.920, p = 0.0951; genotype $F(1,41)$ = 0.995, p = 0.3244; interaction $F(1,41)$ = 4.787, p = 0.0344; Bonferroni's *post hoc* $^*p < 0.05$ c-Fos(+) WT vs. c-Fos(−) WT]. The impaired increase in spine density on c-Fos(+) neurons compared to c-Fos(−) neurons in OE mice may explain impaired contextual recall in OE mice (**Supplementary Figure 1K**, *t*-test $p < 0.05$). In addition, a decreased proportion of smaller spines and an increased number of larger spines was seen in c-Fos(+) neurons compared to c-Fos(−) neurons (**Figure 3E**; two-way ANOVA c-fos $F(2,141)$ = 837.4, $p < 0.0001$), but there was no genotype difference [**Figure 3E**; two-way ANOVA genotype $F(3,141)$ = 1.194, p = 0.3145]. No significant differences were also seen between trained WT and OE mice in synaptic PSD-95, GluA1 (**Figures 3F–H**; WT: 1.006 ± 0.063 vs. OE: 1.251 ± 0.161, $t_{(8)}$ = 1.637, p = 0.140, *t*-test), or GluA2/3 levels (**Figures 3F,I**; WT: 1.007 ± 0.065 vs. OE: 0.757 ± 0.238, $t_{(8)}$ = 1.221, p = 0.257, *t*-test).

Taken together the results suggest that impaired formation of spines on c-Fos(+) CA1 hippocampal neurons may underlie the deficits in contextual recall in astrocyte-specific ephrin-B1 OE mice without affecting dendritic spine maturation.

Increased Spine Clustering Is Observed on c-Fos(+) Neurons in WT and KO Mice, but Not OE Mice

To examine if new spines were added in a close proximity of neighboring spines we analyzed inter-spine intervals (distances between neighboring spines) on c-Fos(+) and c-Fos(−) CA1 neurons in WT mice. As expected, we observed an overall reduction in inter-spine intervals between neighboring spines in c-Fos(+) neurons compared to c-Fos(−) neurons due to an increase in spine density. However, spines were not distributed uniformly as we found a specific increase in the percentage of spines with inter-spine intervals <2.0 μm on c-Fos(+) neurons compared to c-Fos(−) neurons (**Supplementary Figures 4A–C**; WT c-Fos−: 50.91 ± 1.65 vs. WT c-Fos+: 56.58 ± 1.00, $t_{(10)}$ = 2.766, p = 0.019, *t*-test). We further analyzed clusters of these spines that were <2.0 μm from each other in c-Fos(+) and c-Fos(−) neurons. We observed a significant increase in the number of the spine clusters on c-Fos(+) CA1 neurons compared to c-Fos(−) neurons in WT [**Figure 4B**; two-way ANOVA; $F_{c-Fos}(1,50)$ = 6.698, p = 0.0126], in particular smaller clusters containing three spines [**Table 3**; WT c-Fos− (3): 3.42 ± 0.50 vs. WT c-Fos+ (3): 4.59 ± 0.34; Bonferroni's *post hoc* test, $^*p < 0.05$].

This suggests that spine formation occurs at specific locations, in a close proximity to neighboring spines, on the dendrites of c-Fos(+) CA1 neurons activated during contextual recall.

Interestingly, we also observed a significant increase in number of spine clusters in c-Fos(+) neurons compared to c-Fos(−) neurons in ephrin-B1 KO mice [**Figure 4D**, two-way ANOVA $F_{c-Fos}(1,130)$ = 15.5, p_{c-Fos} = 0.0001; **Supplementary Figures 4D–F**], specifically smaller clusters containing three spines [**Table 3**; KO c-Fos− (3): 3.00 ± 0.41 vs. KO c-Fos+ (3): 5.67 ± 0.80; Bonferroni's *post hoc* test, $^{****}p < 0.0001$]. In contrast, we observed no difference in the number of clusters between c-Fos(+) and c-Fos(−) CA1 neurons in ephrin-B1 OE mice [**Figure 4F**; two-way ANOVA $F_{c-Fos}(1,60)$ = 0.9948, p_{c-Fos} = 0.3226; **Supplementary Figures 4G–I**].

Astrocytic ephrin-B1 may affect up-regulation of dendritic spine density on c-Fos(+) neurons by impacting new spine formation at selective dendritic domains.

Synaptic Excitatory Sites Are Up-Regulated in CA1 Hippocampus of Astrocyte-Specific Ephrin-B1 KO Mice Following Fear Conditioning

To determine if KO mice also show an increased number of excitatory synapses in the CA1 hippocampus following fear conditioning, excitatory synaptic sites were identified by co-immunostaining against pre-synaptic vGlut1 and postsynaptic PSD95 (**Figures 5A,B**). Although no changes in vGlut1 positive puncta were detected between trained WT (3.549 ± 0.173) and KO (3.601 ± 0.1753; $t_{(29)}$ = 0.213, p = 0. 833; **Figure 5E**), a significant increase in vGlut1/PSD95 co-localization was seen in trained KO (2.678 ± 0.116) compared to their WT counterparts (1.999 ± 0.215; $t_{(29)}$ = 2.828, p = 0. 008; **Figure 5G**). We also observed an increased number of PSD95 positive puncta in trained KO (5.592 ± 0.088) compared to their WT counterparts (4.727 ± 0.425; $t_{(32)}$ = 2.104, p = 0. 043; **Figure 5F**). In contrast,

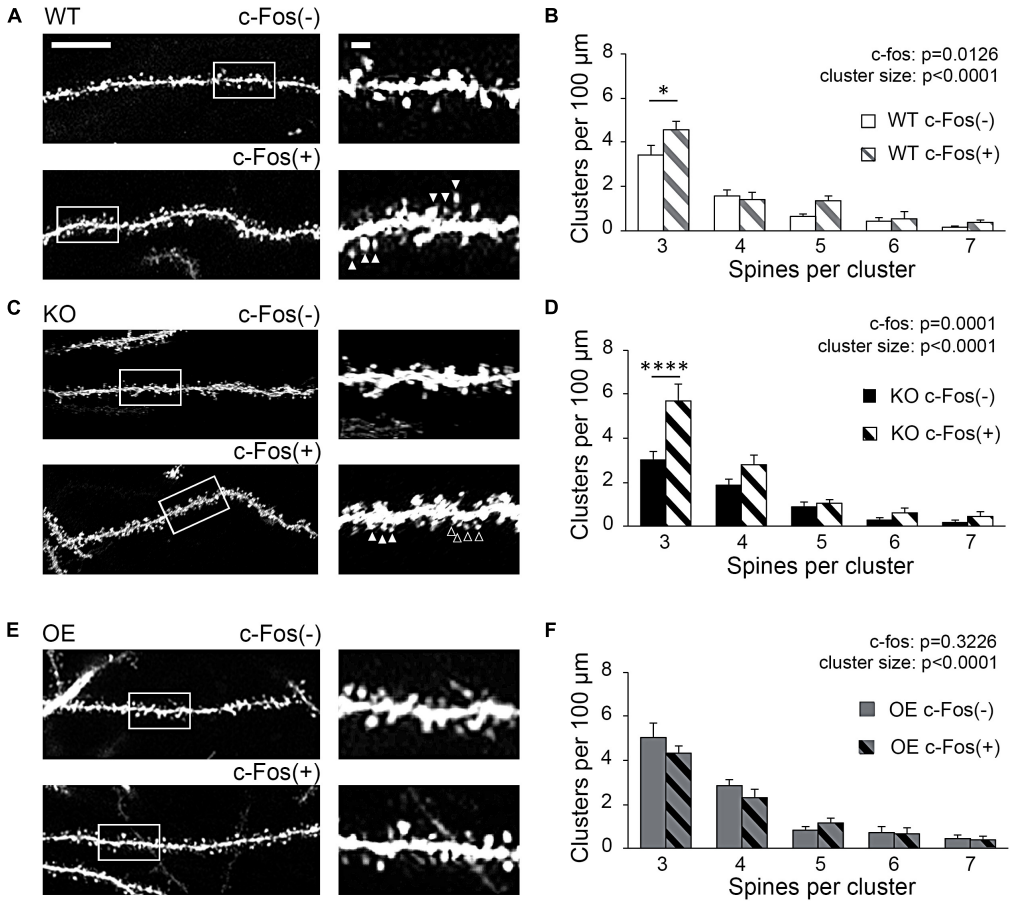

FIGURE 4 | Increased spine clustering is observed on c-Fos(+) neurons in WT and KO mice, but not OE mice. **(A,C,E)** Confocal images of dendritic spines in c-Fos(–) or c-Fos(+) CA1 hippocampal neurons from WT **(A)**, KO **(C)**, and OE **(E)** mice 1 h after contextual recall; scale bar is 10 μm for low magnification images and 2 μm for high magnification images. **(B,D,F)** Graphs show number of clusters containing three, four, five, six, or seven spines (with inter-spine interval < 2 μm) per cluster in c-Fos(–) or c-Fos(+) CA1 neurons from WT **(B)**, KO **(D)** or OE **(F)** mice. **(B)** WT c-Fos(+) neurons had significantly higher number of clusters with three spines than WT c-Fos(–) neurons [cluster size $F(4,50) = 69.19$, $p < 0.0001$; c-Fos $F(1,50) = 6.698$, $p = 0.0126$; two-way ANOVA followed by Bonferroni's *post hoc*, $^{*}p = 0.0109$]. **(D)** There was a higher number of clusters with three spines in KO c-Fos(+) neurons compared to KO c-Fos(–) neurons [cluster size $F(4,130) = 45.77$, $p < 0.0001$; c-Fos $F(1,130) = 15.5$, $p = 0.0001$; two-way ANOVA followed by Bonferroni's *post hoc*, $^{****}p < 0.0001$]. **(F)** There was no difference in the number of clusters with three spines between OE c-Fos(+) and OE c-Fos(–) neurons. Graphs show mean values and error bars represent SEM; $^{*}p < 0.05$, $^{****}p < 0.0001$.

we observed a significant reduction in vGlut1/PSD95 co-localization (**Figure 5G**) in trained OE (2.036 ± 0.232) compared to their WT counterparts (**Figures 5C,D,J**; 2.719 ± 0.158; $t_{(32)} = 2.433$, $p = 0.022$, *t*-test). However, no differences were observed between WT and OE when vGlut1 (WT: 5.736 ± 0.275; OE: 5.352 ± 0.1588, $t_{(32)} = 1.120$, $p = 0.159$, *t*-test) and PSD-95 (WT: 5.600 ± 0.336; OE: 4.835 ± 0.148; $t_{(32)} = 2.084$, $p = 0.078$, *t*-test) puncta were analyzed separately (**Figures 5H,I**).

To determine if astrocytic ephrin-B1 also regulates excitatory inputs on inhibitory cells, dorsal hippocampal sections were co-immunostained for vGlut1 and PV (**Figure 6A**). No significant differences were seen in the number of vGlut1-positive puncta on PV-positive cells between trained WT and KO mice 1 h after contextual recall in SP areas of CA1 hippocampus (**Figure 6B**; WT: 1.280 ± 0.070 vs. KO: 1.451 ± 0.083; $t_{(663)} = 1.516$, $p = 0.114$). We also observed no significant differences in inhibitory GAD65-positive puncta in the CA1 hippocampus between trained WT and KO mice (**Figures 6C,D**; SR WT: 2.07 ± 0.21; KO: 2.49 ± 0.30; $t_{(34)} = 1.159$, $p = 0.255$; SLM WT: 2.90 ± 0.44; KO 3.57 ± 0.46; $t_{(23)} = 1.047$, $p = 0.306$) or between trained WT and OE mice (**Figures 6E,F**; SR WT: 3.10 ± 0.16; OE: 3.02 ± 0.23; $t_{(31)} = 0.9001$, $p = 0.38$; SLM WT 3.02 ± 0.23; KO 3.01 ± 0.32; $t_{(28)}$ ± 0.02563, $p = 0.98$, *t*-test). Whole cell recording from CA1 hippocampal neurons also showed no differences in the amplitude or latency of evoked IPSCs, as well as mIPSC amplitude and frequency between WT and KO mice (**Supplementary Figures 3A,B**).

The results suggest that excess excitatory synapse formation on excitatory CA1 neurons most likely contribute to enhanced contextual recall in astrocyte-specific ephrin-B1 KO mice, whereas reduced number of excitatory synapses/spines following ephrin-B1 OE in adult astrocytes, in particular on activated c-Fos(+) CA1 neurons, would contribute to impaired contextual recall.

TABLE 3 | (Extended data table supporting **Figure 4**.) The number of spine clusters with 3, 4, 5, 6, and 7 spines in c-Fos(–) and c-Fos(+) CA1 neurons of WT, KO, and OE mice.

	Spine clusters per 100 μm dendritic length				
Spines per cluster	**3**	**4**	**5**	**6**	**7**
WT					
c-Fos(–) (*n* = 6)	3.42 ± 0.46	1.56 ± 0.26	0.62 ± 0.13	0.42 ± 0.14	0.16 ± 0.06
c-Fos(+) (*n* = 6)	4.59 ± 0.34	1.41 ± 0.29	1.36 ± 0.21	0.54 ± 0.30	0.38 ± 0.09
Statistics	*t* = 3.232	*t* = 0.404	*t* = 2.032	*t* = 0.333	*t* = 0.593
	*p = 0.0109	$p > 0.999$	$p = 0.2374$	$p > 0.999$	$p > 0.999$
KO					
c-Fos(–) (*n* = 15)	3.00 ± 0.41	1.84 ± 0.30	0.86 ± 0.26	0.28 ± 0.11	0.18 ± 0.08
c-Fos(+) (*n* = 13)	5.67 ± 0.80	2.77 ± 0.48	1.04 ± 0.19	0.61 ± 0.19	0.45 ± 0.18
Statistics	*t* = 5.360	*t* = 1.853	*t* = 0.369	*t* = 0.659	*t* = 0.561
	****$p < 0.0001$	$p = 0.3306$	$p > 0.999$	$p > 0.999$	$p > 0.999$
OE					
c-Fos(–) (*n* = 7)	5.03 ± 0.66	2.86 ± 0.27	0.84 ± 0.17	0.70 ± 0.28	0.46 ± 0.16
c-Fos(+) (*n* = 7)	4.35 ± 0.29	2.32 ± 0.37	1.18 ± 0.18	0.66 ± 0.31	0.37 ± 0.16
Statistics	*t* = 1.503	*t* = 1.197	*t* = 0.760	*t* = 0.099	*t* = 0.191
	$p = 0.6906$	$p > 0.999$	$p > 0.999$	$p > 0.999$	$p > 0.999$

*Statistical analysis of differences between c-Fos(–) and c-Fos(+) expression was performed using two-way ANOVA (c-Fos and cluster size as factors) with Bonferroni post hoc test: *P < 0.05, ****P < 0.001.*

DISCUSSION

Astrocytes are well positioned to influence learning and memory consolidation by influencing dendritic spine formation and maturation in the adult hippocampus, but molecular mechanisms are not clear. Our data suggest that astrocytic ephrin-B1 controls learning and memory consolidation during contextual fear conditioning by regulating new dendritic spine formation on activated CA1 hippocampal neurons. First, we found that the deletion of ephrin-B1 in astrocytes enhances learning-induced formation of new dendritic spines on CA1 hippocampal neurons, while its OE impairs new synapse formation. Second, ephrin-B1 OE in hippocampal astrocytes selectively affects dendritic spine formation and clustering on hippocampal neurons activated during contextual recall. Third, despite the changes to excitatory synapses, deletion or OE of ephrin-B1 in adult astrocytes does not affect the density of inhibitory GAD65-positive puncta in the CA1 hippocampus. Finally, deletion of ephrin-B1 in astrocytes does not affect learning-induced changes in spine volume, as we observed enlargement of dendritic spines in ephrin-B1 KO mice similar to their WT counterparts. Our results suggest that the deficits in dendritic spine formation and clustering, but not spine maturation, in particular on activated CA1 neurons may underlie impaired contextual memory recall in ephrin-B1 OE mice. These studies implicate astrocytic ephrin-B1 as a negative regulator of synapse formation in the adult hippocampus during learning, which can influence spatial memory.

One major finding of this study is that modulation of ephrin-B1 levels in astrocytes negatively affects the formation of new dendritic spines on activated CA1 hippocampal neurons following learning and contextual recall. Hippocampal excitatory neurons play an integral role in associative memory formation. Activation of CA1 pyramidal neurons is observed during contextual recall in mice (Ji and Maren, 2008). Several studies also report formation of new spines on hippocampal neurons during fear conditioning (Matsuo et al., 2008; Restivo et al., 2009; Giachero et al., 2013; Frank et al., 2018). Indeed, dendritic spines can be considered physical representation of memory (Matsuzaki et al., 2004; Holtmaat and Svoboda, 2009; Kasai et al., 2010). Acquisition of new memories facilitates hippocampal spine formation and spine maturation following contextual fear learning and memory recall, particularly more recent memories (Restivo et al., 2009; Giachero et al., 2013), coinciding with the increased synthesis and recruitment of GluR1 to mature mushroom-type spines in the adult hippocampus (Matsuo et al., 2008). The strong memory trace associated with the fear conditioned response is consistent with an increase of total number of mature dendritic spines. Conversely, extinction of a fear memory induces spine loss, specifically dendritic spines that were formed during the learning phase (Lai et al., 2018). Further, reconditioning following extinction induces formation of new dendritic spines near the sites of spine formation that were induced during initial fear conditioning (Lai et al., 2018). In our study we observed an increase in the number of spines on CA1 neurons in trained astrocytes-specific ephrin-B1 KO mice compared to their WT counterparts, suggesting that astrocytic ephrin-B1 may act as a negative regulator of new spine formation in the adult hippocampus during learning. Astrocytic ephrin-B1 may affect new synapse formation during learning by competing with neuronal ephrin-B for binding to neuronal EphB receptors. Loss of several EphB receptors is known to affect synapse and dendritic spine formation in the hippocampus (Ethell et al., 2001; Henkemeyer et al., 2003).

Another finding of this study is that there is a selective formation of new spines on activated CA1 hippocampal

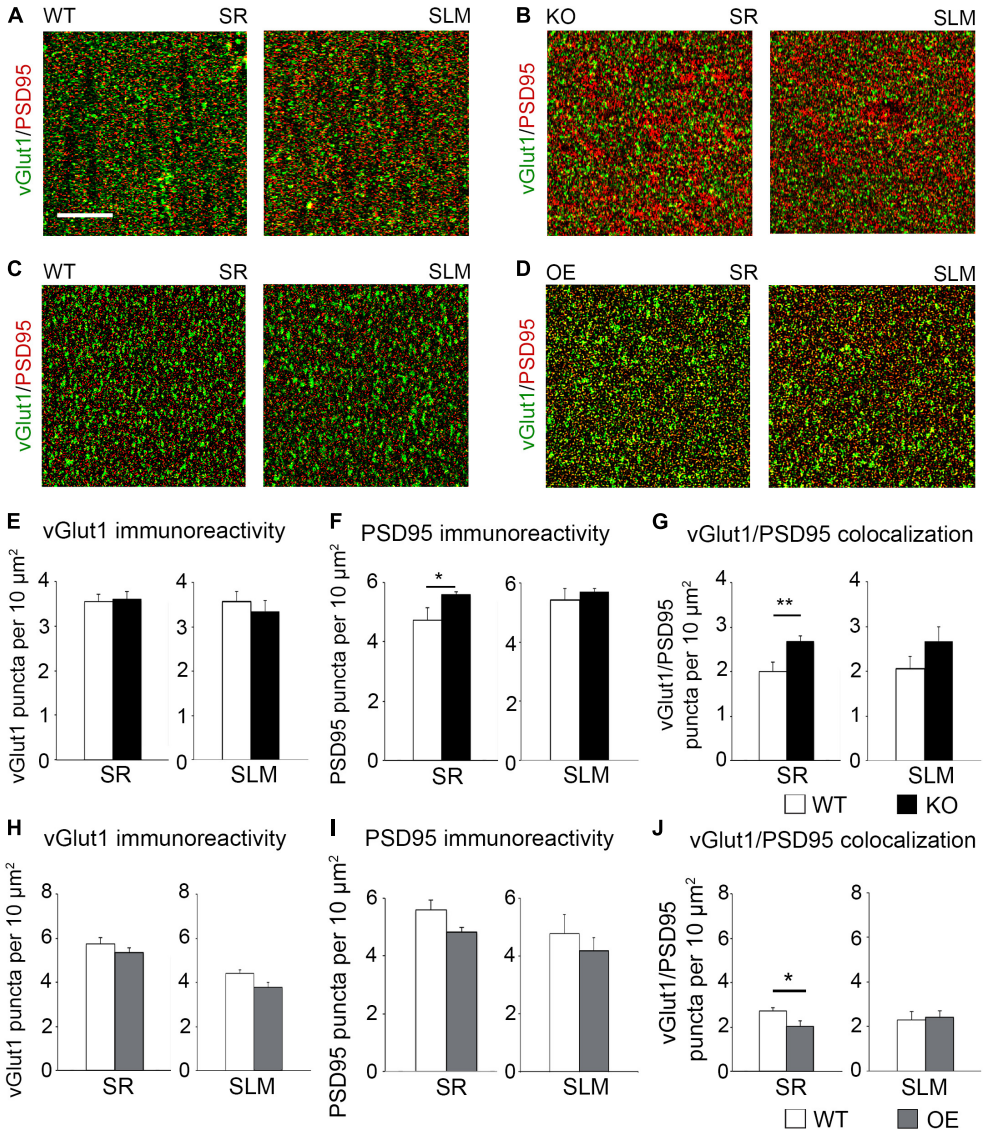

FIGURE 5 | Astrocytic ephrin-B1 negatively regulates the number of excitatory synaptic sites in CA1 hippocampus after fear conditioning. **(A–D)** Confocal images showing vGlut1 (green) and PSD95 (red) immunolabeling in WT **(A,C)**, KO **(B)**, and OE **(D)** in SR and SLM areas of the adult CA1 hippocampus 1 h after contextual recall. Scale bar is 20 µm. **(E–G)** Graphs show the density of vGlut1-positive puncta **(E)**, PSD95-postive puncta **(F)**, and vGlut1/PSD95 co-localization **(G)** per 10 μm^2 in the SR and SLM areas of the CA1 hippocampus of WT and KO mice. There was no difference in vGlut1 positive puncta between WT and KO mice. However, KO mice showed a significant increase in PSD95 puncta (**F**, *t*-test, $t_{(32)} = 2.104$, $p = 0.043$) and vGlut1/PSD95 colocalization (**G**, *t*-test, $t_{(29)} = 2.828$, $p = 0.008$) in the SR CA1 hippocampus. Graphs show mean values and error bars represent SEM. **(H–J)** Graphs show the density of vGlut1-positive puncta **(H)**, PSD95-positive puncta **(I)**, and vGlut1/PSD95 co-localization **(J)** in the SR and SLM areas of the CA1 hippocampus of WT and OE mice. There was no significant difference in vGlut1 **(H)** or PSD95 **(I)** puncta between WT and OE mice. OE mice showed a significant decrease in vGlut1/PSD95 colocalization (**J**, *t*-test, $t_{(32)} = 2.433$, $p = 0.022$). Graphs show mean values and error bars represent SEM; $^*p < 0.05$, $^{**}p < 0.01$.

neurons in WT mice. These new spines form in a close proximity of neighboring spines resulting in an overall increase in the number of spine clusters containing three spines. This is consistent with the published work showing that there are hotspots or preferential dendritic regions for spine clustering of two or more spines following contextual fear conditioning (Frank et al., 2018). Clustering of dendritic spines with learning have been demonstrated in layer 5 pyramidal neurons of mouse primary motor cortex following motor learning tasks (Fu et al., 2012) and clusters of axon-dendritic contacts were also observed in vestibular systems of barn owl following prism adaptation (McBride et al., 2008). In our study, we see a selective increase in the number of dendritic spines on activated c-Fos(+) CA1 hippocampal neurons in both WT and KO mice after contextual fear conditioning. However, the increase in spine density is impaired in OE group and we observed no difference in the number of spines and spine clusters between c-Fos(+)

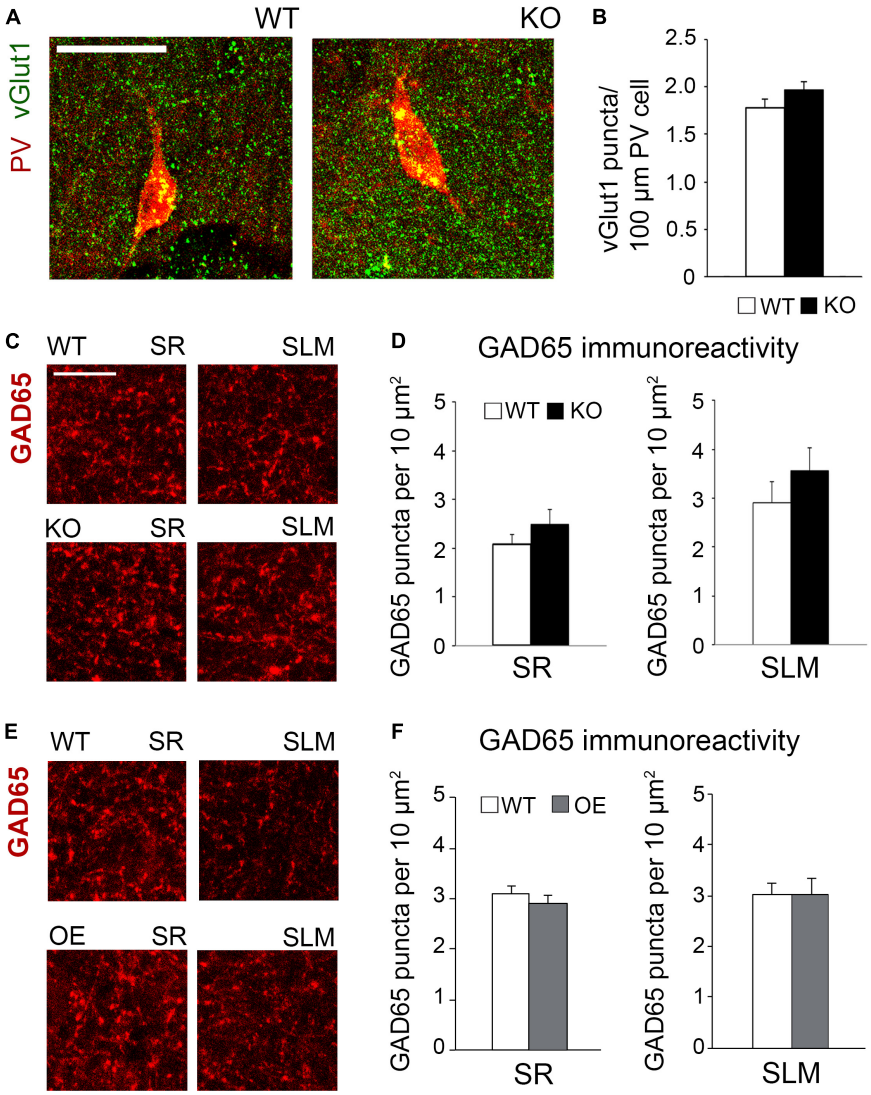

FIGURE 6 | Changes in astrocytic ephrin-B1 levels did not affect the excitatory vGlut1-positive puncta on PV interneurons in SP areas of CA1 hippocampus and inhibitory GAD65-positive puncta. **(A)** Confocal images showing vGlut1 (green) and PV (red) co-immunolabeling in the dorsal CA1 hippocampus of WT and KO adult mice 1 h after contextual recall. Scale bar is 100 µm. **(B)** Graphs show immunoreactivity of vGlut1 positive puncta per 100 µm PV cell in dorsal CA1 hippocampus of trained WT and KO mice. There was no significant difference in vGlut1/PV colocalization between trained WT and KO mice. **(C,E)** Confocal images showing GAD65 (red) immunolabeling in SR and SLM areas of the CA1 hippocampus of KO **(C)** or OE **(E)** mice and their WT counterparts 1 h after contextual recall. Scale bar is 50 µm. **(D)** Graphs show GAD65-positive puncta in the SR and SLM area of the CA1 hippocampus of trained WT and KO mice. There was no significant difference in the number of inhibitory GAD65-positive puncta between WT and KO mice. **(F)** Graphs show GAD65 puncta in the SR and SLM area of the CA1 hippocampus of trained WT and OE mice. No significant differences were seen in GAD65 immunoreactivity between WT and OE mice. Graphs show mean values and error bars represent SEM.

and c-Fos(−) CA1 neurons in the presence of ephrin-B1 overexpressing astrocytes. This is potentially due to reduced formation or increased elimination of dendritic spines on CA1 neurons, which most likely underlie impaired contextual recall in OE mice.

While the OE of ephrin-B1 in astrocytes affected spine numbers, the modulation of ephrin-B1 levels in astrocytes did not affect dendritic spine volume. Activity-dependent maturation of hippocampal synapses during memory formation was shown to promote structural changes to dendritic spines (Lichtman and Colman, 2000; Knott et al., 2006; Draft and Lichtman, 2009; Holtmaat and Svoboda, 2009) and to increase synaptic AMPA receptor levels in CA1 hippocampal neurons (Matsuo et al., 2008). Dendritic spines are diverse in structure and undergo activity-dependent morphological changes (Matsuzaki et al., 2004; Matsuo et al., 2008). The structural plasticity of hippocampal dendritic spines allows for spine maturation following learning and memory acquisition (Restivo et al., 2009; Giachero et al., 2013). Neuronal EphB receptors are shown to regulate dendritic spine maturation in hippocampal

neurons (Ethell et al., 2001; Henkemeyer et al., 2003) and clustering of AMPARs (Kayser et al., 2006). Activation of EphB2 forward signaling can facilitate the recruitment of AMPARs to synaptic sites (Kayser et al., 2006; Hussain et al., 2015), and ephrin-B reverse signaling can antagonize the internalization of GluR2 subunit of AMPAR allowing for the retention of AMPAR at the cell surface (Essmann et al., 2008). However, our studies show no changes in dendritic spine size between training WT and OE groups. Despite impaired increase in spine density and clustering on the dendrites of c-Fos(+) CA1 hippocampal neurons in OE mice, average size of dendritic spines was not significantly different between WT and KO or WT and OE groups.

Mature spines are larger in size and have larger postsynaptic densities (Harris et al., 1992), allowing for more AMPAR recruitment and anchorage (Ashby et al., 2006; Matsuzaki, 2007). As we observed no differences in dendritic spine size in both KO and OE mice compared to their WT counterparts, we also expected to see normal AMPAR recruitment. Indeed, we detected no differences in synaptic AMPAR levels between the groups, further confirming that the changes in astrocytic ephrin-B1 levels did not affect synaptic AMPAR levels. Although CA1 hippocampal neurons showed increased evoked AMPAR and NMDAR responses in trained KO mice compared to their WT counterparts, the ratio of AMPAR/NMDAR currents was comparable between WT and KO mice suggesting similar mature state of dendritic spines. It is most likely that mESPC amplitude is increased due to an overall increase in the number of functional dendritic spines/synapses on CA1 hippocampal neurons in KO compared to WT mice. In addition, we observed increased mEPSC frequency and amplitude in trained KO mice compared to naïve KO mice, suggesting an increase in number of functional synapses in KO mice following training, which is in agreement with dendritic spine analysis showing an increase in the number of spines on activated c-Fos (+) neurons compared to c-Fos (−) neurons.

Increased AMPAR and NMDAR responses both contribute to enhanced synaptic strength and long-term potentiation (LTP), which is an essential mechanism underlying learning (Bliss and Collingridge, 1993). EphB2 was also shown to modulate synaptic transmission by regulating trafficking and function of NMDAR (Dalva et al., 2000; Henderson et al., 2001; Takasu et al., 2002; Nolt et al., 2011). The ability of synaptic EphB2 receptor to regulate both AMPAR and NMDAR trafficking may influence hippocampal LTP and long-term depression (LTD; Grunwald et al., 2001; Henderson et al., 2001). Indeed, EphB2 loss was shown to attenuate LTP (Grunwald et al., 2001; Henderson et al., 2001) and to impair LTD (Grunwald et al., 2001). While the loss of EphB2 function impairs long-term memory formation, photo-activation of EphB2 using optogenetics during fear conditioning learning enhances long-term memory (Alapin et al., 2018). However, our previous study showed no effects of astrocytic ephrin-B1 deletion on LTP induction and consolidation in the adult hippocampus of naïve WT and KO mice (Koeppen et al., 2018).

Finally, we found no changes in GAD65-immunoreactivity in both ephrin-B1 KO and OE mice. Hippocampal dependent memory formation also requires input from local inhibitory neurons. In fact, ablation of $GABA_A$ receptor α5 subunit increased contextual recall (Crestani et al., 2002; Yee et al., 2004) and enhanced spatial learning in mice (Collinson et al., 2002). In addition, an inverse agonist to α5 subunit increased spatial learning (Chambers et al., 2004; Sternfeld et al., 2004). As $GABA_A$ receptor α5 subunit is highly expressed on hippocampal

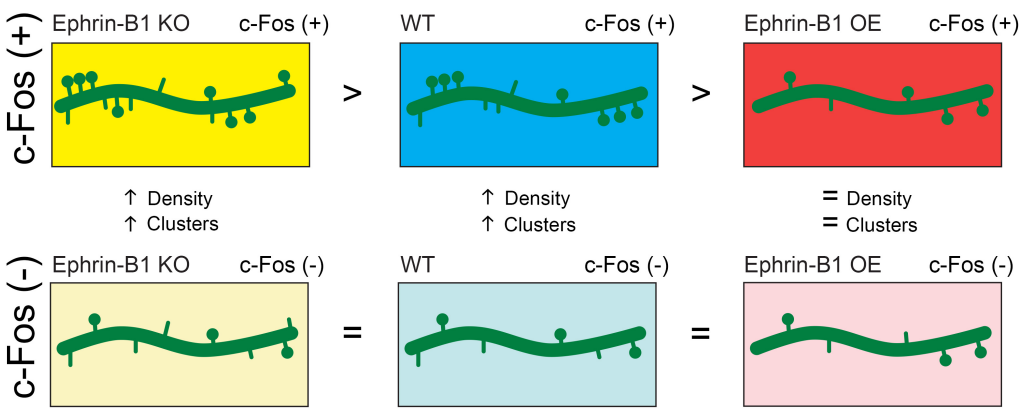

FIGURE 7 | Schematic depiction of the effect of astrocytic ephrin-B1 KO or OE on dendritic spine formation following training. Astrocytic ephrin-B1 regulates excitatory connections in the CA1 hippocampus during contextual memory formation in an activity dependent manner. c-Fos(+) neurons activated during contextual memory recall show higher dendritic spine density and clustering compared to non-activated c-Fos(–) neurons in WT and KO mice. In contrast, no changes in dendritic spine density and clustering were observed between c-Fos(+) and c-Fos(–) neurons in CA1 hippocampus containing astrocytes that overexpress ephrin-B1 (OE). There was a higher number of spines on c-Fos(+) neurons of KO mice compared to WT mice, whereas a lower spine density was observed on c-Fos(+) neurons of OE mice compared to WT mice, coinciding with the enhanced or impaired memory recall, respectively. No differences were detected in spine density on non-activated c-Fos(–) neurons between WT, KO, and OE mice. All together our findings suggest that astrocytic ephrin-B1 is a negative regulator of learning-induced spine formation on activated CA1 neurons.

pyramidal neurons (Pirker et al., 2000; Rudolph and Mohler, 2006), changes in inhibitory cell activity may be potentially involved in the observed effects of ephrin-B1 KO or OE in astrocytes on memory consolidation. However, after deletion or OE of ephrin-B1 in the adult astrocytes we observed no differences in overall numbers of GAD65 positive sites in the hippocampus of trained mice. Whole cell recording from CA1 hippocampal neurons also showed no differences in the amplitude or latency of evoked IPSCs, as well as mIPSC amplitude and frequency between adult WT and KO mice. In addition, deletion of astrocytic ephrin-B1 did not affect the number of vGlut1-positive puncta on PV-positive inhibitory interneurons in trained KO mice compared to WT mice. Previous studies suggest involvement of hippocampal PV cells in learning and memory. While activation of hippocampal PV interneurons was suggested to contribute to reduced contextual recall after fear extinction (Caliskan et al., 2016), interneurons in CA3 hippocampus expressing high levels of PV were shown to receive higher excitatory input following fear conditioning and also play a role in memory consolidation (Donato et al., 2013, 2015). High-PV expressing interneurons were shown to exhibit a higher excitatory to inhibitory input ratio compared to low-PV expressing interneurons (Donato et al., 2015). Although in our study astrocytic ablation and OE of ephrin-B1 affected the overall number of excitatory sites in the CA1 hippocampus, we did not see changes in inhibitory function between adult KO and WT mice.

The studies presented here suggest that astrocytic ephrin-B1 regulates excitatory connections in the CA1 hippocampus during contextual memory formation in an activity dependent manner (**Figure 7**). While deletion of ephrin-B1 in astrocytes does not affect formation of new spines on activated CA1 neurons, OE of ephrin-B1 in astrocytes impairs it, suggesting that ephrin-B1 is a negative regulator of learning-induced spine formation. Astrocytes have been shown to preferentially contact larger synapses and contribute to synapse stabilization and regulate synaptic activity (Haber et al., 2006; Witcher et al., 2007). However, the role of astrocytes in the formation of new synapses in the adult hippocampus during learning has not been explored yet. We propose that ephrin-B1 plays an important role in astrocyte-mediated new synapse formation during learning. However, it is still unclear whether synaptic activity directly regulate levels of ephrin-B1 in astrocytes and if selective up-regulation or down-regulation of ephrin-B1 in some astrocytes may, respectively, suppress or facilitate new synapse formation at specific dendritic domains induced by local changes in synaptic activity during learning, and potentially underlie memory encoding.

DATA AVAILABILITY STATEMENT

The raw data supporting the conclusions of this article will be made available by the authors, without undue reservation, to any qualified researcher.

ETHICS STATEMENT

The animal study was reviewed and approved by the UC Riverside Animal Care and Use Program.

AUTHOR CONTRIBUTIONS

AN, JK, and IE designed and performed the research, and wrote the manuscript. AN, JK, SW, and KM contributed to the unpublished reagents and analytic tools. AN, JK, SW, KM, ZF, and IE analyzed the data.

FUNDING

This research was supported by MH67121 grant from the NIMH (IE) and 1S10OD020042-01 grant from the Research Infrastructure Programs of the NIH. The authors declare no competing financial interests.

ACKNOWLEDGMENTS

The authors thank members of Drs. IE, Obenaus, and Hickmott laboratories for helpful discussions and comments. The authors also thank Arnold Palacios for technical support, Dr. Razak's lab for help with fear conditioning test, and David Carter for advice on confocal microscopy.

SUPPLEMENTARY MATERIAL

The Supplementary Material for this article can be found online at: https://www.frontiersin.org/articles/10.3389/fnsyn.2020.00010/full#supplementary-material

REFERENCES

Adamsky, A., Kol, A., Kreisel, T., Doron, A., Ozeri-Engelhard, N., Melcer, T., et al. (2018). Astrocytic activation generates de novo neuronal potentiation and memory enhancement. *Cell* 174, 59–71.e14. doi: 10.1016/j.cell.2018.05.002

Alapin, J. M., Dines, M., Vassiliev, M., Tamir, T., Ram, A., Locke, C., et al. (2018). Activation of EphB2 forward signaling enhances memory consolidation. *Cell Rep.* 23, 2014–2025. doi: 10.1016/j.celrep.2018.04.042

Alberini, C. M., Cruz, E., Descalzi, G., Bessieres, B., and Gao, V. (2018). Astrocyte glycogen and lactate: new insights into learning and memory mechanisms. *Glia* 66, 1244–1262. doi: 10.1002/glia.23250

Allen, N. J., Bennett, M. L., Foo, L. C., Wang, G. X., Chakraborty, C., Smith, S. J., et al. (2012). Astrocyte glypicans 4 and 6 promote formation of excitatory synapses via GluA1 AMPA receptors. *Nature* 486, 410–414. doi: 10.1038/nature11059

Allen, N. J., and Eroglu, C. (2017). Cell biology of astrocyte-synapse interactions. *Neuron* 96, 697–708. doi: 10.1016/j.neuron.2017.09.056

Anagnostaras, S. G., Gale, G. D., and Fanselow, M. S. (2001). Hippocampus and contextual fear conditioning: recent controversies and advances. *Hippocampus* 11, 8–17. doi: 10.1002/1098-1063(2001)11:1<8::aid-hipo1015>3.0.co;2-7

Araque, A., Parpura, V., Sanzgiri, R. P., and Haydon, P. G. (1999). Tripartite synapses: glia, the unacknowledged partner. *Trends Neurosci.* 22, 208–215. doi: 10.1016/s0166-2236(98)01349-6

Arvanitis, D. N., Behar, A., Drougard, A., Roullet, P., and Davy, A. (2014). Cortical abnormalities and non-spatial learning deficits in a mouse model of CranioFrontoNasal syndrome. *PLoS One* 9:e88325. doi: 10.1371/journal.pone.0088325

Ashby, M. C., Maier, S. R., Nishimune, A., and Henley, J. M. (2006). Lateral diffusion drives constitutive exchange of AMPA receptors at dendritic spines and is regulated by spine morphology. *J. Neurosci.* 26, 7046–7055. doi: 10.1523/jneurosci.1235-06.2006

Bliss, T. V., and Collingridge, G. L. (1993). A synaptic model of memory: long-term potentiation in the hippocampus. *Nature* 361, 31–39. doi: 10.1038/361031a0

Caliskan, G., Muller, I., Semtner, M., Winkelmann, A., Raza, A. S., Hollnagel, J. O., et al. (2016). Identification of parvalbumin interneurons as cellular substrate of fear memory persistence. *Cereb. Cortex* 26, 2325–2340. doi: 10.1093/cercor/bhw001

Castaneda-Castellanos, D. R., Flint, A. C., and Kriegstein, A. R. (2006). Blind patch clamp recordings in embryonic and adult mammalian brain slices. *Nat. Protoc.* 1, 532–542. doi: 10.1038/nprot.2006.75

Chambers, M. S., Atack, J. R., Carling, R. W., Collinson, N., Cook, S. M., Dawson, G. R., et al. (2004). An orally bioavailable, functionally selective inverse agonist at the benzodiazepine site of GABAA alpha5 receptors with cognition enhancing properties. *J. Med. Chem.* 47, 5829–5832. doi: 10.1021/jm040863t

Christopherson, K. S., Ullian, E. M., Stokes, C. C., Mullowney, C. E., Hell, J. W., Agah, A., et al. (2005). Thrombospondins are astrocyte-secreted proteins that promote CNS synaptogenesis. *Cell* 120, 421–433. doi: 10.1016/j.cell.2004.12.020

Chung, W. S., Allen, N. J., and Eroglu, C. (2015). Astrocytes control synapse formation, function, and elimination. *Cold Spring Harb. Perspect. Biol.* 7:a020370. doi: 10.1101/cshperspect.a020370

Chung, W. S., Clarke, L. E., Wang, G. X., Stafford, B. K., Sher, A., Chakraborty, C., et al. (2013). Astrocytes mediate synapse elimination through MEGF10 and MERTK pathways. *Nature* 504, 394–400. doi: 10.1038/nature12776

Clarke, L. E., and Barres, B. A. (2013). Emerging roles of astrocytes in neural circuit development. *Nat. Rev. Neurosci.* 14, 311–321. doi: 10.1038/nrn3484

Collinson, N., Kuenzi, F. M., Jarolimek, W., Maubach, K. A., Cothliff, R., Sur, C., et al. (2002). Enhanced learning and memory and altered GABAergic synaptic transmission in mice lacking the alpha 5 subunit of the GABAA receptor. *J. Neurosci.* 22, 5572–5580. doi: 10.1523/jneurosci.22-13-05572.2002

Crestani, F., Keist, R., Fritschy, J. M., Benke, D., Vogt, K., Prut, L., et al. (2002). Trace fear conditioning involves hippocampal alpha5 GABA(A) receptors. *Proc. Natl. Acad. Sci. U.S.A.* 99, 8980–8985. doi: 10.1073/pnas.142288699

Dalva, M. B., Takasu, M. A., Lin, M. Z., Shamah, S. M., Hu, L., Gale, N. W., et al. (2000). EphB receptors interact with NMDA receptors and regulate excitatory synapse formation. *Cell* 103, 945–956. doi: 10.1016/s0092-8674(00)00197-5

Dines, M., Grinberg, S., Vassiliev, M., Ram, A., Tamir, T., and Lamprecht, R. (2015). The roles of Eph receptors in contextual fear conditioning memory formation. *Neurobiol. Learn. Mem.* 124, 62–70. doi: 10.1016/j.nlm.2015.07.003

Donato, F., Chowdhury, A., Lahr, M., and Caroni, P. (2015). Early- and late-born parvalbumin basket cell subpopulations exhibiting distinct regulation and roles in learning. *Neuron* 85, 770–786. doi: 10.1016/j.neuron.2015.01.011

Donato, F., Rompani, S. B., and Caroni, P. (2013). Parvalbumin-expressing basket-cell network plasticity induced by experience regulates adult learning. *Nature* 504, 272–276. doi: 10.1038/nature12866

Draft, R. W., and Lichtman, J. W. (2009). It's lonely at the top: winning climbing fibers ascend dendrites solo. *Neuron* 63, 6–8. doi: 10.1016/j.neuron.2009.07.001

Essmann, C. L., Martinez, E., Geiger, J. C., Zimmer, M., Traut, M. H., Stein, V., et al. (2008). Serine phosphorylation of ephrinB2 regulates trafficking of synaptic AMPA receptors. *Nat. Neurosci.* 11, 1035–1043. doi: 10.1038/nn.2171

Ethell, I. M., Irie, F., Kalo, M. S., Couchman, J. R., Pasquale, E. B., and Yamaguchi, Y. (2001). EphB/syndecan-2 signaling in dendritic spine morphogenesis. *Neuron* 31, 1001–1013. doi: 10.1016/s0896-6273(01)00440-8

Fellin, T., Pascual, O., Gobbo, S., Pozzan, T., Haydon, P. G., and Carmignoto, G. (2004). Neuronal synchrony mediated by astrocytic glutamate through activation of extrasynaptic NMDA receptors. *Neuron* 43, 729–743. doi: 10.1016/j.neuron.2004.08.011

Frank, A. C., Huang, S., Zhou, M., Gdalyahu, A., Kastellakis, G., Silva, T. K., et al. (2018). Hotspots of dendritic spine turnover facilitate clustered spine addition and learning and memory. *Nat. Commun.* 9:422. doi: 10.1038/s41467-017-02751-2

Fu, M., Yu, X., Lu, J., and Zuo, Y. (2012). Repetitive motor learning induces coordinated formation of clustered dendritic spines in vivo. *Nature* 483, 92–95. doi: 10.1038/nature10844

Gao, V., Suzuki, A., Magistretti, P. J., Lengacher, S., Pollonini, G., Steinman, M. Q., et al. (2016). Astrocytic beta2-adrenergic receptors mediate hippocampal long-term memory consolidation. *Proc. Natl. Acad. Sci. U.S.A.* 113, 8526–8531. doi: 10.1073/pnas.1605063113

Garrett, A. M., and Weiner, J. A. (2009). Control of CNS synapse development by {gamma}-protocadherin-mediated astrocyte-neuron contact. *J. Neurosci.* 29, 11723–11731. doi: 10.1523/JNEUROSCI.2818-09.2009

Gerlai, R., Shinsky, N., Shih, A., Williams, P., Winer, J., Armanini, M., et al. (1999). Regulation of learning by EphA receptors: a protein targeting study. *J. Neurosci.* 19, 9538–9549. doi: 10.1523/jneurosci.19-21-09538.1999

Giachero, M., Calfa, G. D., and Molina, V. A. (2013). Hippocampal structural plasticity accompanies the resulting contextual fear memory following stress and fear conditioning. *Learn. Mem.* 20, 611–616. doi: 10.1101/lm.031724.113

Goshen, I., Brodsky, M., Prakash, R., Wallace, J., Gradinaru, V., Ramakrishnan, C., et al. (2011). Dynamics of retrieval strategies for remote memories. *Cell* 147, 678–689. doi: 10.1016/j.cell.2011.09.033

Grunwald, I. C., Korte, M., Wolfer, D., Wilkinson, G. A., Unsicker, K., Lipp, H. P., et al. (2001). Kinase-independent requirement of EphB2 receptors in hippocampal synaptic plasticity. *Neuron* 32, 1027–1040. doi: 10.1016/s0896-6273(01)00550-5

Haber, M., Zhou, L., and Murai, K. K. (2006). Cooperative astrocyte and dendritic spine dynamics at hippocampal excitatory synapses. *J. Neurosci.* 26, 8881–8891. doi: 10.1523/jneurosci.1302-06.2006

Halladay, A. K., Tessarollo, L., Zhou, R., and Wagner, G. C. (2004). Neurochemical and behavioral deficits consequent to expression of a dominant negative EphA5 receptor. *Brain Res. Mol. Brain Res.* 123, 104–111. doi: 10.1016/j.molbrainres.2004.01.005

Hama, H., Hara, C., Yamaguchi, K., and Miyawaki, A. (2004). PKC signaling mediates global enhancement of excitatory synaptogenesis in neurons triggered by local contact with astrocytes. *Neuron* 41, 405–415. doi: 10.1016/s0896-6273(04)00007-8

Harris, K. M., Jensen, F. E., and Tsao, B. (1992). Three-dimensional structure of dendritic spines and synapses in rat hippocampus (CA1) at postnatal day 15 and adult ages: implications for the maturation of synaptic physiology and long-term potentiation. *J. Neurosci.* 12, 2685–2705. doi: 10.1523/jneurosci.12-07-02685.1992

Hayashi-Takagi, A., Yagishita, S., Nakamura, M., Shirai, F., Wu, Y. I., Loshbaugh, A. L., et al. (2015). Labelling and optical erasure of synaptic memory traces in the motor cortex. *Nature* 525, 333–338. doi: 10.1038/nature15257

Henderson, J. T., Georgiou, J., Jia, Z., Robertson, J., Elowe, S., Roder, J. C., et al. (2001). The receptor tyrosine kinase EphB2 regulates NMDA-dependent synaptic function. *Neuron* 32, 1041–1056. doi: 10.1016/s0896-6273(01)00553-0

Henkemeyer, M., Itkis, O. S., Ngo, M., Hickmott, P. W., and Ethell, I. M. (2003). Multiple EphB receptor tyrosine kinases shape dendritic spines in the hippocampus. *J. Cell Biol.* 163, 1313–1326. doi: 10.1083/jcb.200306033

Henneberger, C., Papouin, T., Oliet, S. H., and Rusakov, D. A. (2010). Long-term potentiation depends on release of D-serine from astrocytes. *Nature* 463, 232–236. doi: 10.1038/nature08673

Hollingsworth, E. B., McNeal, E. T., Burton, J. L., Williams, R. J., Daly, J. W., and Creveling, C. R. (1985). Biochemical characterization of a filtered synaptoneurosome preparation from guinea pig cerebral cortex: cyclic adenosine 3′:5′-monophosphate-generating systems, receptors, and enzymes. *J. Neurosci.* 5, 2240–2253. doi: 10.1523/jneurosci.05-08-02240.1985

Holtmaat, A., and Svoboda, K. (2009). Experience-dependent structural synaptic plasticity in the mammalian brain. *Nat. Rev. Neurosci.* 10, 647–658. doi: 10.1038/nrn2699

Hussain, N. K., Thomas, G. M., Luo, J., and Huganir, R. L. (2015). Regulation of AMPA receptor subunit GluA1 surface expression by PAK3 phosphorylation. *Proc. Natl. Acad. Sci. U.S.A.* 112, E5883–E5890. doi: 10.1073/pnas.1518382112

Ji, J., and Maren, S. (2008). Differential roles for hippocampal areas CA1 and CA3 in the contextual encoding and retrieval of extinguished fear. *Learn. Mem.* 15, 244–251. doi: 10.1101/lm.794808

Kasai, H., Fukuda, M., Watanabe, S., Hayashi-Takagi, A., and Noguchi, J. (2010). Structural dynamics of dendritic spines in memory and cognition. *Trends Neurosci.* 33, 121–129. doi: 10.1016/j.tins.2010.01.001

Kayser, M. S., McClelland, A. C., Hughes, E. G., and Dalva, M. B. (2006). Intracellular and trans-synaptic regulation of glutamatergic synaptogenesis by EphB receptors. *J. Neurosci.* 26, 12152–12164. doi: 10.1523/JNEUROSCI.3072-06.2006

Knott, G. W., Holtmaat, A., Wilbrecht, L., Welker, E., and Svoboda, K. (2006). Spine growth precedes synapse formation in the adult neocortex in vivo. *Nat. Neurosci.* 9, 1117–1124. doi: 10.1038/nn1747

Koeppen, J., Nguyen, A. Q., Nikolakopoulou, A. M., Garcia, M., Hanna, S., Woodruff, S., et al. (2018). Functional consequences of synapse remodeling following astrocyte-specific regulation of Ephrin-B1 in the adult hippocampus. *J. Neurosci.* 38, 5710–5726. doi: 10.1523/JNEUROSCI.3618-17.2018

Lai, C. S., Franke, T. F., and Gan, W. B. (2012). Opposite effects of fear conditioning and extinction on dendritic spine remodelling. *Nature* 483, 87–91. doi: 10.1038/nature10792

Lai, C. S. W., Adler, A., and Gan, W. B. (2018). Fear extinction reverses dendritic spine formation induced by fear conditioning in the mouse auditory cortex. *Proc. Natl. Acad. Sci. U.S.A.* 115, 9306–9311. doi: 10.1073/pnas.1801504115

Lichtman, J. W., and Colman, H. (2000). Synapse elimination and indelible memory. *Neuron* 25, 269–278. doi: 10.1016/s0896-6273(00)80893-4

Liebl, D. J., Morris, C. J., Henkemeyer, M., and Parada, L. F. (2003). mRNA expression of ephrins and Eph receptor tyrosine kinases in the neonatal and adult mouse central nervous system. *J. Neurosci. Res.* 71, 7–22. doi: 10.1002/jnr.10457

Liu, X., Ramirez, S., Pang, P. T., Puryear, C. B., Govindarajan, A., Deisseroth, K., et al. (2012). Optogenetic stimulation of a hippocampal engram activates fear memory recall. *Nature* 484, 381–385. doi: 10.1038/nature11028

Matsuo, N., Reijmers, L., and Mayford, M. (2008). Spine-type-specific recruitment of newly synthesized AMPA receptors with learning. *Science* 319, 1104–1107. doi: 10.1126/science.1149967

Matsuzaki, M. (2007). Factors critical for the plasticity of dendritic spines and memory storage. *Neurosci. Res.* 57, 1–9. doi: 10.1016/j.neures.2006.09.017

Matsuzaki, M., Honkura, N., Ellis-Davies, G. C., and Kasai, H. (2004). Structural basis of long-term potentiation in single dendritic spines. *Nature* 429, 761–766. doi: 10.1038/nature02617

McBride, T. J., Rodriguez-Contreras, A., Trinh, A., Bailey, R., and Debello, W. M. (2008). Learning drives differential clustering of axodendritic contacts in the barn owl auditory system. *J. Neurosci.* 28, 6960–6973. doi: 10.1523/jneurosci.1352-08.2008

Milner, B., Squire, L. R., and Kandel, E. R. (1998). Cognitive neuroscience and the study of memory. *Neuron* 20, 445–468.

Neves, G., Cooke, S. F., and Bliss, T. V. (2008). Synaptic plasticity, memory and the hippocampus: a neural network approach to causality. *Nat. Rev. Neurosci.* 9, 65–75. doi: 10.1038/nrn2303

Newman, L. A., Korol, D. L., and Gold, P. E. (2011). Lactate produced by glycogenolysis in astrocytes regulates memory processing. *PLoS One* 6:e28427. doi: 10.1371/journal.pone.0028427

Nikolakopoulou, A. M., Koeppen, J., Garcia, M., Leish, J., Obenaus, A., and Ethell, I. M. (2016). Astrocytic ephrin-B1 regulates synapse remodeling following traumatic brain injury. *ASN Neuro* 8, 1–18. doi: 10.1177/1759091416630220

Nishiyama, H., Knopfel, T., Endo, S., and Itohara, S. (2002). Glial protein S100B modulates long-term neuronal synaptic plasticity. *Proc. Natl. Acad. Sci. U.S.A.* 99, 4037–4042. doi: 10.1073/pnas.052020999

Nolt, M. J., Lin, Y., Hruska, M., Murphy, J., Sheffler-Colins, S. I., Kayser, M. S., et al. (2011). EphB controls NMDA receptor function and synaptic targeting in a subunit-specific manner. *J. Neurosci.* 31, 5353–5364. doi: 10.1523/JNEUROSCI.0282-11.2011

Pirker, S., Schwarzer, C., Wieselthaler, A., Sieghart, W., and Sperk, G. (2000). GABA(A) receptors: immunocytochemical distribution of 13 subunits in the adult rat brain. *Neuroscience* 101, 815–850. doi: 10.1016/s0306-4522(00)00442-5

Restivo, L., Vetere, G., Bontempi, B., and Ammassari-Teule, M. (2009). The formation of recent and remote memory is associated with time-dependent formation of dendritic spines in the hippocampus and anterior cingulate cortex. *J. Neurosci.* 29, 8206–8214. doi: 10.1523/jneurosci.0966-09.2009

Rudolph, U., and Mohler, H. (2006). GABA-based therapeutic approaches: GABAA receptor subtype functions. *Curr. Opin. Pharmacol.* 6, 18–23. doi: 10.1016/j.coph.2005.10.003

Sala, C., and Segal, M. (2014). Dendritic spines: the locus of structural and functional plasticity. *Physiol. Rev.* 94, 141–188. doi: 10.1152/physrev.00012.2013

Segal, M. (2017). Dendritic spines: morphological building blocks of memory. *Neurobiol. Learn. Mem.* 138, 3–9. doi: 10.1016/j.nlm.2016.06.007

Sternfeld, F., Carling, R. W., Jelley, R. A., Ladduwahetty, T., Merchant, K. J., Moore, K. W., et al. (2004). Selective, orally active gamma-aminobutyric acidA alpha5 receptor inverse agonists as cognition enhancers. *J. Med. Chem.* 47, 2176–2179. doi: 10.1021/jm031076j

Strekalova, T., Zorner, B., Zacher, C., Sadovska, G., Herdegen, T., and Gass, P. (2003). Memory retrieval after contextual fear conditioning induces c-Fos and JunB expression in CA1 hippocampus. *Genes Brain Behav.* 2, 3–10. doi: 10.1034/j.1601-183x.2003.00001.x

Suzuki, A., Stern, S. A., Bozdagi, O., Huntley, G. W., Walker, R. H., Magistretti, P. J., et al. (2011). Astrocyte-neuron lactate transport is required for long-term memory formation. *Cell* 144, 810–823. doi: 10.1016/j.cell.2011.02.018

Tadi, M., Allaman, I., Lengacher, S., Grenningloh, G., and Magistretti, P. J. (2015). Learning-induced gene expression in the hippocampus reveals a role of neuron -astrocyte metabolic coupling in long term memory. *PLoS One* 10:e0141568. doi: 10.1371/journal.pone.0141568

Takasu, M. A., Dalva, M. B., Zigmond, R. E., and Greenberg, M. E. (2002). Modulation of NMDA receptor-dependent calcium influx and gene expression through EphB receptors. *Science* 295, 491–495. doi: 10.1126/science.1065983

Tonegawa, S., Liu, X., Ramirez, S., and Redondo, R. (2015). Memory engram cells have come of age. *Neuron* 87, 918–931. doi: 10.1016/j.neuron.2015.08.002

Trabalza, A., Colazingari, S., Sgobio, C., and Bevilacqua, A. (2012). Contextual learning increases dendrite complexity and EphrinB2 levels in hippocampal mouse neurons. *Behav. Brain Res.* 227, 175–183. doi: 10.1016/j.bbr.2011.11.008

Twigg, S. R., Kan, R., Babbs, C., Bochukova, E. G., Robertson, S. P., Wall, S. A., et al. (2004). Mutations of ephrin-B1 (EFNB1), a marker of tissue boundary formation, cause craniofrontonasal syndrome. *Proc. Natl. Acad. Sci. U.S.A.* 101, 8652–8657. doi: 10.1073/pnas.0402819101

Wieland, I., Jakubiczka, S., Muschke, P., Cohen, M., Thiele, H., Gerlach, K. L., et al. (2004). Mutations of the ephrin-B1 gene cause craniofrontonasal syndrome. *Am. J. Hum. Genet.* 74, 1209–1215. doi: 10.1086/421532

Willi, R., Winter, C., Wieske, F., Kempf, A., Yee, B. K., Schwab, M. E., et al. (2012). Loss of EphA4 impairs short-term spatial recognition memory performance and locomotor habituation. *Genes Brain Behav.* 11, 1020–1031. doi: 10.1111/j.1601-183X.2012.00842.x

Witcher, M. R., Kirov, S. A., and Harris, K. M. (2007). Plasticity of perisynaptic astroglia during synaptogenesis in the mature rat hippocampus. *Glia* 55, 13–23. doi: 10.1002/glia.20415

Yang, Y., Wang, X. B., Frerking, M., and Zhou, Q. (2008). Spine expansion and stabilization associated with long-term potentiation. *J. Neurosci.* 28, 5740–5751. doi: 10.1523/JNEUROSCI.3998-07.2008

Yee, B. K., Hauser, J., Dolgov, V. V., Keist, R., Mohler, H., Rudolph, U., et al. (2004). GABA receptors containing the alpha5 subunit mediate the trace effect in aversive and appetitive conditioning and extinction of conditioned fear. *Eur. J. Neurosci.* 20, 1928–1936. doi: 10.1111/j.1460-9568.2004.03642.x

Conflict of Interest: The authors declare that the research was conducted in the absence of any commercial or financial relationships that could be construed as a potential conflict of interest.

frontiers in Synaptic Neuroscience

REVIEW
published: 17 April 2020
doi: 10.3389/fnsyn.2020.00012

The Role of Rac GTPase in Dendritic Spine Morphogenesis and Memory

*Joana Freitas Costa, Monica Dines and Raphael Lamprecht**

Sagol Department of Neurobiology, Faculty of Natural Sciences, University of Haifa, Haifa, Israel

The ability to form memories in the brain is needed for daily functions, and its impairment is associated with human mental disorders. Evidence indicates that long-term memory (LTM)-related processes such as its consolidation, extinction and forgetting involve changes of synaptic efficacy produced by alterations in neural transmission and morphology. Modulation of the morphology and number of dendritic spines has been proposed to contribute to changes in neuronal transmission mediating such LTM-related processes. Rac GTPase activity is regulated by synaptic activation and it can affect spine morphology by controlling actin-regulatory proteins. Recent evidence shows that changes in Rac GTPase activity affect memory consolidation, extinction, erasure and forgetting and can affect spine morphology in brain areas that mediate these behaviors. Altered Rac GTPase activity is associated with abnormal spine morphology and brain disorders. By affecting Rac GTPase activity we can further understand the roles of spine morphogenesis in memory. Moreover, manipulation of Rac GTPase activity may serve as a therapeutic tool for the treatment of memory-related brain diseases.

Keywords: dendritic spines, Rac1 GTPase, actin cytoskeleton, memory consolidation, memory forgetting, memory extinction, memory erasure

OPEN ACCESS

Edited by:
Menahem Segal,
Weizmann Institute of Science, Israel

Reviewed by:
Christine Gall,
University of California, Irvine, United States
Peter Penzes,
Northwestern University, United States

***Correspondence:**
Raphael Lamprecht
rlamp@research.haifa.ac.il

Received: *07 November 2019*
Accepted: *04 March 2020*
Published: *17 April 2020*

Citation:
Costa JF, Dines M and Lamprecht R (2020) The Role of Rac GTPase in Dendritic Spine Morphogenesis and Memory. Front. Synaptic Neurosci. 12:12. doi: 10.3389/fnsyn.2020.00012

DENDRITIC SPINES AND THEIR ROLE IN MEMORY

Much evidence show that memories are created by alterations in synaptic transmission. These synaptic modifications can be formed by structural changes at postsynaptic sites that can be then actively stabilized over hours or days. These alterations are suggested to form a new neuronal circuit that constitutes the memory trace that, upon memory retrieval, will lead to new intrinsic and possibly behavioral responses. It has been shown that learning leads to structural and functional changes of dendritic spines and that such changes are correlated with memory strength and its retention (Lamprecht and LeDoux, 2004; Caroni et al., 2012; Bailey et al., 2015; Basu and Lamprecht, 2018). Moreover, disruption of such structural changes is associated with memory impairment.

Structure and Function of Dendritic Spines

Dendritic spines are neuronal dendritic protrusions that contain mainly excitatory synapses (Nimchinsky et al., 2002; Lamprecht and LeDoux, 2004; Newpher and Ehlers, 2009;

Nishiyama and Yasuda, 2015). Dendritic spines are subdivided into several categories according to their morphology (Peters and Kaiserman-Abramof, 1970) that include spines with no visible neck (stubby spines), thin spines with a discernable neck and a small head, mushroom spines and branched spines. Mushroom spines are easily distinguished by their short length neck and large head and branched spines have multiple heads that emerge from a common origin (Harris et al., 1992). Interestingly, Tønnesen et al. (2014) showed, using stimulated emission depletion (STED) microscopy, that stubby spines seem to be overreported since short-necked spines may appear to have a stubby appearance in light microscopy (Tønnesen et al., 2014). Dendritic filopodia are protrusions that are involved in sampling for presynaptic partners and are considered as precursors of dendritic spines (Hering and Sheng, 2001; Matus, 2005). As mentioned above, dendritic spines are known to receive mainly excitatory synaptic inputs. However, in recent years, it has been shown that dendritic spines can contain inhibitory synapses and become dually innervated by excitatory and inhibitory inputs (Villa et al., 2016).

Dendritic spines include a dense structure called the postsynaptic density (PSD), which contains necessary components for synaptic transmission such as α-amino-3-hydroxy-5-methyl-4-isoxazolepropionic acid (AMPA) receptors and *N*-methyl-D-aspartate (NMDA) receptors, PSD organization proteins (e.g. scaffolding proteins), and proteins involved in formation and modulation of synaptic structure and transmission (e.g. Eph and ephrins and neurotrophic receptors) and adhesion (Verpelli et al., 2014). In addition to these proteins, spines also contain actin and actin-binding and regulatory proteins that affect spine morphology (Hotulainen and Hoogenraad, 2010; Chazeau et al., 2014; Verpelli et al., 2014). These proteins include F-actin regulatory proteins that are involved in actin nucleation such as formins, WAVE and Arp2/3, proteins that regulate actin polymerization such as cofilin and profilin that are involved in actin depolymerization and polymerization, respectively, and F-actin capping proteins that block the exchange of actin subunits at F-actin barbed end. These actin regulatory proteins are controlled by upstream molecules such as small GTPases that are in turn regulated by guanine nucleotide exchange factors (GEFs) and GTPase-accelerating proteins (GAPs) (Duman et al., 2015). Small GTPase GEFs and GAPs are responsive to synaptic stimulation and thus can mediate between synaptic activation, changes in actin dynamics and structure and spine morphogenesis.

Changes in the morphology of spines may influence neuronal functions that subserve the formation of memory, such as synaptic transmission and efficacy. For example, synaptic transmission is correlated with the dimension of spine structure. It is shown that a higher level of AMPA receptors tends to be found in spines with large postsynaptic densities (PSDs) than in spines with smaller PSDs (e.g. Takumi et al., 1999). Since the dimensions of the spine head are correlated with the area of the PSD (Harris and Stevens, 1989), it is implied that more glutamate receptors are expressed in the spine with larger head than that with smaller head. In addition, a correlation between the spine head volume and the amplitudes of currents in the spine is detected, showing that spine head volume is approximately proportional to the distribution of functional AMPA receptors (Noguchi et al., 2011).

Synaptic efficacy is also affected by the geometry of the spine neck. Changes in the morphology of spine neck appears to affect the amplification of local voltage in the spine and the compartmentalization of biochemical components, such as of Ca^{2+}, within the spine head (Noguchi et al., 2005) and affect bidirectional diffusion of material from dendrite to spines and signal transduction (Bloodgood and Sabatini, 2005; Gray et al., 2006; Santamaria et al., 2006). Spines with thinner longer necks confine more molecules. Thus, synaptic efficacy and also neuronal function may be affected by changes in the spine neck (Araya et al., 2006, 2014). For example, small somatic voltage contributions are detected in spines with a long neck. The pairing of synaptic stimulation with postsynaptic activity can lead to the shortening of the spine neck, alterations in the input/output gain and increase in synaptic efficacy in pyramidal neurons (Araya et al., 2014). Tønnesen et al. (2014) show that the spine neck becomes wider and shorter after long-term potentiation. They predict that such morphological changes will preserve overall biochemical compartmentalization and lead to a drop in spine head excitatory postsynaptic potential (EPSP).

The aforementioned observations show that dendritic spine morphology and the content and the activity of molecules within the spine can affect synaptic efficacy and neuronal transmission. Spine morphology and molecular function can be regulated by synaptic activity that is similar to that detected during learning. In turn, changes in these spine parameters that affect neuronal function, such as alteration in the response of the neuron to incoming inputs, may constitute the memory trace. Such a memory trace is expected to last and to subserve long-term memory (LTM) persistence. Indeed, studies indicate that spine structure can last for a long period of time and thus may support an enduring memory trace (Basu and Lamprecht, 2018).

Dendritic Spines in Memory Formation

Several lines of evidence have shown that changes in dendritic spine morphology and density and modifications in spine PSD are associated with memory formation (Lamprecht and LeDoux, 2004; Bailey et al., 2015). For example, the density of dendritic spines in the anterior cingulate cortex and hippocampal cornu ammonis 1 (CA1) is increased following contextual fear conditioning (Restivo et al., 2009; Vetere et al., 2011). Auditory fear conditioning extinction leads to an increased spine formation in pyramidal neurons located in layer V in the mouse frontal association cortex, whereas fear conditioning induces spine elimination in this brain region (Lai C. S. et al., 2012). Fear conditioning decreases spine head volume in the lateral amygdala (LA) and leads to an increase in the PSD area in the smooth endoplasmic reticulum (sER)-free spines in LA (Ostroff et al., 2010). Auditory fear conditioning leads to putative LA–auditory cortex (ACx) synaptic pairs, as it increases the pathway-specific formation of LA axons buttons in ACx and dendritic spines of pyramidal cells in layer V of ACx (Yang et al., 2016). Animals trained with conditioned place preference show increased levels of spine density within the basolateral amygdala complex (Young

et al., 2014). Changes in spines are formed in the motor cortex by learning and is therefore suggested to provide a structural basis for spatial coding of motor memory (Fu et al., 2012). In addition, evidence indicates that spines morphological changes and new spines induced by learning can become stable for a long period of time to maintain LTM. For example, it was shown that the amount of the stable spines is correlated with performance after learning (Yang et al., 2009). Training for a forelimb reaching task leads to new dendritic spine growth that is preferentially stabilized by subsequent training sessions (Xu et al., 2009).

These results show that learning leads to changes in spine morphology and density and that some of the changes in spines persist over a long period of time. However, several questions remain to be clarified. Does spine morphogenesis underlie memory formation and maintenance? What are the molecular mechanisms that mediate such changes and are they involved in memory? Can we affect spine morphology to treat brain diseases? The study of Rac GTPase allows an insight into the role of spine morphogenesis in memory and may provide critical answers for these questions.

Rac GTPase AND SPINE MORPHOGENESIS

Rac GTPase and Its Regulation

Rac is a small (∼21 kDa) GTPase and is a member of the Rho family of GTPases. Rac GTPase family consists of four members Rac1–3 and RhoG. Rac GTPase cycles between GTP (active)-bound state and GDP (inactive)-bound state (Heasman and Ridley, 2008). The GTP/GDP cycle is regulated by proteins that activate Rac GTPases by catalyzing GDP/GTP exchange (GEFs) or inhibit Rac GTPases by stimulating GTP hydrolysis (GAPs) (Duman et al., 2015).

Rac1 GTPase activity is regulated by synaptic extracellular signaling through synaptic receptors involved in spine morphogenesis (Penzes et al., 2008; **Figure 1**). For example, it has been shown that NMDA receptor-induced CaMKII activation is important for spine plasticity (Maletic-Savatic et al., 1999; Jourdain et al., 2003; Matsuzaki et al., 2004). NMDA receptor activation induces phosphorylation of the GEF kalirin-7, in a CaMKII-dependent manner, leading to the activation of small GTPase Rac1 and rapid enlargement of spines. Moreover, it is shown that kalirin is required for the long-term maintenance of spines (Xie et al., 2007). Additional study has shown a role for kalirin-7 regulator disrupted-in-schizophrenia 1 (DISC1) and Rac1 in modulating the structure and function of spines (Hayashi-Takagi et al., 2010). Another example of a Rac-GEF that is responsive to glutamate stimulation is Tiam1 that can be phosphorylated by CaMKII (Fleming et al., 1999). NMDA-receptor-mediated increase in calcium results in phosphorylation of Tiam1 and the increase in its GEF activation (Tolias et al., 2005). Tiam1 knockdown was shown to reduce dendritic spine density and lead to the simplification of neuronal dendritic tree (Tolias et al., 2005). Tiam1 is also activated by brain-derived neurotrophic factor (BDNF) and its receptor tropomyosin-related kinase B (TrkB). TrkB phosphorylation at S478 controls its interaction with Tiam1 leading to Rac1 activation during activity-dependent dendritic spine remodeling (Lai K. O. et al., 2012). In neurons that express a dominant-negative form of Tiam1, the induction of spine formation and enlargement by BDNF was abolished (Lai K. O. et al., 2012). Another study has shown that the spreading of Rac1 signaling out of the stimulated spine, mediated by BDNF–TrkB activation, is needed for facilitating structural long-term potentiation (sLTP) in nearby spines (Hedrick et al., 2016). Rac1 GTPase is also regulated by additional synaptic receptors such as EphB, whose activation leads to Rho-GEF kalirin translocation to the synapse and activation of Rac1 and its downstream effector p21-activated kinase (PAK). Overexpression of dominant-negative EphB receptor eliminates ephrin-induced spine development (Penzes et al., 2003). EphA-mediated spine morphogenesis in hippocampal neurons is suppressed by disruption of the Rac-GAP α2-chimaerin (Iwata et al., 2015). Synaptic signaling that activates PKC is also involved in Rac1-mediated synaptic morphogenesis, as it was shown that molecular pathways that involve Rac1 and Rho-A and are activated by PKC produce actin-based structural plasticity in dendrites and spines (Pilpel and Segal, 2004).

Thus, Rac GTPase is regulated by synaptic receptors and signaling molecules that have been shown to be involved in memory formation, such as NMDAR, EphB, and TrkB. Therefore, Rac GTPase can mediate between synaptic activation during learning and cellular and molecular activities that affect changes in spine morphology and synaptic transmission that underlie synaptic plasticity and memory formation. The actin cytoskeleton subserves neuronal morphology and synaptic transmission, and its dynamics and structure are intimately mediated by synaptic activation and Rac GTPase activity. Thus, the actin cytoskeleton appears to mediate between learning-induced Rac GTPase activity and cellular events that mediate memory formation.

Rac GTPase-Regulated Pathways and Their Effects on the Neuronal Actin Cytoskeleton

The active Rac GTPase exerts its effects by binding and activating different effectors. One such example is the activation of PAK by Rac. Active PAK, in turn, phosphorylates LIM kinase (LIMK), which will then phosphorylate cofilin inhibiting, consequently, its actin depolymerization activity affecting, therefore, the content of actin filaments (Lappalainen and Drubin, 1997; Arber et al., 1998; Yang et al., 1998; Edwards et al., 1999). This pathway affects the actin cytoskeleton network in the dendritic spine and spine morphology. For example, the normal distribution of filamentous actin (higher level of filamentous actin in spines compared to the adjacent dendritic area) in hippocampal neurons, was disrupted in LIMK-1 knockout (KO) neurons. These KO neurons show a low level of actin filaments in spines, which is not significantly higher than that of other dendritic areas, as opposed to neurons from wild-type animals showing higher filamentous actin in spine heads compared to the adjacent dendritic area. These results indicate that the high level of actin filaments in

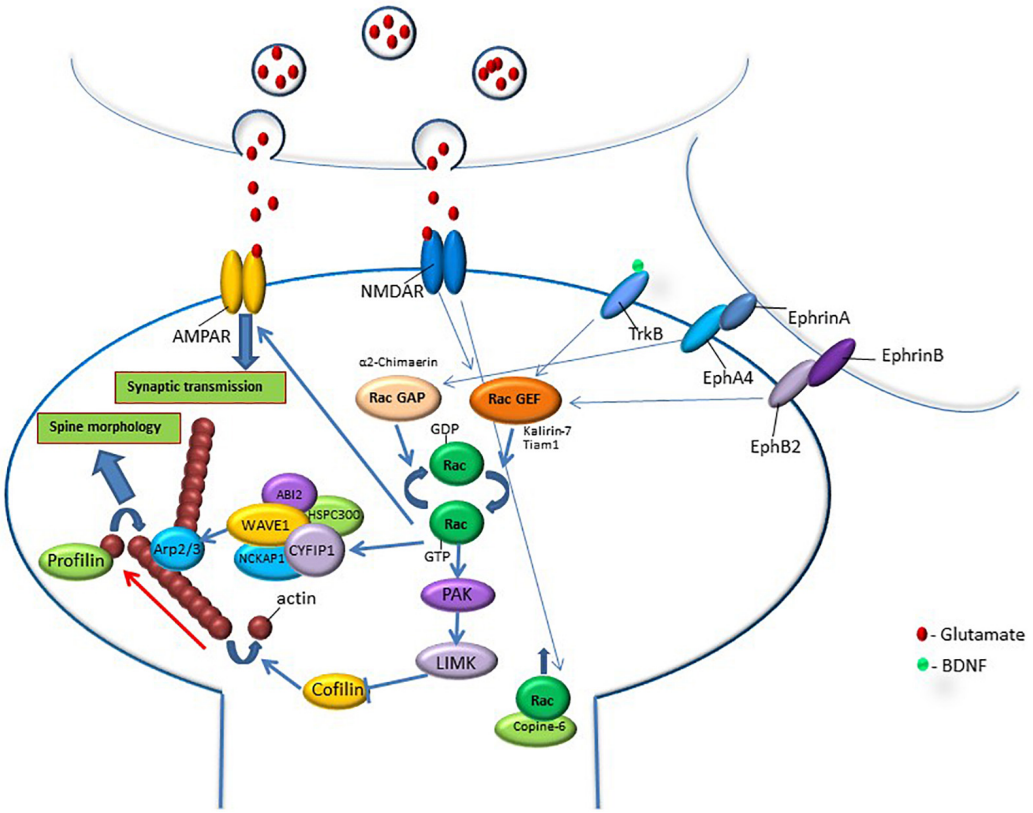

FIGURE 1 | Rac GTPase activity is regulated by synaptic activation through synaptic receptors that are known to be involved in memory formation such as NMDA, Trk, and Eph receptors. Activation of these synaptic receptors leads to the regulation of RacGEFs or RacGAPs that activate or inhibit Rac GTPase, respectively. Rac GTPase regulates downstream effectors that can affect spine morphology and synaptic transmission. Rac GTPase exerts its effects on spine morphology through the regulation of molecules that affect signaling pathways that control actin-regulatory proteins. In its active state, Rac GTPase activates the PAK-LIMK-cofilin pathway that can control actin dynamics through the inhibition of cofilin, an actin-depolymerizing protein. Rac GTPase also regulates actin network through the modulation of the WAVE-Arp2/3 pathway that, in turn, regulates actin nucleation and actin branching. Both cofilin and Arp2/3 regulation of the actin cytoskeleton affect spine morphology. In addition, Rac GTPase may regulate synaptic efficacy by controlling AMPA receptor content in the synapse. Rac1 GTPase protein level in the spine and its effects on spine functions can be regulated by calcium-induced translocation of Rac1 GTPase into the spine by copine-6. The correlation between Rac GTPase activity and changes in spine morphology, synaptic transmission and memory indicates that Rac GTPase regulates spine functions that can mediate various stages of memory formation, erasure, extinction and forgetting.

spines is maintained by LIMK activity (Meng et al., 2002). LIMK regulates actin polymerization by phosphorylation and inhibition of cofilin (Arber et al., 1998). Cofilin regulates actin dynamics and spine morphology. Mice in which n-cofilin (a non-muscle cofilin) was removed postnatally (N-cofflx/flx,CaMKII-cre) from principal neurons exhibit an increase of 50–60% in the F/G-actin ratio in hippocampus and cortex synaptosomes when compared to controls (Rust et al., 2010). Decreased amounts of cofilin-1 lead to a decrease in actin filament turnover rates in spines (Hotulainen et al., 2009).

The aforementioned observations show that molecules in this Rac1-cofilin pathway (Rac, PAK, LIMK, and cofilin), as well as in other pathways (e.g. Rac1-WAVE, see below), are intimately involved in the regulation of actin cytoskeleton structure. The actin cytoskeleton was shown to mediate the formation and elimination, morphology, motility and stability of dendritic spines (Halpain et al., 1998; Matus, 2000; Schubert and Dotti, 2007; Honkura et al., 2008; Hotulainen and Hoogenraad, 2010; Chazeau et al., 2014). Actin polymerization affects spine head structure. For example, glutamate-stimulation-induced spine head enlargement is dependent on actin polymerization (Matsuzaki et al., 2004). In addition, actin may be involved in affecting the morphology of the spine neck. A biophysical model suggests that the stabilization of spines is assisted by the constriction of the spine neck, thus pointing to a role in stabilization and maintenance for F-actin ring-like structures that are consistently found in the spine neck (Miermans et al., 2017). Thus, Rac GTPase can affect spine morphology through the control of actin-regulatory proteins.

Rac GTPase Effects on Dendritic Spine Morphogenesis

Modulation of Rac GTPase activity leads to changes in neuronal morphology of dendritic spine. For example, expression of a dominant-negative form of Rac1 results in the elimination of

dendritic spines in the hippocampus (Nakayama et al., 2000), and RacV12 (constitutively active mutant) increases spine density and reduces spine size (Tashiro et al., 2000). Spines in Purkinje neurons of transgenic mice expressing constitutively active Rac1 are reduced in size but increased in number (Luo et al., 1996). The mean spine head area is significantly larger, and the mean PSD length is significantly increased in mice that are devoid of Rac1 in excitatory neurons in the forebrain (Haditsch et al., 2009). Overexpression of a dominant-negative Rac1 (Rac1-DN) in cultured primary hippocampal neurons led to a reduced spine density, to longer and thin filopodia-like spine, and reduced synaptic motility. On the other hand, more lamellipodia-like synapses with a large spine head are produced following the expression of constitutively active Rac1 (Rac1-CA) (Liu et al., 2016). Activation by light of a photoactivatable Rac1 GTPase (activated synapse targeting photoactivatable Rac1; AS-PA-Rac1) in selected spines of neurons in the motor cortex leads to shrinkage of the AS-PA-Rac1-containing spines (Hayashi-Takagi et al., 2015). Overexpression of Rac1 in hippocampal slices induced a significant increase in spine density and AMPAR clustering, leading to an increase in both frequency and amplitude of miniature excitatory synaptic currents (mEPSCs) (Wiens et al., 2005). Besides Rac1 role in spine morphogenesis, Rac3 isoform also displays a role in spine morphology since overexpression of either Rac1 or Rac3 GTPases leads to an increase in spine density (Pennucci et al., 2019). Rac3 is more effective in promoting mature spine enlargement and Rac1 appears to be more efficient in inducing spine formation. Double knockout of both Rac1 and Rac3 genes inhibits the formation of dendritic spines and induces an increase in dendritic protrusions such as filopodia (Corbetta et al., 2009; Pennucci et al., 2019).

Rac GTPase effectors are also involved in the regulation of spine morphology. PAK is involved in neuronal morphogenesis. Cortical neurons in the forebrain of dominant-negative PAK (dnPAK) transgenic mice exhibit fewer spines and an increase in the proportion of larger synapses (Hayashi et al., 2004). PAK exerts its effects through LIMK and cofilin. LIMK can be directly phosphorylated and activated by PAK (Edwards et al., 1999). In LIMK knockout mice, most of the spines have thick neck and small head in contrast to wild-type mice where the majority of spines have large head and thin neck (Meng et al., 2002). LIMK phosphorylates and inhibits cofilin function (Arber et al., 1998). Active cofilin promotes actin depolymerization and is an essential regulator of actin dynamics in neurons (Rust, 2015). N-cofflx/flx,CaMKII-cre mice (n-cofilin removed postnatally) exhibit enlargement of dendritic spines and an increase in synapse density in the hippocampus (Rust et al., 2010). A decrease in cofilin leads to abnormal spine morphology and neurons typically contain abnormal filopodia-like protrusions or have aberrantly long spine necks (Hotulainen et al., 2009). In addition to LIMK/cofilin effectors, Rac1 affects actin cytoskeleton rearrangements in spine, through the regulation of the WAVE protein that consequently acts upon actin nucleator actin-related protein 2/3 (Arp2/3) to drive Arp2/3 activities, leading to the formation of dendritic spines (Sanchez et al., 2009). Arp2/3-containing complex binds to the side of a preexisting actin filament to form a new branch of actin filament (Pollard, 2007). Arp2/3 is concentrated in dendritic spines and is necessary for activity-dependent spine enlargement for spine head growth (Kim et al., 2006, 2013; Rácz and Weinberg, 2008; Wegner et al., 2008; Hotulainen et al., 2009). Arp2/3 activity was shown to be essential for the formation of LTM (e.g. Basu et al., 2016).

Interestingly, Rac1 activity is involved in the maintenance of spine morphology. Induction of sLTP (structural enlargement of dendritic spine) using uncaging of glutamate on a single spine led to the activation of Rac1 that lasted more than 30 min (Saneyoshi et al., 2019). Inhibition of Rac1 by EHT1864 postinduction blocked sLTP, showing that consistent activation of Rac1 by RacGEF is needed for the maintenance of sLTP. Furthermore, single spine stimulation leads to the rapid formation of a complex consisting of CaMKII and Tiam1 and to constitutive CaMKII activation, which persistently phosphorylates Tiam1. Spine structure is maintained during LTP by phosphorylation of Tiam1 that promotes stable actin-polymerization through Rac1.

Additional Neuronal Functions Regulated by Rac GTPase

In addition to its role in spine regulation, Rac is also involved in other neuronal functions that may contribute to alterations in synaptic efficacy and changes in neuronal ensembles. For example, Rac is involved in axonal morphogenesis (e.g. Spillane and Gallo, 2014) that may contribute to the formation of new neuronal connectivity that subserves memory. Furthermore, Rac1 is also involved in neurogenesis since a learning-induced increase in neurogenesis in the adult mouse hippocampus is impaired in neurons that are devoid of Rac1 (Haditsch et al., 2013). Neurogenesis is involved in memory formation (Gonçalves et al., 2016). Rac has been associated with the determination of the molecular composition and function at the synapse, such as the regulation of AMPA receptor functions. It was shown that breakpoint cluster region (BCR) protein, a RacGAP (see below), is important for regulating AMPA receptor localization on the neuronal surface, both at basal level and in response to EphB activation (Um et al., 2014). Moreover, Rac1 activation enhances recruiting AMPARs to the synapses during spinogenesis (Wiens et al., 2005). Another recent study shows that, on memory retrieval after long cocaine withdrawal, matured synapses become AMPAR silent again, followed by rematuration ∼6 h later. Increase and decrease in Rac1 activities control these synaptic dynamics, leading to the closing and opening, respectively, of the silent synapse-mediated destabilization window (Wright et al., 2020).

Taken together, the aforementioned results show that Rac GTPase is intimately involved, through its effectors, in regulating spine morphology. The effect of Rac GTPase on spine morphology may depend on the localization of the neurons in the brain and the time of activation. Moreover, different experimental protocols can account for different effects. Since spine morphogenesis is involved in memory formation and Rac GTPase is involved in this process, the observations

beg the questions: Is Rac necessary for memory and does its involvement in memory correlates with its effects on spine morphogenesis?

Rac1 GTPase IN MEMORY FORMATION, FORGETTING, ERASURE AND EXTINCTION

Rac1 GTPase in Learning and Memory Formation

The above observations show that Rac GTPase is involved in different cellular events such as changes in neuronal morphology and synaptic transmission that are believed to be necessary for memory formation. Indeed, Rac1 GTPase is shown to be involved in memory formation. Several studies have demonstrated a role for Rac1 GTPase in learning and memory formation in the amygdala. Light stimulation of photoactivatable Rac1 (PA-Rac1) during auditory fear conditioning in the LA led to an increase in PAK phosphorylation and to an impairment in long- but not in short-term auditory fear conditioning memory (Das et al., 2017). Inhibiting the downstream effector PAK in LA enhanced long- but not short-term fear conditioning memory. Rac1 function in astrocytes in the basolateral amygdala (BLA) is also important for long-term fear memory formation. Photoactivation of PA-Rac1 in astrocytes led to their structural alterations, and activation of Rac1 in astrocytes in BLA during fear conditioning attenuated fear memory formation (Liao et al., 2017). In another study, short- and long-term auditory fear conditioning memories are impaired when Rac1 is deleted from excitatory neurons but not from parvalbumin inhibitory neurons. Conditional knockout of Rac1 before fear conditioning training in the BLA impaired short- and long-term fear memories. The expression of a dominant-negative mutant of Rac1 in BLA, or infusion into BLA of Rac1 inhibitor NSC23766 before or after fear conditioning, blocked both fear conditioning short- and long-term memories (Gao et al., 2015). Taken together, the results show that alteration of Rac1 activity in the amygdala during or after fear conditioning affects memory formation.

In addition to memory consolidation, Rac1 is also involved in memory reconsolidation in the BLA. Reconsolidation of auditory Pavlovian fear memory was impaired when NSC23766 was microinjected into the BLA but not into the central amygdala (CeA) or hippocampal CA1 immediately after retrieval of auditory fear conditioning memory (Wu et al., 2014).

Other types of memories such as spatial and contextual memories are also mediated by Rac1 activity. Systemic administration of NSC23766 improved contextual fear memory at 1.5 and 24 h memory tests (Gan et al., 2016). Microinjection of NSC23766 after fear memory retrieval into the hippocampal CA1, but not into CeA or BLA, disrupted contextual fear conditioning memory reconsolidation (Wu et al., 2014).

Rac1-deficient mice (by CaMKII promoter-driven excision of Rac1 using a Cre-lox system) are impaired in learning and memory. More time was required to locate the hidden platform in the Morris water maze task in these Rac1-deficient mice, suggesting that learning is impaired in these mice. In the delayed matching-to-place (DMP) Morris water maze version, a behavior that depends on the integrity of NMDA receptor activation in hippocampus (Steele and Morris, 1999), the escape latency was reduced in a much faster rate in the control mice compared to that in the Rac1-deficient mice, showing that the ability to acquire a memory of the platform location is impaired in the Rac1 mutants (Haditsch et al., 2009). In another study, the authors (Haditsch et al., 2013) show that the selective ablation of Rac1 in postmitotic forebrain projection neurons leads to an impairment in working memory in the DMP task.

Rac1 in nucleus accumbens (NAc) is also involved in cocaine conditioned place preference (CPP) and in cocaine-induced spine morphogenesis (Dietz et al., 2012). Expression of a constitutively active mutant of Rac1 (Rac1-CA) in NAc blocked place preference conditioning and the acute locomotor-activating effect of the drug. Supporting these results, the authors show that activation of PA-Rac1 prevented CPP formation to cocaine. In contrast, intra-NAc injection of a dominant-negative mutant of Rac1 (Rac1-DN) promoted CPP to cocaine without altering locomotor responses. Constitutive active cofilin (cofilin-CA) expression in the NAc also increased the rewarding effects of cocaine. The study further showed that five doses of cocaine led to an increase in the number of dendritic spines on NAc medium spiny neurons, compared with the control mice that were treated with saline when tested 4 h after the last dose. Rac1-CA completely blocked this increase. However, in basal conditions, Rac1-CA had no effect on spine density. Cocaine induction of spines was also blocked by PA-Rac1 when it was activated by light following each injection of cocaine. In contrast, an increase in spine density in saline-treated mice is observed when Rac1-DN is overexpressed. Spine density increase that is induced by cocaine was largely driven by an increase in the number of thin spines. Such an increase was blocked by Rac1-CA and mimicked by Rac1-DN overexpression. The number of mushroom spines is reduced by Rac1-CA but not by Rac1-DN or cofilin-CA.

Rac1 signaling is also crucial for methamphetamine (METH)-induced CPP and structural plasticity (Tu et al., 2019). Expression of Rac1-CA in nucleus accumbens blocked the METH-induced increase in dendritic complexity, length, and branch number and significantly decreased the CPP scores in the group trained for METH CPP. In the saline CPP group, the total spine density is increased by Rac1-DN (mainly by the increased thin spine density), whereas mushroom spine density is significantly increased by Rac1-CA. In the METH CPP group, total spine density was increased and was blocked by Rac1-CA.

The aforementioned results show that the integrity of Rac1 activity is needed for memory formation. Interference, with Rac1 activity, by either activation or inhibition, affects normal memory consolidation (or reconsolidation). Moreover, interference with Rac1 levels of activity also affects neuronal morphology. Thus, precise spatiotemporal Rac1 activity is necessary to form normal memory.

The above studies show that altering Rac1 level or activity directly by pharmacology, by mutating the Rac1 protein or

altering Rac1 level by genetic manipulation in the brain, affect LTM formation. Rac1 activity is also modified by controlling Rac GEFs and GAPs. BCR and active BCR-related (ABR) proteins (Heisterkamp et al., 1989) show Rac-GAP activities (Diekmann et al., 1991; Heisterkamp et al., 1993; Tan et al., 1993; Chuang et al., 1995; Voncken et al., 1995; Kaartinen et al., 2001; Cho et al., 2007). Mice deficient of BCR or ABR exhibit enhanced basal Rac1 activity and a small increase in spine density (Oh et al., 2010). The study indicates that the maintenance ability, but not induction, of LTP measured in Schaffer collateral (SC)–CA1 pyramidal neuron synapses of $BCR^{-/-}$ and $ABR^{-/-}$ hippocampus is reduced in mice deficient of BCR or ABR. In contrast, LTD was comparable in wild-type (WT) and knockout (KO) mice. A slight increase in dendritic spine density is observed in the $BCR^{-/-}$ and $ABR^{-/-}$. $BCR^{-/-}$ and $ABR^{-/-}$ mice showed reduced learning relative to WT mice in the Morris water maze. In the probe test, $ABR^{-/-}$ mice, but not $BCR^{-/-}$ mice, spent less time in the target quadrant when compared with WT mice, and in both $BCR^{-/-}$ and $ABR^{-/-}$ mice, the number of exact crossings over the former location of the platform was reduced, suggesting that mice that are deficient in BCR/ABR are impaired in spatial learning and memory (Oh et al., 2010). In the object recognition task, $BCR^{-/-}$ and $ABR^{-/-}$ mice exhibit an equal preference for the two objects, whereas the WT mice show preference to the novel object, suggesting that object recognition memory is impaired in the BCR/ABR-deficient mice. A different Rac GAP protein is encoded by the ArhGAP15 gene (Seoh et al., 2003). It was found that there are fewer CR+, PV+, and SST+ inhibitory neurons in the CA3 and DG regions of the hippocampus of the $ArhGAP15^{-/-}$ mice (Zamboni et al., 2016). The balance between excitatory and inhibitory synapses is altered in primary cultures of hippocampal neurons from the mutant mice, showing overexcitation and reduced synchronicity. Neuritogenesis in primary cultures of dissociated embryonic brains of mutant mice also displayed reduced efficiency of neurite elongation and branching and a simpler neuronal morphology. Anti-ArhGAP15 short hairpin RNA (shRNA) application led to a reduction in spine density compared to controls in hippocampal-cultured neurons. It was also found that hippocampus-dependent working and associative memories are impaired in adult $ArhGAP15^{-/-}$ mice. $ArhGAP15^{-/-}$ mice exhibited normal ability to learn hidden-platform water maze; however, they showed difficulties to locate the new platform position during the reversal phase. $ArhGAP15^{-/-}$ mice also have defects in radial maze acquisition and repetition. Mutant mice were impaired in freezing responses during auditory trace fear-conditioning training and the subsequent tone and context tests subjected 24 h later.

Rac GEFs are also involved in the regulation of spine morphology and memory formation. Kalirin is a brain-specific GEF. In kalirin KO mice, Rac1 activity was shown to be reduced in the cortex but not in the hippocampus (Cahill et al., 2009). Spine density in the KO mice frontal cortex, but not in the hippocampus, is significantly reduced as revealed by Golgi staining of neurons. Two-trial matching to sample in the Morris water maze task was impaired in these mutant KO mice. Moreover, in the five testing days, the KO mice failed to improve their performance in the second vs. the first trial, indicating that their spatial working memory abilities are impaired. The same KO mice also presented severe difficulties in the Y-maze arm recognition task, which indicates an impairment in working memory.

Rac1 localization in neurons can also be regulated by neuronal activity and may affect neuronal morphogenesis, synaptic plasticity and memory. One protein that affects Rac1 localization is copine-6 (Reinhard et al., 2016). Copine-6 binds Rac1 and recruits it to the postsynaptic spine membrane in response to calcium influx. Chemical LTP (cLTP)-triggered calcium transients translocate copine-6 from the dendrite to the membrane of postsynaptic spine. Copine-6 translocation into postsynaptic spines is also triggered by calcium influx via NMDA receptors. Rac1 accumulates in spines following cLTP induction but not in the presence of the calcium mutant Copine-6D167N-myc. cLTP leads to an increase in spine head width but not in neurons of Cpne6 KO mice. Moreover, hippocampal learning and memory and synaptic plasticity require copine-6. Stimulation of Schaffer collaterals in acute hippocampal slices leads to LTP in WT mice, but the increase in the EPSPs responses in Cpne6 KO mice returns to baseline within 60 min. Cpne6 KO mice show impairment in fear-conditioning learning and in context, but not cued, dependent long-term fear memory.

The aforementioned results show that Rac activity is regulated in the brain by upstream GAPs and GEFs and is affected by synaptic activity. Moreover, impairment in Rac1 activity and cellular localization leads to alterations in spine morphology and memory formation. Thus, Rac1 can mediate between synaptic activation (e.g. during learning) and cellular events that underlie memory.

Rac1 GTPase in Memory Erasure

To understand the role of Rac1 in the regulation of spine morphology and to further elucidate the roles of spine structure in memory, an AS-PA-Rac1 was developed (Hayashi-Takagi et al., 2015). This construct contains a modified photoactivatable Rac1 GTPase that is fused to PSDΔ1.2 and is regulated by dendritic targeting element (DTE) of Arc mRNA. In this manner, NMDA receptor-dependent synaptic activation leads to the target and translation of the construct in activated dendritic segments. Indeed, in mice trained with the rotarod training task, spines were labeled, and the mice exhibited significantly more structural potentiation (enlargement or formation of spines) compared with the non-trained mice in cortical layers II/III of the primary motor cortex (M1). The authors further show that the specific AS-PA-Rac1-containing spines shrink following low-frequency pulsed photoactivation of AS-PA-Rac1. Light activation of M1 immediately after or 1 day, but not 2 days, after training disrupted the acquired learning. The authors suggest that spine potentiation visualized by AS-PA-Rac1 that are evoked by learning (at +1 day), but not spontaneous potentiation (at +2 day), accounts for the memory traces. Thus, the study suggests that shrinkage of potentiated spines by Rac1 GTPase disrupts long-term motor memory in the cortex.

The current results show that Rac1 activity affects learning-acquired task a day after training and that this Rac1 activation leads to shrinkage of the spine. Thus, the results indicate that Rac1 activity should be controlled after training in neurons to maintain the learning-induced neuronal ensembles that mediate the acquired task.

Rac1 GTPase in Memory Forgetting

Memory is stored in the brain after acquisition and consolidation. Owing to a large number of memory engrams that can be stored over time, it seems reasonable that the brain has a mechanism to remove memories that become unused, also termed as "active forgetting". Active forgetting may be achieved by the degradation of the cellular and molecular memory traces or the engram cell circuit (Davis and Zhong, 2017). Several studies have shown that Rac1 is involved in memory forgetting. For example, expressing a constitutively active form of Rac1 in the mushroom body neurons (MBn) of *Drosophila* accelerates forgetting of Pavlovian odor-shock olfactory aversive conditioning, whereas expressing a dominant-negative form of Rac1 transgene in MBn inhibits intrinsic forgetting (Shuai et al., 2010). Rac1 downstream effectors are also involved in active forgetting. Memory decay is slowed by constitutively active cofilin, and overexpression of constitutively active Rac1 mutant that is unable to bind PAK fails to accelerate memory decay. The scaffolding protein Scribble forms a signaling complex that includes Rac1, PAK3, and cofilin in the MBn (Cervantes-Sandoval et al., 2016). Scribble knockdown significantly reduces the level of p-cofilin, and when Scribble expression is reduced, memory loss is impaired. Scribble consequently has been pointed out as a mediator of active forgetting in *Drosophila* (Cervantes-Sandoval et al., 2016).

The roles of Rac1 in memory forgetting have also been tested in mice. Toward that end, the investigators expressed Rac1-DN or Rac1-CA in the hippocampus and studied the effects on forgetting of hippocampal-dependent memory (Liu et al., 2016). The inhibition of Rac1 activity in hippocampal neurons, through the targeted expression of a Rac1-DN, extended object recognition memory from less than 72 h to over 72 h, whereas accelerated memory is decayed by Rac1 activation to less than 24 h. In addition, interference-induced forgetting of this memory [where retroactive interference objects were introduced 22 h after sampling (training)] was correlated with Rac1 activation and was blocked by inhibition of Rac1 activity. LTP decay in the Schaffer collateral pathway is also highly regulated by Rac1 activity. Rac1 activation accelerated the decay of LTP, whereas its inhibition slowed LTP decay. Paired pulse low-frequency stimulation (PP-LFS; 900 paired pulses delivered at a frequency of 1 Hz; at 50-ms interval) failed to reverse LTP in the Rac1-DN slices when it was introduced 1 h after the LTP recordings, but significantly induced LTD in the Rac1-CA slices. These patterns are similar to the roles of Rac in memory forgetting. Thus, the aforementioned observations show that activation of Rac1 within excitatory neurons in the hippocampus causes time-based natural decay and interference-induced forgetting of object recognition memory.

A recent study shows that contextual fear conditioning induces Rac1 activation and expression of α2-chimaerin, a RacGAP, in the hippocampus. Furthermore, it is shown that Rac1 activity mediates reversible forgetting. α2-Chimaerin, through inhibition of Rac1 activity during the maintenance stage, reverses forgetting to sustain memory (Lv et al., 2019).

Rac1 is also involved in forgetting of social recognition memory (SRM). A recent study shows that social isolation does not affect SRM (social discrimination paradigm) formation but rather accelerated SRM decay, suggesting enhanced forgetting (Liu et al., 2018). Inhibition of Rac1 activity in both the dorsal and ventral regions of the hippocampus, using Rac1-DN, blocked forgetting of SRM in isolated mice. Activation of Rac1 in the hippocampus, using Rac1-CA, accelerated forgetting in group-housed mice. Accelerated LTP decay in hippocampal slices from isolated mice was rescued by inhibition of Rac1 activity. The observations show that enhanced Rac1-dependent forgetting mediates social memory impairments in isolated mice.

These results further support the observations that controlled Rac1 activity posttraining, in various behavioral paradigms, regulates the strength of memory and that manipulating Rac1 activity affects the maintenance of memory and can lead to memory erasure and forgetting.

Rac1 GTPase and Memory Extinction

Memory extinction occurs when the conditioned stimulus (CS) cues are subjected alone after learning without the unconditioned stimulus (Pavlov, 1927) leading to relearning of a new association of the CS with the absence of the original reinforcement. Memory extinction does not reflect the forgetting of the original learning (Rescorla, 1996). Rac1 GTPase is also involved in memory extinction. Mass extinction of contextual fear conditioning in rats upregulated Rac1 activity in the hippocampus and led to long-term extinction of contextual fear in rats. Extinction of contextual fear memory is prevented by intrahippocampal injection of the Rac1 inhibitor NSC23766 immediately after extinction trial (Jiang et al., 2016). Long-spaced extinction downregulated Rac1 activity in the hippocampus and led to lesser extinction. Intrahippocampal injection of Rac1 activator CN04-A during extinction trials facilitated the extinction of contextual fear in long-spaced extinction trained rats.

Extinction of conditioned place aversion (CPA) to naloxone-precipitated opiate withdrawal activates Rac1 in the ventromedial prefrontal cortex (vmPFC) of rats. Active Rac1 is needed and sufficient for $GABA_A$ receptors ($GABA_AR$) endocytosis and CPA extinction (Wang et al., 2017). Knockdown of Rac1 by shRNA within the vmPFC suppressed endocytosis of $GABA_AR$ and extinction of CPA, whereas expression of a constitutively active Rac1 accelerated $GABA_AR$ endocytosis and CPA extinction.

Rac1 GTPase IN BRAIN DISORDERS

Taking into consideration the central role of Rac1 in memory and neuronal morphogenesis, it is not surprising that this small GTPase has been associated with several brain diseases, that lead to cognitive and psychiatric dysfunctions and neurodegeneration, that involve also abnormalities in

neuronal morphology (Newey et al., 2005). Here, we present several examples.

Fragile X Syndrome (FXS) is caused by a reduced or loss of expression of the fragile X mental retardation 1 (FMR1) gene that encodes the Fragile X mental retardation protein (FMRP). FMRP regulates mRNA translation (Bagni et al., 2012; Bhakar et al., 2012). FXS causes impaired cognition, social/language deficits, hyperactivity, hypersensitivity to sensory stimuli, increased susceptibility to seizures, sleep disturbances, attentional deficits and motor incoordination. The neuroanatomical hallmark of FXS is an overabundance of immature dendritic spines in mammals (Rudelli et al., 1985; Irwin et al., 2001). Studying Fmr1 in *Drosophila* revealed that Fmr1 affects dendritic development and that Rac1 is involved in promoting dendritic branching (Lee et al., 2003). Moreover, the study shows that Fmr1 and Rac1 interact genetically with each other in controlling the formation of fine dendritic branches. Another study has shown that in *Drosophila*, the cytoplasmic FMRP-interacting protein (CYFIP) associates Rac-dependent cytoskeleton remodeling and dFMR1-dependent control of translation (Schenck et al., 2003). Studies using Fmr1 KO mice reveal memory impairments (Dutch-Belgian Fragile X Consortium., 1994) and altered spines morphology in these mice (He and Portera-Cailliau, 2013). Rac1 is upregulated in Fmr1 knockout mice (Bongmba et al., 2011). Activation of Rac1 and its effector p21-activated kinase (PAK), by theta burst afferent stimulation (TBS), is impaired at hippocampal synapses in the Fmr1 KO, an FXS mouse model (Chen et al., 2010). Aberrantly increased activity of Rac1 inhibited the actin-depolymerizing factor cofilin and led to spine abnormalities, which are associated with the disease, in the somatosensory cortex of FXS model mice (Pyronneau et al., 2017). Expression of a constitutively active cofilin mutant (cofilinS3A) in the somatosensory cortex of the Fmr1-deficient mice rescued immature dendritic spine and increased spine density phenotypes. Inhibition of PAK1 rescued synaptic signaling and improved sensory processing in FXS mice. Fmr1 KO mice treated with NSC23766, which blocks Rac1 activation by GEFs, exhibited an increase in contextual memory after delayed fear conditioning (Martinez and Tejada-Simon, 2018). Contextual memory is impaired in untreated KO mice compared to that in wild-type mice. In addition, treatment of Fmr1 KO with a Rac1 inhibitor improves cue memory in mice trained for trace fear conditioning training. Treatment with NSC23766 also increases LTP in the Fmr1 KO hippocampus. Inhibition of PAK rescues morphological (spine density and morphology) and behavioral symptoms of fragile X syndrome in mice (Hayashi et al., 2007).

Dock4 is a risk gene for autism spectrum disorder (ASD) and other neuropsychiatric disorders. Dock4 encodes for a Rac1 guanine nucleotide exchange factor. Dock4 KO mice exhibited ASD-like behaviors, including elevated anxiety, abnormal isolation-induced pup vocalizations, impaired social novelty preference and perturbed object and spatial learning. Hippocampal neurons of KO mice show attenuation in excitatory synaptic transmission (in CA1), decreased spine density (in CA1 and DG), and synaptic content of AMPA and NMDA receptors (in whole hippocampus). Rac1 activity is reduced in the Dock4-deficient hippocampus, leading to the downregulation of protein synthesis and reduced expression of AMPA and NMDA receptor subunits. Injection of lentivirus expressing Rac1 into Dock4 KO mice hippocampal CA1 rescued excitatory synaptic transmission and plasticity impairments and corrected the impaired social deficits in these mice (Guo et al., 2019).

Rac1 has also been associated with major depressive disorder (MDD). A repressive chromatin state surrounding the Rac1 promoter and reduced Rac1 transcription in the NAc is found in subjects with MDD. In mice that underwent social defeat, a model of depression-like behavior, Rac1 mRNA level is downregulated. This reduction in Rac1 mRNA level is associated with a repressive chromatin state surrounding the proximal promoter of Rac. Reduction in Rac1 activity or its expression in the NAc of mice increases social defeat-induced social avoidance and anhedonia. The observations in the study indicate that the chronic social defeat stress-induced decrease in Rac1 expression results in concurrent stubby spine formation and cofilin localization within these spines. Expression in the NAc of constitutively active Rac1 after chronic social defeat stress reversed the induction of stubby spines and depression-related behaviors in mice (Golden et al., 2013).

In addition to psychiatric disorders, Rac1 is also associated with neurodegenerative brain disorders such as Alzheimer's disease (AD). The pathological hallmarks of AD range from an extracellular accumulation of amyloid β plaques and neurofibrillary tangles to alterations in synaptic activity and memory loss (Small and Duff, 2008; Selkoe and Hardy, 2016; Femminella et al., 2018). Recently, Rac1 activity was demonstrated to be enhanced not only in AD patients but also in the hippocampus of APP/PS1 AD mice model and in a transgenic fly model of AD in comparison to the controls (Wu et al., 2019). This study further shows that Aβ42 oligomer application to HEK-293 leads to an increase in Rac1 activity. In addition, it is demonstrated that the impaired performance in APP/PS1 mice during the Morris water maze task could be rescued by the intragastric application of a Rac1 inhibitor, EHop-016. Furthermore, injection of a dominant-negative form of Rac1 into the hippocampus was able to inhibit the accelerated memory decay in the mutant mice. Lastly, LTP fast decay in the AD model was rescued as well by the application of the Rac1 inhibitor EHop-016 (Wu et al., 2019). Rac1 is also involved in another type of AD mice model, the 3xTg-AD. It is shown that Rac1 activity is increased in 6-week-old 3xTg-AD mice (Borin et al., 2018). Moreover, in primary cortical neurons, Rac1 or constitutively active mutant forms of Rac1 constructs led to the creation of pathogenic Aβ fragments and the translocation of SET from the nucleus to the cytoplasm, which also resulted in increased phosphorylation of tau. The authors also show that the levels of Rac1 in AD patients and 7-month-old 3xTg-AD mouse appeared to be significantly lower, which coincides with the decline of cognitive function in the mouse model. Additional to the decline of cognitive function and abnormal level of Rac1, dendritic spines were shown to be significantly reduced in the 7-month-old mouse model. The authors suggest a possible dual role of Rac1 according to the different stages of the pathology. Taken together,

the results suggest that alteration in Rac1 activity is involved in AD-related memory abnormalities and the pathological changes that occur in the AD brain. Moreover, it appears that the reversal of the abnormal activity of Rac1 might restore some cognitive functions and morphological alterations, making this small GTPase an interesting target for study as a molecular marker and a possible target for pharmacological treatment.

Rac1 activity is also associated with Huntington's disease (HD) that usually causes movement and cognitive and psychiatric disorders with an extensive spectrum of symptoms and signs (Walker, 2007). Rac1 activity levels are increased in the striatum of a 1.5-month-old mouse of HD Q140/Q140 mice (Knockin mouse with a chimeric mouse/human exon 1 containing 140 CAG repeats inserted in the murine huntingtin gene) but reduced in 4.5 months old mouse compared to controls. Huntingtin was found to associate with p85α subunit of the PI 3-kinase, actinin-2 and preferentially with active Rac1 (Tousley et al., 2019). Puigdellívol et al. (2015) detected a decrease in Rac1 activity in HD-mutant mice (Q7/Q111) (containing alleles with 7 CAG repeats and with targeted insertion of 109 CAG repeats that extends the glutamine segment in huntingtin to 111 residues) in the cortex. Kalirin-7, an activator of Rac1, was found to be significantly reduced in the cortex of these mice. The $Hdh^{Q7/Q111}$ mouse model presented smaller spine density in the motor cortex but not striatum. In addition, the mice were impaired in the ability to learn new motor skills (Puigdellívol et al., 2015).

The above examples show that a dysfunctional Rac1 activity and level in the brain leads to neuronal morphological abnormalities, including these of dendritic spines. Moreover, the results indicate that such dysfunctions are involved with behavioral abnormalities associated with mental disorders. These observations give incentive to further explore the possibility that intervention in Rac1 level of activity can rescue such abnormalities in human brain structure and behavior.

CONCLUSION

Rac GTPase regulates several signaling pathways in neurons including pathways that control actin cytoskeleton dynamics and structure. Such changes in actin dynamics and structure mediate spines morphogenesis and density and synaptic transmission in spine. As described above, several studies have shown that Rac-induced alterations in spine morphology correlate with the effects of Rac on memory formation.

The following model can be deduced from the aforementioned observations. It is possible that synaptic activation, for example during learning or memory extinction, leads to changes in Rac activity that in turn affects the actin cytoskeleton. Changes in actin cytoskeleton alter neuronal morphology. Such changes in the actin cytoskeleton are preserved over time [see for possible mechanisms of preserving such molecular and morphological changes over time in Basu and Lamprecht (2018)]. These modifications in neuronal morphology alter the responsiveness of the neurons to incoming sensory input, such that subjecting the animal to the sensory stimulus that participated in learning and led to the formation of memory (i.e. the conditioned stimulus) will lead to an activation of the memory trace neuronal circuit in the brain and to memory retrieval.

Rac1 GTPase is also important for postlearning functions such as erasure and forgetting. Thus, Rac1 activity can be used to modulate neuronal morphology after learning to control memory. Therefore, a balanced and controlled Rac activity following memory consolidation will determine whether the memory will be preserved or will deteriorate.

The above studies also show that the activity of Rac is essential for normal brain functions. Indeed, spine abnormal morphology and densities are observed in brain disorders where Rac and its regulators can be found in abnormal levels or dysregulated in terms of activity. It would be important to examine the possibility that controlling Rac activity can rescue memory-related brain disorders.

AUTHOR CONTRIBUTIONS

All authors listed have made a substantial, direct and intellectual contribution to the work, and approved it for publication.

REFERENCES

Araya, R., Jiang, J., Eisenthal, K. B., and Yuste, R. (2006). The spine neck filters membrane potentials. *Proc. Natl. Acad. Sci. U.S.A.* 103, 17961–17966. doi: 10.1073/pnas.0608755103

Araya, R., Vogels, T. P., and Yuste, R. (2014). Activity-dependent dendritic spine neck changes are correlated with synaptic strength. *Proc. Natl. Acad. Sci. U.S.A.* 111, E2895–E2904. doi: 10.1073/pnas.1321869111

Arber, S., Barbayannis, F. A., Hanser, H., Schneider, C., Stanyon, C. A., Bernard, O., et al. (1998). Regulation of actin dynamics through phosphorylation of cofilin by LIM-kinase. *Nature* 393, 805–809. doi: 10.1038/31729

Bagni, C., Tassone, F., Neri, G., and Hagerman, R. (2012). Fragile X syndrome: causes, diagnosis, mechanisms, and therapeutics. *J. Clin. Invest.* 122, 4314–4322. doi: 10.1172/JCI63141

Bailey, C. H., Kandel, E. R., and Harris, K. M. (2015). Structural components of synaptic plasticity and memory consolidation. *Cold Spring Harb. Perspect. Biol.* 7:a021758. doi: 10.1101/cshperspect.a021758

Basu, S., Kustanovich, I., and Lamprecht, R. (2016). Arp2/3 and VASP are essential for fear memory formation in lateral amygdala. *eNeuro* 3: ENEURO.0302-16.2016.

Basu, S., and Lamprecht, R. (2018). The role of actin cytoskeleton in dendritic spines in the maintenance of long-term memory. *Front. Mol. Neurosci.* 11:143. doi: 10.3389/fnmol.2018.00143

Bhakar, A. L., Dölen, G., and Bear, M. F. (2012). The pathophysiology of fragile X (and what it teaches us about synapses). *Annu. Rev. Neurosci.* 35, 417–443. doi: 10.1146/annurev-neuro-060909-153138

Bloodgood, B. L., and Sabatini, B. L. (2005). Neuronal activity regulates diffusion across the neck of dendritic spines. *Science* 310, 866–869. doi: 10.1126/science.1114816

Bongmba, O. Y., Martinez, L. A., Elhardt, M. E., Butler, K., and Tejada-Simon, M. V. (2011). Modulation of dendritic spines and synaptic function by Rac1: a possible link to Fragile X syndrome pathology. *Brain Res.* 1399, 79–95. doi: 10.1016/j.brainres.2011.05.020

Borin, M., Saraceno, C., Catania, M., Lorenzetto, E., Pontelli, V., Paterlini, A., et al. (2018). Rac1 activation links tau hyperphosphorylation and Aβ dysmetabolism in Alzheimer ' s disease. *Acta Neuropathol. Commun.* 6, 1–17.

Cahill, M. E., Xie, Z., Day, M., Photowala, H., Barbolina, M. V., Miller, C. A., et al. (2009). Kalirin regulates cortical spine morphogenesis and disease-related behavioral phenotypes. *Proc. Natl. Acad. Sci. U.S.A.* 106, 13058–13063. doi: 10.1073/pnas.0904636106

Caroni, P., Donato, F., and Muller, D. (2012). Structural plasticity upon learning: regulation and functions. *Nat. Rev. Neurosci.* 13, 478–490. doi: 10.1038/nrn3258

Cervantes-Sandoval, I., Chakraborty, M., MacMullen, C., and Davis, R. L. (2016). Scribble scaffolds a signalosome for active forgetting. *Neuron* 90, 1230–1242. doi: 10.1016/j.neuron.2016.05.010

Chazeau, A., Mehidi, A., Nair, D., Gautier, J. J., Leduc, C., Chamma, I., et al. (2014). Nanoscale segregation of actin nucleation and elongation factors determines dendritic spine protrusion. *EMBO J.* 33, 2745–2764. doi: 10.15252/embj.201488837

Chen, L. Y., Rex, C. S., Babayan, A. H., Kramár, E. A., Lynch, G., Gall, C. M., et al. (2010). Physiological activation of synaptic Rac>PAK (p-21 activated kinase) signaling is defective in a mouse model of fragile X syndrome. *J. Neurosci.* 30, 10977–10984. doi: 10.1523/JNEUROSCI.1077-10.2010

Cho, Y. J., Cunnick, J. M., Yi, S. J., Kaartinen, V., Groffen, J., and Heisterkamp, N. (2007). Abr and Bcr, two homologous Rac GTPase-activating proteins, control multiple cellular functions of murine macrophages. *Mol. Cell. Biol.* 27, 899–911. doi: 10.1128/mcb.00756-06

Chuang, T. H., Xu, X., Kaartinen, V., Heisterkamp, N., Groffen, J., and Bokoch, G. M. (1995). Abr and Bcr are multifunctional regulators of the Rho GTP-binding protein family. *Proc. Natl. Acad. Sci. U.S.A.* 92, 10282–10286. doi: 10.1073/pnas.92.22.10282

Corbetta, S., Gualdoni, S., Ciceri, G., Monari, M., Zuccaro, E., Tybulewicz, V. L. J., et al. (2009). Essential role of Rac1 and Rac3 GTPases in neuronal development. *FASEB J.* 23, 1347–1357. doi: 10.1096/fj.08-121574

Das, A., Dines, M., Alapin, J. M., and Lamprecht, R. (2017). Affecting long-term fear memory formation through optical control of Rac1 GTPase and PAK activity in lateral amygdala. *Sci. Rep.* 7:13930.

Davis, R. L., and Zhong, Y. (2017). The biology of forgetting-a perspective. *Neuron* 95, 490–503. doi: 10.1016/j.neuron.2017.05.039

Diekmann, D., Brill, S., Garrett, M. D., Totty, N., Hsuan, J., Monfries, C., et al. (1991). Bcr encodes a GTPase-activating protein for p21rac. *Nature* 351, 400–402. doi: 10.1038/351400a0

Dietz, D. M., Sun, H., Lobo, M. K., Cahill, M. E., Chadwick, B., Gao, V., et al. (2012). Rac1 is essential in cocaine-induced structural plasticity of nucleus accumbens neurons. *Nat. Neurosci.* 15, 891–896. doi: 10.1038/nn.3094

Duman, J. G., Mulherkar, S., Tu, Y. K., Cheng, J., and Tolias, K. F. (2015). Mechanisms for spatiotemporal regulation of Rho-GTPase signaling at synapses. *Neurosci. Lett.* 601, 4–10. doi: 10.1016/j.neulet.2015.05.034

Dutch-Belgian Fragile X Consortium. (1994). Fmr1 knockout mice: a model to study fragile X mental retardation. *Cell* 78, 23–33.

Edwards, D. C., Sanders, L. C., Bokoch, G. M., and Gill, G. N. (1999). Activation of LIM-kinase by Pak1 couples Rac/Cdc42 GTPase signalling to actin cytoskeletal dynamics. *Nat. Cell Biol.* 1, 253–259. doi: 10.1038/12963

Femminella, G. D., Thayanandan, T., Calsolaro, V., Komici, K., Rengo, G., Corbi, G., et al. (2018). Imaging and molecular mechanisms of Alzheimer's disease: a review. *Int. J. Mol. Sci.* 19, 1–23. doi: 10.3390/ijms20225722

Fleming, I. N., Elliott, C. M., Buchanan, F. G., Downes, C. P., and Exton, J. H. (1999). Ca2+/calmodulin-dependent protein kinase II regulates Tiam1 by reversible protein phosphorylation. *J. Biol. Chem.* 274, 12753–12758. doi: 10.1074/jbc.274.18.12753

Fu, M., Yu, X., Lu, J., and Zuo, Y. (2012). Repetitive motor learning induces coordinated formation of clustered dendritic spines *in vivo*. *Nature* 483, 92–95. doi: 10.1038/nature10844

Gan, P., Ding, Z. Y., Gan, C., Mao, R. R., Zhou, H., Xu, L., et al. (2016). Corticosterone regulates fear memory via Rac1 activity in the hippocampus. *Psychoneuroendocrinology* 71, 86–93. doi: 10.1016/j.psyneuen.2016.05.011

Gao, Q., Yao, W., Wang, J., Yang, T., Liu, C., Tao, Y., et al. (2015). Post-training activation of Rac1 in the basolateral amygdala is required for the formation of both short-term and long-term auditory fear memory. *Front. Mol. Neurosci.* 8:65. doi: 10.3389/fnmol.2015.00065

Golden, S. A., Christoffel, D. J., Heshmati, M., Hodes, G. E., Magida, J., Davis, K., et al. (2013). Epigenetic regulation of RAC1 induces synaptic remodeling in stress disorders and depression. *Nat. Med.* 19, 337–344. doi: 10.1038/nm.3090

Gonçalves, J. T., Schafer, S. T., and Gage, F. H. (2016). Adult neurogenesis in the hippocampus: from stem cells to behavior. *Cell* 167, 897–914. doi: 10.1016/j.cell.2016.10.021

Gray, N. W., Weimer, R. M., Bureau, I., and Svoboda, K. (2006). Rapid redistribution of synaptic PSD-95 in the neocortex *in vivo*. *PLoS Biol.* 4:e0040370. doi: 10.1371/journal.pbio.0040370

Guo, D., Peng, Y., Wang, L., Sun, X., Wang, X., Liang, C., et al. (2019). Autism-like social deficit generated by Dock4 deficiency is rescued by restoration of Rac1 activity and NMDA receptor function. *Mol. Psychiatry* [Epub ahead of print]. doi: 10.1038/s41380-019-0472-7

Haditsch, U., Anderson, M. P., Freewoman, J., Cord, B., Babu, H., Brakebusch, C., et al. (2013). Neuronal Rac1 is required for learning-evoked neurogenesis. *J. Neurosci.* 33, 12229–12241. doi: 10.1523/JNEUROSCI.2939-12.2013

Haditsch, U., Leone, D. P., Farinelli, M., Chrostek-Grashoff, A., Brakebusch, C., Mansuy, I. M., et al. (2009). A central role for the small GTPase Rac1 in hippocampal plasticity and spatial learning and memory. *Mol. Cell Neurosci.* 41, 409–419. doi: 10.1016/j.mcn.2009.04.005

Halpain, S., Hipolito, A., and Saffer, L. (1998). Regulation of F-actin stability in dendritic spines by glutamate receptors and calcineurin. *J. Neurosci.* 18, 9835–9844. doi: 10.1523/jneurosci.18-23-09835.1998

Harris, K. M., Jensen, F., and Tsao, B. (1992). Three-dimensional structure of dendritic spines and synapses in rat hippocampus (CA1) at postnatal day 15 and adult ages: implications for the maturation of synaptic physiology and long-term potentiation. *J. Neurosci.* 12, 2685–2705. doi: 10.1523/jneurosci.12-07-02685.1992

Harris, K. M., and Stevens, J. K. (1989). Dendritic spines of CA1 pyramidal cells in the rat hippocampus: serial electron microscopy with reference to their biophysical characteristics. *J. Neurosci.* 9, 2982–2997. doi: 10.1523/jneurosci.09-08-02982.1989

Hayashi, M. L., Choi, S. Y., Rao, B. S., Jung, H. Y., Lee, H. K., Zhang, D., et al. (2004). Altered cortical synaptic morphology and impaired memory consolidation in forebrain- specific dominant-negative PAK transgenic mice. *Neuron* 42, 773–787. doi: 10.1016/j.neuron.2004.05.003

Hayashi, M. L., Rao, B. S., Seo, J. S., Choi, H. S., Dolan, B. M., Choi, S. Y., et al. (2007). Inhibition of p21-activated kinase rescues symptoms of fragile X syndrome in mice. *Proc. Natl. Acad. Sci. U.S.A.* 104, 11489–11494. doi: 10.1073/pnas.0705003104

Hayashi-Takagi, A., Takaki, M., Graziane, N., Seshadri, S., Murdoch, H., Dunlop, A. J., et al. (2010). Disrupted-in-schizophrenia 1 (DISC1) regulates spines of the glutamate synapse via Rac1. *Nat. Neurosci. Mar.* 13, 327–332. doi: 10.1038/nn.2487

Hayashi-Takagi, A., Yagishita, S., Nakamura, M., Shirai, F., Wu, Y. I., Loshbaugh, A. L., et al. (2015). Labelling and optical erasure of synaptic memory traces in the motor cortex. *Nature* 525, 333–338. doi: 10.1038/nature15257

He, C. X., and Portera-Cailliau, C. (2013). The trouble with spines in fragile X syndrome: density, maturity and plasticity. *Neuroscience* 251, 120–128. doi: 10.1016/j.neuroscience.2012.03.049

Heasman, S. J., and Ridley, A. J. (2008). Mammalian Rho GTPases: new insights into their functions from *in vivo* studies. *Nat. Rev. Mol. Cell Biol.* 9, 690–701. doi: 10.1038/nrm2476

Hedrick, N. G., Harward, S. C., Hall, C. E., Murakoshi, H., McNamara, J. O., and Yasuda, R. (2016). Rho GTPase complementation underlies BDNF-dependent homo- and heterosynaptic plasticity. *Nature* 538, 104–108. doi: 10.1038/nature19784

Heisterkamp, N., Kaartinen, V., van Soest, S., Bokoch, G. M., and Groffen, J. (1993). Human ABR encodes a protein with GAPrac activity and homology to the DBL nucleotide exchange factor domain. *J. Biol. Chem.* 268, 16903–16906.

Heisterkamp, N., Morris, C., and Groffen, J. (1989). ABR, an active BCR-related gene. *Nucleic Acids Res.* 17, 8821–8831. doi: 10.1093/nar/17.21.8821

Hering, H., and Sheng, M. (2001). Dendritic spines: structure, dynamics and regulation. *Nat. Rev. Neurosci.* 2, 880–888. doi: 10.1038/35104061

Honkura, N., Matsuzaki, M., Noguchi, J., Ellis-Davies, G. C., and Kasai, H. (2008). The subspine organization of actin fibers regulates the structure and plasticity of dendritic spines. *Neuron* 57, 719–729. doi: 10.1016/j.neuron.2008.01.013

Hotulainen, P., and Hoogenraad, C. C. (2010). Actin in dendritic spines: connecting dynamics to function. *J. Cell Biol.* 189, 619–629. doi: 10.1083/jcb.201003008

Hotulainen, P., Llano, O., Smirnov, S., Tanhuanpää, K., Faix, J., Rivera, C., et al. (2009). Defining mechanisms of actin polymerization and depolymerization during dendritic spine morphogenesis. *J. Cell. Biol.* 185, 323–339. doi: 10.1083/jcb.200809046

Irwin, S. A., Patel, B., Idupulapati, M., Harris, J. B., Crisostomo, R. A., Larsen, B. P., et al. (2001). Abnormal dendritic spine characteristics in the temporal and visual cortices of patients with fragile-X syndrome: a quantitative examination. *Am. J. Med. Genet.* 98, 161–167. doi: 10.1002/1096-8628(20010115)98:2<161::aid-ajmg1025>3.0.co;2-b

Iwata, R., Matsukawa, H., Yasuda, K., Mizuno, H., Itohara, S., and Iwasato, T. (2015). Developmental RacGAP α2-chimaerin signaling is a determinant of the morphological features of dendritic spines in adulthood. *J. Neurosci.* 35, 13728–13744. doi: 10.1523/jneurosci.0419-15.2015

Jiang, L., Mao, R., Tong, J., Li, J., Chai, A., Zhou, Q., et al. (2016). Inhibition of Rac1 activity in the hippocampus impaired extinction of contextual fear. *Neuropharmacology* 109, 216–222. doi: 10.1016/j.neuropharm.2016.06.017

Jourdain, P., Fukunaga, K., and Muller, D. (2003). Calcium/calmodulin-dependent protein kinase II contributes to activity-dependent filopodia growth and spine formation. *J. Neurosci.* 23, 10645–10649. doi: 10.1523/jneurosci.23-33-10645.2003

Kaartinen, V., Gonzalez-Gomez, I., Voncken, J. W., Haataja, L., Faure, E., Nagy, A., et al. (2001). Abnormal function of astroglia lacking Abr and Bcr RacGAPs. *Development* 128, 4217–4227.

Kim, I. H., Racz, B., Wang, H., Burianek, L., Weinberg, R., Yasuda, R., et al. (2013). Disruption of Arp2/3 results in asymmetric structural plasticity of dendritic spines and progressive synaptic and behavioral abnormalities. *J. Neurosci.* 33, 6081–6092. doi: 10.1523/JNEUROSCI.0035-13.2013

Kim, Y., Sung, J. Y., Ceglia, I., Lee, K. W., Ahn, J. H., Halford, J. M., et al. (2006). Phosphorylation of WAVE1 regulates actin polymerization and dendritic spine morphology. *Nature* 442, 814–817. doi: 10.1038/nature04976

Lai, C. S., Franke, T. F., and Gan, W. B. (2012). Opposite effects of fear conditioning and extinction on dendritic spine remodelling. *Nature* 48, 87–91. doi: 10.1038/nature10792

Lai, K. O., Wong, A. S., Cheung, M. C., Xu, P., Liang, Z., Lok, K. C., et al. (2012). TrkB phosphorylation by Cdk5 is required for activity-dependent structural plasticity and spatial memory. *Nat. Neurosci.* 15, 1506–1515. doi: 10.1038/nn.3237

Lamprecht, R., and LeDoux, J. (2004). Structural plasticity and memory. *Nat. Rev. Neurosci.* 5, 45–54.

Lappalainen, P., and Drubin, D. G. (1997). Cofilin promotes rapid actin filament turnover *in vivo*. *Nature* 388, 78–82 doi: 10.1038/40418

Lee, A., Li, W., Xu, K., Bogert, B. A., Su, K., and Gao, F. B. (2003). Control of dendritic development by the Drosophila fragile X-related gene involves the small GTPase Rac1. *Development* 130, 5543–5552. doi: 10.1242/dev.00792

Liao, Z., Tao, Y., Guo, X., Cheng, D., Wang, F., Liu, X., et al. (2017). Fear conditioning downregulates Rac1 activity in the basolateral amygdala astrocytes to facilitate the formation of fear memory. *Front. Mol. Neurosci.* 10:396. doi: 10.3389/fnmol.2017.00396

Liu, Y., Du, S., Lv, L., Lei, B., Shi, W., Tang, Y., et al. (2016). Hippocampal activation of RAC1 regulates the forgetting of object recognition memory. *Curr. Biol.* 26, 2351–2357. doi: 10.1016/j.cub.2016.06.056

Liu, Y., Lv, L., Wang, L., and Zhong, Y. (2018). Social isolation induces RAC1-dependent forgetting of social memory. *Cell Rep.* 25, 288–295. doi: 10.1016/j.celrep.2018.09.033

Luo, L., Hensch, T. K., Ackerman, L., Barbel, S., Jan, L. Y., and Jan, Y. N. (1996). Differential effects of the Rac GTPase on Purkinje cell axons and dendritic trunks and spines. *Nature* 379, 837–840. doi: 10.1038/379837a0

Lv, L., Liu, Y., Xie, J., Wu, Y., Zhao, J., Li, Q., et al. (2019). Interplay between α2-chimaerin and Rac1 activity determines dynamic maintenance of long-term memory. *Nat. Commun.* 10:5313.

Maletic-Savatic, M., Malinow, R., and Svoboda, K. (1999). Rapid dendritic morphogenesis in CA1 hippocampal dendrites induced by synaptic activity. *Science* 283, 1923–1927. doi: 10.1126/science.283.5409.1923

Martinez, L. A., and Tejada-Simon, M. V. (2018). Pharmacological rescue of hippocampal fear learning deficits in fragile X syndrome. *Mol. Neurobiol.* 55, 5951–5961. doi: 10.1007/s12035-017-0819-5

Matsuzaki, M., Honkura, N., Ellis-Davies, G. C., and Kasai, H. (2004). Structural basis of long-term potentiation in single dendritic spines. *Nature* 429, 761–766. doi: 10.1038/nature02617

Matus, A. (2000). Actin-based plasticity in dendritic spines. *Science* 290, 754–758. doi: 10.1126/science.290.5492.754

Matus, A. (2005). Growth of dendritic spines: a continuing story. *Curr. Opin. Neurobiol.* 15, 67–72. doi: 10.1016/j.conb.2005.01.015

Meng, Y., Zhang, Y., Tregoubov, V., Janus, C., Cruz, L., Jackson, M., et al. (2002). Abnormal spine morphology and enhanced LTP in LIMK-1 knockout mice. *Neuron* 35, 121–133. doi: 10.1016/s0896-6273(02)00758-4

Miermans, C. A., Kusters, R. P., Hoogenraad, C. C., and Storm, C. (2017). Biophysical model of the role of actin remodeling on dendritic spine morphology. *PLoS One* 12:e0170113. doi: 10.1371/journal.pone.0170113

Nakayama, A. Y., Harms, M. B., and Luo, L. (2000). Small GTPases Rac and Rho in the maintenance of dendritic spines and branches in hippocampal pyramidal neurons. *J. Neurosci.* 20, 5329–5338. doi: 10.1523/jneurosci.20-14-05329.2000

Newey, S. E., Velamoor, V., Govek, E. E., and Van Aelst, L. (2005). Rho GTPases, dendritic structure, and mental retardation. *J. Neurobiol.* 64, 58–74. doi: 10.1002/neu.20153

Newpher, T. M., and Ehlers, M. D. (2009). Spine microdomains for postsynaptic signaling and plasticity. *Trends Cell Biol.* 19, 218–227. doi: 10.1016/j.tcb.2009.02.004

Nimchinsky, E. A., Sabatini, B. L., and Svoboda, K. (2002). Structure and function of dendritic spines. *Annu. Rev. Physiol.* 64, 313–353.

Nishiyama, J., and Yasuda, R. (2015). Biochemical computation for spine structural plasticity. *Neuron* 87, 63–75. doi: 10.1016/j.neuron.2015.05.043

Noguchi, J., Matsuzaki, M., Ellis-Davies, G. C. R., and Kasai, H. (2005). Spine-neck geometry determines NMDA receptor-dependent Ca2+signaling in dendrites. *Neuron* 46, 609–622. doi: 10.1016/j.neuron.2005.03.015

Noguchi, J., Nagaoka, A., Watanabe, S., Ellis-Davies, G. C., Kitamura, K., Kano, M., et al. (2011). *In vivo* two-photon uncaging of glutamate revealing the structure-function relationships of dendritic spines in the neocortex of adult mice. *J. Physiol.* 589, 2447–2457. doi: 10.1113/jphysiol.2011.207100

Oh, D., Han, S., Seo, J., Lee, J. R., Choi, J., Groffen, J., et al. (2010). Regulation of synaptic Rac1 activity, long-term potentiation maintenance, and learning and memory by BCR and ABR Rac GTPase-activating proteins. *J. Neurosci.* 30, 14134–14144. doi: 10.1523/jneurosci.1711-10.2010

Ostroff, L. E., Cain, C. K., Bedont, J., Monfils, M. H., and Ledoux, J. E. (2010). Fear and safety learning differentially affect synapse size and dendritic translation in the lateral amygdala. *Proc. Natl. Acad. Sci. U.S.A.* 107, 9418–9423. doi: 10.1073/pnas.0913384107

Pavlov, I. P. (1927). *Conditioned Reflexes: An Investigation of the Physiological Activity of the Cerebral Cortex*. London: Oxford University Press.

Pennucci, R., Gucciardi, I., and de Curtis, I. (2019). Rac1 and Rac3 GTPases differently influence the morphological maturation of dendritic spines in hippocampal neurons. *PLoS One* 14:e0220496. doi: 10.1371/journal.pone.0220496

Penzes, P., Beeser, A., Chernoff, J., Schiller, M. R., Eipper, B. A., Mains, R. E., et al. (2003). Rapid induction of dendritic spine morphogenesis by trans-synaptic ephrinB-EphB receptor activation of the Rho-GEF kalirin. *Neuron* 37, 263–274. doi: 10.1016/s0896-6273(02)01168-6

Penzes, P., Cahill, M. E., Jones, K. A., and Srivastava, D. P. (2008). Convergent CaMK and RacGEF signals control dendritic structure and function. *Trends Cell Biol.* 8, 405–413. doi: 10.1016/j.tcb.2008.07.002

Peters, A., and Kaiserman-Abramof, I. R. (1970). The small pyramidal neuron of the rat cerebral cortex. The perikaryon, dendrites and spines. *Am. J. Anat.* 127, 321–355. doi: 10.1002/aja.1001270402

Pilpel, Y., and Segal, M. (2004). Activation of PKC induces rapid morphological plasticity in dendrites of hippocampal neurons via Rac and Rho-dependent mechanisms. *Eur. J. Neurosci.* 19, 3151–3164. doi: 10.1111/j.0953-816x.2004.03380.x

Pollard, T. D. (2007). Regulation of actin filament assembly by Arp2/3 complex and formins. *Annu. Rev. Biophys. Biomol. Struct.* 36, 451–477. doi: 10.1146/annurev.biophys.35.040405.101936

Puigdellívol, M., Cherubini, M., Brito, V., Suelves, N., Ballesteros, J., Zamora-Moratalla, A., et al. (2015). A role for Kalirin-7 in corticostriatal synaptic dysfunction in Huntington's disease. *Hum. Mol. Genet.* 24, 7265–7285. doi: 10.1093/hmg/ddv426

Pyronneau, A., He, Q., Hwang, J. Y., Porch, M., Contractor, A., and Zukin, R. S. (2017). Aberrant Rac1-cofilin signaling mediates defects in dendritic spines, synaptic function, and sensory perception in fragile X syndrome. *Sci. Signal.* 10:eaan0852. doi: 10.1126/scisignal.aan0852

Rácz, B., and Weinberg, R. J. (2008). Organization of the Arp2/3 complex in hippocampal spines. *J. Neurosci.* 28, 5654–5659. doi: 10.1523/JNEUROSCI.0756-08.2008

Reinhard, J. R., Kriz, A., Galic, M., Angliker, N., Rajalu, M., Vogt, K. E., et al. (2016). The calcium sensor Copine-6 regulates spine structural plasticity and learning and memory. *Nat. Commun.* 7:11613. doi: 10.1038/ncomms11613

Rescorla, R. A. (1996). Preservation of pavlovian associations through extinction. *Q. J. Exp. Psychol.* 49B, 245–258.

Restivo, L., Vetere, G., Bontempi, B., and Ammassari-Teule, M. (2009). The formation of recent and remote memory is associated with time-dependent formation of dendritic spines in the hippocampus and anterior cingulate cortex. *J. Neurosci.* 29, 8206–8214. doi: 10.1523/JNEUROSCI.0966-09.2009

Rudelli, R. D., Brown, W. T., Wisniewski, K., Jenkins, E. C., Laure-Kamionowska, M., Connell, F., et al. (1985). Adult fragile X syndrome. Clinico-neuropathologic findings. *Acta Neuropathol.* 67, 289–295. doi: 10.1007/bf00687814

Rust, M. B. (2015). ADF/cofilin: a crucial regulator of synapse physiology and behavior. *Cell. Mol. Life Sci.* 72, 3521–3529. doi: 10.1007/s00018-015-1941-z

Rust, M. B., Gurniak, C. B., Renner, M., Vara, H., Morando, L., Görlich, A., et al. (2010). Learning, AMPA receptor mobility and synaptic plasticity depend on n-cofilin-mediated actin dynamics. *EMBO J.* 29, 1889–1902. doi: 10.1038/emboj.2010.72

Sanchez, A. M., Flamini, M. I., Fu, X. D., Mannella, P., Giretti, M. S., Goglia, L., et al. (2009). Rapid signaling of estrogen to WAVE1 and moesin controls neuronal spine formation via the actin cytoskeleton. *Mol. Endocrinol.* 23, 1193–1202. doi: 10.1210/me.2008-0408

Saneyoshi, T., Matsuno, H., Suzuki, A., Murakoshi, H., Hedrick, N. G., Agnello, E., et al. (2019). Reciprocal activation within a kinase-effector complex underlying persistence of structural LTP. *Neuron* 102, 1199–1210. doi: 10.1016/j.neuron.2019.04.012

Santamaria, F., Wils, S., De Schutter, E., and Augustine, G. J. (2006). Anomalous diffusion in Purkinje cell dendrites caused by spines. *Neuron* 52, 635–648. doi: 10.1016/j.neuron.2006.10.025

Schenck, A., Bardoni, B., Langmann, C., Harden, N., Mandel, J. L., and Giangrande, A. (2003). CYFIP/Sra-1 controls neuronal connectivity in Drosophila and links the Rac1 GTPase pathway to the fragile X protein. *Neuron* 38, 887–898. doi: 10.1016/s0896-6273(03)00354-4

Schubert, V., and Dotti, C. G. (2007). Transmitting on actin: synaptic control of dendritic architecture. *J. Cell. Sci.* 120, 205–212. doi: 10.1242/jcs.03337

Selkoe, D. J., and Hardy, J. (2016). The amyloid hypothesis of Alzheimer's disease at 25 years. *EMBO Mol. Med.* 8, 595–608.

Seoh, M. L., Ng, C. H., Yong, J., Lim, L., and Leung, T. (2003). ArhGAP15, a novel human RacGAP protein with GTPase binding property. *FEBS Lett.* 539, 131–137. doi: 10.1016/s0014-5793(03)00213-8

Shuai, Y., Lu, B., Hu, Y., Wang, L., Sun, K., and Zhong, Y. (2010). Forgetting is regulated through Rac activity in *Drosophila*. *Cell* 140, 579–589. doi: 10.1016/j.cell.2009.12.044

Small, S. A., and Duff, K. (2008). Linking Abeta and tau in late-onset Alzheimer's disease: a dual pathway hypothesis. *Neuron* 60, 534–542. doi: 10.1016/j.neuron.2008.11.007

Spillane, M., and Gallo, G. (2014). Involvement of Rho-family GTPases in axon branching. *Small GTPases* 5:e27974. doi: 10.4161/sgtp.27974

Steele, R. J., and Morris, R. G. (1999). Delay-dependent impairment of a matching-to-place task with chronic and intrahippocampal infusion of the NMDA-antagonist D-AP5. *Hippocampus* 9, 118–136. doi: 10.1002/(sici)1098-1063(1999)9:2<118::aid-hipo4>3.0.co;2-8

Takumi, Y., Ramírez-León, V., Laake, P., Rinvik, E., and Ottersen, O. P. (1999). Different modes of expression of AMPA and NMDA receptors in hippocampal synapses. *Nat. Neurosci.* 2, 618–624. doi: 10.1038/10172

Tan, E. C., Leung, T., Manser, E., and Lim, L. (1993). The human active breakpoint cluster region-related gene encodes a brain protein with homology to guanine nucleotide exchange proteins and GTPase-activating proteins. *J. Biol. Chem.* 268, 27291–27298.

Tashiro, A., Minden, A., and Yuste, R. (2000). Regulation of dendritic spine morphology by the rho family of small GTPases: antagonistic roles of Rac and Rho. *Cereb. Cortex* 10, 927–938. doi: 10.1093/cercor/10.10.927

Tolias, K. F., Bikoff, J. B., Burette, A., Paradis, S., Harrar, D., Tavazoie, S., et al. (2005). The Rac1-GEF Tiam1 couples the NMDA receptor to the activity-dependent development of dendritic arbors and spines. *Neuron* 45, 525–538. doi: 10.1016/j.neuron.2005.01.024

Tønnesen, J., Katona, G., Rózsa, B., and Nägerl, U. V. (2014). Spine neck plasticity regulates compartmentalization of synapses. *Nat. Neurosci.* 17, 678–685. doi: 10.1038/nn.3682

Tousley, A., Iuliano, M., Weisman, E., Sapp, E., Zhang, N., Vodicka, P., et al. (2019). Rac1 activity is modulated by huntingtin and dysregulated in models of Huntington's disease. *J. Huntington's Dis.* 8, 53–69. doi: 10.3233/jhd-180311

Tu, G., Ying, L., Ye, L., Zhao, J., Liu, N., Li, J., et al. (2019). Dopamine D1 and D2 receptors differentially regulate Rac1 and Cdc42 signaling in the nucleus accumbens to modulate behavioral and structural plasticity after repeated methamphetamine treatment. *Biol. Psychiatry* 86, 820–835. doi: 10.1016/j.biopsych.2019.03.966

Um, K., Niu, S., Duman, J. G., Cheng, J. X., Tu, Y. K., Schwechter, B., et al. (2014). Dynamic control of excitatory synapse development by a Rac1 GEF/GAP regulatory complex. *Dev. Cell* 29, 701–715. doi: 10.1016/j.devcel.2014.05.011

Verpelli, C., Heise, C., and Sala, C. (2014). *Structural and Functional Organization of the Postsynaptic Density*. Amsterdam: Elsevier, 129–153.

Vetere, G., Restivo, L., Cole, C. J., Ross, P. J., Ammassari-Teule, M., Josselyn, S. A., et al. (2011). Spine growth in the anterior cingulate cortex is necessary for the consolidation of contextual fear memory. *Proc. Natl. Acad. Sci. U.S.A.* 108, 8456–8460. doi: 10.1073/pnas.1016275108

Villa, K. L., Berry, K. P., Subramanian, J., Cha, J. W., Oh, W. C., Kwon, H. B., et al. (2016). Inhibitory synapses are repeatedly assembled and removed at persistent sites *in vivo* article inhibitory synapses are repeatedly assembled and removed at persistent sites *in vivo*. *Neuron* 89, 756–769. doi: 10.1016/j.neuron.2016.01.010

Voncken, J. W., van Schaick, H., Kaartinen, V., Deemer, K., Coates, T., Landing, B., et al. (1995). Increased neutrophil respiratory burst in bcr-null mutants. *Cell* 80, 719–728. doi: 10.1016/0092-8674(95)90350-x

Walker, F. O. (2007). Huntington's disease. *Lancet* 369, 218–228.

Wang, W., Ju, Y. Y., Zhou, Q. X., Tang, J. X., Li, M., Zhang, L., et al. (2017). The Small GTPase Rac1 Contributes to Extinction of Aversive Memories of Drug Withdrawal by Facilitating GABAA Receptor Endocytosis in the vmPFC. *J. Neurosci.* 37, 7096–7110. doi: 10.1523/JNEUROSCI.3859-16.2017

Wegner, A. M., Nebhan, C. A., Hu, L., Majumdar, D., Meier, K. M., Weaver, A. M., et al. (2008). N-wasp and the arp2/3 complex are critical regulators of actin in the development of dendritic spines and synapses. *J. Biol. Chem.* 283, 15912–15920. doi: 10.1074/jbc.M801555200

Wiens, K. M., Lin, H., and Liao, D. (2005). Rac1 induces the clustering of AMPA receptors during spinogenesis. *J. Neurosci.* 25, 10627–10636. doi: 10.1523/jneurosci.1947-05.2005

Wright, W. J., Graziane, N. M., Neumann, P. A., Hamilton, P. J., Cates, H. M., Fuerst, L., et al. (2020). Silent synapses dictate cocaine memory destabilization and reconsolidation. *Nat. Neurosci.* 23, 32–46. doi: 10.1038/s41593-019-0537-6

Wu, P., Ding, Z. B., Meng, S. Q., Shen, H. W., Sun, S. C., Luo, Y. X., et al. (2014). Differential role of Rac in the basolateral amygdala and cornu ammonis 1 in the reconsolidation of auditory and contextual Pavlovian fear memory in rats. *Psychopharmacology* 231, 2909–2919. doi: 10.1007/s00213-014-3462-0

Wu, W., Du, S., Shi, W., Liu, Y., Hu, Y., Xie, Z., et al. (2019). Inhibition of Rac1-dependent forgetting alleviates memory deficits in animal models of Alzheimer's disease. *Protein Cell* 10, 745–759. doi: 10.1007/s13238-019-0641-0

Xie, Z., Srivastava, D. P., Photowala, H., Kai, L., Cahill, M. E., Woolfrey, K. M., et al. (2007). Kalirin-7 controls activity-dependent structural and functional plasticity of dendritic spines. *Neuron* 56, 640–656. doi: 10.1016/j.neuron.2007.10.005

Xu, T., Yu, X., Perlik, A. J., Tobin, W. F., Zweig, J. A., Tennant, K., et al. (2009). Rapid formation and selective stabilization of synapses for enduring motor memories. *Nature* 462, 915–919. doi: 10.1038/nature08389

Yang, G., Pan, F., and Gan, W. B. (2009). Stably maintained dendritic spines are associated with lifelong memories. *Nature* 462, 920–924. doi: 10.1038/nature08577

Yang, N., Higuchi, O., Ohashi, K., Nagata, K., Wada, A., Kangawa, K., et al. (1998). Cofilin phosphorylation by LIM-kinase 1 and its role in Racmediated actin reorganization. *Nature* 393, 809–812. doi: 10.1038/31735

Yang, Y., Liu, D. Q., Huang, W., Deng, J., Sun, Y., Zuo, Y., et al. (2016). Selective synaptic remodeling of amygdalocortical connections associated with fear memory. *Nat. Neurosci.* 19, 1348–1355. doi: 10.1038/nn.4370

Young, E. J., Aceti, M., Griggs, E. M., Fuchs, R. A., Zigmond, Z., Rumbaugh, G., et al. (2014). Selective, retrieval-independent disruption of methamphetamine-associated memory by actin depolymerization. *Biol. Psychiatry* 75, 96–104. doi: 10.1016/j.biopsych.2013.07.036

Zamboni, V., Armentano, M., Sarò, G., Ciraolo, E., Ghigo, A., Germena, G., et al. (2016). Disruption of ArhGAP15 results in hyperactive Rac1, affects the architecture and function of hippocampal inhibitory neurons and causes cognitive deficits. *Sci. Rep.* 6:34877. doi: 10.1038/srep 34877

Conflict of Interest: The authors declare that the research was conducted in the absence of any commercial or financial relationships that could be construed as a potential conflict of interest.

frontiers in Synaptic Neuroscience

REVIEW
published: 28 August 2020
doi: 10.3389/fnsyn.2020.00036

Dendritic Spine Plasticity: Function and Mechanisms

*Karen Runge, Carlos Cardoso and Antoine de Chevigny**

Institut de Neurobiologie de la Méditerranée (INMED) INSERM U1249, Aix-Marseille University, Marseille, France

Dendritic spines are small protrusions studding neuronal dendrites, first described in 1888 by Ramón y Cajal using his famous Golgi stainings. Around 50 years later the advance of electron microscopy (EM) confirmed Cajal's intuition that spines constitute the postsynaptic site of most excitatory synapses in the mammalian brain. The finding that spine density decreases between young and adult ages in fixed tissues suggested that spines are dynamic. It is only a decade ago that two-photon microscopy (TPM) has unambiguously proven the dynamic nature of spines, through the repeated imaging of single spines in live animals. Spine dynamics comprise formation, disappearance, and stabilization of spines and are modulated by neuronal activity and developmental age. Here, we review several emerging concepts in the field that start to answer the following key questions: What are the external signals triggering spine dynamics and the molecular mechanisms involved? What is, in return, the role of spine dynamics in circuit-rewiring, learning, and neuropsychiatric disorders?

Keywords: dendritic spine plasticity, molecular controls, neurodevelopmental disorders, two photon imaging, structural plasticity

OPEN ACCESS

Edited by:
Menahem Segal,
Weizmann Institute of Science, Israel

Reviewed by:
Shigeo Okabe,
The University of Tokyo, Japan
Akos Kulik,
University of Freiburg, Germany

***Correspondence:**
Antoine de Chevigny
antoine.de-chevigny@inserm.fr

Received: *27 May 2020*
Accepted: *28 July 2020*
Published: *28 August 2020*

Citation:
Runge K, Cardoso C and de Chevigny A (2020) Dendritic Spine Plasticity: Function and Mechanisms. Front. Synaptic Neurosci. 12:36. doi: 10.3389/fnsyn.2020.00036

INTRODUCTION

Dendritic spines are the postsynaptic sites of most excitatory synapses, found along the dendrites of neurons. *Ramón y Cajal in 1888* was the first to observe these small protrusions 1.0–1.5 μm in length in Golgi stainings (Cajal, 1888). He proposed them to be points of contact between neurons. Towards the end of the century, theories emerged proposing that changes in brain activity and function could be driven by morphological modifications of spines (reviewed by DeFelipe, 2015). Following years of speculations, it was only in 1959 with the development of electron microscopy (EM) that spines were confirmed to be the points of contact between neurons, by forming the postsynaptic element of synapses (Gray, 1959). Comparing brain tissue at immature vs. old ages (Feldman and Dowd, 1975) or after being exposed to an enriched or impoverished environment (Globus et al., 1973) showed striking differences in spine densities, indicating that dendritic spines must be to some degree plastic. Ziv and Smith (1996) and Fischer et al. (1998) eventually observed dendritic spine dynamics for the first time in cultured hippocampal neurons and were intrigued by the unexpected rapidity of spine formation and elimination. With the development of two-photon microscopy (TPM; Denk et al., 1990) and the emergence of transgenic animals expressing fluorochromes in neurons in the early 2000s (Feng et al., 2000; Keller-Peck et al., 2001), researchers became able to follow spine changes over time *in vivo* (Grutzendler et al., 2002; Trachtenberg et al., 2002). These revolutionizing studies gathered information on spine dynamics in basal vs. specific contexts, for example, motor tasks (Xu et al., 2009) or sensory deprivations

(Zuo et al., 2005a; Keck et al., 2008). Nowadays, *in vivo* TPM has gained in precision owing to improvements in optical tools and the ability to express high-quality fluorophores in defined subsets of neurons. In addition to the use of transgenic mouse lines, e.g., Thy1-GFP (Feng et al., 2000), other techniques as viral transmission (Kuhlman and Huang, 2008), *in utero* electroporation (Villa et al., 2016; Subramanian et al., 2019) and single-cell electroporation (Pagès et al., 2015) have allowed controlled spatial and temporal expression of fluorescent dyes and other genetic constructs in desired cell types across the cortex.

To excite the target neurons with a two-photon laser within the living brain, one has to remove or thin a part of the animal's skull. Since the beginnings of *in vivo* TPM, two techniques have emerged. The first is cranial window surgery (Trachtenberg et al., 2002; Villa et al., 2016), where a piece of bone is removed and replaced with a transparent window. The second is thinned-skull cranial window surgery (Grutzendler et al., 2002; Isshiki et al., 2014), where, in an attempt to be less invasive, the skull is thinned using micro-surgical blades to a thickness of approximately 20 μm (Zuo et al., 2005b), rendering the bone translucent. While cranial window implantation has been associated with inflammation-induced spine turnover (Xu et al., 2007) for more than 20 days post-surgery, cranial thinning in turn does not require a recovery period, is less associated with inflammation and allows immediate imaging (Yang et al., 2010). However, the thinned skull technique is more challenging and, due to the natural regrowth of the thinned bone, one has to re-thin the window to image repeatedly (Zuo et al., 2005b). Nowadays, both techniques are largely employed. For more details on the cranial window and thinned-skull cranial window surgeries please refer to Xu et al. (2007) and Yang et al. (2010).

In the last decades, spine dynamics have taken a prominent role in explaining the brain's adaptability. Deciphering the intrinsic and extrinsic mechanisms that underlie specific turnover properties shall help to elucidate the functional changes that in turn lead to complex cognitive abilities or drive pathological outcomes. Here, we review the most recent literature in the field of spine dynamics with a particular focus on *in vivo* TPM. We address the following questions: What are the intrinsic and experience-dependent signals that control spine dynamic and how? What is, in return, the role of spine-dynamics in behavior?

SPINOGENESIS AND SPINE SUBTYPES

For a list of the main studies with *in vivo* TPM of spine dynamics during development, see **Table 1**. Spines are commonly classified into filopodia, stubby, thin, and mushroom spines, according to their shape and size (Peters and Kaiserman-Abramof, 1970). These fixed categories have been challenged, though, as in physiological conditions spines are constantly evolving and morphological stages are transitory (Tønnesen et al., 2014).

Filopodia are long and thin protrusions without bulbous heads whose contribution is high in early postnatal life and rapidly drops down in adulthood. They are the most dynamic dendritic protrusions as they can appear and disappear in as little as 10 min (Ziv and Smith, 1996). Thin spines have small heads separated from the dendrite by long, thin necks. Stubby spines were initially described as containing a bulbous head directly budding from the dendrite without intermediate neck structures. However, recent superresolution imaging based on stimulated emission depletion (STED) microscopy has indicated that stubby spines in fact would have very short necks connecting the head to the dendrite and that those short necks would be visible only by STED (Tønnesen et al., 2014). Further time-lapse experiments suggested that mushroom spines undergo neck length reduction upon stimulation, indicating that stubby spines could be a form of active mushroom spines with very short necks (Tønnesen et al., 2014). Thus, the structural and functional roles of stubby spines need to be reevaluated. Stubby and thin spines are less dynamic than filopodia and can persist over several days (Holtmaat et al., 2005). The least dynamic spines are the large-headed mushroom spines that can be stable over several months (Grutzendler et al., 2002). Mushroom spines are commonly seen as functional spines and synaptically connected to an axonal bouton. Following stimulation, thin spines were shown to acquire a full functional synapse and transit simultaneously into stable mushroom spines (Matsuzaki et al., 2004); this need to be reevaluated now that some stubby spines are mushroom spines with short necks (Tønnesen et al., 2014). However, the presence of synapses in small spines does not always predict stability nor the future acquisition of a mushroom morphology. Using *in vivo* TPM imaging and EM, it has been shown that fractions of small transient spines are also able to form temporary synapse components and to participate in functional circuits before being eliminated (Cane et al., 2014).

Whether spine formation reflects some intrinsic properties of postsynaptic dendrites that precede synaptogenesis or if it is induced by extrinsic factors associated with presynaptic axonal terminals during synaptogenesis is still under debate. However, strong lines of evidence indicate that dendritic filopodia are involved in the initial stages of spinogenesis and synaptogenesis in most, if not 100%, of cases. First, time-lapse observations from neuron cultures and brain organotypic slices have revealed that dendritic filopodia can initiate contacts with presynaptic axons and are occasionally transformed into spines (Dailey and Smith, 1996; Ziv and Smith, 1996). Second, the presence of synaptic contacts between a fraction of filopodia and axons was confirmed by EM studies (Fiala et al., 1998). These findings suggest that filopodia are spine precursors acting as samplers of the local synaptic neighborhood. Later, *in vivo* imaging in YFP-expressing young mice demonstrated that dendritic filopodia are indeed highly dynamic and can transform into spines (Grutzendler et al., 2002; Zuo et al., 2005b). In juvenile mice, ∼12% of all dendritic protrusions in different cortical regions are filopodia, the remaining being spines. Whereas most filopodia at a given time point underwent rapid turnover within a few hours, ∼15% rapidly transformed into spine-like protrusions, of which 20% survived long term (Zuo et al., 2005b). These newly persistent protrusions were morphologically indistinguishable from preexisting spines. In sum, in the brain of young mice, a small percentage of filopodia observed at a given time point are

TABLE 1 | Spine plasticity during development.

Brain region	Age animals	Impact on spine stability	Main results	Methods	Reference
Visual cortex					
Visual cortex, PN, Layer 5	P30	73% stable spines over 30 days	Spines become more stable from juvenile to adult ages.	Two-photon laser scanning, Thinned skull cranial window, YFP-labeled dendrites	Grutzendler et al. (2002)
	4 months	96% stable spines over 30 days			
Visual cortex, auditory cortex, somatosensory cortex, PN, Layer 5	P40-P61	VC: 78% of spines stable over 3 weeks SS: 88% of spines stable over 3 weeks AC: 89% of spines stable over 3 weeks	Most (∼80%) spines in the cortex are stable over 3 weeks.	Two-photon laser scanning, Thinned skull cranial window, GFP or YFP-labeled dendrites	Majewska et al. (2006)
Somatosensory cortex					
Somatosensory cortex, visual cortex, PN, Layer 5	P16-25	SS: 35% stable spines over ≥8 days	Spines become more stable from juvenile to adult ages. Stability in SS and VC is similar.	Two-photon laser scanning, Craniotomy, GFP or YFP-labeled dendrites	Holtmaat et al. (2005)
	P35-80	SS: 54% stable spines over ≥8 days			
	P80-120	SS: 66% stable spines over ≥8 days			
	P175-225	SS: 73% stable spines over ≥8 days			
	3-6 months	VC: 75% stable spines over ≥8 days			
Barrel cortex, Motor cortex, Frontal cortex, PN Layer 5	P30	60% stable over 22 months	Spines become more stable in adulthood and a majority of them can last throughout life.	Two-photon laser scanning, Thinned skull cranial window, YFP-labeled dendrites	Zuo et al. (2005b)
	4-6 months	74% stable over 18 months			
Barrel cortex, PN, Layer 2/3	P56	78% of stable spines observed over 17 days contain a PSD	Most stable spines have a PSD.	Two-photon laser scanning, Craniotomy, DsRedExpress-labeled dendrites, GFP-labeled PSD-95	Cane et al. (2014)

transformed into stable thin or mushroom-like dendritic spines, while other filopodia are eliminated. These *in vivo* observations reinforce the notion that dendritic filopodia are spine precursors that sample the environment in search of axonal partners to elicit spinogenesis and synaptogenesis.

Although the aforementioned data indicate that spines are born from filopodia that have found a presynaptic axonal partner during dynamic sampling, several studies have suggested that other modes of spinogenesis might also occur at specific developmental time points. First, EM studies in early development have suggested that excitatory shaft synapses precede the formation of spine synapses (Fiala et al., 1998; Zuo et al., 2005b). These observations were reinforced by time-lapse imaging studies showing that at this stage spines can form directly from dendritic shafts without passing by a filopodial stage (Dailey and Smith, 1996). Such observations were confirmed more recently in studies showing that glutamate and γ-aminobutyric acid (GABA) uncaging can induce spine formation without the need for a filopodial intermediate (Kwon and Sabatini, 2011; Oh et al., 2016). These observations suggest that spinogenesis during very early development might skip a filopodial sampling phase, although the requirement for presynaptic axon proximity seems preserved.

Overall, the current knowledge strongly supports the hypothesis that, at least in young mice, axonal growth and neurotransmitter release may be the triggering events in dendritic spine formation such that axonal bouton localization and activity are important triggers of spinogenesis.

SPINE PRUNING IN YOUTH, STABILITY IN ADULTHOOD

Since the first studies on fixed tissues, striking differences in spine densities were observed between developmental ages. Across several mammalian species, including humans, projection neurons in young brains show a much higher spine density compared to those in adults (Rakic et al., 1986; Markus and Petit, 1987; Lübke and Albus, 1989; Huttenlocher, 1990; Duan et al., 2003). This suggests that during youth, neuronal networks undergo significant modifications mediated, at least in part, by synapse elimination. However, these analyses on fixed postmortem tissues did not allow determining the dynamic

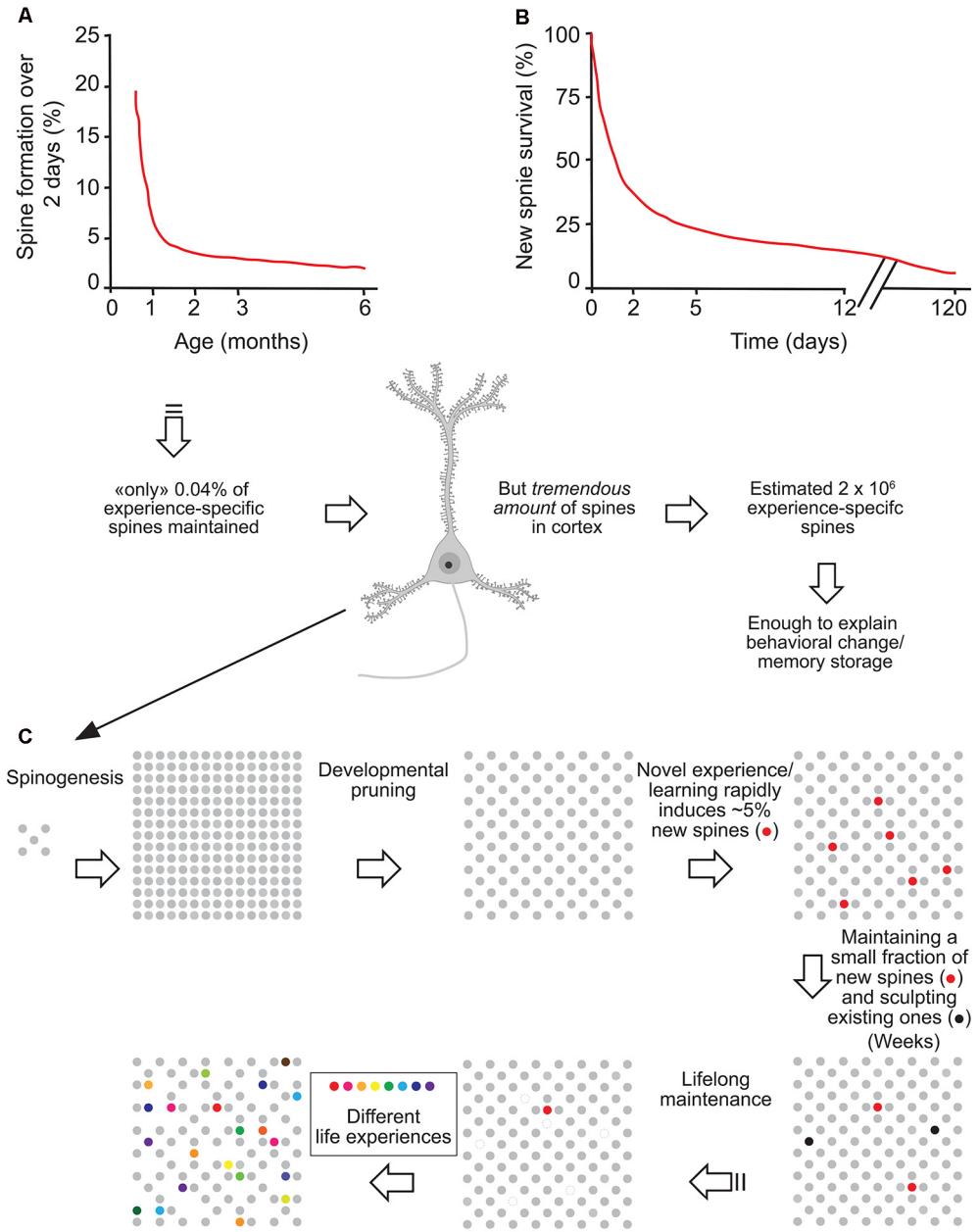

FIGURE 1 | Experience-specific spines constitute a tiny fraction of total spines but can encode memory. **(A)** Spine formation rate declined rapidly from P19 to P30 and remained low thereafter. **(B)** Regardless of animals' ages, ~5% of new spines formed over 2 days were maintained over a protracted process. **(C)** Schematic summary of spine remodeling and maintenance throughout life. Spines are rapidly formed after birth, undergo experience-dependent pruning during postnatal development, and remain largely stable in adulthood. Learning or novel sensory experience induces the rapid formation of new spines (5% of total spines) within 1–2 days. Only a tiny fraction of new spines (0.04% of total spines) survive the first few weeks in synaptic circuits and are stably maintained later in life. Novel experience also results in the pruning of a small fraction of existing spines formed early during development. New stable spines induced by novel experience, together with existing spines formed during early development and surviving experience-dependent pruning, provide an integrated and stable structural basis for lifelong memory storage, despite ongoing plasticity in synaptic networks. Modified with permission from Yang et al. (2009).

behavior of dendritic spines. This is important because, as spines are dynamically formed and eliminated over time, the decrease in net spine density with increasing age may be due to an increase in the elimination of existing spines, the addition of fewer new spines, or a combination of both. To address this issue, dendritic spines of layer 5 (L5) neurons were longitudinally

imaged by *in vivo* TPM. Such studies showed that in juvenile mice, 13–20% of spines were eliminated and 5–8% were formed over a 2-week interval in barrel, motor, visual and frontal cortical areas, indicating a cortex wide elimination of spines during this developmental period (Grutzendler et al., 2002; Zuo et al., 2005b). Because the amount of spine elimination is more than two-fold higher than that of spine formation between adolescence and adulthood, these *in vivo* studies indicate that the net spine loss observed in fixed tissue is mainly due to the elimination, also called "pruning," of existing synaptic connections.

The question of the stability of spines in adulthood was first treated in 2002 by two groups who initially came to different conclusions: Trachtenberg et al. (2002) found that in 6–10 week old young adult mice only 60% of spines were stable over 8 days, suggesting a relative instability of adult spines (Trachtenberg et al., 2002). Grutzendler et al. (2002), in contrast, when imaging 4 months old animals, observed a massive 96% of spines to be stable over at least 30 days (Grutzendler et al., 2002). Further quantitative predictions resulted in a spine half-life of more than 13 months, which implies that most adult spines would be stable lifelong. Besides the differences in mouse age and cortical area examined, the differences in spine stability between the two studies likely arose primarily from the use of an open-skull glass window vs. a thinned-skull window for imaging. As mentioned earlier, cranial surgery for an open-skull glass window is associated with strong inflammatory responses that can last up to 20 days and strongly increase spine plasticity (Xu et al., 2007). Trachtenberg et al. (2002) started imaging as early as 7 days post-surgery, which raises the possibility that the observed spine instability was in large part artifactual, due to inflammatory-associated processes. Later TPM studies confirmed the long-term stability of most adult spines (Holtmaat et al., 2005; Zuo et al., 2005b). Overall, although open-skull imaging studies tend to artificially enhance basal spine turnover rates, the consensus is that in adulthood dendritic spines are largely long-term stable.

The above imaging studies were performed on L5 neurons of visual and motor areas. Since, then, other studies have shown that, although globally held, baseline spine dynamics in adulthood can differ to some degree between cortical areas and cell types. At the areal level, basal spine dynamics are reduced in the visual cortex compared to the somatosensory and auditory areas (Majewska et al., 2006). At the laminar level, Tjia et al. (2017) showed that baseline spine turnover is much higher in cortical L2/3 than in L5 and that L5 but not L2/3 neurons undergo spine pruning between juvenile and adult stages (Tjia et al., 2017). Also, learning-induced spine formation is branch-specific in L5 neurons, but this rule does not apply to L2/3 neurons (Ma et al., 2015). Even at the single-cell level, spine dynamics might vary between dendritic compartments. Such variations were reported for example between basal (Gu et al., 2014) and apical dendrites (Attardo et al., 2015) in CA1 pyramidal neurons of the hippocampus, albeit this has to be treated with care as Pfeiffer et al. (2018) demonstrated that insufficient resolution in TPM compared to super-resolution STED microscopy can lead to significant underestimations of spine turnover.

Using *in vivo* TPM, imaging basal spine dynamics of deep-layer neurons have been unachievable due to the high distance from the brain surface. For this reason, most studies on spine dynamics have focused on apical dendrites in L1. The recent advent of three-photon microscopy, however (Ouzounov et al., 2017) shall soon pave the way towards *in vivo* imaging of basal dendrites in cortical neurons.

Importantly, although in adulthood most adult spines remain stable and might provide a physical substrate for long-term information storage, the observed small degree of spine turnover, together with rapid changes in synaptic strength of existing spines (Baltaci et al., 2019), may underlie learning and plasticity in the mature brain. Based on formation rates and long-term survival of new spines formed over 2 days, Yang et al. (2009) estimated that the number of such task-specific spines persisting at the end of life should be ∼0.04% of the total spines in motor or barrel cortex. However, given the immense quantity of spines in the mouse cortex (∼10,000 per neuron), the number of learning-induced and subsequently maintained new spines could be around 2×10^6, large enough to have a significant and lifelong impact on neural network functions and animal's behavior (Arenz et al., 2008; Houweling and Brecht, 2008; **Figure 1**).

Although the adult brain is less plastic than the young brain, it is still retaining the fundamental capability of removing spines and forming new ones, which might be essential for the encoding and processing of novel experiences and learning. But how do experiences influence spine dynamics?

EXPERIENCE-DEPENDENT SPINE DYNAMICS

Experience-dependent spine remodeling has been shown in a variety of learning tasks and deprivation assays, and the corresponding changes in spine dynamics allowed us to better understand the possible function of spine remodeling in adaptive behaviors, learning, and memory. For a list of the main studies with *in vivo* TPM of spine dynamics during development, see **Table 2**.

Whisker Deprivation in the Barrel Cortex

A group of studies has investigated spine remodeling in the somatosensory barrel cortex, in normal and deprived or stimulated conditions. Naturally, in the juvenile barrel cortex, spine elimination overcomes spine formation, which corresponds to the synaptic pruning that shapes neuronal circuits (Zuo et al., 2005a). Interestingly, sensory deprivation by complete contralateral whisker trimming over 2 weeks in juveniles attenuates spine elimination rates without affecting spine formation, hence reducing the pruning and increasing net spine density (Zuo et al., 2005a; Ma et al., 2015). This indicates that sensory experience is required for synaptic pruning during adolescence. Reproducing complete whisker trimming in adults has a similar, albeit much smaller effect that requires prolonged deprivation (8 weeks of deprivation are required; Zuo et al., 2005a). These studies suggest that experience plays an important

TABLE 2 | Experience-dependent spine plasticity.

Modulation	Brain region	Age animals	Impact on spine formation/elimination	Main results	Methods	Reference
Whisker trimming						
Chessboard whisker trimming	Barrel cortex, PN, Layer 5	6-10 weeks	Control: 40% stable spines over 4 days Trimmed: 30% stable spines over 4 days	Sensory deprivation increases spine turnover and reduces stability.	Two-photon laser scanning, Craniotomy, GFP-labeled dendrites	Trachtenberg et al. (2002)
Unilateral whisker trimming	Barrel cortex, PN, Layer 5	P30	Control: 17% of spines eliminated and 6% formed over 2 weeks Trimmed: 10% of spines eliminated, 5% formed after 2 weeks	Long-term sensory deprivation in young mice reduces the rate of spine elimination but has no significant effect on spine formation. Spines in adulthood are less affected.	Two-photon laser scanning, Thinned skull cranial window, YFP-labeled dendrites	Zuo et al. (2005a)
		>4 months	Control: 5% of spines eliminated and 4% formed over 2 weeks Trimmed: No changes in spine turnover after 2 weeks			
Chessboard whisker trimming	Barrel cortex, PN, Layer 5	2-5 months	Control: ∼63% of spines stable over 28 days Trimmed: ∼60% of spines stable over 28 days, turnover increased	Sensory deprivation induces loss of old persistent spines and forms new persistent spines.	Two-photon laser scanning, Craniotomy, GFP-labeled dendrites, Electron microscopy	Holtmaat et al. (2006)
Motor learning						
Motor task, Neonatal bilateral whisker trimming	Barrel cortex, Motor cortex, PN, Layer 2/3, Layer 5	P30	Control, MC, L2/3: ∼18% spine elimination, ∼18% spine formation over 4 days Motor task, MC, L2/3: ∼16% spine elimination, ∼17% spine formation Control, MC, L5: ∼9% spine elimination, ∼6% spine formation over 4 days Motor task, MC, L5: ∼14% spine elimination ∼14% spine formation Control, BC, L2/3: ∼15% spine elimination, ∼15% spine formation After neo. trimming, BC, L2/3: ∼17% spine elimination, ∼7% spine formation Control, BC, L5: ∼12% spine elimination, ∼7% spine formation After neo. trimming, BC, L5: ∼12% spine elimination, ∼7% spine formation	Motor task-induced increase in spine dynamics happens only in L5, but not in L2/3 of MC. Neonatal whisker trimming reduces spine formation in L2/3, but not in L5 of the somatosensory cortex.	Two-photon laser scanning, Thinned skull cranial window, GFP-labeled dendrites	Tjia et al. (2017)
Forelimb reaching	Motor cortex, PN, L5	P30	Control: ∼7% spine elimination, ∼5% spine formation over 2 days	Motor learning selectively stabilizes learning-induced new spines into adulthood.	Two-photon laser scanning, Thinned skull cranial window and craniotomy, YFP-labeled dendrites	Xu et al. (2009)

(Continued)

TABLE 2 | Continued

Modulation	Brain region	Age animals	Impact on spine formation/elimination	Main results	Methods	Reference
			Reaching: Spine elimination increased after 2 days (∼15%), spine formation increased to 11% within 1 h after training			
Rotarod motor task	Motor cortex, PN, Layer 5	P30	Control MC: ∼9% elimination, ∼7% spine formation over 2 days Rotarod MC: ∼9% elimination, ∼15% spine formation over 2 days	Learning induces formation of new spines.	Two-photon laser scanning, Thinned skull cranial window, YFP-labeled dendrites	Yang et al. (2009)
		>4 months	Control MC: ∼3% elimination, ∼3% spine formation over 2 days Rotarod MC: ∼4% elimination, ∼8% spine formation over 2 days			
Visual deprivation						
Monocular deprivation	Visual cortex, PN, Layer 2/3, Layer 5	P45-100	Control L2/3: 8% spine elimination, 7% spines formation over 8 days Control L5: 7% spine elimination, 6% spines formation over 4 days MD L2/3: no changes in spine turnover over 4+ days MD L5: spine elimination unchanged, ∼11% of spines formed over 4 days	Visual deprivation increases spine formation.	Two-photon laser scanning, Craniotomy, GFP- labeled dendrites	Hofer et al. (2009)
Monocular- and Binocular deprivation	Visual cortex, PN, Layer 5	P28	Control: ∼11% spine elimination, ∼8% spine formation over 3 days MD: ∼19% spine elimination, ∼9% spine formation over 3 days BD: ∼10% spine elimination, ∼7% spine formation over 3 days	MD over 3 days significantly increases spine elimination without affecting spine formation. BD does not change spine dynamics.	Two-photon laser scanning, Thinned skull cranial window, YFP-labeled dendrites	Zhou et al. (2017)
Fear conditioning						
Fear conditioning, Fear extinction	Frontal association cortex, PN, Layer 5	P30	Control: ∼18% spine elimination, ∼14% spine formation over 9 days Fear cond.: ∼23% spine elimination, ∼11% spine formation over 9 days Fear ext.: ∼10% spine elimination, ∼17% spine formation after 2 days	Fear conditioning promotes spine elimination. Fear extinction induces spine formation.	Two-photon laser scanning, Thinned skull cranial window, YFP-labeled dendrites	Lai et al. (2012)
Fear conditioning	Auditory cortex, PN, Layer 5	3-6 months	Control: ∼7% spine elimination, ∼8% spine formation over 2 h Fear cond.: ∼11% spine elimination, ∼17% spine formation over 2 h	Auditory fear conditioning causes an increase of spine turnover	Two-photon laser scanning, Craniotomy, GFP-labeled dendrites	Lai et al. (2018)

(Continued)

TABLE 2 | Continued

Modulation	Brain region	Age animals	Impact on spine formation/elimination	Main results	Methods	Reference
Fear conditioning	Auditory cortex, PN, Layer 5	7–10 weeks	Control: ∼13% spine elimination, ∼7% spine formation over 3 days Fear cond.: ∼13% spine elimination, ∼15% spine formation	Fear conditioning increases formation of new Amygdala–Auditory cortex connections consistent with the consolidation of fear memory.	Two-photon laser scanning, Craniotomy, YFP, tdTomato and GFP-labeled dendrites and axons	Yang et al. (2016)
Fear conditioning, Fear extinction	Auditory cortex, PN, Layer 5	P30	Control: ∼9% spine elimination, ∼9% spine formation over 3 days Fear cond.: ∼10% spine elimination, ∼16% spine formation over 3 days Fear ext.: ∼17% spine elimination, ∼5% spine formation over 2 days	Persistent new spines are induced by auditory fear conditioning. Fear extinction selectively eliminates new spines.	Two-photon laser scanning, Thinned skull cranial window, YFP-labeled dendrites	Lai et al. (2018)
Stress						
Corticosterone administration (stress)	Barrel cortex, PN, Layer 5	P23-30	Control: ∼4% elimination, ∼5% spine formation over 1 day Acute cort.: ∼12% elimination, ∼7% spine formation over 1 day Chronic cort.: Elimination increases to 22%, Spine formation unchanged over 10 days	Acute corticosterone increases spine turnover. Chronic stress increases spine elimination.	Two-photon laser scanning, Thinned skull cranial window, YFP-labeled dendrites	Liston and Gan (2011)
Motor task, corticosterone administration (stress)	Motor cortex, PN, Layer 5	P30	Untrained: ∼7% spine formation over 2 days Training with additional cort: ∼17% spine formation over 2 days Chronic cort.: elimination of training associated and pre-training spines over 10 days	Corticosterone increases formation of lasting task-associated spines. Chronic corticosterone causes loss of spines and reduces motor performance.	Two-photon laser scanning, Thinned skull cranial window, YFP-labeled dendrites	Liston et al. (2013)

role in the net loss of synapses over most of an animal's lifespan, particularly during adolescence.

In contrast to complete whisker trimming, alternated "chessboard" trimming in juvenile mice increases spine formation over 2 days in the contralateral barrel cortex, while causing no change in elimination rates (Pan et al., 2010). In young adult mice imaged over 1 month, chessboard trimming does not alter net spine density but increases spine turnover by eliminating previously stable spines and stabilizing newly formed ones (Holtmaat et al., 2006). Moreover, spine gains are especially localized in regions encompassing the border between different barrel columns. These experiments illustrate on one hand how the developing brain is much more plastic than the adult one, and on the other hand, that the type and severity of sensory deprivation critically influence the formation and abandonment of connections.

Visual Deprivation

Another type of sensory deprivation task is the blocking of visual input. The binocular visual cortex in a given hemisphere receives sensory input predominantly from the contralateral eye, while the contribution of the ipsilateral eye is much lower. This is commonly referred to as ocular dominance (OD). Depriving visual input of one eye, also called monocular deprivation (MD), and recording visual signals in the contralateral visual cortex show increased responsiveness towards the non-deprived, ipsilateral eye while the deprived eye responses fade (Shatz and Stryker, 1978). This is called OD plasticity, which is maximal during a critical period in young mice and requires longer-lasting MD in adults, typically during at least 5 days (Gordon and Stryker, 1996). However, OD plasticity upon short-lasting MD can be reinstated in adult mice under the condition that another, OD plasticity-inducing MD episode took place earlier in the life of the animal (Kind et al., 2002; Hofer et al., 2006). Thus, a transient adaptation to altered visual input leaves a "trace" in cortical circuits that facilitates similar adaptations in the future. To investigate whether and how morphological alterations in dendritic spines could participate in this memory trace, *in vivo* TPM has been used to observe spine dynamics during OD plasticity. The Huebener group studied dendritic spine turnover in adult mice submitted to two subsequent episodes of MD (Hofer et al., 2009). During the first deprivation, binocular visual cortex neurons increased spine formation, while spine elimination remained unchanged, leading to a net spine gain. Interestingly, newly formed spines persisted but shrunk during the recovery phase in between the two deprivation episodes (Hofer et al., 2009). The second deprivation did not modify spine dynamics or density but selectively re-enlarged the spines formed during the first deprivation. Thus, spines added during the first MD may provide a structural basis for subsequent OD shifts. These data point out a strong link between functional plasticity and specific synaptic rearrangements, revealing a mechanism of how prior experiences could be stored in cortical circuits through specific spines. Of note, binocular deprivation in juveniles and adults has not been connected to any significant changes in spine turnover (Majewska and Sur, 2003; Zhou et al., 2017). This indicates that sensory competition between contralateral and ipsilateral inputs is required to modify spine turnover.

Motor Learning

The idea that selected dendritic spines represent a structural memory trace of specific experiences can be challenged in experiments involving learning and the retention of certain skills. Researchers in the field have been using motor learning tasks, such as the paw reaching task, where the animal learns how to reach a food pellet by passing its paw through a narrow gap (Xu et al., 2009), or the accelerated rotarod learning task, which requires the mouse to find balance on a rotating cylinder (Yang et al., 2009). Mice exposed for the first time to the paw reaching task rapidly formed new spines within the contralateral forepaw motor cortex (Xu et al., 2009). As approximately half of these new spines stabilized over 8 days (which is higher than the average spine survival in basal conditions), the general motor performance of the animal concomitantly increased, and the level of performance correlated with the amount of retained new spines. Prolonging training not only stabilized the newly-formed spines long term but also increased the elimination of preexisting spines compared to baseline elimination rates, resulting in a total spine density that eventually matched control levels (Xu et al., 2009). In another study, Yang et al. (2009) subjected mice to the rotarod task and made similar observations. Rotarod learning led to new spine formation and elimination of pre-existing spines. The survival rate of learning-induced new spines and the elimination rate of pre-existing spines both increased with the training duration and were long-lasting. The extent of spine remodeling correlated with behavioral improvement after learning, suggesting a crucial role of synaptic structural plasticity in memory formation. Trained animals were able to maintain successful motor performance in the long term, even if they did not execute the task for months, indicating that stable learning-induced spines might underlie the controlled execution of specific motor skills (Xu et al., 2009; Yang et al., 2009).

Thus, successful retention of a motor task does not only require the formation of new synaptic contacts but involves equally permanent removal of some pre-existing spines. These time-dependent spine density changes contribute to the creation of a neuronal network that serves as the foundation of durable motor memory. Overall, these studies indicate that learning and daily sensory experience leave small but permanent marks on cortical connections and suggest that lifelong memories can be stored in largely stably connected synaptic networks (Yang et al., 2009; **Figure 1**).

Sleep

Maret et al. (2011) studied the effect of sleep on L5 apical tuft spine dynamics in adolescent Thy1-GFP mice using a thinned skull approach. Interestingly, they found that spine elimination over a 24-h circadian cycle preferentially occurs during sleep. More specifically, during sleep spine elimination overcomes spine formation, leading to a net spine loss, while conversely, spine formation exceeds elimination during wakefulness, such that over a complete 24 h cycle net spine number remains stable. Moreover, daily spine elimination is down-tuned in

sleep-deprived mice (Maret et al., 2011). On the other hand, it was shown that sleep after motor learning promotes the formation of dendritic spines on a subset of branches specific for this task (Yang et al., 2014). Sleep deprivation directly after a motor training inhibited learning-induced new spine formation and resulted in reduced retention of motor memory. This is in line with the idea that sleep contributes to memory consolidation. Notably, using Ca^{2+} imaging the researchers further described that cells active during the motor task are reactivated during sleep, and disrupting this neuronal reactivation prevents learning and branch-specific spine formation. Another study from the same team further showed that natural elimination of a fraction of newly formed spines in response to a motor task happens in the hours following training, notably during sleep (Li et al., 2017). Deprivation of REM sleep eliminates fewer task-associated new spines compared to control mice. This indicates that REM sleep is necessary for the selective elimination of presumably unnecessary experience-associated spines, which allows to free up space in neuronal circuits. The work by Li et al. (2017) further demonstrates that the newly-formed task-associated spines that are destined to become stable undergo an increase of size during REM sleep, unlike REM-deprived mice. The latter observation is in line with other seminal studies indicating that sleep is essential for synaptic scaling (Diering et al., 2014; De Vivo et al., 2017). In sum, sleep bidirectionally shapes neuronal circuits, by the elimination of unnecessary spines and strengthening of essential task-associated synapses.

Fear Conditioning and Extinction

Changes in spine turnover can be caused by complex environmental influences, for example, such that trigger fear. One extensively studied paradigm is fear conditioning. Rodents typically respond to a foot shock with freezing behavior. If the foot shock, called unconditioned stimulus (US), is paired with a neutral stimulus such as a sound or an environmental context (conditioned stimulus or CS), the animal rapidly learns to associate the CS with the US and will now freeze whenever the CS is presented alone (Kim and Jung, 2006). Strikingly, a single conditioning session is sufficient to form immediate and long-lasting fear memories (Poulos et al., 2016). Fear conditioning is encoded in the amygdala (Davis, 1997), hippocampus (Phillips and LeDoux, 1992) and prefrontal cortex (PFC; Quinn et al., 2008), of which hippocampus, anterior cingulate cortex, and infralimbic cortex show an increase of spine densities upon fear induction (Vetere et al., 2011; Pignataro et al., 2013). Reversal of fear conditioning is possible by exposing the test animal numerous times to the CS only; this is referred to as fear extinction. Interestingly, after fear extinction, spine density gets restored to pre-fear conditioned levels in the basolateral amygdala (BLA) *in vitro* (Heinrichs et al., 2013).

Lai et al. (2012) used TPM to monitor the frontal association cortex—a part of the dorsal PFC—of juvenile mice during auditory fear conditioning and extinction. They focused on L5 projection neurons using Thy1-YFP mice (line H). TPM analyses showed that fear conditioning induces a long-lasting increase in spine elimination while spine formation is unaffected (Lai et al., 2012; Chu et al., 2019). In contrast, fear extinction triggers the formation of new long-lasting spines that tend to appear near the location of formerly erased ones, thus re-establishing pre-fear levels of global spine density. Strikingly, repeating the fear conditioning protocol on these animals induces the selected elimination of those spines that were reformed after fear extinction (Lai et al., 2012). This shows that fear conditioning and extinction lead to opposing alterations at the level of selected spines and synapses.

In contrast to the frontal association cortex, neurons in the auditory cortex, which is involved in fear memory recall, respond to fear conditioning by increased spinogenesis, and fear extinction favors the elimination of those new spines (Lai et al., 2018). But conceptually similar to the association cortex findings, extinction in the auditory cortex eliminated the very spines formed by fear conditioning and reconditioning induced reformation of new dendritic spines close to the sites of new spine formation induced by previous fear conditioning. Notably, persisting new spines induced by fear conditioning were auditory cue-specific and clustered within branch segments (Lai et al., 2018). Together, results from the two seminal studies from Lai et al. (2012, 2018) show that fear conditioning, extinction, and reconditioning induce cue- and location-specific dendritic spine remodeling in the frontal association and auditory cortical areas. They also indicate that changes of synaptic connections induced by fear conditioning are reversed after fear extinction, which contradicts prior hypotheses that fear extinction corresponds to a new form of learning (Myers and Davis, 2007).

Another study attempted to identify the specific neuronal input partners that might be responsible for forming axonal boutons onto auditory cortex neurons with altered spine remodeling, using tracing techniques and dual-color TPM (Yang et al., 2016). They discovered that a direct connection between the lateral amygdala and L5 pyramidal neurons in the auditory cortex is involved in the aforementioned dendritic spine plasticity after fear conditioning (Yang et al., 2016). In an elegant setup, they simultaneously imaged amygdalar axonal boutons and dendritic spines in auditory L1 *in vivo* and found that fear-induced synaptic contacts are formed by adding new partners to already existing pre- or postsynaptic elements between these two structures. This resulted in a net increase in both spine and axonal bouton formation.

Although the fear-induced changes in spine dynamics vary highly between different brain regions, they have in common that they are rapid and usually long-lasting without the necessity of repeating fear-inducing experiments. This is consistent with the fact that in the natural world the recognition of potentially life-threatening situations is crucial for survival. Almost all of the formerly presented studies report likewise that the extent of fear-associated changes in spine elimination or formation is directly correlated with the animal's behavior (Lai et al., 2012; Yang et al., 2016; Chu et al., 2019).

Stress and Corticosterone

Other environmental stimuli that modify spine dynamics are variations in stress levels. A predominant role is given to

glucocorticoids. The main glucocorticoid in humans is cortisol and in rodents corticosterone (Joëls et al., 2018). Corticosterone regulates the stress response by binding two receptors: the glucocorticoid (GR, also called NR3C1) and mineralocorticoid receptors (MR or NR3C2; De Kloet et al., 1998). Acute, short-term stress typically ameliorates physical performance and supports the consolidation of memories (Cordero and Sandi, 2007; Liston et al., 2013). In contrast to acute stress, chronic stress lowers performance (see review by Joëls et al., 2006), especially in memory acquisition and consolidation (Conrad et al., 1996; de Quervain et al., 1998; Mizoguchi et al., 2002).

Concomitantly to their behavioral effects, stresses induced by exposure to external stressors or by corticosterone administration have profound effects on the structure of dendrites and spines across numerous brain areas, such as the PFC (Radley et al., 2006; Liu and Aghajanian, 2008), the somatosensory cortex (Jeanneteau et al., 2018), the motor cortex (Liston and Gan, 2011), hippocampus (Patel et al., 2018), amygdala (Patel et al., 2018) and striatum (Dias-Ferreira et al., 2009). This points to a universal role of glucocorticoids in the dendritic and spine morphogenesis in the brain. *In vivo*, TPM has shown that acute administration of corticosterone in mice induces a rapid increase of both spine formation and elimination in the barrel cortex of juveniles and adult mice (Liston and Gan, 2011). In contrast, prolonging the stressful episode by rendering it chronic leads to exaggerated spine elimination that largely exceeds spine formation and thus results in strongly reduced net spine density (Liston and Gan, 2011). Further, chronic stress also induces the elimination of pre-existing stable spines that were not affected by short episodes of stress (Liston and Gan, 2011). Recently, these structural spine changes were shown to causally underlie chronic stress-induced behavior, at least in the PFC (Moda-Sava et al., 2019); this is detailed in the discussion below.

As all these dendritic and spine phenotypes have been observed both by exposing the animal to a stressful situation or by administering corticosterone, it is evident that the stress hormone plays a major role in dendrite and spine remodeling. This is further supported by the fact that blocking GR or MR significantly modulates spine formation and elimination over 24 h (Liston and Gan, 2011). Applying an MR antagonist reduces spine formation and elimination by approximately 75%, while a GR antagonist lowers only spine formation without influencing elimination rates. Liston et al. (2013) used transcriptional inhibitors and were able to identify that spine elimination is most likely modulated *via* MR and transcriptional pathways, whereas spine formation depends on faster non-transcriptional processes. Nonetheless, the exact underlying signaling pathways of stress-induced spine dynamics and stabilization are so far incompletely delineated. They most likely depend on a combination of distinct transcriptional and non-transcriptional actions and the activity of complex co-regulatory elements (Weikum et al., 2017; see discussion below). Notably, besides stress, age-related cognitive decline is similarly associated with dendritic atrophy and spine loss (reviewed by Dickstein et al., 2013), raising the possibility that glucocorticoid signaling might also participate in this process.

Spatial Confinement of Experience-Induced Spine Changes

We have seen that remodeling of dendritic spines accompanies the learning of motor tasks (Xu et al., 2009), fear-inducing experiences (Yang et al., 2016), and new sensory inputs (Yang et al., 2009). Interestingly, such experience-induced spine remodeling occurs at non-random locations on dendrites as they tend to spatially cluster. First, several studies report clustered spine formation in spatial proximity at sites of synaptic potentiation. De Roo et al. (2008) described that LTP induction by theta-burst stimulation leads to the formation of new functional spines close to activated spines in slice preparations. Fu et al. (2012) showed by *in vivo* TPM of the motor cortex that after repeated training of a specific motor task many of the new task-associated spines form entirely new clusters or clusters near already existing spines. Moreover, they revealed that clustered spines are stable for the long term as opposed to non-clustered spines, even if the associated motor task training stops. A similar *in vivo* experiment by Frank et al. (2018) demonstrated as well that more than 42% of nascent spines appeared in clusters after repeated episodes of contextual learning in the retrosplenial cortex and likewise, these clusters remained largely stable over weeks following the initial learning task.

Consistent with the observed clusterization of spines devoted to the same task, it was also shown that certain motor tasks tend to activate selected branches on the apical dendrite of a given neuron. Indeed, *in vivo* Ca^{2+} imaging showed that dendritic segments of the same neuron generate branch-specific Ca^{2+} spikes with little to no overlap in response to even subtly different motor tasks. Furthermore, spines that happen to be active at the moment of branch-specific Ca^{2+} spikes, undergo functional potentiation (Cichon and Gan, 2015). This indicates that spine formation and synaptic potentiation do not only cluster on a given dendritic branch but are also enriched in specific dendritic branches compared to sister branches (separated by a node on the same neuron). In sum, spatially clustered spines appear to participate in the same task or memory-related circuit. Upon repeated activation of the corresponding circuit, these grouped synapses are potentiated and the associated spines become stable over a long period.

DYSREGULATION OF SPINE DYNAMICS IN NEUROPATHOLOGIES

In this review, we focus on neuropsychiatric disorders. Dendritic spine abnormalities in neurodegenerative disorders have been treated in the review by Herms and Dorostkar (2016). The first indications that mental illnesses were based on abnormal spine numbers and morphology came from the analysis of human post-mortem tissues. Patients diagnosed with intellectual disability (ID) showed reduced spine density and abnormal long and thin spines on apical dendrites of pyramidal neurons in the motor cortex (Purpura, 1974). Reduced spine density was also reported in the auditory cortex of patients with schizophrenia (SCZ; Sweet et al., 2009) and in the PFC of patients with bipolar disorder (BD; Konopaske et al., 2014).

On the other hand, autism spectrum disorders (ASD)—a term comprising disorders involving developmental deficits in social interaction, communication and the appearance of repetitive behaviors and stereotypies (Rapin, 1997)—are generally associated with increased spine densities, at least across the temporal lobe (Hutsler and Zhang, 2010). For a complete review of spinopathies in neurodevelopmental disorders, please refer to Forrest et al. (2018).

Although spine morphological abnormalities have been well described in most neurodevelopmental disorders, the molecular pathways that trigger irregular spine turnover are largely unknown. While the genetic component plays an important role, the environmental impact on the onset and severity of mental diseases cannot be neglected as they add tremendously to the final neurofunctional- and behavioral outcome (Chini et al., 2020). Yet, genetic mouse models of disorders allow testing hypotheses about the molecular pathways. In any case, the fact that spine alterations are the main convergence point between neurodevelopmental disorders raises the general hypothesis that spinopathies are an underlying cause.

ASD-ID

ASDs have been classified into syndromic and nonsyndromic, a distinction that is based on clinical criteria (Sztainberg and Zoghbi, 2016). In "syndromic" ASD the autistic phenotypes occur in conjunction with additional phenotypes and/or dysmorphic features. The etiology in most syndromic ASD cases is known and can involve chromosomal abnormalities, copy number variations, and mutations in a single gene, such as in fragile X syndrome, Angelman syndrome or tuberous sclerosis complex. The term "nonsyndromic" typically refers to "classic autism," in which no additional symptoms are present. For most nonsyndromic ASD cases the etiology is unknown, and the term "idiopathic autism" has been used alternatively. Interestingly, ASD and ID likely have overlapping origins as 8–20% of ID patients also meet the criteria for ASD (Kaufman et al., 2010) and 50–80% of ASD patients display ID (Simonoff et al., 2008). Despite a tremendous research effort in the field, only a few high confidence genes or copy number variations responsible for ASD have been discovered, most of which are associated with syndromic ASDs. Some of the best-studied syndromic ASD genes are *FMR1* (Fragile X syndrome), *TSC* (Tuberous sclerosis), and *UBE3a* (Angelman syndrome; Bourgeron, 2015; Sztainberg and Zoghbi, 2016). One well studied syndromic ASD deletion is the 22q11 microdeletion (Di George syndrome).

Fragile X Syndrome: FMR1

Mutations of the activity-dependent RNA-binding protein FMRP, encoded by the *FMR1* gene found on the X chromosome, cause Fragile X syndrome, a disorder associating ID and ASD. *Fmr1* knockout mice show hyperactivity and abnormal social interactions (Bernardet and Crusio, 2006). Consistent with findings in brain tissue from Fragile X syndrome subjects (Irwin et al., 2001), studies on L5 cortical neurons found that *Fmr1* knockout mice display increased spine densities with immature, abnormally elongated, spine morphologies even at adult ages (Comery et al., 1997; Nimchinsky et al., 2001; Galvez and Greenough, 2005). Conversely, other studies reported no change in spine shape or density in L5 as well as other neuronal types (Harlow et al., 2010; Till et al., 2012; Wijetunge et al., 2014). These differences may be attributed to age, the brain area that is examined, the genetic background, and/or methodology. In any case, fixed tissues only provide a snapshot of processes that are in reality dynamic and thus may not capture abnormalities in spine remodeling. In fact, *in vivo* TPM has revealed abnormally high baseline spine turnover ratios in various cortical areas of *Fmr1* knockout mice (Cruz-Martín et al., 2010; Pan et al., 2010; Padmashri et al., 2013; Nagaoka et al., 2016). *In vivo* imaging of L2/3 in the barrel-cortex shows no differences in spine density or morphology between wild type and *Fmr1* knockout mice (Cruz-Martín et al., 2010). The same knockout mice, however, present increased spine turnover and fail to downregulate spine dynamics at 2 weeks of age (Cruz-Martín et al., 2010). This is due to the defective transition from early protrusions to mature spines, entailing that fewer spines undergo stabilization. Pan et al. (2010) observed L5 of the barrel cortex and concluded likewise, that *Fmr1* knockout mice have a larger pool of unstable spines which accounts for the increased dynamics.

Interestingly, while spine turnover is enhanced in *Fmr1* knockout mice in basal conditions, it is much less sensitive to motor learning and experience than in control animals (Cruz-Martín et al., 2010; Pan et al., 2010; Padmashri et al., 2013; Nagaoka et al., 2016). Pan et al. (2010) found that sensory deprivation by chessboard whisker trimming would not induce new spine formation in *Fmr1* knockout mice. Similarly, such mice fail to learn a motor task, as motor training-associated new spines fail to form (Padmashri et al., 2013). Furthermore, *Fmr1* knockout mice do not undergo increased spine formation under an enriched environment as wildtype mice do (Arroyo et al., 2019). Therefore, *Fmr1* deficiency alters experience-dependent spine dynamics and thus behavioral adaptation to the external world.

FMRP malfunction dysregulates the local activity-dependent translation of numerous mRNAs at the synapse (Bassell and Warren, 2008; Sethna et al., 2014). As FMRP is considered a translational repressor, mutations induce an augmentation of synapse-relevant proteins that could act upon spine dynamics (Sidorov et al., 2013). For example, activity-regulated cytoskeleton-associated protein (ARC), a synaptic protein critical for the internalization of α-amino-3-hydroxy-5-methyl-4-isoxazolepropionic acid (AMPA) receptor trafficking at synapses, is one mRNA target of FMRP at the synapses (Waung et al., 2008; Ebert and Greenberg, 2013). For more information regarding the molecular mechanisms of synaptic dysfunction in Fmr1 knockout mice, please refer to Nishiyama (2019).

Angelman Syndrome: Ube3a

Loss of expression of the ubiquitin-protein ligase E3a (UBE3A) is associated with most cases of Angelman syndrome, which is a rare syndrome of developmental delay, ID and ASD (Buiting et al., 2016). Opposed to loss-of-function mutations, duplications or triplications of the gene are also highly common among patients diagnosed with ASD (Vatsa and Jana, 2018), which points to a highly regulated role of UBE3A in the

organism. Greer et al. (2010) identified that UBE3A controls the activity-dependent degradation of ARC in spines, which is involved in the internalization of glutamate AMPA receptors. Consequently, absence or mutation of UBE3A can reduce AMPA receptors at postsynaptic sites and thereby modify excitatory synaptic transmission.

In mouse models of Angelman syndrome that lack *Ube3a*, dendritic spines present abnormal morphologies and reduced densities in the hippocampus and neocortex (Dindot et al., 2008; Yashiro et al., 2009). *In vivo*, TPM allowed gaining more insight into the basal and experience-dependent spine dynamics in such mice. Yashiro et al. (2009) and Kim et al. (2016) described that dendritic spines of *Ube3a* deleted mice undergo excessive pruning while spine formation remains unchanged (Kim et al., 2016), thus resulting in a net loss of spines. However, in *Ube3a* deleted mice that are raised in darkness, spine density and dynamics were indistinguishable with controls, which indicates that decreased spine density in Angelman syndrome model mice reflects impaired experience-driven spine maintenance. The general notion of impaired experience-dependent plasticity in Angelman syndrome is reinforced by the observation that MD, which usually induces an OD shift in the visual cortex of wild type mice, does not have such an effect in *Ube3a*-deleted animals (Yashiro et al., 2009). These abnormalities point to a function of UBE3A in experience-dependent plasticity during development that could play a role in the cognitive deficits observed in Angelman syndrome.

22q11 Deletion Syndrome

Another genetic predisposition for SCZ and ASD is chromosomal microdeletions on position 22q11 encompassing up to 40 different genes that can lead to 22q11 deletion syndrome. As numerous genes are affected, patients can present various additional phenotypes as facial dysmorphia, thymic hypoplasia, or cardiovascular anomalies (Squarcione et al., 2013). Nevertheless, there is a strong component for neuropsychiatric disorders: 22q11 deletion syndrome induces SCZ in 30% of patients (Earls and Zakharenko, 2014). As this region is conserved in mice, 22q11 deletion syndrome can be relatively easily modeled to study the physiopathology of the syndrome. Analysis of cultured hippocampal 22q11 deleted mouse neurons shows reduced spine density, smaller mushroom spine heads, and reduced dendritic complexity, suggesting morphological immaturity (Xu et al., 2013). Interestingly, Moutin et al. (2017) observed in hippocampal organotypic cultures that 22q11 deleted neurons present higher spine formation and elimination rates than wild type neurons, such that the total spine turnover is balanced and not responsible for the observed reduced spine density. Instead, they observed decreased long-term spine stabilization. This short-livity eventually drives the observed reduced number of dendritic spines and thus most likely cognitive impairments. The exact genes within the deletion that drive these neuronal changes have not been identified yet. Strong candidates are proteins that are involved in cell metabolism pathways and regulation of neurotransmission, such as COMT, PRODH, or ZDHHC8 (see review by Squarcione et al., 2013), and the micro-RNA mIR-185 (Xu et al., 2013).

SCZ: The DISC1 Case

SCZ is characterized by psychotic symptoms that include disorganized thoughts, delusions, or hallucinations and, unlike ASD, finds its typical onset in late adolescence. Studies on human tissue describe reduced dendritic spine density (Sweet et al., 2009; Konopaske et al., 2014). Meta-analyses of twin studies allow estimating that the heritability of SCZ is around 81% (Sullivan et al., 2003), indicating a strong genetic component. One important SCZ risk factor is *DISC1* (Mathieson et al., 2011). Originally, a chromosomal translocation of *DISC1* was found in members of a large Scottish family who developed SCZ (St Clair et al., 1990). In neurons, DISC1 acts as a scaffolding protein and associates with a great number of synapse- and microtubule-associated proteins during cortical development and adulthood (Brandon and Sawa, 2011). Hayashi-Takagi et al. (2010) demonstrated that knockdown of DISC1 in cultured rat cortical neurons leads to spine shrinkage. They further determined that DISC1 regulates activation of the Rho-GTPase RAC1 in the PSD, RAC1 being a protein whose activity modulates spine shape through regulation of actin dynamics (see discussion below). The same group went on to determine the signaling pathway downstream of RAC1 that was regulated by DISC1. Chemical inhibition of p21-activated kinases in DISC1-knockdown neurons partially reversed some of the knockdown-induced spine defects (Hayashi-Takagi et al., 2014). Finally, using TPM in the PFC of DISC1 knockdown mice, they confirmed increased spine elimination between P35 and P60 and found that this was reversed by administering a p21-activated kinase inhibitor. These experiments show that DISC1 defects produce a synaptic phenotype reminiscent of the reduced spine density observed in cases of SCZ and that these defects are communicated *via* the RAC1 pathway, which in turn represents a potential target for therapeutic interventions.

Rett Syndrome: MECP2

Rett syndrome is induced by loss-of-function mutations in the transcriptional regulator gene *MECP2*. MECP2 is an activity-dependent transcriptional repressor protein that acts by binding to methylated CpG dinucleotides and induces remodeling of the chromatin structure (Nan et al., 1997; Amir et al., 1999; Cohen et al., 2011). *MECP2* is an X-linked gene and most affected patients are females, who present stereotypies, motor capability regression and cognitive impairments that reflect in post-mortem brain tissue by reduced dendritic complexity and reduced spine densities in the hippocampus and across all layers of the cortex (Belichenko et al., 1994; Chapleau et al., 2009). Although some of its symptoms at first remind of ASD, Rett syndrome has been classified as a neurodevelopmental disorder, notably due to its critical motor coordination defects. Approximately 95% of Rett syndrome cases are directly linked to *MECP2* mutations, and their phenotypic severity depends on the type of mutation or the pattern of somatic X-chromosome inactivation in the patient (Chahrour and Zoghbi, 2007). Mouse models of Rett syndrome either express point mutations from

patients (Cohen et al., 2011) or are *Mecp2* knockouts (Belichenko et al., 2009). Diverse genetic models develop impressively similar phenotypes that resemble human symptoms, including failure to thrive, cognitive deterioration in early postnatal life, and premature death (Chahrour and Zoghbi, 2007). Anatomically, mouse models of Rett syndrome present reduced spine density but also abnormal axonal orientation and dendritic swelling, which also coincides with observations made in humans and thus renders them suitable for studying the disease (Fukuda et al., 2005; Belichenko et al., 2009).

Since Rett syndrome manifests itself in early postnatal life when experience shapes neuronal circuit wiring, and since *Mecp2* is activity-dependently regulated (Cohen et al., 2011), it is hypothesized that *Mecp2* might mediate experience-dependent processes of synapse development. First, loss of *Mecp2* leads to impairments in LTP and LTD, and in a reduced number of glutamatergic synapses and spines in the hippocampus (Asaka et al., 2006; Moretti et al., 2006). Landi et al. (2011) performed TPM over 1 h in the somatosensory cortex of juvenile *Mecp2* knockout mice. They found a reduced number of filopodia, which accounts for reduced protrusion density, and described spine heads as a lot more stable than in wild type mice in terms of volume fluctuations. This is observed during a critical period where spines normally mature and coincides with the disease onset in the mouse model. In adult mice, spine short term motility does not differ anymore between mutant and control animals, as motility naturally declines also in wild type mice. However, the reduced spine density in the mutant persists (Landi et al., 2011).

Overall, the current data show that dysfunctional MECP2 underlies defective spine turnover during a critical window in development, which induces spine loss. The experience-dependency of MECP2's role in dendritic spine turnover requires further investigations. Molecular mechanisms underlying RTT have been extensively studied in the past decades and are out of the scope of this study (Luikenhuis et al., 2004; Chang et al., 2006; Giacometti et al., 2007; Guy et al., 2007; Larimore et al., 2009).

Major Depressive Disorder

Major depressive disorder (MDD) is a psychiatric illness that is characterized by low mood and lack of feeling pleasure. MDD patients show altered glucocorticoid levels, which speaks for dysregulation of the HPA axis (Gold et al., 2015). Similarly to what is observed after exposure to chronic stress in mice (see discussion above), individuals with MDD present reduced spine synapses and decreased brain volume, especially in PFC and hippocampus (Hastings et al., 2004; Kang et al., 2012).

To model MDD in animals, chronic stress paradigms are employed, such as social stress (Hollis and Kabbaj, 2014) or chronic mild stress, where the mouse is exposed to phases of unpredictable stressors (Willner et al., 1992). As discussed above, numerous studies including some, with *in vivo* TPM showed that chronic stress in rodents strongly increases spine elimination, notably in the PFC, leading to a reduced spine density (Radley et al., 2006; Liston and Gan, 2011; Moda-Sava et al., 2019). Besides dendritic spine reduction, the MDD rat model of learned helplessness is also associated with reduced PSD-95 protein levels in the hippocampus (Reinés et al., 2008). This is similar to the analysis of human MDD PFC tissue, which also shows reduced protein expression of PSD-95 and synapse-related genes (Feyissa et al., 2009; Kang et al., 2012). The most common antidepressant drugs that are proven to be effective in humans, such as the NMDA-receptor antagonist ketamine (Murrough et al., 2013), also alleviate symptoms in mice as they overturn reduced animal mobility in the tail suspension tests (Cryan et al., 2005). Interestingly, ketamine is also able to restore, at least partially, dendritic spines eliminated by chronic stress in the mouse PFC (Moda-Sava et al., 2019). Also, the other well-known antidepressant fluoxetine similarly restores higher levels of PSD-95 in the hippocampus of stressed rats (Reinés et al., 2008). Strikingly, an elegant experiment took advantage of the paRac1 approach to demonstrate the causal relationship between spine reformation and behavioral recovery induced by ketamine in mice (see discussion below; Moda-Sava et al., 2019).

In sum, spine defects are a convergence point of many neuropsychiatric disorders (Forrest et al., 2018). Further functional analyses of both existing and new models for neuropsychiatric disorders will be essential to uncover generic and specific mechanisms leading to spine pathology. In this quest, state-of-the-art "omics" technologies will be essential to deconstruct the global pathway alterations taking place in model systems. The fact that spine pathology appears before cognitive defects in certain disorders suggests that there are critical periods for treatment to prevent disease onset (Marín, 2016). Furthermore, several mouse models, such *Mecp2* (Luikenhuis et al., 2004; Giacometti et al., 2007; Guy et al., 2007) and *Shank3* (Mei et al., 2016) have also shown that some structural and behavioral deficits can be reversed in adult animals, offering hope for treating human conditions (Ehninger et al., 2008).

THE CAUSATIVE ROLE OF SPINE DYNAMICS IN LEARNING AND BEHAVIOR

There is a strong correlation between spine formation/elimination/stabilization and retention of learned tasks (Xu et al., 2009; Yang et al., 2009). However, due to technical limitations, it has long been impossible to assess the causality link between new spines and learning. Hayashi-Takagi et al. (2015) developed a revolutionary approach that finally allowed tackling this question. They developed a photoactivatable form of the Rho GTPase RAC1, known to regulate spine dynamics through the modulation of actin polymerization (Costa et al., 2020), which they called paRAC1. RAC1 normally accumulates in recently formed, nascent spines, and constitutive RAC1 activation leads to spine shrinkage and elimination (Tashiro et al., 2000). The photoactivation form of paRAC1 renders RAC1 constitutively active and thus eliminates RAC1-expressing recently formed spines. With this tool, Hayashi-Takagi et al. (2015) selectively eliminated new spines induced by rotarod learning. They observed that this elimination blocked memory recall, demonstrating for the first time that task-induced spines are causally involved in memorizing the task. Moda-Sava et al. (2019) employed the

same technique to demonstrate that ketamine-induced restored spines in chronically stressed mice are causally involved in the maintenance (but not the induction) of behavioral recovery after treatment. They photoactivated virally-expressed paRAC1 in PFC neurons to selectively reverse the positive effects of ketamine on spine formation; by this approach, they found that the newly formed spines are required to sustain ketamine's antidepressant effects on motivated escape behavior (Moda-Sava et al., 2019). Interestingly, ketamine-induced spine reformation was required for the maintenance of antidepressant effects but not for their initiation, as ketamine's effects on behavior and cell ensemble activity preceded its effects on spine formation by several hours.

MOLECULAR MECHANISMS OF DENDRITIC SPINE PLASTICITY

Experiments showing that a massive local release of glutamate or GABA can induce the formation of postsynaptic dendritic spines have indicated that presynaptic neurotransmitter release is likely the main trigger for synapse formation, proving that synaptogenesis is an activity-dependent process that likely depends on the presence of presynaptic axonal boutons (Kwon and Sabatini, 2011; Oh et al., 2016). The post-synaptic mechanisms by which synaptic activity modulates the structure of existing spines have been thoroughly investigated, mostly using global or spine-specific long term potentiation (LTP) or long term depression (LTD) paradigms. The capacity of a stimulated spine to display enlargement or shrinkage upon LTP or LTD, respectively, is called structural plasticity (sLTP and sLTD). Although much fewer studies have investigated the molecular control of *de novo* spine formation/elimination, the current evidence indicates that they share similar mechanisms with spine enlargement/shrinkage (Caroni et al., 2012). Spine dynamics are largely controlled by local actin polymerization/depolymerization. Upon stimulation of dendrites and spines, early inducers of initial spine formation or enlargement comprise cascades of activation of actin-binding proteins (ABPs) including CaMKII and Rho GTPases. Later on, local translation at the spine level is induced to maintain the architecture of spines. Even later, activity-dependent transcriptional mechanisms followed by putative synaptic tagging and capture of plasticity-related genes are required for long-lasting stabilization. We briefly review the molecular mechanisms governing these different phases of spine formation. The specific mechanisms underlying spine shrinkage and elimination during LTD are in part redundant with the ones underlying spine formation/enlargement and are the subject of recent reviews (Segal, 2017; Stein and Zito, 2019).

Actin Underlies Spine Dynamics

The cytoskeleton of the dendritic spine is predominantly composed of actin filaments (Matus, 2000). Actin monomers (globular or G-actin) polymerize to form actin filaments (filamentous or F-actin) *via* the complex interaction with a variety of actin-binding proteins (ABPs). F-actin provides the force necessary for the formation of nascent protrusions and modifications in spine shape, such that actin polymerization/depolymerization is the main determinant of spine structural dynamics. A LTP inducing stimulation increases actin polymerization in spines (Fukazawa et al., 2003; Okamoto et al., 2004; Lin et al., 2005a). Importantly, actin networks are associated with the PSD, which contains hundreds of proteins that organize and stabilize synaptic receptors, cytoskeletal proteins, and signaling proteins (Kasai et al., 2003; Carlisle and Kennedy, 2005; Ethell and Pasquale, 2005). Also, recent genetic studies have shown that many mutations associated with neurodevelopmental disorders involve genes encoding regulators of the spine actin cytoskeleton (Borovac et al., 2018), validating the hypothesis that mechanisms regulating the actin cytoskeleton may contribute to spine pathology in neurodevelopmental disorders. For a more complete review of actin and ABPs in spinogenesis, please refer to Costa et al. (2020) in this issue of Frontiers in Synaptic Neuroscience, and Borovac et al. (2018).

Initiation of Spine Enlargement

Glutamate binding to NMDAR triggers rapid Ca^{2+} accumulation, which can be visualized by combining fluorescent Ca^{2+} indicators with live TPM (Higley and Sabatini, 2012). Glutamate uncaging experiments have shown that Ca^{2+} accumulation lasts short (0.1 s) and is mainly restricted to the stimulated spine (Mainen et al., 1999; Sobczyk and Svoboda, 2007), suggesting that dendritic spines can act as independent signaling compartments. Calcium flowing into the spine through NMDA receptors binds to the Ca^{2+}-binding protein calmodulin (CaM), and the Ca^{2+}-CaM complex then activates the holoenzyme CaMKII that is necessary and sufficient for LTP induction (Lisman et al., 2012). CaMKII is one of the most abundant proteins in neurons and plays a primary role in spine plasticity, learning, and memory. After activation by autophosphorylation, CaMKII rapidly translocates from the parent dendrite to the stimulated spine. Activated CaMKII has two functions in the early stages of spine plasticity: a kinase function on AMPA receptors and a structural function on actin dynamics (**Figure 2**).

Concerning the kinase function, activated CaMKII translocates to the postsynaptic density (PSD) where it forms complexes with NMDA receptor and other PSD molecules, allowing its stabilization. There, CamKII kinase activity enhances AMPAR-mediated transmission in two ways. First, CaMKII phosphorylates AMPA receptors, which leads to an increase in the average conductance of such channels (Lisman et al., 2012). Second, CaMKII phosphorylates the AMPAR auxiliary protein stargazin, which causes stargazin to bind PSD95, thereby increasing the number of AMPARs at the synapse (Tomita et al., 2005; Opazo et al., 2010; **Figure 2**).

These processes are confined to stimulated spines and are thought to account for the synapse-specificity of LTP expression, although the causal relationship between CaMKII-derived modulation of AMPA receptor conductivity/synaptic capture and LTP expression remains to be proven.

Concerning its structural impact on actin remodeling in spines, activated CamKII plays a dual function. First, inactive

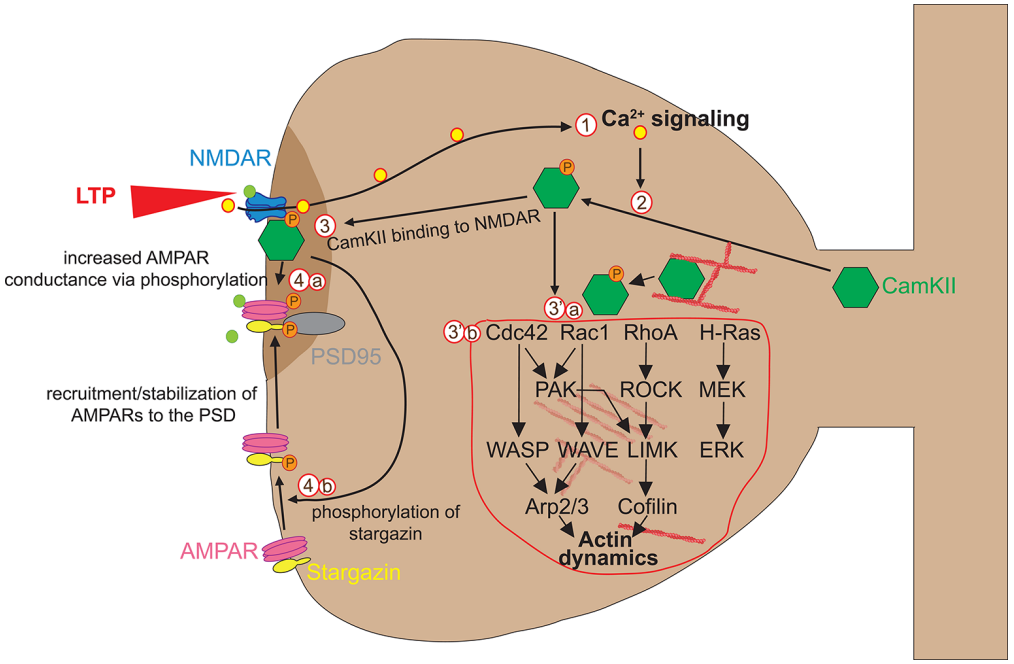

FIGURE 2 | Early phase of spine enlargement/formation. Calcium flowing into the spine through NMDAR (1) binds to the Ca^{2+}-binding protein calmodulin (CaM) and Ca^{2+}-CaM complex activates CaMKIIα by allowing its auto-phosphorylation (2). Activated CaMKII has two functions in the early stages of spine plasticity: a kinase function (3) and a structural function on actin dynamics (3′). Concerning the kinase function, activated CaMKII translocates to the postsynaptic density (PSD) where it forms complexes with NMDA receptor and other PSD molecules, allowing its stabilization. There, CamKII kinase activity enhances AMPAR-mediated transmission in two ways. First, CaMKII phosphorylates AMPA receptors, which leads to an increase in the average conductance of such channels (4a). Second, CaMKII phosphorylates the AMPAR auxiliary protein stargazin, which causes stargazin to bind PSD95, thereby increasing the number of AMPARs at the synapse (4b). Concerning its structural impact on actin remodeling in spines, CamKII plays a dual function. First, CamKII binds actin directly in its basal state and transiently detaches when phosphorylated to allow F-actin assembly/disassembly that is necessary for actin reorganization underlying spine enlargement (3′a). Second, CamKII activates *via* unknown mechanisms numerous small GTPases including Cdc42, Rac1, RhoA, and H-Ras (3′b). Those small GTPases in turn activate ABPs such as Cofilin and Arp2/3 *via* several kinase pathways, which in turn regulate structural LTP *via* actin remodeling. For more detailed information about the regulation of the spine actin cytoskeleton please refer to Nishiyama and Yasuda (2015).

CamKII binds actin directly and transiently detaches when activated to allow F-actin assembly/disassembly events that are necessary for actin reorganization underlying spine enlargement (for more details, see Borovac et al., 2018). Second, CamKII activates mechanisms numerous small GTPases including Cdc42, Rac1, RhoA, and H-Ras to reorganize actin networks in the spine. This was demonstrated thanks to the introduction of FRET and two-photon fluorescence lifetime imaging microscopy (2pFLIM), which made it possible to study dynamic signaling responses in stimulated spines at least in acute slice paradigms (Nishiyama and Yasuda, 2015; Nishiyama, 2019). CaMKIIα activity in individual stimulated spines has been imaged using 2pFLIM of a FRET-based biosensor (Okamoto et al., 2004; Lee et al., 2009). LTP induction by glutamate uncaging triggers rapid activation of CaMKIIα that is restricted to the stimulated spine. CaMKIIα activity decays with a time constant of ∼10 s, 100 times longer than the Ca^{2+} transient, suggesting that CaMKII plays a role in prolonging Ca^{2+} initiation signal in the spine. Downstream of CaMKII, Ras, RhoA, Cdc42, and Rac1, are key regulators of actin cytoskeleton dynamics, spine morphogenesis, and LTP (Nishiyama and Yasuda, 2015; Nishiyama, 2019). These signaling proteins cycle between an inactive GDP-bound form and an active GTP-bound form. Guanine nucleotide exchange factors (GEFs) stimulate Rho GTPase enzymatic activity by catalyzing GDP-GTP exchange, whereas GTPase-activating proteins (GAPs) inhibit their activity by catalyzing the hydrolysis of GTP to GDP (Negishi and Katoh, 2005). Using 2pFLIM, the Rho GTPase H-Ras has recently been discovered as a major downstream effector of CaMKII in actin reorganization for structural spine plasticity (Harvey et al., 2008). Indeed, the activity of H-Ras was found rapidly increased at stimulated spines but suppressed after CaMKII inhibition (Harvey et al., 2008). Furthermore, in contrast to CaMKII that stays restricted to the stimulated spine, H-Ras activation spreads along the parent dendritic shaft for over 10 μm. For H-Ras, the spatiotemporal activity of Rac1, RhoA, and Cdc42 has been measured using 2pFLIM of FRET biosensors. These studies show that while like CamKII and Cdc42 activities remain highly restricted to the stimulated spine, Rac1 and RhoA activities, like H-Ras, spread into the dendrite and neighboring spines (Murakoshi et al., 2011; Hedrick et al., 2016). Although hypothetic at this stage, the spread of activated H-Ras or other Ras family members such as Rac1 and RhoA during induction of structural plasticity at the stimulated spine may "predispose" neighboring spines

or spine sites for heterosynaptic plasticity (Van Bommel and Mikhaylova, 2016; Hedrick and Yasuda, 2017). It is tempting to speculate that new spine clustering or branch specificity during repetitive task learning might be facilitated by such mechanisms (Lai et al., 2012). One should keep in mind that the aforementioned 2p-FLIM-FRET studies dealt with structural potentiation of existing spines, not with *de novo* spine formation from smooth stretches of the dendrite. Another limitation of these studies is that for technical reasons they were performed on acute slices rather than *in vivo*. A single study has applied the 2p-FLIM-FRET approach *in vivo* in the context of sensory deprivation in the visual cortex (Mower et al., 2011). Although this study provides a proof-of-principle that FRET studies can theoretically be done *in vivo*, Spatio-temporal resolution is lower than in slices, which might in part explain why such *in vivo* experiments have not been reproduced. Finally, it remains to be determined by which mechanisms CamKII activates small GTPases.

Downstream effectors of small GTPases are several kinases including p21-activated kinase (PAK), Rho kinase (ROCK), and LIM kinase (LIMK; Murakoshi et al., 2011). These kinases ultimately activate numerous ABPs including Cofilin and Arp2/3 that play essential roles in actin reorganization. The mechanisms by which ABPs induce actin reorganization upon synaptic potentiation have been abundantly studied in other reviews (Borovac et al., 2018; Costa et al., 2020).

In sum, activation of Rho GTPases and associated ABPs *via* CaMKII activation controls actin polymerization, leading to profound and rapid (within minutes) structural changes at single stimulated dendritic spines. A growing number of genetic studies have linked neurodevelopmental disorders to various synaptic GEFs and GAPs for Rho GTPases (Hamdan et al., 2009; Alber et al., 2017; Stressman et al., 2017). Further studies are required to determine how CaMKII, Rho GTPases, and associated GEFs and GAPs participate in spine formation/elimination under physiological learning conditions *in vivo*.

Spine Stabilization

The long term stabilization of new spines requires specific mechanisms (Subramanian et al., 2019) and is believed to be the structural correlate of long-lasting LTP (also called late-phase LTP; Baltaci et al., 2019). Long term structural plasticity is mediated by NMDA-receptor-dependent and/or by L-type voltage-sensitive calcium channels (L-VSCCActb Limk1Actb)-dependent calcium influx (Ebert and Greenberg, 2013). In contrast to short term structural spine plasticity, long-lasting plasticity requires protein synthesis, *via* local mRNA translation and gene transcription in the nucleus. The main signaling cascade for local translation at spines requires glutamate binding to metabotropic glutamate receptors (mGluR), which triggers protein-synthesis-dependent forms of spine plasticity by activating extracellular signal-regulated kinase (ERK) or mammalian target of rapamycin (mTOR) pathways (Ebert and Greenberg, 2013). Activity-dependent locally translated mRNAs important for spine plasticity include *Camk2a*, *Actb*, or *Limk1*; for a more complete list please refer to Holt et al. (2019).

The neuronal activity also triggers programs of gene transcription that affect dendritic spine development and plasticity on the longer run (Cohen and Greenberg, 2008; Greer and Greenberg, 2008; Zhai et al., 2013). Activity-dependent gene transcription requires Ca^{2+} signaling (Bading et al., 1993; Dolmetsch et al., 2001; Zhai et al., 2013). Activity-induced calcium entry triggers the activation of several distinct but sometimes converging signaling molecules, including CaMKII, protein kinase A (PKA), MAPK, or the phosphatase calcineurin pathways, each of which phosphorylates or dephosphorylate multiple transcriptional regulators within the nucleus. The best-studied activity-regulated transcriptional regulator is CREB, which upon phosphorylation at Ser 133 by such calcium-dependent pathways activates gene transcription that promotes spine development (Cohen and Greenberg, 2008; Greer and Greenberg, 2008). Other known activity-dependent transcription factors include myocyte enhancer factor 2 (MEF2), serum response factor (SRF), or CREST (Norman et al., 1988; Aizawa et al., 2004; Flavell et al., 2006). Like CREB, other activity-dependent transcription factors such as MEF2 and SRF/ELK are constitutively expressed, and their activation depends on their ability to integrate signals from multiple calcium-dependent pathways *via* post-transcriptional modifications, such as phosphorylation (Cohen and Greenberg, 2008; Greer and Greenberg, 2008; Ebert and Greenberg, 2013). The literature on the signaling mechanisms triggering activity-dependent transcription has been comprehensively reviewed elsewhere (Deisseroth and Tsien, 2002; Lonze and Ginty, 2002; Flavell and Greenberg, 2008; Hagenston and Bading, 2011; Benito and Barco, 2015).

Activity-dependent transcription factors, once phosphorylated by calcium signaling pathways, immediately activate an early transcriptional program corresponding to immediate early genes (IEGs), such as *Fosb*, *Fosl1*, *Fosl2*, *Jun*, *Junb*, *Egr1*, *Egr3*, and *Nr4a1* (Lyons and West, 2011). These IEGs then induce a program of late-response genes (LRGs) that will provide new spines with plasticity-related proteins (Hrvatin et al., 2018; Yap and Greenberg, 2018). One big question is how only stimulated spines can be selectively provided with plasticity-related proteins when activity-induced transcription typically changes gene expression in the whole cell. A body of studies indicates that activity-dependent mRNAs and proteins can preferentially be transported and captured at stimulated spines for local translation *via* a synaptic tagging and capture mechanism (**Figure 3**) that remains to be elucidated (Martin et al., 1997; Martin and Kosik, 2002; Redondo and Morris, 2011; Okuno et al., 2012; Pinho et al., 2020).

Numerous neuronal activity-dependent LRGs have been characterized (Loebrich and Nedivi, 2009; Leslie and Nedivi, 2011), but only a few genes have been linked with structural spine dynamics. A recent example is *Cpg15* (for Candidate Plasticity Gene 15, also known as *Neurontin*), an activity-regulated gene highly expressed at developmental times of synaptogenesis (Nedivi et al., 1996; Corriveau et al., 1999; Lee and Nedivi, 2002). *Cpg15* KO mice show defects in synapse formation (Fujino et al., 2011). Recently, *in vivo* TPM in the visual cortex showed that CPG15 is not required for rapid spine formation

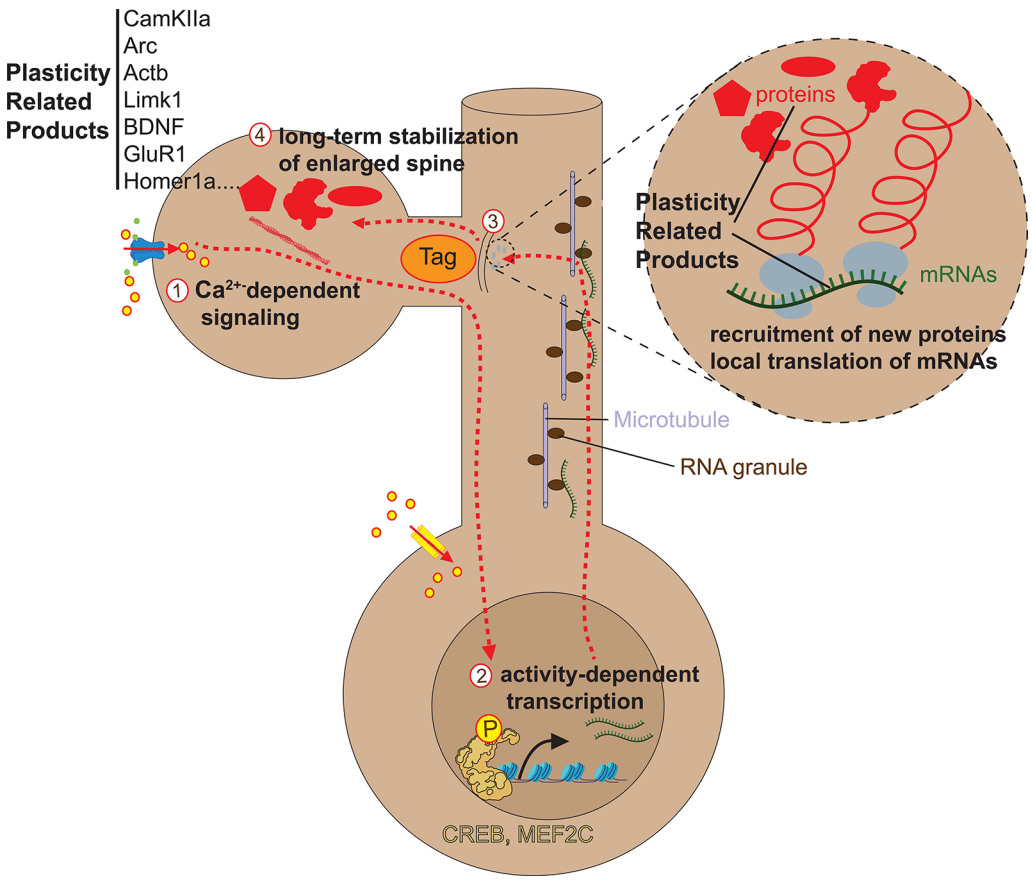

FIGURE 3 | Late phase of spine enlargement/formation. Glutamate release at synapses can induce long-lasting forms of synaptic plasticity that are mediated by NMDA-receptor and/or L-VSCC dependent calcium influx (1) and typically require activity-dependent protein synthesis, which is a consequence of the local mRNA translation within the dendrite (3) or of gene transcription within the nucleus (2,3). The mechanisms underlying activity-dependent local mRNA translation are currently unclear. Concerning gene transcription in the nucleus and transport of new mRNAs/proteins to activated spines, Ca^{2+} influx induces a cascade of kinase/phosphatase signaling pathways that propagate from the spine to the nucleus to phosphorylate/dephosphorylate activity-dependent transcription factors such as CREB or MEF2c. In turn, these factors induce the gene expression of plasticity-related products (PRPs) in the cytoplasm, either proteins or mRNAs. These PRPs are then transported and selectively captured by stimulated spines *via* a synaptic tagging and capture mechanism whose precise nature is still debated (3).

(Subramanian et al., 2019). Surprisingly, visual experience was also not required. However, PSD95 recruitment to nascent spines for their subsequent stabilization requires both visual input and CPG15. Notably, elegant experiments using conditional deletion in *Cpg15* floxed mice showed that CPG15 is necessary post-synaptically for spine stabilization. Further, CPG15 is not only required but sufficient for spine stabilization as its forced expression in post-synaptic neurons compensates for visual deprivation in allowing spine stabilization. Mechanistically, the data indicate that CPG15 physically interacts with AMPA receptors at the nascent spine and then recruits PSD95 for stabilization.

Many of the proteins that constitute the activity-dependent signaling network controlling gene transcription are implicated in neurodevelopmental disorders, in particular ASD (Ebert and Greenberg, 2013; Yap and Greenberg, 2018). This suggests that dysregulation of activity-dependent signaling networks, in general, may contribute significantly to the synaptic dysfunction that occurs in such neurodevelopmental disorders.

"External" Triggers of Spinogenesis

The current knowledge based on uncaging experiments states that the principal initial triggers for spinogenesis are the binding of the neurotransmitters, glutamate, and GABA through their binding to NMDA and GABA-A receptors, respectively (Kwon and Sabatini, 2011; Oh et al., 2016). Glutamate triggers spinogenesis lifelong, while the spinogenic effect of GABA is restricted to early life when the neurotransmitter is depolarizing.

Although neurotransmitter/receptor interactions are essential to determine where spine formation/elimination occurs on dendrite stretches, other external molecules have been recently shown to coregulate spine dynamics. Studies in the ventral tegmental area (VTA) and hippocampus have enlightened the role of the neuromodulators dopamine and serotonin in spine enlargement and elongation. In slices, dopamine secreted by VTA neurons was shown to promote glutamate-induced spinogenesis in nucleus accumbens medium spiny neurons. Researchers optically stimulated dopaminergic and glutamatergic inputs separately and found that dopamine

promoted spine enlargement only during a narrow time window (0.3–2 s) after the glutamatergic inputs. The downstream spine effector mechanisms included calcium entry, cAMP, and PKA activation (Yagishita et al., 2014). These data uncover a molecular basis and spine mechanism for the concept of reinforcement of animal behavior. Concerning serotonin, Bijata et al. (2017) have found in dissociated hippocampal cultures a signaling module involving the 5-HT7 receptor (5-HT7R), matrix metalloproteinase 9 (MMP-9), the hyaluronan receptor CD44, and the small GTPase Cdc42. Stimulation of 5-HT7R results in MMP-9 activation, which, in turn, cleaves CD44. This results in local detachment from the extracellular matrix, which facilitates spine elongation.

The predominant influence of stress and the circadian cycle highlights the critical role of glucocorticoid in spine dynamics. The two receptors for glucocorticoids GR and MR are involved in glucocorticoid actions (Liston and Gan, 2011; Liston et al., 2013). Tritiated labeling first showed that GR and MR exist as transcription factors bound to genomic DNA (Sarrieau et al., 1984; Alexis et al., 1990). However, EM analyses indicated that GR and MR can also be found at the cell membrane, in particular at pre and postsynaptic sites (Prager et al., 2010). The canonical model of action of GR and MR upon glucocorticoid binding is to activate a specific gene transcription program. This program can be triggered either by DNA-bound GR/MR since glucocorticoid can cross cell and nuclear membranes, or by synaptic GR/MR that can translocate to the nucleus after glucocorticoid binding. Strikingly, a non-transcriptional role of GR has been shown in the rapid formation of nascent spines *in vivo*, already 1 h after local corticosterone infusion (Liston et al., 2013). Molecular analyses indicated that activation of dendritic GR initiates spine formation through local interaction with the LIMK1-cofilin pathway and subsequent modulations of actin polymerization. Nevertheless, glucocorticoid-induced new spines then tend to stabilize and survive long term, which requires longer-lasting, transcriptional mechanisms that largely remain to be determined (Leslie and Nedivi, 2011). In contrast to GR, pharmacologic manipulations indicate that MR is predominantly involved in spine elimination and that the mechanisms at play are purely transcriptional (Liston et al., 2013). To add a level of complexity, recent studies have indicated that the transcriptional activities of GR and MR upon glucocorticoid activation require the interaction with the NEUROD family of bHLH transcription factors (Van Weert et al., 2017, 2019). In particular genomic DNA binding sites for MR are all found near NEUROD binding sites on genomic DNA, and both MR and GR depend on NEUROD2 for efficient transactivation of their target genes, as demonstrated on a luciferase assay (Van Weert et al., 2017). *Neurod2* is expressed in pyramidal neurons of the cortex and hippocampus starting from their birth up until animal death. Interestingly, NEUROD2 was identified by the elegant "transactivator trap" genetic screen designed by the Ghosh team as an activity-dependent transcription factor, like CREB. Indeed, NEUROD2 transactivation activity is potentiated by neuronal activity in a calcium-dependent manner (Ince-Dunn et al., 2006). Interestingly, a mouse study has suggested that Neurod2 KO mice are insensitive to stress in the elevated plus-maze and fear conditioning box (Lin et al., 2005b). We recently found that NEUROD2 loss-of-function mutations are causally involved in a neurodevelopment syndrome including ASD and ID in humans (Runge et al., 2020). When analyzing *Neurod2* KO mice, we observed alterations of spine densities in apical tuft dendrites of somatosensory L5 neurons. Spine variations differed in juvenile and adult ages: juvenile mice had fewer spines while adult mice more spines compared to wild type controls. *In vivo*, TPM of apical dendrites helped explain these results as it showed abnormally elevated spine formation rates in juvenile mice, while spine elimination was normal, such that formation took over elimination. Whether NEUROD2's effect on spine dynamics is entirely dependent on glucocorticoid signaling or whether it can act independently as a mediator of activity-dependent gene transcription for late-phase sLTP remains to be determined. Nevertheless, our bulk (Runge et al., 2020) and ongoing single-cell RNA-seq analyses show that plasticity-related post-synaptic genes are the most enriched set of genes among *Neurod2* KO differentially expressed genes (37/227 genes), which suggests that NEUROD2 is a nexus in a gene network that controls spine turnover in the postnatal cortex.

CONCLUSION AND PERSPECTIVES

We have described the current knowledge about the causes and consequences of dendritic spine plasticity, with a particular focus on recent *in vivo* TPM. Such studies have shown that spine plasticity is caused by several forms of functional plasticity and learning, and that, in return, it is causally involved in the storage of the memory of these experiences on the long-term (Hayashi-Takagi et al., 2015; Moda-Sava et al., 2019). Developmentally, spine plasticity is prominent until adolescence and then drops down in adulthood to very low levels. However, the tremendous number of spines in each brain area allows to compensate for this very low-level adult plasticity and can explain a lifelong causative impact on neural network functions and animal's behavior (Arenz et al., 2008; Houweling and Brecht, 2008; Yang et al., 2009; **Figure 1**).

In the future, several approaches might be indicated to accelerate knowledge in the field. in utero electroporation of more than a single fluorochrome will allow capturing not only each spine's morphology and location but also its subtype identity in real-time *in vivo*. As shown by the work of Nedivi and colleagues (Chen et al., 2012; Villa et al., 2016; Subramanian et al., 2019), the ability to visualize PSD-95, *via* the *in utero* electroporation of a PSD95-mCherry construct, revealed that spines fall into two main subtypes corresponding to different maturation stages. The majority of spines (∼80% in adults), correspond to mature excitatory synapses, and these contain PSD-95. Most of these PSD-95 positive spines are stable, but, in the rare cases that they lose PSD-95 and disappear, or are formed *de novo* and gain PSD-95, their dynamics result in a persistent synapse gain or loss and permanent circuit rewiring associated with learning and memory, respectively. The remaining 20% of adult spines are PSD-95 negative. Most of them have immature synaptic currents due to low AMPA receptor contents and thus form unstable synapses. PSD-95

negative spines are highly dynamic and mostly transient, rarely gaining PSD-95 or persisting. Their dynamics likely reflect a sampling strategy for searching potential presynaptic partners in the extracellular space, and the rare spines gaining PSD-95 would be the ones inducing permanent circuit rewiring. In sum, the recent *in vivo* TPM experiments have shown that PSD95 is necessary for spine stabilization but not for spine initiation (Subramanian et al., 2019). Interestingly, adult TPM of *in utero* electroporated plasmids can also allow visualizing the dynamics of molecular determinants of spine plasticity in real-time *in vivo*. As a proof-of-principle, two studies from Huganir and colleagues have shown that *in utero* electroporation of a SEP-tagged GluA1 (an AMPA receptor subunit) plasmid can be used to image experience-dependent AMPA receptor trafficking in real-time *in vivo* (Zhang et al., 2015; Roth et al., 2020). Many molecules other than PSD-95 and AMPA receptors are important for spine plasticity (Sala and Segal, 2014; Schreiner et al., 2017), but their *in vivo* role remains to be assessed, possibly *via* similar approaches.

Importantly, the development of 2pFLIM on organotypic slices has allowed exploring the spatiotemporal dynamics of biochemical signaling in dendritic spines, and a proof-of-principle *in vivo* has been published (Mower et al., 2011). One current limitation of this strategy is that it typically requires the over-expression of FRET-based biosensors (Nishiyama, 2019), which likely disrupts native cell signaling and thus limits the applicability of the method. In this regard, the recent development of CRISP-Cas9 based techniques to fluorescently tag endogenous proteins may open better avenues to image endogenous signal transduction without the effects of overexpressed FRET sensors, and this rather *in vivo* than in slice cultures (Mikuni et al., 2016; Suzuki et al., 2016; Nishiyama et al., 2017).

Besides spines, inhibitory synapses can now be imaged longitudinally by TPM of Gephyrin-fused fluorophores. Nedivi et al. (1996) found that, in cortical pyramidal neuron dendrites, ∼30% of inhibitory synapses form on dendritic spines (they called them inhibitory spine synapses) while the rest are shaft synapses. Then, by TPM they discovered that inhibitory spine synapses are much more dynamic than dendritic spines and inhibitory shaft synapses (Chen et al., 2012) and that they are repeatedly assembled and removed at persistent sites (Villa et al., 2016). This could provide flexible, input-specific gating of stable excitatory synapses. Studying further the interplay between inhibitory synapse subtypes and excitatory spines has exciting implications for the understanding of cortical network function in health and neuropsychiatric disorders, which often strongly affect inhibitory neurons (Han et al., 2012; Judson et al., 2016; Ip et al., 2018).

Another prospective advance in the field will be to track presynaptic axons and circuits connecting the dendritic spines whose dynamics are observed. The Gan team has nicely shown that axonal boutons are largely stable in the barrel cortex of adult mice (Qiao et al., 2016). However, for all but one study in the field to date (Yang et al., 2016), the identity of axonal inputs that form connections with learning-induced spines have not been searched. The recent improvements in intersectional genetics and retrograde/anterograde tracers should help to address this issue, which will be essential to deconstruct how specific circuits are modulated by experience and disease.

AUTHOR CONTRIBUTIONS

AC and KR wrote the article. KR designed the tables. AC made the figures. All authors contributed to the article and approved the submitted version.

FUNDING

This work was supported by Fédération pour la Recherche sur le Cerveau, Fondation Jérôme Lejeune, and Agence Nationale de la Recherche.

REFERENCES

Aizawa, H., Hu, S.-C., Bobb, K., Balakrishnan, K., Ince, G., Gurevich, I., et al. (2004). Dendrite development regulated by CREST, a calcium-regulated transcriptional activator. *Science* 303, 197–202. doi: 10.1126/science.1089845

Alber, M., Kalscheuer, V. M., Marco, E., Sherr, E., Lesca, G., Till, M., et al. (2017). ARHGEF9 disease: phenotype clarification and genotype-phenotype correlation. *Neurol. Genet.* 3:e148. doi: 10.1212/NXG.0000000000000148

Alexis, M. N., Kitraki, E., Spanou, K., Stylianopoulou, F., and Sekeris, C. E. (1990). Ontogeny of the glucocorticoid receptor in the rat brain. *Adv. Exp. Med. Biol.* 265, 269–276. doi: 10.1007/978-1-4757-5876-4_25

Amir, R. E., Van den Veyver, I. B., Wan, M., Tran, C. Q., Francke, U., and Zoghbi, H. Y. (1999). Rett syndrome is caused by mutations in X-linked MECP2, encoding methyl-CpG-binding protein 2. *Nat. Genet.* 23, 185–188. doi: 10.1038/13810

Arenz, A., Silver, R. A., Schaefer, A. T., and Margrie, T. W. (2008). The contribution of single synapses to sensory representation *in vivo*. *Science* 321, 977–980. doi: 10.1126/science.1158391

Arroyo, E. D., Fiole, D., Mantri, S. S., Huang, C., and Portera-Cailliau, C. (2019). Dendritic spines in early postnatal fragile X mice are insensitive to novel sensory experience. *J. Neurosci.* 39, 412–419. doi: 10.1523/jneurosci.1734-18.2018

Asaka, Y., Jugloff, D. G., Zhang, L., Eubanks, J. H., and Fritzsimonds, R. M. (2006). Hippocampal synaptic plasticity in impaired in the Mecp2-null mouse model of rett syndrome. *Neurobiol. Dis.* 21, 217–227. doi: 10.1016/j.nbd.2005.07.005

Attardo, A., Fitzgerald, J. E., and Schnitzer, M. J. (2015). Impermanence of dendritic spines in live adult CA1 hippocampus. *Nature* 523, 592–596. doi: 10.1038/nature14467

Bading, H., Ginty, D. D., and Greenberg, M. E. (1993). Regulation of gene expression in hippocampal neurons by distinct calcium signaling pathways. *Science* 260, 181–186. doi: 10.1126/science.8097060

Baltaci, S. B., Mogulkoc, R., and Baltaci, A. K. (2019). Molecular mechanisms of early and late LTP. *Neurochem. Res.* 44, 281–296. doi: 10.1007/s11064-018-2695-4

Bassell, G. J., and Warren, S. T. (2008). Fragile X syndrome: loss of local MRNA regulation alters synaptic development and function. *Neuron* 60, 201–214. doi: 10.1016/j.neuron.2008.10.004

Belichenko, P. V., Oldfords, A., Hagberg, B., and Dahlström, A. (1994). Rett syndrome: 3-D confocal microscopy pf cortical pyramidal dendrites and afferents. *Neuroreport.* 5, 1509–1513.

Belichenko, P. V., Wright, E. E., Belichenko, N. P., Masliah, E., Li, H. H., Mobley, W. C., et al. (2009). Widespread changes in dendritic and axonal morphology in Mecp2-mutant mouse models of rett syndrome: evidence

for disruption of neuronal networks. *J. Comp. Neurol.* 514, 240–258. doi: 10.1002/cne.22009

Benito, E., and Barco, A. (2015). The neuronal activity-driven transcriptome. *Mol. Neurobiol.* 51, 1071–1088. doi: 10.1007/s12035-014-8772-z

Bernardet, M., and Crusio, W. E. (2006). Fmr1 KO mice as a possible model of autistic features. *Sci. World J.* 6, 1164–1176. doi: 10.1100/tsw.2006.220

Bijata, M., Labus, J., Guseva, D., Stawarski, M., Butzlaff, M., Dzwonek, J., et al. (2017). Synaptic remodeling depends on signaling between serotonin receptors and the extracellular matrix. *Cell Rep.* 19, 1767–1782. doi: 10.1016/j.celrep.2017.05.023

Borovac, J., Bosch, M., and Okamoto, K. (2018). Regulation of actin dynamics during structural plasticity of dendritic spines: signaling messengers and actin-binding proteins. *Mol. Cell. Neurosci.* 91, 122–130. doi: 10.1016/j.mcn.2018.07.001

Bourgeron, T. (2015). From the genetic architecture to synaptic plasticity in autism spectrum disorder. *Nat. Rev. Neurosci.* 16, 551–563. doi: 10.1038/nrn3992

Brandon, N. J., and Sawa, A. (2011). Linking neurodevelopmental and synaptic theories of mental illness through DISC1. *Nat. Rev. Neurosci.* 12, 707–722. doi: 10.1038/nrn3120

Buiting, K., Williams, C., and Horsthemke, B. (2016). Angelman syndrome—insights into a rare neurogenetic disorder. *Nat. Rev. Neurol.* 12, 584–593. doi: 10.1038/nrneurol.2016.133

Cajal, S. R. (1888). Estructura de los centros nerviosos de las aves. *Rev. Trim. Histol. Norm. patol.* 1, 1–10.

Cane, M., Maco, B., Knott, G., and Holtmaat, A. (2014). The relationship between PSD-95 clustering and spine stability *in vivo*. *J. Neurosci.* 34, 2075–2086. doi: 10.1523/JNEUROSCI.3353-13.2014

Carlisle, H. J., and Kennedy, M. B. (2005). Spine architecture and synaptic plasticity. *Trends Neurosci.* 28, 182–187. doi: 10.1016/j.tins.2005.01.008

Caroni, P., Donato, F., and Muller, D. (2012). Structural plasticity upon learning: regulation and functions. *Nat. Rev. Neurosci.* 13, 478–490. doi: 10.1038/nrn3258

Chahrour, M., and Zoghbi, H. Y. (2007). The story of rett syndrome: from clinic to neurobiology. *Neuron* 56, 422–437. doi: 10.1016/j.neuron.2007.10.001

Chang, Q., Khare, G., Dani, V., Nelson, S., and Jaenisch, R. (2006). The disease progression of Mecp2 mutant mice is affected by the level of BDNF expression. *Neuron* 49, 341–348. doi: 10.1016/j.neuron.2005.12.027

Chapleau, C. A., Calfa, G. D., Lane, M. C., Albertson, A. J., Larimore, J. L., Kudo, S., et al. (2009). Dendritic spine pathologies in hippocampal pyramidal neurons from rett syndrome brain and after expression of rett-associated MECP2 mutations. *Neurobiol. Dis.* 35, 219–233. doi: 10.1016/j.nbd.2009.05.001

Chen, J. L., Villa, K. L., Cha, J. W., So, P. T. C., Kubota, Y., and Nedivi, E. (2012). Clustered dynamics of inhibitory synapses and dendritic spines in the adult neocortex. *Neuron* 74, 361–373. doi: 10.1016/j.neuron.2012.02.030

Chini, M., Pöpplau, J. A., Lindemann, C., Carol-Perdiguer, L., Hnida, M., Oberländer, V., et al. (2020). Resolving and rescuing developmental miswiring in a mouse model of cognitive impairment. *Neuron* 105, 60.e7–74.e7. doi: 10.1016/j.neuron.2019.09.042

Chu, C., Murdock, M. H., Jing, D., Won, T. H., Chung, H., Kressel, A. M., et al. (2019). The microbiota regulate neuronal function and fear extinction learning. *Nature* 574, 543–548. doi: 10.1038/s41586-019-1644-y

Cichon, J., and Gan, W. (2015). Branch-specific dendritic Ca(2+) spikes cause persistent synaptic plasticity. *Nature* 520, 180–185. doi: 10.1038/nature14251

Cohen, S. and Greenberg, M. E. (2008). Communication between the synapse and the nucleus in neuronal development, plasticity and disease. *Annu. Rev. Cell. Dev. Biol.* 24, 183–209. doi: 10.1146/annurev.cellbio.24.110707.175235

Cohen, S., Gabel, H. W., Hemberg, M., Hutchinson, A. N., Sadacca, L. A., Ebert, D. H., et al. (2011). Genome-wide activity-dependent MeCP2 phosphorylation regulates nervous system development and function. *Neuron* 72, 72–85. doi: 10.1016/j.neuron.2011.08.022

Comery, T. A., Harris, J. B., Willems, P. J., Oostra, B. A., Irwin, S. A., Weiler, I. J., et al. (1997). Abnormal dendritic spines in fragile X knockout mice: maturation and pruning deficits. *Proc. Natl. Acad. Sci. U S A* 94, 5401–5404. doi: 10.1073/pnas.94.10.5401

Conrad, C. D., Galea, L. A. M., Kuroda, Y., and McEwen, B. S. (1996). Chronic stress impairs rat spatial memory on the y maze and this effect is blocked by tianeptine pretreatment. *Behav. Neurosci.* 110, 1321–1334. doi: 10.1037/0735-7044.110.6.1321

Cordero, I. M., and Sandi, C. (2007). Stress amplifies memory for social hierarchy. *Front. Neurosci.* 1, 175–184. doi: 10.3389/neuro.01.1.1.013.2007

Corriveau, R. A., Shatz, C. J., and Nedivi, E. (1999). Dynamic regulation of cpg15 during activity-dependent synaptic development in the mammalian visual system. *J. Neurosci.* 19, 7999–8008. doi: 10.1523/JNEUROSCI.19-18-07999.1999

Costa, J. F., Dines, M., and Lamprecht, R. (2020). The role of rac GTPase in dendritic spine morphogenesis and memory. *Front. Synaptic Neurosci.* 12:12. doi: 10.3389/fnsyn.2020.00012

Cruz-Martín, A., Crespo, M., and Portera-Cailliau, C. (2010). Delayed stabilization of dendritic spines in fragile X mice. *J. Neurosci.* 30, 7793–7803. doi: 10.1523/JNEUROSCI.0577-10.2010

Cryan, J. F., Mombereau, C., and Vassout, A. (2005). The tail suspension test as a model for assessing antidepressant activity: review of pharmacological and genetic studies in mice. *Neurosci. Biobehav. Rev.* 29, 571–625. doi: 10.1016/j.neubiorev.2005.03.009

Dailey, M. E., and Smith, S. J. (1996). The dynamics of dendritic structure in developing hippocampal slices. *J. Neurosci.* 16, 2983–2994. doi: 10.1523/JNEUROSCI.16-09-02983.1996

Davis, M. (1997). Neurobiology of fear responses: the role of the amygdala. *J. Neuropsychiatry Clin. Neurosci.* 9, 382–402. doi: 10.1176/jnp.9.3.382

De Kloet, E. R., Vreugdenhil, E., Oitzl, M. S., and Joëls, M. (1998). Brain corticosterone receptor balance in health and disease. *Endocr. Rev.* 19, 269–301. doi: 10.1210/edrv.19.3.0331

de Quervain, D. J., Roozendaal, B., and McGaugh, J. L. (1998). Stress and glucocorticoids impair retrieval of long-term spatial memory. *Nature* 394, 787–790. doi: 10.1038/29542

De Roo, M., Klauser, P., and Muller, D. (2008). LTP promotes a selective long-term stabilization and clustering of dendritic spines. *PLoS Biol* 6:e219. doi: 10.1371/journal.pbio.0060219

De Vivo, L., Bellesi, M., Marshall, W., Bushong, E. A., Ellisman, M. H., Tononi, G., et al. (2017). Ultrastructural evidence for synaptic scaling across the wake/sleep cycle. *Science* 355, 507–510. doi: 10.1126/science.aah5982

DeFelipe, J. (2015). The dendritic spine story: an intriguing process of discovery. *Front. Neuroanat.* 9:14. doi: 10.3389/fnana.2015.00014

Deisseroth, K., and Tsien, R. W. (2002). Dynamic multiphosphorylation passwords for activity-dependent gene expression. *Neuron* 34, 179–182. doi: 10.1016/s0896-6273(02)00664-5

Denk, W., Strickler, J. H., and Webb, W. W. (1990). Two-photon laser scanning fluorescence microscopy. *Science* 248, 73–76. doi: 10.1126/science.2321027

Dias-Ferreira, E., Sousa, J. C., Melo, I., Morgado, P., Mesquita, A. R., Cerqueira, J. J., et al. (2009). Chronic stress causes frontostriatal reorganization and affects decision-making. *Science* 325, 621–625. doi: 10.1126/science.1171203

Dickstein, D. L., Weaver, C. M., Luebke, J. I., and Hof, P. R. (2013). Dendritic spine changes associated with normal aging. *Neuroscience* 251, 21–32. doi: 10.1016/j.neuroscience.2012.09.077

Diering, G. H., Gustina, A. S., and Huganir, R. L. (2014). PKA-GluA1 coupling *via* AKAP5 controls AMPA receptor phosphorylation and cell-surface targeting during bidirectional homeostatic plasticity. *Neuron* 84, 790–805. doi: 10.1016/j.neuron.2014.09.024

Dindot, S. V., Antalffy, B. A., Bhattacharjee, M. B., and Beaudet, A. L. (2008). The angelman syndrome ubiquitin ligase localizes to the synapse and nucleus and maternal deficiency results in abnormal dendritic spine morphology. *Hum. Mol. Genet.* 17, 111–118. doi: 10.1093/hmg/ddm288

Dolmetsch, R. E., Pajvani, U., Fife, K., Spotts, J. M., and Greenberg, M. E. (2001). Signaling to the nucleus by an L-type calcium channel-calmodulin complex through the map kinase pathway. *Science* 294, 333–339. doi: 10.1126/science.1063395

Duan, H., Wearne, S. L., Rocher, A. B., Macedo, A., Morrison, J. H., and Hof, P. R. (2003). Age-related dendritic and spine changes in corticocortically projecting neurons in macaque monkeys. *Cereb. Cortex* 13, 950–961. doi: 10.1093/cercor/13.9.950

Earls, L. R., and Zakharenko, S. S. (2014). A synaptic function approach to investigating complex psychiatric diseases. *Neuroscientist* 20, 257–271. doi: 10.1177/1073858413498307

Ebert, D. H., and Greenberg, M. E. (2013). Activity-dependent neuronal signalling and autism spectrum disorder. *Nature* 493, 327–337. doi: 10.1038/nature11860

Ehninger, D., Li, W., Fox, K., Stryker, M. P., and Silva, A. J. (2008). Reversing neurodevelopmental disorders in adults. *Neuron* 60, 950–960. doi: 10.1016/j.neuron.2008.12.007

Ethell, I. M., and Pasquale, E. B. (2005). Molecular mechanisms of dendritic spine development and remodeling. *Prog. Neurobiol.* 75, 161–205. doi: 10.1016/j.pneurobio.2005.02.003

Feldman, M. L., and Dowd, C. (1975). Loss of dendritic spines in aging cerebral cortex. *Anat. Embryol.* 148, 279–301. doi: 10.1007/BF00319848

Feng, G., Mellor, R. H., Bernstein, M., Keller-Peck, C., Nguyen, Q. T., Wallace, M., et al. (2000). Imaging neuronal subsets in transgenic mice expressing multiple spectral variants of GFP. *Neuron* 28, 41–51. doi: 10.1016/s0896-6273(00)00084-2

Feyissa, A. M., Chandran, A., Stockmeier, C. A., and Karolewicz, B. (2009). Reduced levels of NR2A and NR2B subunits of NMDA receptor and PSD-95 in the prefrontal cortex in major depression. *Prog. Neuropsychopharmacol. Biol. Psychiatry* 33, 70–75. doi: 10.1016/j.pnpbp.2008.10.005

Fiala, J. C., Feinberg, M., Popov, V., and Harris, K. M. (1998). Synaptogenesis *via* dendritic filopodia in developing hippocampal area CA1. *J. Neurosci.* 18, 8900–8911. doi: 10.1523/JNEUROSCI.18-21-08900.1998

Fischer, M., Kaech, S., Knutti, D., and Matus, A. (1998). Rapid actin-based plasticity in dendritic spines. *Neuron* 20, 847–854. doi: 10.1016/S0896-6273(00)80467-5

Flavell, S. W., and Greenberg, M. E. (2008). Signaling mechanisms linking neuronal activity to gene expression and plasticity of the nervous system. *Annu. Rev. Neurosci.* 31, 563–590. doi: 10.1146/annurev.neuro.31.060407.125631

Flavell, S. W., Cowan, C. W., Kim, T., Greer, P. L., Lin, Y., Paradis, S., et al. (2006). Activity-dependent regulation of MEF2 transcription factors suppresses excitatory synapse number. *Science* 311, 1008–1012. doi: 10.1126/science.1122511

Forrest, M. P., Parnell, E., and Penzes, P. (2018). Dendritic structural plasticity and neuropsychiatric disease. *Nat. Rev. Neurosci.* 19, 215–234. doi: 10.1038/nrn.2018.16

Frank, A. C., Huang, S., Zhou, M., Gdalyahu, A., Kastellakis, G., Silva, T. K., et al. (2018). Hotspots of dendritic spine turnover facilitate clustered spine addition and learning and memory. *Nat. Commun.* 9:422. doi: 10.1038/s41467-017-02751-2

Fu, M., Yu, X., Lu, J., and Zuo, Y. (2012). Repetitive motor learning induces coordinated formation of clustered dendritic spines *in vivo*. *Nature* 483, 92–95. doi: 10.1038/nature10844

Fujino, T., Leslie, J. H., Eavri, R., Chen, J. L., Lin, W. C., Flanders, G. H., et al. (2011). CPG15 regulates synapse stability in the developing and adult brain. *Genes Dev.* 25, 2674–2685. doi: 10.1101/gad.176172.111

Fukazawa, Y., Saitoh, Y., Ozawa, F., Ohta, Y., Mizuno, K., and Inokuchi, K. (2003). Hippocampal LTP is accompanied by enhanced F-actin content within the dendritic spine that is essential for late LTP maintenance *in vivo*. *Neuron* 38, 447–460. doi: 10.1016/s0896-6273(03)00206-x

Fukuda, T., Itoh, M., Ichikawa, T., Washiyama, K., and Goto, Y. (2005). Delayed maturation of neuronal architecture and synaptogenesis in cerebral cortex of MeCP2-deficient mice. *J. Neuropathol. Exp. Neurol.* 64, 537–544doi: 10.1093/jnen/64.6.537

Galvez, R., and Greenough, W. T. (2005). Sequence of abnormal dendritic spine development in primary somatosensory cortex of a mouse model of the fragile X mental retardation syndrome. *Am. J. Med. Genet.* 135, 155–160. doi: 10.1002/ajmg.a.30709

Giacometti, E., Luikenhuis, S., Beard, C., and Jaenisch, R. (2007). Partial rescue of MeCP2 deficiency by postnatal activation of MeCP2. *Proc. Natl. Acad. Sci. U S A* 104, 1931–1936. doi: 10.1073/pnas.0610593104

Globus, A., Rosenzweig, M. R., Bennett, E. L., and Diamond, M. C. (1973). Effects of differential experience on dendritic spine counts in rat cerebral cortex. *J. Comp. Physiol. Psychol.* 82, 175–181. doi: 10.1037/h0033910

Gold, P. W., Machado-Vieira, R., and Pavlatou, M. G. (2015). Clinical and biochemical manifestations of depression: relation to the neurobiology of stress. *Neural Plast.* 2015:581976. doi: 10.1155/2015/581976

Gordon, J. A., and Stryker, M. P. (1996). Experience-dependent plasticity of binocular responses in the primary visual cortex of the mouse. *J. Neurosci.* 16, 3274–3286. doi: 10.1523/JNEUROSCI.16-10-03274.1996

Gray, E. G. (1959). Axo-somatic and axo-dendritic synapses of the cerebral cortex: an electron microscope study. *J. Anat.* 93, 420–433.

Greer, P. L., and Greenberg, M. E. (2008). From synapse to nucleus: calcium-dependent gene transcription in the control of synapse development and function. *Neuron* 59, 846–860. doi: 10.1016/j.neuron.2008.09.002

Greer, P. L., Hanayama, R., Bloodgood, B. L., Mardinly, A. R., Lipton, D. M., Flavell, S. W., et al. (2010). The angelman syndrome protein Ube3A regulates synapse development by ubiquitinating arc. *Cell* 140, 704–716. doi: 10.1016/j.cell.2010.01.026

Grutzendler, J., Kasthuri, N., and Wen, B. (2002). Long-term dendritic spine stability in the adult cortex. *Nature* 420, 812–816. doi: 10.1038/nature01276

Gu, L., Kleiber, S., Schmid, L., Nebeling, F., Chamoun, M., Steffen, J., et al. (2014). Long-term *in vivo* imaging of dendritic spines in the hippocampus reveals structural plasticity. *J. Neurosci.* 34, 13948–13953. doi: 10.1523/JNEUROSCI.1464-14.2014

Guy, J., Gan, J., Selfridge, J., Cobb, S., and Bird, A. (2007). Reversal of neurological defects in a mouse model of rett syndrome. *Science* 315, 1143–1147. doi: 10.1126/science.1138389

Hagenston, A. M., and Bading, H. (2011). Calcium signaling in synapse-to-nucleus communication. *Cold Spring Harb. Perspect. Biol.* 3:a004564. doi: 10.1101/cshperspect.a004564

Hamdan, F. F., Gauthier, J., Spiegelman, D., Noreau, A., Yang, Y., Pellerin, S., et al. (2009). Mutations in SYNGAP1 in autosomal nonsyndromic mental retardation. *N. Engl. J. Med.* 360, 599–605. doi: 10.1056/NEJMoa0805392

Han, S., Tai, C., Westenbroek, R. E., Yu, F. H., Cheah, C. S., Potter, G. B., et al. (2012). Autistic-like behaviour in Scn1a+/- mice and rescue by enhanced GABA-mediated neurotransmission. *Nature* 489, 385–390. doi: 10.1038/nature11356

Harlow, E. G., Till, S. M., Russel, T. A., Wijetunge, L. S., Kind, P., and Contractor, A. (2010). Critical period plasticity is disrupted in the barrel cortex of FMR1 knockout mice. *Neuron* 65, 385–398. doi: 10.1016/j.neuron.2010.01.024

Harvey, C. D., Yasuda, R., Zhong, H., and Svoboda, K. (2008). The spread of ras activity triggered by activation of a single dendritic spine. *Science* 321, 136–140. doi: 10.1126/science.1159675

Hastings, R. S., Parsey, R. V., Oquendo, M. A., Arango, V., and Mann, J. J. (2004). Volumetric analysis of the prefrontal cortex, amygdala and hippocampus in major depression. *Neuropsychopharmacol.* 29, 952–959. doi: 10.1038/sj.npp.1300371

Hayashi-Takagi, A., Araki, Y., Nakamura, M., Vollrath, B., Duron, S. G., Yan, Z., et al. (2014). PAKs inhibitors ameliorate schizophrenia-associated dendritic spine deterioration *in vitro* and *in vivo* during late adolescence. *Proc. Natl. Acad. Sci. U S A* 111, 6461–6466. doi: 10.1073/pnas.1321109111

Hayashi-Takagi, A., Takaki, M., Graziane, N., Seshadri, S., Murdoch, H., Dunlop, A. J., et al. (2010). Disrupted-in-schizophrenia 1 (DISC1) regulates spines of the glutamate synapse *via* Rac1. *Nat. Neurosci.* 13, 327–332. doi: 10.1038/nn.2487

Hayashi-Takagi, A., Yagishita, S., Nakamura, M., Shirai, F., Wu, Y. I., Loshbaugh, A. L., et al. (2015). Labelling and optical erasure of synaptic memory traces in the motor cortex. *Nature* 525, 333–338. doi: 10.1038/nature15257

Hedrick, N. G., and Yasuda, R. (2017). Regulation of Rho GTPase proteins during spine structural plasticity for the control of local dendritic plasticity. *Curr. Opin. Neurobiol.* 45, 193–201. doi: 10.1016/j.conb.2017.06.002

Hedrick, N. G., Harward, S. C., Hall, C. E., Murakoshi, H., McNamara, J. O., and Yasuda, R. (2016). Rho GTPase complementation underlies BDNF-dependent homo- and heterosynaptic plasticity. *Nature* 538, 104–108. doi: 10.1038/nature19784

Heinrichs, S. C., Leite-Morris, K. A., Guy, M. D., Goldberg, L. R., Young, A. J., and Kaplan, G. B. (2013). Dendritic structural plasticity in the basolateral amygdala

after fear conditioning and its extinction in mice. *Behav. Brain Res.* 248, 80–84. doi: 10.1016/j.bbr.2013.03.048

Herms, J., and Dorostkar, M. M. (2016). Dendritic spine pathology in neurodegenerative diseases. *Annu. Rev. Pathol.* 11, 221–250. doi: 10.1146/annurev-pathol-012615-044216

Higley, M. J., and Sabatini, B. L. (2012). Calcium signaling in dendritic spines. *Cold Spring Harb. Perspect. Biol.* 4:a005686. doi: 10.1101/cshperspect.a005686

Hofer, S. B., Mrsic-Flogel, T. D., Bonhoeffer, T., and Hübener, M. (2006). Prior experience enhances plasticity in adult visual cortex. *Nat. Neurosci.* 9, 127–132. doi: 10.1038/nn1610

Hofer, S. B., Mrsic-Flogel, T. D., Bonhoeffer, T., and Hübener, M. (2009). Experience leaves a lasting structural trace in cortical circuits. *Nature* 457, 313–317. doi: 10.1038/nature07487

Hollis, F., and Kabbaj, M. (2014). Social defeat as an animal model for depression. *ILAR J.* 55, 221–232. doi: 10.1093/ilar/ilu002

Holt, C. E., Martin, K. C., and Schuman, E. M. (2019). Local translation in neurons: visualization and function. *Nat. Struct. Mol. Biol.* 26, 557–566. doi: 10.1038/s41594-019-0263-5

Holtmaat, A., Wilbrecht, L., Knott, G. W., Welker, E., and Svoboda, K. (2006). Experience-dependent and cell-type-specific spine growth in the neocortex. *Nature* 441, 979–983. doi: 10.1038/nature04783

Holtmaat, A. J. G. D., Trachtenberg, J. T., Wilbrecht, L., Shepherd, G. M., Zhang, X., Knott, G. W., et al. (2005). Transient and persistent dendritic spines in the neocortex *in vivo*. *Neuron* 45, 279–291. doi: 10.1016/j.neuron.2005.01.003

Houweling, A. R., and Brecht, M. (2008). Behavioural report of single neuron stimulation in somatosensory cortex. *Nature* 451, 65–68. doi: 10.1038/nature06447

Hrvatin, S., Hochbaum, D. R., Nagy, M. A., Cicconet, M., Robertson, K., Cheadle, L., et al. (2018). Single-cell analysis of experience-dependent transcriptomic states in the mouse visual cortex. *Nat. Neurosci.* 21, 120–129. doi: 10.1038/s41593-017-0029-5

Hutsler, J. J., and Zhang, H. (2010). Increased dendritic spine densities on cortical projection neurons in autism spectrum disorders. *Brain Res.* 1309, 83–94. doi: 10.1016/j.brainres.2009.09.120

Huttenlocher, P. R. (1990). Morphometric study of human cerebral cortex development. *Neuropsychologia* 28, 517–527. doi: 10.1016/0028-3932(90)90031-i

Ince-Dunn, G., Hall, B. J., Hu, S. C., Ripley, B., Huganir, R. L., Olson, J. M., et al. (2006). Regulation of thalamocortical patterning and synaptic maturation by neuroD2. *Neuron* 49, 683–695. doi: 10.1016/j.neuron.2006.01.031

Ip, J. P. K., Mellios, N., and Sur, M. (2018). Rett syndrome: insights into genetic, molecular and circuit mechanisms. *Nat. Rev. Neurosci.* 19, 368–382. doi: 10.1038/s41583-018-0006-3

Irwin, S. A., Patel, B., Idupulapati, M., Harris, J. B., Crisostomo, R. A., Larsen, B. P., et al. (2001). Abnormal dendritic spine characteristics in the temporal and visual cortices of patients with fragile-X syndrome: a quantitative examination. *Am. J. Med. Genet.* 98, 161–167. doi: 10.1002/1096-8628(20010115)98:2<161::AID-AJMG1025>3.0.CO;2-B

Isshiki, M., Tanaka, S., Kuriu, T., Tabuchi, K., Takumi, T., and Okabe, S. (2014). Enhanced synapse remodelling as a common phenotype in mouse models of autism. *Nat. Commun.* 5:4742. doi: 10.1038/ncomms5742

Jeanneteau, F., Barrère, C., Vos, M., De Vries, C. M. J., Rouillard, C., Levesque, D., et al. (2018). The stress-induced transcription factor NR4A1 adjusts mitochondrial function and synapse number in prefrontal cortex. *J. Neurosci.* 38, 1335–1350. doi: 10.1523/JNEUROSCI.2793-17.2017

Joëls, M., Karst, H., and Sarabdjitsingh, R. A. (2018). The stressed brain of humans and rodents. *Acta Physiol.* 223:e13066. doi: 10.1111/apha.13066

Joëls, M., Pu, Z., Wiegert, O., Oitzl, M. S., and Krugers, H. J. (2006). Learning under stress: how does it work? *Trends Cogni. Sci.* 10, 152–158. doi: 10.1016/j.tics.2006.02.002

Judson, M. C., Wallace, M. L., Sidorov, M. S., Burette, A. C., Gu, B., Van Woerden, G. M., et al. (2016). GABAergic neuron-specific loss of Ube3a causes angelman syndrome-like EEG abnormalities and enhances seizure susceptibility. *Neuron* 90, 56–69. doi: 10.1016/j.neuron.2016.02.040

Kang, H. J., Voleti, B., Hajszan, T., Rajkowska, G., Stockmeier, C. A., Licznerski, P., et al. (2012). Decreased expression of synapse-related genes and loss of synapses in major depressive disorder. *Nat. Med.* 18, 1413–1417. doi: 10.1038/nm.2886

Kasai, H., Matsuzaki, M., Noguchi, J., Yasumatsu, N., and Nakahara, H. (2003). Structure-stability-function relationships of dendritic spines. *Trends Neurosci.* 26, 360–368. doi: 10.1016/S0166-2236(03)00162-0

Kaufman, L., Ayub, M., and Vincent, J. B. (2010). The genetic basis of non-syndromic intellectual disability: a review. *J. Neurodev. Disord.* 2, 182–209. doi: 10.1007/s11689-010-9055-2

Keck, T., Mrsic-Flogel, T. D., Afonso, M. V., Eysel, U. T., Bonhoeffer, T., and Hübener, M. (2008). Massive restructuring of neuronal circuits during functional reorganization of adult visual cortex. *Nat. Neurosci.* 11, 1162–1167. doi: 10.1038/nn.2181

Keller-Peck, C. R., Walsh, M. K., Gan, W., Feng, G., Sanes, J. R., and Lichtman, J. W. (2001). Asynchronous synapse elimination in neonatal motor units: studies using GFP transgenic mice. *Neuron* 31, 381–394. doi: 10.1016/S0896-6273(01)00383-X

Kim, H., Kunz, P. A., Mooney, R., Philpot, B. D., and Smith, S. L. (2016). Maternal loss of ube3a impairs experience-driven dendritic spine maintenance in the developing visual cortex. *J. Neurosci.* 36, 4888–4894. doi: 10.1523/JNEUROSCI.4204-15.2016

Kim, J. J., and Jung, M. W. (2006). Neural circuits and mechanisms involved in pavlovian fear conditioning: a critical review. *Neurosci. Biobehav. Rev.* 30, 188–202. doi: 10.1016/j.neubiorev.2005.06.005

Kind, P. C., Mitchell, D. E., Ahmed, B., Blakemore, C., Bonhoeffer, T., and Sengpiel, F. (2002). Correlated binocular activity guides recovery from monocular deprivation. *Nature* 416, 430–433. doi: 10.1038/416430a

Konopaske, G. T., Lange, N., Coyle, J. T., and Benes, F. M. (2014). Prefrontal cortical dendritic spine pathology in schizophrenia and bipolar disorder. *JAMA Psychiatry* 71, 1323–1331. doi: 10.1001/jamapsychiatry.2014.1582

Kuhlman, S. J., and Huang, Z. J. (2008). High-resolution labeling and functional manipulation of specific neuron types in mouse brain by cre-activated viral gene expression. *PLoS One* 3:e2005. doi: 10.1371/journal.pone.0002005

Kwon, H., and Sabatini, B. L. (2011). Glutamate induces de novo growth of functional spines in developing cortex. *Nature* 474, 100–104. doi: 10.1038/nature09986

Lai, C. S. W., Adler, A., and Gan, W. (2018). Fear extinction reverses dendritic spine formation induced by fear conditioning in the mouse auditory cortex. *Proc. Natl. Acad. Sci. U S A* 115, 9306–9311. doi: 10.1073/pnas.1801504115

Lai, C. S. W., Franke, T. F., and Gan, W. (2012). Opposite effects of fear conditioning and extinction on dendritic spine remodelling. *Nature* 483, 87–91. doi: 10.1038/nature10792

Landi, S., Putignano, E., Boggio, E. M., Giustetto, M., Pizzorusso, T., and Ratto, G. M. (2011). The short-time structural plasticity of dendritic spines is altered in a model of rett syndrome. *Sci. Rep.* 1:45. doi: 10.1038/srep00045

Larimore, J. L., Chapleau, C. A., Kudo, S., Theibert, A., Percy, A. K., and Pozzo-Miller, L. (2009). Bdnf overexpression in hippocampal neurons prevents dendritic atrophy caused by rett-associated MECP2 mutations. *Neurobiol. Dis.* 34, 199–211. doi: 10.1016/j.nbd.2008.12.011

Lee, S. R., Escobodo-Lozoya, Y., Szatmari, E. M., and Yasuda, R. (2009). Activation of CaMKII in single dendritic spines during long-term potentiation. *Nature* 485, 299–304. doi: 10.1038/nature07842

Lee, W. C., and Nedivi, E. (2002). Extended plasticity of visual cortex in dark-reared animals may result from prolonged expression of cpg15-like genes. *J. Neurosci.* 22, 1807–1815. doi: 10.1523/JNEUROSCI.22-05-01807.2002

Leslie, J. H., and Nedivi, E. (2011). Activity-regulated genes as mediators of neural circuit plasticity. *Prog. Neurobiol.* 94, 223–237. doi: 10.1016/j.pneurobio.2011.05.002

Li, W., Ma, L., Yang, G., and Gan, W. (2017). REM sleep selectively prunes and maintains new synapses in development and learning. *Nat. Neurosci.* 20, 427–437. doi: 10.1038/nn.4479

Lin, B., Kramár, E. A., Bi, X., Brucher, F. A., Gall, C. M., and Lynch, G. (2005a). Theta stimulation polymerizes actin in dendritic spines of hippocampus. *J. Neurosci.* 25, 2062–2069. doi: 10.1523/JNEUROSCI.4283-04.2005

Lin, C. H., Hansen, S., Wang, Z., Storm, D. R., Trapscott, S. J., and Olson, J. M. (2005b). The dosage of the neuroD2 transcription factor regulates amygdala

development and emotional learning. *Proc. Natl. Acad. Sci. U S A* 102, 14877–14882. doi: 10.1073/pnas.0506785102

Lisman, J., Yasuda, R., and Raghavachari, S. (2012). Mechanisms of CaMKII action in long-term potentiation. *Nat. Rev. Neurosci.* 13, 169–182. doi: 10.1038/nrn3192

Liston, C., and Gan, W. (2011). Glucocorticoids are critical regulators of dendritic spine development and plasticity *in vivo*. *Proc. Natl. Acad. Sci. U S A* 108, 16074–16079. doi: 10.1073/pnas.1110444108

Liston, C., Cichon, J. M., Jeanneteau, F., Jia, Z., Chao, M. V., and Gan, W. (2013). Circadian glucocorticoid oscillations promote learning-dependent synapse formation and maintenance. *Nat. Neurosci.* 16, 698–705. doi: 10.1038/nn.3387

Liu, R., and Aghajanian, G. K. (2008). Stress blunts serotonin- and hypocretin-evoked EPSCs in prefrontal cortex: role of corticosterone-mediated apical dendritic atrophy. *Proc. Natl. Acad. Sci. U S A* 105, 359–364. doi: 10.1073/pnas.0706679105

Loebrich, S., and Nedivi, E. (2009). The function of activity-regulated genes in the nervous system. *Physiol. Rev.* 89, 1079–1103. doi: 10.1152/physrev.00013.2009

Lonze, B. E., and Ginty, D. D. (2002). Function and regulation of CREB family transcription factors in the nervous system. *Neuron* 35, 605–623. doi: 10.1016/s0896-6273(02)00828-0

Lübke, J., and Albus, K. (1989). The postnatal development of layer VI pyramidal neurons in the cat's striate cortex, as visualized by intracellular lucifer yellow injections in aldehyde-fixed tissue. *Brain Res. Dev. Brain Res.* 45, 29–38. doi: 10.1016/0165-3806(89)90004-7

Luikenhuis, S., Giacometti, E., Beard, C. F., and Jaenisch, R. (2004). Expression of MeCP2 in postmitotic neurons rescues rett syndrome in mice. *Proc. Natl. Acad. Sci. U S A* 101, 6033–6038. doi: 10.1073/pnas.0401626101

Lyons, M. R., and West, A. E. (2011). Mechanisms of specificity in neuronal activity-regulated gene transcription. *Prog. Neurobiol.* 94, 259–295. doi: 10.1016/j.pneurobio.2011.05.003

Ma, L., Qiao, Q., Tsai, J., Yang, G., Li, W., and Gan, W. (2015). Experience-dependent plasticity of dendritic spines of L2/3 pyramidal neurons in the mouse cortex. *Dev. Neurobiol.* 76, 277–286. doi: 10.1002/dneu.22313

Mainen, Z. F., Malinow, R., and Svoboda, K. (1999). Synaptic calcium transients in single spines indicate that NMDA receptors are not saturated. *Nature* 399, 151–155. doi: 10.1038/20187

Majewska, A., and Sur, M. (2003). Motility of dendritic spines in visual cortex *in vivo*: changes during the critical period and effects of visual deprivation. *Proc. Natl. Acad. Sci. U S A* 100, 16024–16029. doi: 10.1073/pnas.2636949100

Majewska, A. K., Newton, J. R., and Sur, M. (2006). Remodeling of synaptic structure in sensory cortical areas *in vivo*. *J. Neurosci.* 26, 3021–3029. doi: 10.1523/JNEUROSCI.4454-05.2006

Maret, S., Faraguana, U., Nelson, A. B., Cirelli, C., and Tononi, G. (2011). Sleep and waking modulate spine turnover in the adolescent mouse cortex. *Nat. Neurosci.* 14, 1418–1420. doi: 10.1038/nn.2934

Marín, O. (2016). Developmental timing and critical windows for the treatment of psychiatric disorders. *Nat. Med.* 22, 1229–1238. doi: 10.1038/nm.4225

Markus, E. J., and Petit, T. L. (1987). Neocortical synaptogenesis, aging and behavior: lifespan development in the motor-sensory system of the rat. *Exp. Neurol.* 96, 262–278. doi: 10.1016/0014-4886(87)90045-8

Martin, K. C., and Kosik, K. S. (2002). Synaptic tagging—who's it? *Nat. Rev. Neurosci.* 3, 813–820. doi: 10.1038/nrn942

Martin, K. C., Casadio, A., Zhu, H., Yaping, E., Rose, J. C., Chen, M., et al. (1997). Synapse-specific, long-term facilitation of aplysia sensory to motor synapses: a function for local protein synthesis in memory storage. *Cell* 91, 927–938. doi: 10.1016/s0092-8674(00)80484-5

Mathieson, I., Munafò, M. R., and Flint, J. (2011). Meta-analysis indicates that common variants at the DISC1 Locus are not associated with schizophrenia. *Mol. Psychiatry* 17, 634–641. doi: 10.1038/mp.2011.41

Matsuzaki, M., Honkura, N., Ellis-Davies, G. C. R., and Kasai, H. (2004). Structural basis of long-term potentiation in single dendritic spines. *Nature* 429, 761–766. doi: 10.1038/nature02617

Matus, A. (2000). Actin-based plasticity in dendritic spines. *Science* 290, 754–758. doi: 10.1126/science.290.5492.754

Mei, Y., Monteiro, P., Zhou, Y., Kim, J. A., Gao, X., Fu, Z., et al. (2016). Adult restoration of shank3 expression rescues selective autistic-like phenotypes. *Nature* 530, 481–484. doi: 10.1038/nature16971

Mikuni, T., Nishiyama, J., Sun, Y., Kamasawa, N., and Yasuda, R. (2016). High-throughput, high-resolution mapping of protein localization in mammalian brain by *in vivo* genome editing. *Cell* 165, 1803–1817. doi: 10.1016/j.cell.2016.04.044

Mizoguchi, K., Yuzurihara, M., Ishige, A., Sasaki, H., and Tabira, T. (2002). Chronic stress impairs rotarod performance in rats: implications for depressive state. *Pharmacol. Biochem. Behav.* 71, 79–84. doi: 10.1016/S0091-3057(01)00636-0

Moda-Sava, R. N., Murdock, M. H., Parekh, P. K., Fetcho, R. N., Huang, B. S., Huynh, T. N., et al. (2019). Sustained rescue of prefrontal circuit dysfunction by antidepressant-induced spine formation. *Science* 364:eaat8078. doi: 10.1126/science.aat8078

Moretti, P., Levenson, J. M., Battaglia, F., Atkinson, R., Teague, R., Antalffy, B., et al. (2006). Learning and memory and synaptic plasticity are impaired in a mouse model of rett syndrome. *J. Neurosci.* 26, 319–327. doi: 10.1523/JNEUROSCI.2623-05.2006

Moutin, E., Nikonenko, I., Stefanelli, T., Wirth, A., Ponimaskin, E., De Roo, M., et al. (2017). Palmitoylation of cdc42 promotes spine stabilization and rescues spine density deficit in a mouse model of 22q11.2 deletion syndrome. *Cereb. Cortex* 27, 3618–3629. doi: 10.1093/cercor/bhw183

Mower, A. F., Kwok, S., Yu, H., Majewska, A. K., Okamoto, K., Hayashi, Y., et al. (2011). Experience-dependent regulation of CaMKII activity within single visual cortex synapses *in vivo*. *Proc. Natl. Acad. Sci. U S A* 108, 21241–21246. doi: 10.1073/pnas.1108261109

Murakoshi, H., Wang, H., and Yasuda, R. (2011). Local, persistent activation of rho gtpases during plasticity of single dendritic spines. *Nature* 472, 100–104. doi: 10.1038/nature09823

Murrough, J., Iosifescu, D. V., Chang, L. C., Al Jurdi, R. K., Green, C. E., Perez, A. M., et al. (2013). Antidepressant efficacy of ketamine in treatment-resistant major depression: a two-site randomized controlled trial. *Am. J. Psychiatry* 170, 1134–1142. doi: 10.1176/appi.ajp.2013.13030392

Myers, K. M., and Davis, M. (2007). Mechanisms of fear extinction. *Mol. Psychiatry* 12, 120–150. doi: 10.1038/sj.mp.4001939

Nagaoka, A., Takehara, H., Hayashi-Takagi, A., Noguchi, J., Ishii, K., Shirai, F., et al. (2016). Abnormal intrinsic dynamics of dendritic spines in a fragile X syndrome mouse model *in vivo*. *Sci. Rep.* 6:26651. doi: 10.1038/srep26651

Nan, X., Campoy, F. J., and Bird, A. (1997). MeCP2 is a transcriptional repressor with abundant binding sites in genomic chromatin. *Cell* 88, 471–481. doi: 10.1016/s0092-8674(00)81887-5

Nedivi, E., Fieldust, S., Theill, L. E., and Hevron, D. (1996). A set of genes expressed in response to light in the adult cerebral cortex and regulated during development. *Proc. Natl. Acad. Sci. U S A* 93, 2048–2053. doi: 10.1073/pnas.93.5.2048

Negishi, M. and Katoh, H. (2005). Rho family GTPases and dendritic plasticity. *Neuroscientist* 11, 187–191. doi: 10.1177/1073858404268768

Nimchinsky, E. A., Oberlander, A. M., and Svoboda, K. (2001). Abnormal development of dendritic spines in FMR1 knock-out mice. *J. Neurosci.* 21, 5139–5146. doi: 10.1523/JNEUROSCI.21-14-05139.2001

Nishiyama, J. (2019). Plasticity of dendritic spines: molecular function and dysfunction in neurodevelopmental disorders. *Psychiatry Clin. Neuros.* 73, 541–550. doi: 10.1111/pcn.12899

Nishiyama, J., and Yasuda, R. (2015). Biochemical computation for spine structural plasticity. *Neuron* 87, 63–75. doi: 10.1016/j.neuron.2015.05.043

Nishiyama, J., Mikuni, T., and Yasuda, R. (2017). Virus-Mediated genome editing *via* homology-directed repair in mitotic and postmitotic cells in mammalian brain. *Neuron* 96, 755.e5–768.e5. doi: 10.1016/j.neuron.2017.10.004

Norman, C., Runswick, M., Pollock, R., and Treisman, R. (1988). Isolation and properties of cDNA clones encoding SRF, a transcription factor that binds to the c-fos serum response element. *Cell* 55, 989–1003. doi: 10.1016/0092-8674(88)90244-9

Oh, W. C., Lutzu, S., Castillo, P. E., and Kwon, H.-B. (2016). De novo synaptogenesis induced by GABA in the developing mouse cortex. *Science* 353, 1037–1040. doi: 10.1126/science.aaf5206

Okamoto, K., Nagai, T., Miyawaki, A., and Hayashi, Y. (2004). Rapid and persistent modulation of actin dynamics regulates postsynaptic reorganization underlying bidirectional plasticity. *Nat. Neurosci.* 7, 1104–1112. doi: 10.1038/nn1311

Okuno, H., Akashi, K., Ishii, Y., Yagishita-Kyo, N., Suzuki, K., Nonaka, M., et al. (2012). Inverse Synaptic tagging of inactive synapses *via* dynamic interaction of Arc/Arg3.1 with CaMKIIβ. *Cell* 149, 886–898. doi: 10.1016/j.cell.2012.02.062

Opazo, P., Labrecque, S., Tigaret, C. M., Frouin, A., Wiseman, P. W., De Koninck, P., et al. (2010). CaMKII triggers the diffusional trapping of surface AMPARs through phosphorylation of stargazin. *Neuron* 67, 239–252. doi: 10.1016/j.neuron.2010.06.007

Ouzounov, D. G., Wang, T., Wang, M., Feng, D. D., Horton, N. G., Cruz-Hernández, J. C., et al. (2017). *In vivo* three-photon imaging of activity of GCaMP6-labeled neurons deep in intact mouse brain. *Nat. Methods* 14, 388–390. doi: 10.1038/nmeth.4183

Padmashri, R., Reiner, B. C., Suresh, A., Spartz, E., and Dunaevsky, A. (2013). Altered structural and functional synaptic plasticity with motor skill learning in a mouse model of fragile X syndrome. *J. Neurosci.* 33, 19715–19723. doi: 10.1523/JNEUROSCI.2514-13.2013

Pagès, S., Cane, M., Randall, J., Capello, L., and Holtmaat, A. (2015). Single cell electroporation for longitudinal imaging of synaptic structure and function in the adult mouse neocortex *in vivo*. *Front. Neuroanat.* 9:36. doi: 10.3389/fnana.2015.00036

Pan, F., Aldridge, G. M., Greenough, W. T., and Gan, W. (2010). Dendritic spine instability and insensitivity to modulation by sensory experience in a mouse model of fragile X syndrome. *Proc. Natl. Acad. Sci. U S A* 107, 17768–17773. doi: 10.1073/pnas.1012496107

Patel, D., Anilkumar, S., Chattarji, S., and Buwalda, B. (2018). Repeated social stress leads to contrasting patterns of structural plasticity in the amygdala and hippocampus. *Behav. Brain Res.* 347, 314–324. doi: 10.1016/j.bbr.2018.03.034

Peters, A., and Kaiserman-Abramof, I. R. (1970). The small pyramidal neuron of the rat cerebral cortex. The perikaryon, dendrites and spines. *Am. J. Anat.* 127, 321–355. doi: 10.1002/aja.1001270402

Pfeiffer, T., Poll, S., Bancelin, S., Angibaud, J., Krishna Inavalli, V. V. G., Keppler, K., et al. (2018). Chronic 2P-STED imaging reveals high turnover of dendritic spines in the hippocampus *in vivo*. *Elife* 7:e34700. doi: 10.7554/eLife.34700

Phillips, R. G., and LeDoux, J. E. (1992). Differential contribution of amygdala and hippocampus to cued and contextual fear conditioning. *Behav. Neurosci.* 106, 274–285. doi: 10.1037//0735-7044.106.2.274

Pignataro, A., Middei, S., Borreca, A., and Ammassari-Teule, M. (2013). Indistinguishable pattern of amygdala and hippocampus rewiring following tone or contextual fear conditioning in C57BL/6 mice. *Front. Behav. Neurosci.* 7:156. doi: 10.3389/fnbeh.2013.00156

Pinho, J., Marcut, C., and Fonseca, R. (2020). Actin remodeling, the synaptic tag and the maintenance of synaptic plasticity. *IUBMB Life* 72, 577–589. doi: 10.1002/iub.2261

Poulos, A. M., Mehta, N., Lu, B., Amir, D., Livingston, B., Santarelli, A., et al. (2016). Conditioning- and time-dependent increases in context fear and generalization. *Learn. Mem.* 23, 379–385. doi: 10.1101/lm.041400.115

Prager, E. M., Brielmaier, J., Bergstrom, H. C., McGuire, J., and Johnson, L. R. (2010). Localization of mineralocorticoid receptors at mammalian synapses. *PLoS One* 5:e14344. doi: 10.1371/journal.pone.0014344

Purpura, D. P. (1974). Dendritic spine "dysgenesis" and mental retardation. *Science* 186, 1126–1128. doi: 10.1126/science.186.4169.1126

Qiao, Q., Ma, L., Li, W., Tsai, J., Yang, G., and Gan, W. (2016). Long-term stability of axonal boutons in the mouse barrel cortex. *Dev. Neurobiol.* 76, 252–261. doi: 10.1002/dneu.22311

Quinn, J. J., Ma, Q. D., Tinsley, M. R., Koch, C., and Fanselow, M. S. (2008). Inverse Temporal Contributions of the Dorsal Hippocampus and Medial Prefrontal cortex to the expression of long-term fear memories. *Learn. Mem.* 15, 368–372. doi: 10.1101/lm.813608

Radley, J. J., Rocher, A. B., Miller, M., Janssen, W. G. M., Liston, C., Hof, P. R., et al. (2006). Repeated stress induces dendritic spine loss in the rat medial prefrontal cortex. *Cereb. Cortex* 16, 313–320. doi: 10.1093/cercor/bhi104

Rakic, P., Bourgeois, J. P., Eckenhoff, M. F., Zecevic, N., and Goldman-Rakig, P. S. (1986). Concurrent overproduction of synapses in diverse regions of the primate cerebral cortex. *Science* 232, 232–235. doi: 10.1126/science.3952506

Rapin, I. (1997). Autism. *N. Engl. J. Med.* 337, 97–104. doi: 10.1056/NEJM199707103370206

Redondo, R. L., and Morris, R. G. M. (2011). Making memories last: the synaptic tagging and capture hypothesis. *Nat. Rev. Neurosci.* 12, 17–30. doi: 10.1038/nrn2963

Reinés, A., Cereseto, M., Ferrero, A., Sifonios, L., Podestá, M. F., and Wikinski, S. (2008). Maintenance treatment with fluoxetine is necessary to sustain normal levels of synaptic markers in an experimental model of depression: correlation with behavioral response. *Neuropsychopharmacology* 33, 1896–1908. doi: 10.1038/sj.npp.1301596

Roth, R. H., Cudmore, R. H., Tan, H. L., Hong, I., Zhang, Y., and Huganir, R. L. (2020). Cortical synaptic AMPA receptor plasticity during motor learning. *Neuron* 105, 895.e5–908.e5. doi: 10.1016/j.neuron.2019.12.005

Runge, K., Mathieu, R., Bugeon, S., Lafi, S., Beurrier, C., Sahu, S., et al. (2020). Disruption of the transcription factor NEUROD2 causes an autism syndrome *via* cell-autonomous defects in cortical projection neurons. *BioRxiv*, 296889. doi: 10.1101/296889

Sala, C., and Segal, M. (2014). Dendritic spines: the locus of structural and functional plasticity. *Physiol. Rev.* 94, 141–188. doi: 10.1152/physrev.00012.2013

Sarrieau, A., Vial, M., Philibert, D., Moguilewsky, M., Dussaillant, M., McEwan, B., et al. (1984). *in vitro* binding of tritiated glucocorticoids directly on unfixed rat brain sections. *J. Steroid Biochem.* 20, 1233–1238. doi: 10.1016/0022-4731(84)90150-x

Schreiner, D., Savas, J. N., Herzog, E., Brose, N., and de Wit, J. (2017). Synapse biology in the "circuit-age"-paths toward molecular connectomics. *Curr. Opin. Neurobiol.* 42, 102–110. doi: 10.1016/j.conb.2016.12.004

Segal, M. (2017). Dendritic spines: morphological building blocks of memory. *Neurobiol. Learn. Mem.* 138, 3–9. doi: 10.1016/j.nlm.2016.06.007

Sethna, F., Moon, C., and Wang, H. (2014). From FMRP function to potential therapies for fragile X syndrome. *Neurochem. Res.* 39, 1016–1031. doi: 10.1007/s11064-013-1229-3

Shatz, C. J., and Stryker, M. P. (1978). Ocular dominance in layer IV of the cat's visual cortex and the effects of monocular deprivation. *J. Physiol.* 281, 267–283. doi: 10.1113/jphysiol.1978.sp012421

Sidorov, M. S., Auerbach, B. D., and Bear, M. F. (2013). Fragile X mental retardation protein and synaptic plasticity. *Mol. Brain* 6:15. doi: 10.1186/1756-6606-6-15

Simonoff, E., Pickles, A., Charman, T., Chandler, S., Loucas, T., and Baird, G. (2008). Psychiatric disorders in children with autism spectrum disorders: prevalence, comorbidity and associated factors in a population-derived sample. *J. Am. Acad. Child Adolesc. Psychiatry* 47, 921–929. doi: 10.1097/CHI.0b013e318179964f

Sobczyk, A., and Svoboda, K. (2007). Activity-dependent plasticity of the NMDA-receptor fractional Ca2+ current. *Neuron* 53, 17–24. doi: 10.1016/j.neuron.2006.11.016

Squarcione, C., Torti, M. C., Fabio, F. D., and Biondi, M. (2013). 22q11 deletion syndrome: a review of the neuropsychiatric features and their neurobiological basis. *Neuropsychiatr. Dis. Treat.* 9, 1873–1884. doi: 10.2147/NDT.S52188

St Clair, D., Blackwood, D., Mior, W., Carothers, A., Walker, M., Spowart, G., et al. (1990). Association within a family of a balanced autosomal translocation with major mental illness. *Lancet* 336, 13–16. doi: 10.1016/0140-6736(90)91520-k

Stein, I. S., and Zito, K. (2019). Dendritic spine elimination: molecular mechanisms and implications. *Neuroscientist* 25, 27–47. doi: 10.1177/1073858418769644

Stressman, H. A., Xiong, B., Coe, B. P., Wang, T., Hoekzema, K., Fenckova, M., et al. (2017). Targeted sequencing identifies 91 neurodevelopmental-disorder risk genes with autism and developmental-disability biases. *Nat. Genet.* 49, 515–526. doi: 10.1038/ng.3792

Subramanian, J., Michel, K., Benoit, M., and Nedivi, E. (2019). CPG15/neuritin mimics experience in selecting excitatory synapses for stabilization by facilitating PSD95 recruitment. *Cell Rep.* 28, 1584.e5–1595.e5. doi: 10.1016/j.celrep.2019.07.012

Sullivan, P. F., Kendler, K. S., and Neale, M. C. (2003). Schizophrenia as a complex trait. *Arch. Gen. Psychiatry* 60, 1187–1192. doi: 10.1001/archpsyc.60.12.1187

Suzuki, K., Tsunekawa, Y., Hernandez-Benitez, R., Wu, J., Zhu, J., Kim, E. J., et al. (2016). *In vivo* genome editing *via* CRISPR/Cas9 mediated homology-independent targeted integration. *Nature* 540, 144–149. doi: 10.1038/nature20565

Sweet, R. A., Henteleff, R. A., Zhang, W., Sampson, A. R., and Lewis, D. A. (2009). Reduced dendritic spine density in auditory cortex of subjects with schizophrenia. *Neuropsychopharmacology* 34, 374–389. doi: 10.1038/npp.2008.67

Sztainberg, Y., and Zoghbi, H. Y. (2016). Lessons learned from studying syndromic autism spectrum disorders. *Nat. Neurosci.* 19, 1408–1417. doi: 10.1038/nn.4420

Tashiro, A., Minden, A., and Yuste, R. (2000). Regulation of dendritic spine morphology by the rho family of small GTPases: antagonistic roles of rac and rho. *Cereb. Cortex* 10, 927–938. doi: 10.1093/cercor/10.10.927

Till, S. M., Wijetunge, L. S., Seidel, V. G., Harlow, E., Wright, A. K., Bagni, C., et al. (2012). Altered maturation of the primary somatosensory cortex in a mouse model of fragile X syndrome. *Hum. Mol. Genet.* 21, 2143–2156. doi: 10.1093/hmg/dds030

Tjia, M., Yu, X., Jammu, L. S., Lu, J., and Zuo, Y. (2017). Pyramidal neurons in different cortical layers exhibit distinct dynamics and plasticity of apical dendritic spines. *Front. Neural Circuits* 11:43. doi: 10.3389/fncir.2017.00043

Tomita, S., Stein, V., Stocker, T. J., Nicoll, R. A., and Bredt, D. S. (2005). Bidirectional synaptic plasticity regulated by phosphorylation of stargazin-like TARPs. *Neuron* 45, 269–277. doi: 10.1016/j.neuron.2005.01.009

Tønnesen, J., Katona, G., Rózsa, B., and Nägerl, U. V. (2014). Spine neck plasticity regulates compartmentalization of synapses. *Nat. Neurosci.* 17, 678–685. doi: 10.1038/nn.3682

Trachtenberg, J. T., Chen, B., Knott, G. W., Feng, G., Sanes, J. R., Welker, E., et al. (2002). Long-term *in vivo* imaging of experience-dependent synaptic plasticity in adult cortex. *Nature* 420, 788–794. doi: 10.1038/nature01273

Van Bommel, B., and Mikhaylova, M. (2016). Talking to the neighbours: the molecular and physiological mechanisms of clustered synaptic plasticity. *Neurosci. Biobehav. Rev.* 71, 352–361. doi: 10.1016/j.neubiorev.2016.09.016

Van Weert, L. T. C. M., Buurstede, J. C., Mahfouz, A., Braakhuis, P. S. M., Polman, J. A. E., Sips, H. C. M., et al. (2017). NeuroD factors discriminate mineralocorticoid from glucocorticoid receptor DNA binding in the male rat brain. *Endocrinology* 158, 1511–1522. doi: 10.1210/en.2016-1422

Van Weert, L. T. C. M., Buurstede, J. C., Sips, H. C. M., Mol, I. M., Puri, T., Damsteegt, R., et al. (2019). Mechanistic insights in NeuroD potentiation of mineralocorticoid receptor signaling. *Int. J. Mol. Sci.* 20:1575. doi: 10.3390/ijms20071575

Vatsa, N., and Jana, N. R. (2018). UBE3A and Its Link With Autism. *Front. Mol. Neurosci.* 11:448. doi: 10.3389/fnmol.2018.00448

Vetere, G., Restivo, L., Novembre, G., Aceti, M., Lumaca, M., and Ammassari-Teule, M. (2011). Extinction partially reverts structural changes associated with remote fear memory. *Learn. Mem.* 18, 554–557. doi: 10.1101/lm.2246711

Villa, K. L., Berry, K. P., Subramanian, J., Cha, J. W., Oh, W., Kwon, H., et al. (2016). Inhibitory synapses are repeatedly assembled and removed at persistent sites *in vivo*. *Neuron* 89, 756–769. doi: 10.1016/j.neuron.2016.01.010

Waung, M. W., Pfeiffer, B. E., Nosyreva, E. D., Ronesi, J. A., and Huber, K. M. (2008). Rapid translation of Arc/Arg3.1 selectively mediates mGluR-dependent LTD through persistent increases in AMPAR endocytosis rate. *Neuron* 59, 84–97. doi: 10.1016/j.neuron.2008.05.014

Weikum, E. R., Knuesel, M. T., Ortlund, E. A., and Yamamoto, K. R. (2017). Glucocorticoid receptor control of transcription: precision and plasticity *via* allostery. *Nat. Rev. Mol. Cell Biol.* 18, 159–174. doi: 10.1038/nrm.2016.152

Wijetunge, L. S., Angibaud, J., Frick, A., Kind, P. C., and Nägerl, U. V. (2014). Stimulated emission depletion (STED) microscopy reveals nanoscale defects in the developmental trajectory of dendritic spine morphogenesis in a mouse model of fragile X syndrome. *J. Neurosci.* 34, 6405–6412. doi: 10.1523/JNEUROSCI.5302-13.2014

Willner, P., Muscat, R., and Papp, M. (1992). Chronic mild stress-induced anhedonia: a realistic animal model of depression. *Neurosci. Biobehav. Rev.* 16, 525–534. doi: 10.1016/S0149-7634(05)80194-0

Xu, B., Hsu, P. K., Stark, K. L., Karayiorgou, M., and Gogos, J. A. (2013). Derepression of a neuronal inhibitor due to miRNA dysregulation in a schizophrenia-related microdeletion. *Cell* 152, 262–275. doi: 10.1016/j.cell.2012.11.052

Xu, H. T., Pan, F., Yang, G., and Gan, W. (2007). Choice of cranial window type for *in vivo* imaging affects dendritic spine turnover in the cortex. *Nat. Neurosci.* 10, 549–551. doi: 10.1038/nn1883

Xu, T., Yu, X., Perlik, A. J., Tobin, W. F., Zweig, J. A., Tennant, K., et al. (2009). Rapid formation and selective stabilization of synapses for enduring motor memories. *Nature* 462, 915–919. doi: 10.1038/nature08389

Yagishita, S., Hayashi-Takagi, A., Ellies-Davies, G. C. R., Urakubo, H., Ishii, S., and Kasai, H. (2014). A critical time window for dopamine actions on the structural plasticity of dendritic spines. *Science* 345, 1616–1620. doi: 10.1126/science.1255514

Yang, G., Lai, C. S. W., Cichon, J., Ma, L., Li, W., and Gan, W. (2014). Sleep promotes branch-specific formation of dendritic spines after learning. *Science* 344, 1173–1178. doi: 10.1126/science.1249098

Yang, G., Pan, F., and Gan, W. (2009). Stably maintained dendritic spines are associated with lifelong memories. *Nature* 462, 920–924. doi: 10.1038/nature08577

Yang, G., Pan, F., Parkhurst, C. N., Grutzendler, J., and Gan, W. (2010). Thinned-skull cranial window technique for long-term imaging of the cortex in live mice. *Nat. Protoc.* 5, 201–208. doi: 10.1038/nprot.2009.222

Yang, Y., Liu, D., Huang, W., Deng, J., Dun, Y., Zuo, Y., et al. (2016). Selective synaptic remodeling of amygdalacortical connections associated with fear memory. *Nat. Neurosci.* 19, 1348–1355. doi: 10.1038/nn.4370

Yap, E. L., and Greenberg, M. E. (2018). Activity-regulated transcription: bridging the gap between neural activity and behavior. *Neuron* 100, 330–348. doi: 10.1016/j.neuron.2018.10.013

Yashiro, K., Riday, T. T., Condon, K. H., Roberts, A. C., Bernardo, D. R., Prakash, R., et al. (2009). Ube3a is required for experience-dependent maturation of the neocortex. *Nat. Neurosci.* 12, 777–783. doi: 10.1038/nn.2327

Zhai, S., Ark, E. D., Parra-Bueno, P., and Yasuda, R. (2013). Long-distance integration of nuclear erk signaling triggered by activation of a few dendritic spines. *Science* 342, 1107–1111. doi: 10.1126/science.1245622

Zhang, Y., Cudmore, R. H., Lin, D. T., Linden, D. J., and Huganir, R. L. (2015). Visualization of NMDA receptor-dependent AMPA receptor synaptic plasticity *in vivo*. *Nat. Neurosci.* 18, 402–407. doi: 10.1038/nn.3936

Zhou, Y., Lai, B., and Gan, W. (2017). Monocular deprivation induces dendritic spine elimination in the developing mouse visual cortex. *Sci. Rep.* 7:4977. doi: 10.1038/s41598-017-05337-6

Ziv, N. E., and Smith, S. J. (1996). Evidence for a role of dendritic filopodia in synaptogenesis and spine formation. *Neuron* 17, 91–102. doi: 10.1016/S0896-6273(00)80283-4

Zuo, Y., Yang, G., Kwon, E., and Gan, W. (2005a). Long-term sensory deprivation prevents dendritic spine loss in primary somatosensory cortex. *Nature* 436, 261–265. doi: 10.1038/nature03715

Zuo, Y., Lin, A., Chang, P., and Gan, W. (2005b). Development of long-term dendritic spine stability in diverse regions of cerebral cortex. *Neuron* 46, 181–189. doi: 10.1016/j.neuron.2005.04.001

Conflict of Interest: The authors declare that the research was conducted in the absence of any commercial or financial relationships that could be construed as a potential conflict of interest.

frontiers in Synaptic Neuroscience

ORIGINAL RESEARCH
published: 04 September 2020
doi: 10.3389/fnsyn.2020.00038

Paternal Deprivation and Female Biparental Family Rearing Induce Dendritic and Synaptic Changes in *Octodon degus*: I. Medial Prefrontal Cortex

Tony de Schultz[1], *Joerg Bock*[2,3] *and Katharina Braun*[1,3]*

[1]Department of Zoology, Developmental Neurobiology, Institute of Biology, Otto von Guericke University Magdeburg, Magdeburg, Germany, [2]PG "Epigenetics and Structural Plasticity," Institute of Biology, Otto von Guericke, University Magdeburg, Magdeburg, Germany, [3]Center for Behavioral Brain Sciences, Magdeburg, Germany

In most mammalian species parent-offspring interactions during early life periods primarily comprise social contacts with the mother, whereas the role of males in parental care is one of the most overlooked and understudied topics. The present study addressed the hypothesis that the complete deprivation of paternal care delays or permanently retards synaptic connectivity in the brain, particularly in the medial prefrontal cortex (mPFC) of the offspring in a sex-specific manner. Another aim of this study was to address the question whether and in which way replacing the father with a female caregiver (in our experiments the "aunt") can "buffer" the detrimental effects of paternal deprivation on neuronal development. The comparison of: (a) single mother rearing; (b) biparental rearing by father and mother; and (c) biparental rearing by two female caregivers revealed that: (i) paternal care represents a critical environmental factor for synaptic and dendritic development of pyramidal neurons in the vmPFC of their offspring; (ii) a second female caregiver ("aunt") does not "buffer" the neuronal consequences of paternal deprivation; and that (iii) neuronal development in the vmPFC is differentially affected in male and female offspring in response to different family constellations.

Keywords: dendritic spines, prefrontal cortex, paternal deprivation, family structure, sex difference, pyramidal neuron

OPEN ACCESS

Edited by:
Menahem Segal,
Weizmann Institute of Science, Israel

Reviewed by:
Atsuo Fukuda,
Hamamatsu University School of Medicine, Japan
Raphael Lamprecht,
University of Haifa, Israel

***Correspondence:**
Katharina Braun
katharina.braun@ovgu.de

Received: *22 January 2020*
Accepted: *31 July 2020*
Published: *04 September 2020*

Citation:
de Schultz T, Bock J and Braun K (2020) Paternal Deprivation and Female Biparental Family Rearing Induce Dendritic and Synaptic Changes in Octodon degus: I. Medial Prefrontal Cortex. Front. Synaptic Neurosci. 12:38. doi: 10.3389/fnsyn.2020.00038

INTRODUCTION

The vast majority of studies emphasize the important role of the mother in supporting infant growth and survival and facilitating cognitive as well social-emotional development (Meaney, 2001; Zhang et al., 2013; Bock et al., 2014; Maccari et al., 2014; Glynn and Baram, 2019). In contrast, the father's contribution to infant development has been less studied. This is surprising since in humans as well as in several other bi-parental mammalian species the father represents a major source of emotional and social interactions (Feldman et al., 2019). Recent studies comparing maternal and paternal behavior in humans showed that fathers provide the same level of sensitivity as mothers during interactions with their children and make a unique contribution to the child's social development and emotion regulation, particularly to the child's later capacity to function adaptively within the social milieu (Feldman, 2016; Kohl et al., 2017, 2018; Abraham and Feldman, 2018). Absence of a paternal caregiver influences the socialization and increases the probability of drug and

alcohol abuse, mental illness, poor educational performance and criminal activity of affected children (Franz et al., 1999; Baskerville, 2002; O'Neill, 2002; Erhard and Janig, 2003; Kindler and Grossmann, 2004; Garfield and Isacco, 2006). Also, a variety of clinical studies provide evidence that adolescents living in single-mother homes develop higher levels of delinquency than those raised in dual-parent households (Juby and Farrington, 2001; Demuth and Brown, 2004) and are at greater risk for incarceration (Harper and McLanahan, 2004).

So far there are no systematic analyses of brain functional changes in father-deprived children, which underlines the importance of research in animal models, which—besides, to use functional imaging techniques—also allow to "zoom in" to the microscopic and molecular/epigenetic level to study the impact of paternal care on neuronal and synaptic development. An increasing number of experimental approaches in various biparental rodent species revealed the important role of fathers and bi-parental care in shaping functional neuronal networks in the brain and the associated socioemotional development of their offspring (Braun and Champagne, 2014; Bales and Saltzman, 2016; Saltzman et al., 2017; Feldman et al., 2019; Pohl et al., 2019). These studies compared the developmental trajectories of offspring from biparental and single-mother families, whereas studies investigating possible influences of an additional (male or female) caregiver are rare.

We have introduced the trumpet-tailed rat *Octodon degus* as an animal model to study developmental processes underlying human psychopathologies in the context of the DOHaD (Developmental Origins of Health and Disease; Hanson and Gluckman, 2014; Heindel et al., 2015). This species is characterized by biparental care that is associated with complex familial structures and an intense social bond between young degus and their parents (Fuchs et al., 2010; Colonnello et al., 2011). Behavioral studies in degus have shown that the father is actively engaged in parent-offspring interactions (Wilson, 1982), including huddling, licking and grooming, and play behavior (Helmeke et al., 2009; Pinkernelle et al., 2009). During the first 3 weeks of life paternal care comprises about 40% of total parent-offspring interactions (Helmeke et al., 2009; Pinkernelle et al., 2009) and it was claimed that degu fathers play a major role as "regulator" of the offspring's behavioral development (Wilson, 1982). Importantly, after the removal of the father single degu mothers do not compensate for the lack of paternal care by intensifying maternal activities (Helmeke et al., 2009), which creates a socio-emotionally deprived environment in fatherless families. Degus share the principal brain anatomy with common laboratory rodents (Wright and Kern, 1992; Kumazawa-Manita et al., 2013, 2018) and they display superior cognitive functions, such as learning to use a tool to retrieve food (Okanoya et al., 2008). Similar to human babies (De Casper and Fifer, 1980; Fifer and Moon, 1994), newborn degus learn to recognize and to respond to their mothers' vocalizations within the first days of life (Poeggel and Braun, 1996; Braun and Scheich, 1997; Braun and Poeggel, 2001), and also similar to humans this vocal communication is important for the establishment and maintenance of the emotional attachment to the parents.

Various experimental studies analyzing the development of sensory and motor systems revealed that the developing brain is "experience-expectant" during circumscribed critical periods and that the establishment and refinement of sensory and emotional brain pathways requires an "enriched" stimulating environment during these life periods (Bryan and Riesen, 1989; Rosenzweig and Bennett, 1996; Bock and Braun, 1999a,b; Poeggel et al., 2003; Markham and Greenough, 2004; Bock et al., 2014). Such an enriched socio-emotional environment is normally provided by an adequate and structured parental care. While biparental care can be envisioned as an "enriched" environment for the offspring, being raised by a single caregiver represents an "impoverished" environment, a family setting which in animal studies can be experimentally applied to assess the impact of paternal care on the development of his offspring. The behavioral pathologies observed in father-deprived individuals likely arise from a socio-emotionally impoverished family setting resulting in functional deficits within specific brain circuits. Indeed, the development and functional maturation of brain regions such as the orbitofrontal cortex (OFC) and the anterior cingulate cortex (ACd) are particularly sensitive towards paternal input as revealed in previous studies (Ovtscharoff et al., 2006; Helmeke et al., 2009; Braun et al., 2011, 2013; Seidel et al., 2011).

One aim of the present study was to address the hypothesis that paternal deprivation delays or permanently retards synaptic connectivity in the brain, particularly in the medial prefrontal cortex (mPFC) of the offspring. Most studies consider paternal absence synonymous with living in a single-parent, non-intact, or mother-headed family, and accordingly, the majority of experimental paternal deprivation studies applied a paradigm in which the father is removed from the family at the birth of his offspring. However, in "real" life an absent father can be replaced by other male or female caregivers, which are integrated into the family setting. Hence, the second aim of this study was to address the question whether the father can be replaced by another female caregiver (in our experiments the "aunt") who may "buffer" the detrimental effects of paternal deprivation on brain development. Since so far, the majority of animal studies have focused on the consequences of paternal deprivation in male offspring, the third aim of this study was to compare the impact of paternal deprivation on neuronal development in male and female siblings.

MATERIALS AND METHODS

Animals

The degus used in this study were bred in our colony at the Institute of Biology, Otto von Guericke University Magdeburg. They were housed in wire cages (l/w/h: 50 cm/42 cm/67 cm) in temperature (22°C) and humidity (55%) controlled rooms under a 12/12 h light/dark cycle. Freshwater and rodent diet pellets were accessible *ad libitum*, vegetables were added occasionally. All experiments were performed following the European Community's Council Directive and according to the German guidelines for the care and use of animals in laboratory research. The experimental protocols were approved by the ethics committee of Saxony-Anhalt.

Experimental Groups

Four weeks after mating a male and female breeding pair the sister of the female (aunt) was introduced to the breeding pair and housed in the same cage. On the day of delivery (postnatal day, PND, 0) the families were assigned to three experimental groups:

Control family (+F group = male and female biparental): after delivery of the pups the aunt was removed from the family, resulting in a bi-parental family in which the pups were raised by the father and mother ($N_{offspring}$ = 7 males, 5 females, each from different families to prevent litter effects). The data presented for this group include a total of 28 neurons for males and a total of 20 neurons for females. The data presented for this group include a total of 28 neurons for males and a total of 20 neurons for females.

Single mother family (−F group = father-deprived): on the day of delivery the father and the aunt were removed from the home cage, resulting in a single-parent family in which the pups were raised by the mother only ($N_{offspring}$ = 6 males, 7 females, each from different families to prevent litter effects). The data presented for this group include a total of 24 neurons for males and a total of 28 neurons for females.

Mother-Aunt family (MA group = female biparental): on the day of delivery the father was removed from the family, resulting in a bi-parental family in which the pups were raised by the mother and her sister (aunt; $N_{offspring}$ = 6 males, 6 females, each from different families to prevent litter effects). The data presented for this group include a total of 24 neurons for males and also a total of 24 neurons for females. All families were group-housed in their home cage until postnatal day 45 (puberty).

Quantitative Neuromorphology

After decapitation, the unfixed brains were impregnated in the Golgi solution for 14 days and embedded in celloidin. One-hundred and fifty micrometre tissue sections were prepared and developed by using a modified Golgi–Cox technique (for methodological details, see Bock et al., 2016). For each hemisphere two pyramidal neurons located in layer II/III of the ventromedial prefrontal cortex (vmPFC) comprising the infralimbic (IL) and prelimbic (PL) cortex were analyzed (**Figure 1A**). The brain region was defined according to the rat brain atlas (Paxinos and Watson, 2004) and the degu brain atlas (Kumazawa-Manita et al., 2018). All neurons were reconstructed at a final magnification of 1,000× using a computer-based neuron tracing system (NEUROLUCIDA®, MicroBright-Field, Williston, VT, USA), which allows the quantitative three-dimensional analysis of complete dendritic trees. For each animal two neurons per hemisphere, that is four neurons per animal, were analyzed. Neurons selected for analysis (representative example in **Figure 1B**) had to fulfill the following criteria: (1) localization within the boundaries of the vmPFC, (2) uniform and complete staining of apical and basal dendritic trees within the 150 μm section, (3) apical dendrites had to branch regularly into a series of bifurcating branches divided into primary, secondary, tertiary, etc. and (4) sufficient distance from neighboring neurons, glia or blood vessels, which could obscure their morphology. All protrusions, thin, stubby, or mushroom type were counted as spines if they were in direct continuity with the dendritic shaft. No attempt was made to correct for hidden spines (Feldman and Peters, 1979), as the use of visible spine counts for comparison between different experimental conditions had been validated previously (Horner and Arbuthnott, 1991). The following parameters for each reconstructed neuron were quantified: (i) dendritic length in μm; (ii) spine frequency representing the number of visible spines per 10 μm dendritic length; (iii) number of visible spines; and (iv) dendritic complexity. All protrusions, thin, stubby, or mushroom type were counted as spines if they were in direct continuity with the dendritic shaft. The length of the dendritic trees was measured by tracing the entire dendrite in three dimensions while counting dendritic spines. Spine frequency was calculated separately for the apical and basal dendrites of each neuron. For a more detailed analysis, three parallel analysis strategies were performed: (1) To assess whether spine changes are confined to specific areas of the dendritic field, the natural branches (segments) of the apical and basal dendritic trees were numbered consecutively (primary, secondary, tertiary, etc.) from proximal to distal (Bock and Braun, 1999a,b; Bock et al., 2016; **Figure 1C**). Spine frequency was calculated: (i) as the average for the complete apical or basal dendrite; and (ii) as the average for the individual branching orders (see above). (2) Since it turned out that the most distal dendritic segments showed the most pronounced differences between the rearing groups we applied an additional analysis: the values for each parameter (dendritic length, spine frequency, spine number) were pooled for the 3rd-5th apical branch order or the 2nd–4th basal branch order, respectively. (3) To obtain more detailed information about changes of dendritic complexity, a three-dimensional version of the Sholl analysis (Sholl, 1953) was performed, in which concentric spheres at 50 μm intervals were placed around the soma and the number of intersections between dendrite and Sholl sphere was calculated (**Figure 1D**). All analyses were conducted by an experimenter who was unaware of the experimental conditions of the animals.

Statistical Analysis

A two-way ANOVA was performed to test for potential differences within the main factors rearing condition (+F, −F, MA) and sex (male, female) and potential interaction of these factors. For a more detailed comparison of the individual experimental groups, a one-way ANOVA for male and female groups was conducted and in case of significance ($p \leq 0.05$) a Student-Newman-Keuls-(SNK-) test *post hoc* tests was applied. The data for each hemisphere were pooled and analyzed separately, resulting in two values per animal. As described above we compared values of dendritic length, spine frequency, and spine number for: (i) complete neurons; and (ii) 3rd–5th order segments for apical dendrites, 2nd–4th order segments for basal dendrites. Also, values for comparison of dendritic complexity were derived from Sholl analysis.

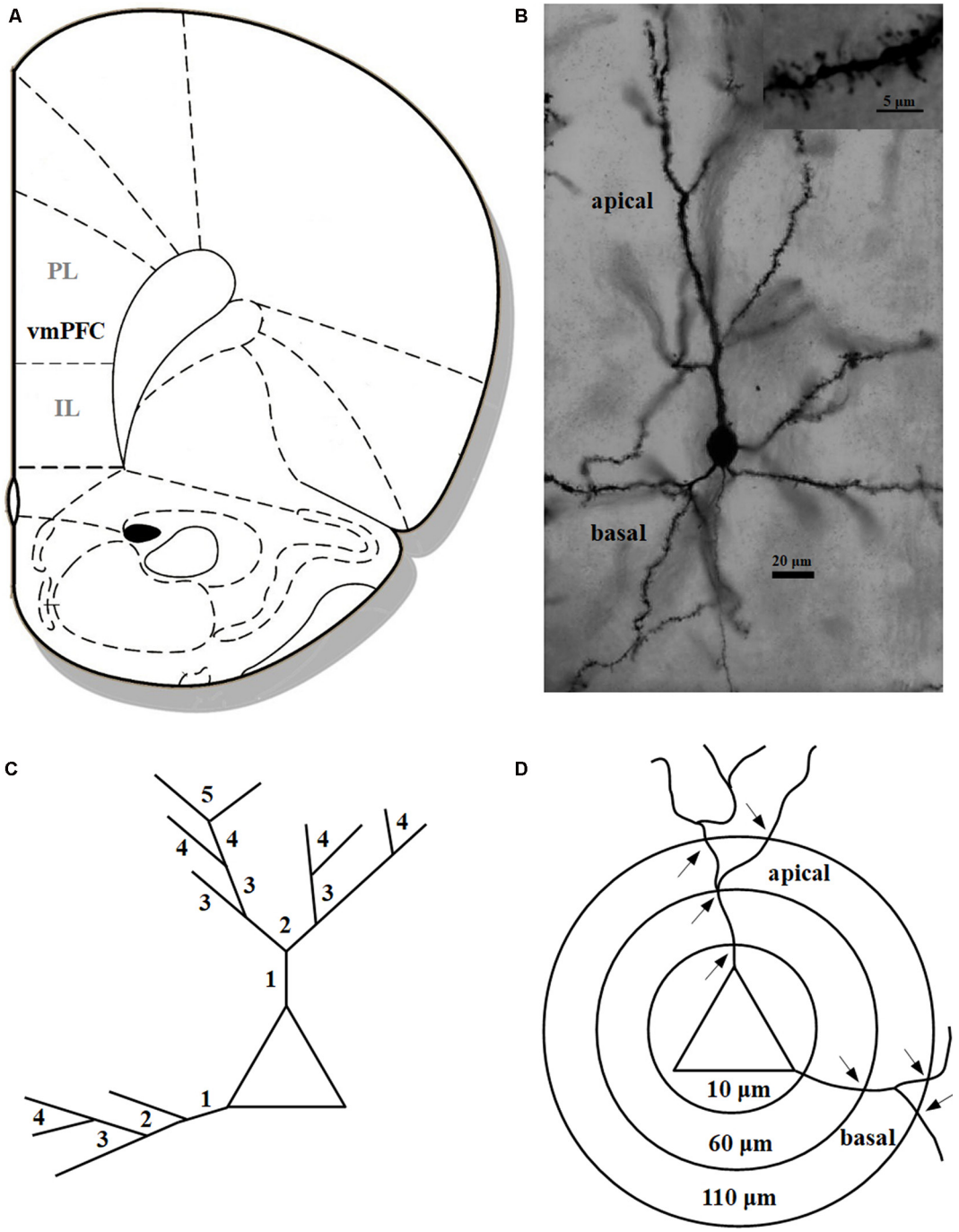

FIGURE 1 | (A) Schematic illustration indicating the vmPFC in the Degu cortex comprising the infralimbic (IL) and prelimbic (PL) cortex (modified after Paxinos and Watson, 2004); **(B)** photomicrograph of a pyramidal neuron in the vmPFC; inset shows a dendritic segment with dendritic spines; **(C)** schematic illustration of dendritic branching with numbers indicating individual branch orders ("natural" dendritic segments); **(D)** schematic illustration of Sholl analysis with concentric spheres around the soma and respective radii in µm; arrows indicate intersections on apical and basal dendrites ("artificial" dendritic segments), respectively, used for the analysis of dendritic complexity.

RESULTS

In the present study, we aimed to analyze if growing up without a male caregiver (single mother family, −F group) may affect neuronal morphology in the vmPFC of periadolescent degu pups when compared to pups from a male and female biparental control family (control group). Moreover, to analyze if differences between these two rearing conditions are specific

for a male caregiver, we introduced an additional biparental group consisting of two female caregivers (mother/aunt family, MA group). Also, we wanted to test for potential differences between male and female offspring. Thus, we first applied a two-way ANOVA to test for differences between the three rearing conditions, between male and female animals and potential interactions between these main factors. Also, a one-way ANOVA with the subsequent *post hoc* test was applied separately for male and female offspring to get a more detailed comparison between the individual rearing conditions.

Rearing-Induced Differences in Spine Frequency, Spine Number, Dendritic Length and Complexity

Two-way ANOVA for factors rearing condition and sex revealed several significant effects or strong tendencies for the factor rearing condition and interaction of rearing condition × sex, no significant effects were detected for factor sex (for details see **Table 1**).

Since two-way ANOVA revealed some evidence for an interaction of rearing conditions × sex (basal spine number and basal dendritic length), we conducted a one-way ANOVA with an SNK posthoc test for males and females separately to test for differences between the individual experimental groups. This analysis revealed that rearing conditions affect neuromorphological parameters and that these effects differ in male and female offspring, as described in detail in the following section.

Male Offspring

Spine frequency: Analysis of vmPFC pyramidal neurons using a one-way ANOVA indicated significant differences in the average spine frequency for the complete basal dendrites between the three treatment groups (p = 0.035). *Post hoc test* revealed a significantly lower spine frequency of offspring from the single mother (−F) group compared to offspring from the biparental (+F) group (p = 0.034, 16% reduced, **Figure 2D**). Similarly, analysis for the pooled values of the 2nd to 4th basal dendritic segments indicated a significant difference between the treatment groups (p = 0.019) and the *post hoc* test revealed a significantly lower spine frequency for the −F group compared to the +F group (p = 0.017, 20% decrease, **Figures 2E,F**) in this basal segments. Also, the *post hoc* test showed a tendency towards a lower basal spine frequency in the mother-aunt (MA) group compared to the offspring of the +F group (p = 0.062, 13% decrease, **Figures 2E,F**). For the apical dendrites, no significant effects in spine frequency were found between the experimental groups (**Figures 2A–C**). Also, no differences neither for spine number (**Figures 2G–L**), dendritic length nor for dendritic complexity were observed in male animals.

Female Offspring

Spine frequency: No significant differences for spine frequency were found between the three rearing conditions neither on basal or on apical dendrites (**Figures 3A–F**).

Spine number: One way ANOVA in female offspring indicated significant differences in the average spine number for the complete basal dendrite between the three treatment groups (p = 0.037). *Post hoc* analysis revealed reduced spine number in female offspring of the MA group compared to −F offspring (p = 0.031, 35% decrease, **Figure 3J**). Similarly, analysis for the pooled values of the 2nd to 4th basal dendritic segments indicated a significant difference between the treatment groups (p = 0.012) and the *post hoc* test revealed a significantly lower spine number for the MA group compared to the +F group (p = 0.015, 36% decrease) as well as for the −F group (p = 0.019, 30% decrease, **Figures 3K,L**). While no significant effects were observed for the complete apical dendrite (**Figure 4A**), significant differences between the experimental groups were also observed for the pooled values of 3rd to 5th dendritic segments of apical dendrites (p = 0.025) and the *post hoc* test revealed a significantly lower number in female animals of the MA group compared to female animals of the +F group (p = 0.026, 26% decrease, **Figure 3G**) as well as of the −F group (p = 0.035, 27% decrease, **Figures 3H,I**).

Dendritic length and complexity: One way ANOVA for total basal dendritic length indicated significant differences between

TABLE 1 | Results of two-way ANOVA for factors rearing, sex, and interaction of rearing condition × sex.

Dendrite	Parameter	Rearing condition	Sex	Rearing condition × sex
apical	spine frequency	0.3	0.67	0.75
	spine number	0.2	0.5	0.3
	dendritic length	0.2	0.2	0.3
	dendritic complexity	*0.074*	0.3	0.28
basal	spine frequency	*0.068*	0.4	0.3
	spine number	*0.058*	0.5	*0.056*
	dendritic length	*0.056*	0.8	*0.069*
	dendritic complexity	**0.05**	0.7	0.27
apical pooled values 3rd–5th segments	spine frequency	0.3	0.5	0.9
	spine number	**0.002**	0.7	0.89
	dendritic length	**0.008**	0.9	0.7
basal pooled values 2nd–4th segments	spine frequency	*0.091*	0.7	0.1
	spine number	**0.026**	0.5	0.2
	dendritic length	0.1	0.2	0.2

Bold numbers with grey background indicate significant differences ($p \leq 0.05$); numbers in italics indicate a trend towards significance ($p < 0.1$).

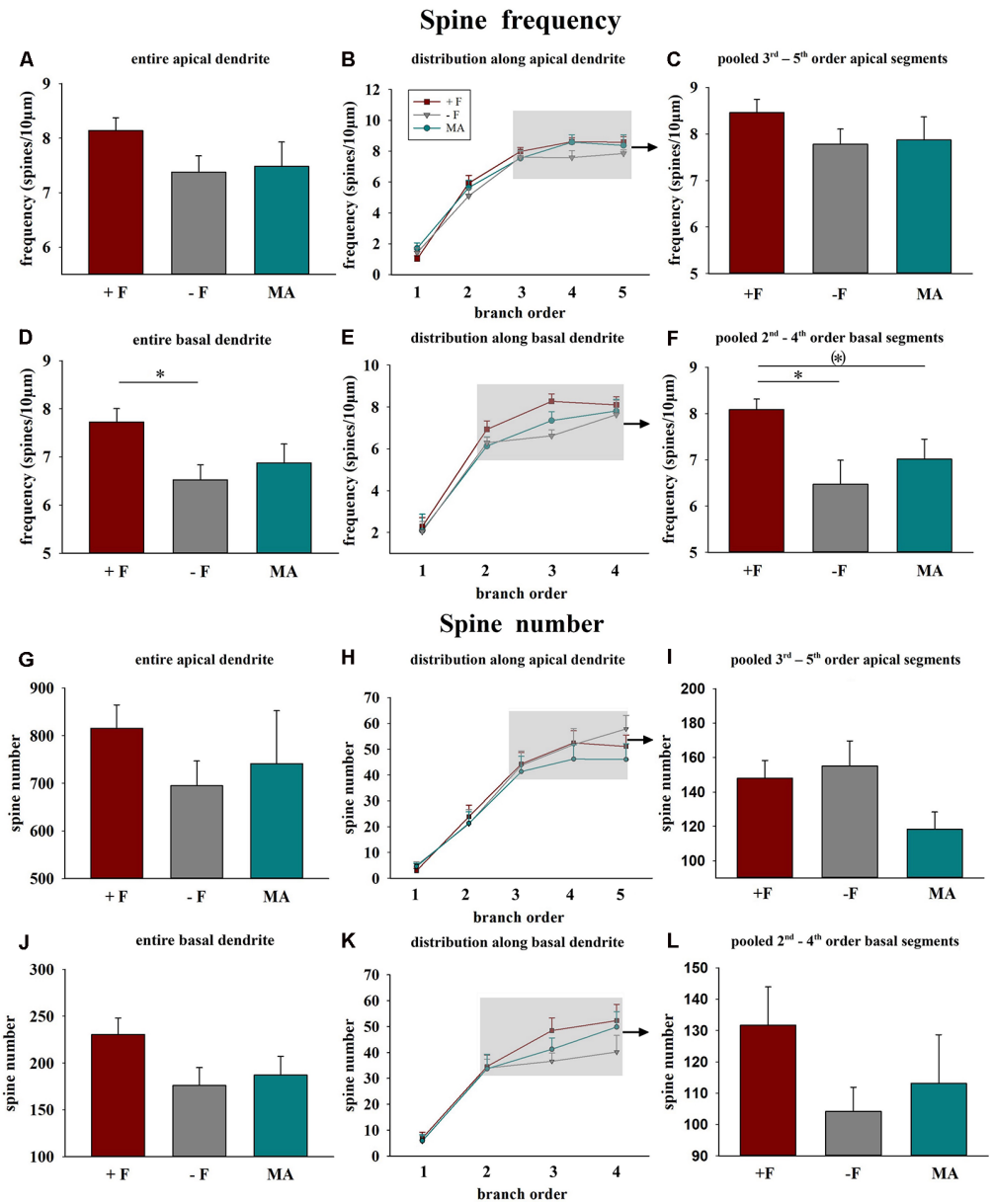

FIGURE 2 | Effects of different rearing conditions on dendritic spine frequency and spine number in male degu offspring. **(A,D,G,J)** Mean dendritic spine frequency and spine number for entire apical **(A,G)** or basal dendrites **(D,J)**. **(B,E,H,K)** Distribution of spine frequency and spine number within the individual dendritic segments (branch orders) along apical and basal dendrites; rectangles in figures in the central column indicate the branch orders used for pooled segment analysis. **(C,F,I,L)** Mean spine frequency and spine number of pooled 3rd to 5th branch order segments in apical and the 2nd to 4th branch order segments in basal dendrites. +F, male and female biparental control group; −F, fatherless single mother group; MA, female biparental (mother and aunt) group. $^{*}p \leq 0.05$; $^{(*)}p \leq 0.1$, SNK *post hoc* test.

the three experimental groups (p = 0.027), and the *post hoc* test revealed reduced dendritic length in offspring from the MA group compared to offspring from the −F group (p = 0.021, 38% reduction, **Figure 4D**). Also, analysis for the pooled values of the 2nd to 4th basal dendritic segments indicated a significant difference between the treatment groups (p = 0.006), and the *post hoc* test revealed for this basal segments reduced dendritic length in the MA group compared to the +F group (p = 0.006, 30% reduction) as well as to the −F group (p = 0.028, 22% reduction, **Figures 4E,F**). While no significant effects were observed for the entire apical dendrites, one way ANOVA indicated differences for the pooled 3rd to 5th dendritic segments of apical dendrites between the experimental groups (p = 0.04) and the *post hoc* test revealed significantly reduced length of these apical segments in females from the MA group compared to females from −F group (p = 0.044, 22% reduction) as well as a strong tendency compared to the −F group (p = 0.053, 20% reduction, **Figures 4B,C**).

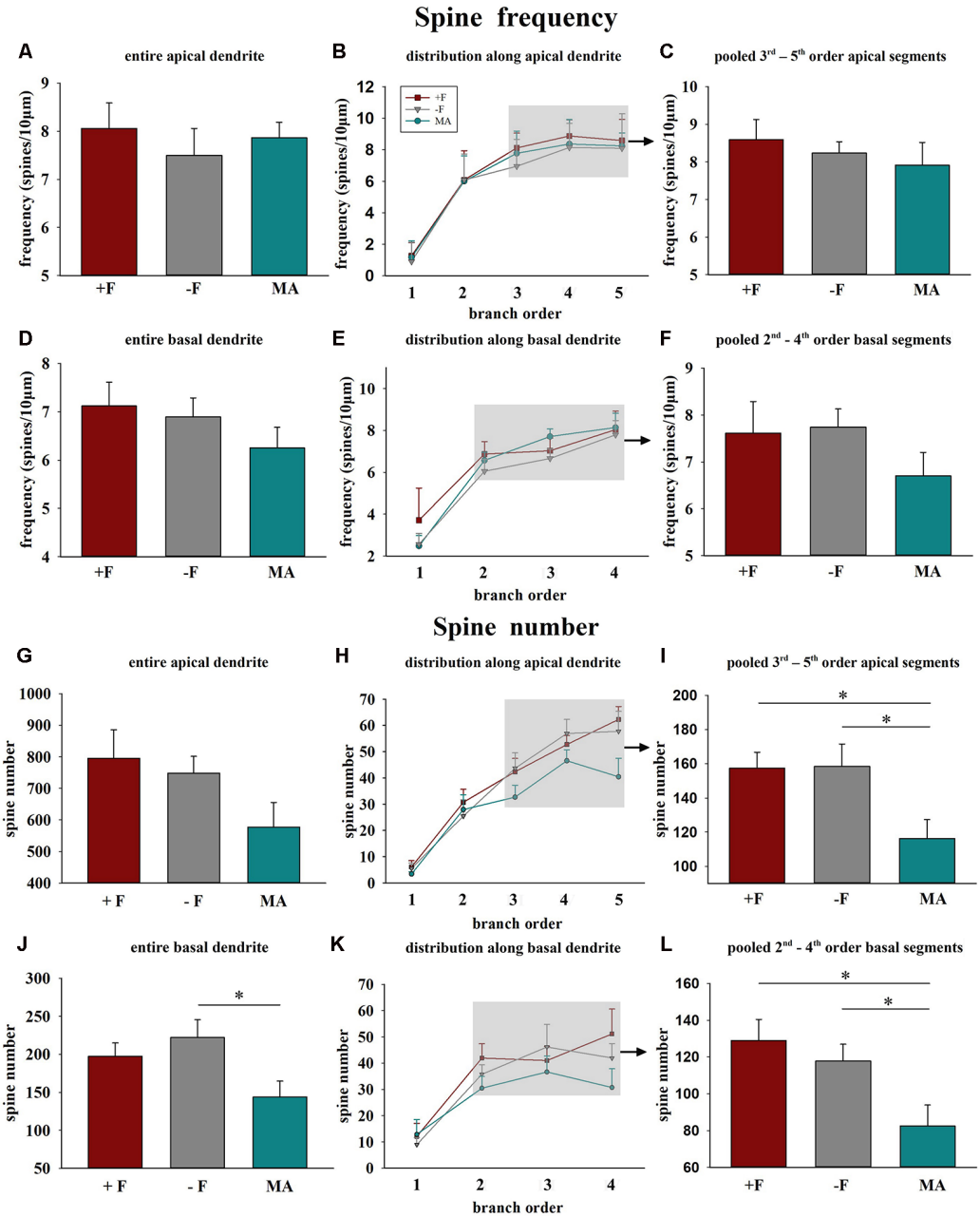

FIGURE 3 | Effects of different rearing conditions on dendritic spine frequency and spine number in female degu offspring. Diagrams in the left column illustrate mean dendritic spine frequency and spine number for entire apical **(A,G)** or basal dendrites **(D,J)**. The diagrams in the center column illustrate the distribution of spine frequency **(B,E)** and spine number **(H,K)** along the individual dendritic segments (branch orders) of apical and basal dendrites. The grey shaded rectangles indicate the branch orders that were used for the pooled segment analysis (for details see "Materials and Methods" section). Diagrams in the right column illustrate the results of the pooled segment analysis, mean spine frequency, and spine number of the pooled 3rd to 5th branch order segments in apical **(C,I)** and the 2nd to 4th branch order segments in basal dendrites **(F,L)**. +F, male and female biparental control group; −F, fatherless single mother group; MA, female biparental (mother and aunt) group. *$p \leq 0.05$, SNK *post hoc* test.

For dendritic complexity as analyzed with Sholl analysis ANOVA indicated a difference between the experimental groups in the basal dendrite ($p = 0.05$) and *post hoc* analysis revealed reduced basal dendritic complexity in the MA female group compared to the −F female group ($p = 0.039$, 36% reduction, **Figures 4I,J**). Also, for dendritic complexity of apical dendrites, ANOVA indicated a difference between the female experimental groups ($p = 0.018$) and the *post hoc* test revealed a reduction apical dendritic complexity in the MA group compared to the +F group ($p = 0.024$, 28% reduction) as well as to

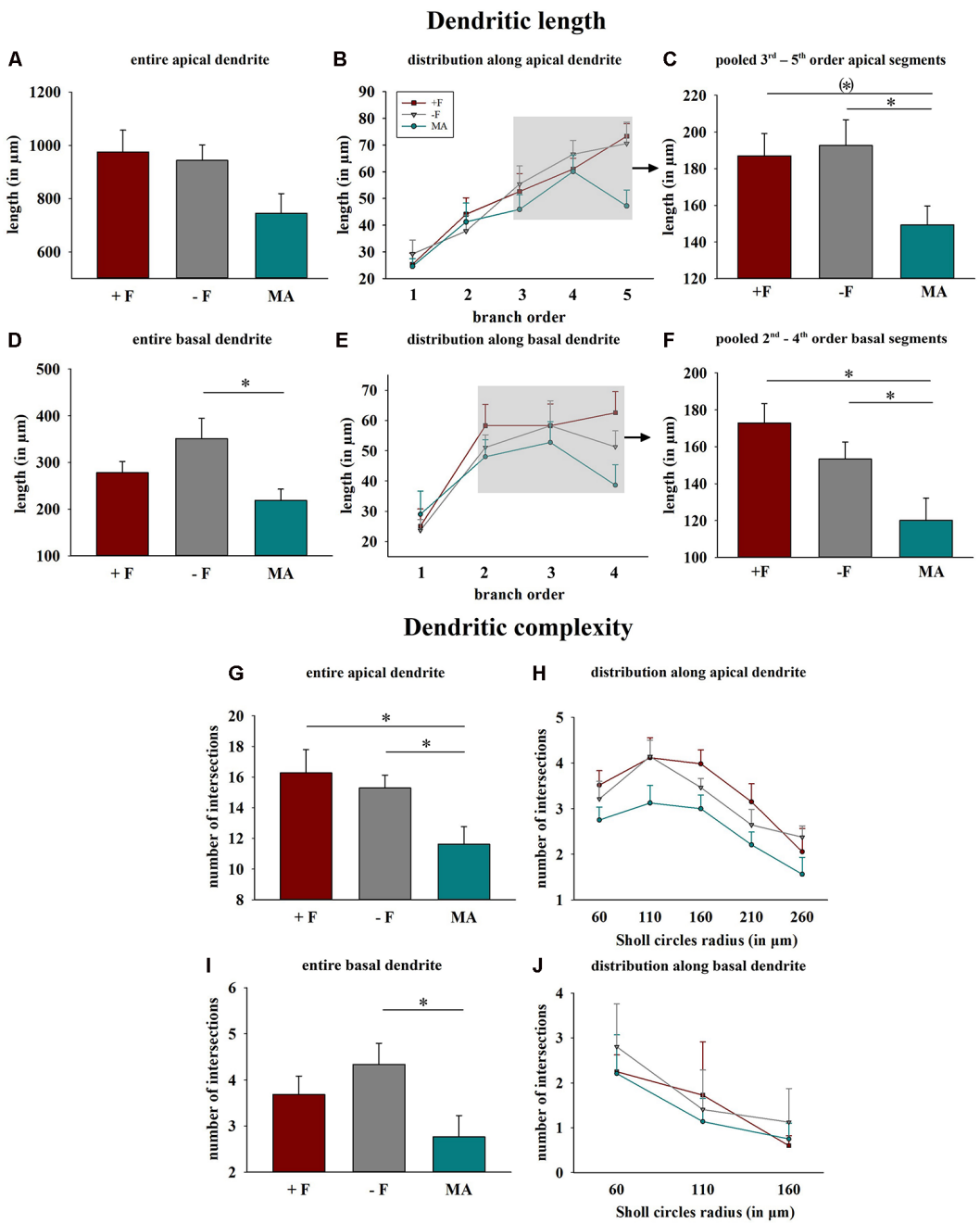

FIGURE 4 | Effects of different rearing conditions on dendritic length and complexity in female degu offspring. **(A,D)** Dendritic length for entire apical **(A)** or basal **(D)** dendrites. **(B,E)** Distribution of mean dendritic length within the individual dendritic segments (branch orders) along apical and basal dendrites; rectangles in figures in the central column indicate the branch orders used for pooled segment analysis. **(C,F)** Dendritic length of the pooled 3rd to 5th branch order segments in apical and the 2nd to 4th branch order segments in basal dendrites. **(G,H,I,J)** Dendritic complexity indicated as intersections as a result of Sholl analysis; **(G,I)** sum across entire apical or basal dendrites, **(H,J)** distribution along apical and basal dendrites. +F, male and female biparental control group; −F, fatherless single mother group; MA, female biparental (mother and aunt) group. $^{*}p \leq 0.05$, $^{(*)}p \leq 0.1$, SNK *post hoc* test.

the −F group (p = 0.023, 24% reduction, **Figures 4G,H**). Results for dendritic complexity are illustrated as representative dendrograms and reconstructions of representative pyramidal neurons in **Figure 5** (dendrograms **Figures 5A,B**; representative reconstructions **Figure 5C**).

DISCUSSION

The target area of the present study, the vmPFC, is implicated in various behavioral aspects and specifically related to the control of socio-emotional behavior, behavioral flexibility,

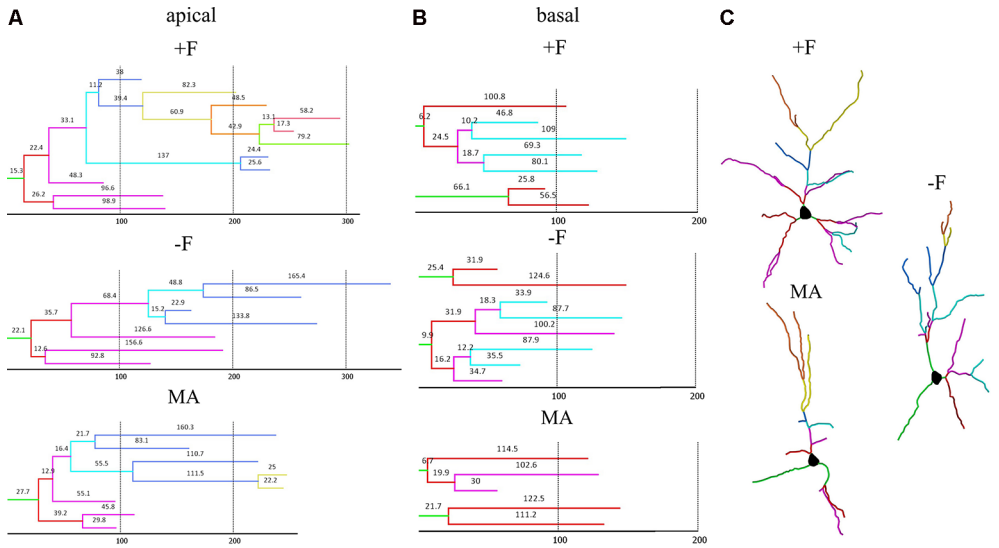

FIGURE 5 | Dendrograms and reconstructions of representative neurons in the different rearing groups to visualize the differences in dendritic length and complexity in female offspring. **(A,B)** Representative dendrograms for apical and basal dendrites; hatched vertical lines and numbers on each segment indicate length in μm. **(C)** Reconstructions of representative pyramidal neurons; branch orders are labeled by individual colors. +F = biparental control group, −F, fatherless group reared by mother; MA, reared by mother and aunt.

and cognitive functions. Although the homology of vmPFC subregions between humans and rodents is still under debate, it is important to note that the vmPFC is a key modulatory area of specific cortical and subcortical networks that include the amygdala, hippocampus, bed nucleus of stria terminalis, periaqueductal grey, anterior cingulate cortex and nucleus accumbens (Ko, 2017; Hiser and Koenigs, 2018). Previous studies in *Octodon degus* revealed that growing up in fatherless family results in various alterations of neuronal networks, which are indicative of a shift in homeostatic synaptic plasticity, i.e., the balance of excitatory and inhibitory activity in the prefrontal cortex. This view is supported by findings demonstrating that reduced excitatory input onto neurons in the PFC (reflected by decreased spine density and/or number) is paralleled by an increase in the density of different subtypes of inhibitory interneurons in the OFC as well as in the vmPFC (PL/IL; Braun et al., 2011). Although it is premature, without behavioral correlates indicative for prefrontal dysfunction, to offer a functional interpretation for the reduced synaptic density in father-deprived male offspring, it is tempting to speculate that these neuroanatomical changes in response to paternal deprivation might indicate that prefrontal regions may become hypofunctional. In support for this interpretation, we observed in degu pups, which were repeatedly separated from their parents and family during the first 3 weeks of life, that they display decreased metabolic brain activity in several brain areas including prefrontal cortical areas such as ACd, OFC as well as the PL and IL (Bock et al., 2017). This finding matches observations of functional imaging studies, which revealed that children suffering from early neglect and emotional deprivation display prefrontal hypofunction (Chugani et al., 2001).

Paternal Care Influences Dendritic and Synaptic Development

So far, only a few studies compared the effect of paternal care on the brain and behavioral development in male and female offspring. Although on the "mathematical level" the two-way ANOVA revealed no clear significant effects for the factor sex, a trend for interaction between rearing conditions and sex was detected. The comparison of individual groups—reflecting the "biological" view—revealed that paternal care affects dendrites and spine synapses in the vmPFC differently in male and female offspring. While in paternally deprived male offspring spine frequency on basal dendrites was reduced without changes in dendritic length and complexity, this effect was completely absent in paternally deprived females. In contrast, reductions of spine number and dendritic length and complexity in the mother/aunt group were restricted to female offspring, whereas male offspring appeared not to be affected by this rearing condition (see below). Sex-specific consequences of paternal deprivation have also been observed in other species, where either males or females were more severely affected. Moreover, the impact of paternal deprivation on brain development of his offspring is not confined to degus but has also been observed in other biparental rodents and non-human primates, which suggests that similar neuronal changes may occur in the human brain in response to paternal deprivation. For instance, electrophysiological studies in the mPFC of California mice observed lower firing rates of low-spiking pyramidal neurons in father-deprived females compared to biparentally raised females, whereas no significant differences in basal firing rates of both low-spiking and high-spiking neurons were seen in father-deprived and biparentally raised males (Bambico et al., 2015).

Paternal deprivation-induced neuronal changes have also been reported in limbic brain regions, which are connected to the mPFC, including the hippocampal formation. In father-deprived prairie voles (Microtus ochrogaster) glucocorticoid receptor β (GRβ) protein expression was elevated in the hippocampus of females, increased corticotropin-releasing hormone receptor 2 (CRHR2) protein expression was observed in the hippocampus of males, while in both sexes paternal deprivation resulted in decreased hippocampal CRHR2 mRNA (Tabbaa et al., 2017). A recent study in the biparental mandarin vole demonstrated that pre-weaning paternal deprivation at postnatal days 14–21 reduced neurogenesis in the dentate gyrus, predominantly in female offspring (Wu et al., 2014), and only female offspring showed decreased expression of Brain-Derived Neurotrophic Factor (BDNF) and the glucocorticoid receptor (NR3C1; Wu et al., 2014). In contrast, decreased dendritic spine density was observed in the dentate gyrus of both males and females (He et al., 2018).

A Female Caregiver Cannot "Buffer" the Neuronal Consequences of Paternal Deprivation

Most experimental studies in bi-parental non-human species apply paternal deprivation paradigms, where the father is removed from the social unit. These studies demonstrate that the absence of the father affects various behavioral traits in the progeny, including anxiety, aggression, social behavior and response to reward (Bester-Meredith and Marler, 2003; Frazier et al., 2006; McGraw and Young, 2010; Wang et al., 2012; Yu et al., 2012; Birnie et al., 2013). When interpreting findings from paternal deprivation studies in animal models it has, however, to be kept in mind that the observed consequences on the brain and behavioral development might not be specific to the absence of a male caregiver but might rather be due to single-parent rearing conditions. This question was experimentally addressed in our study by replacing the father with another female caregiver (the sister of the dam, i.e., the "aunt") resulting in a female biparental family. Our results revealed that a female caregiver cannot protect from or compensate for the neuronal changes induced by growing-up in a fatherless environment, but rather induces additional neuronal changes, particularly in the vmPFC of female offspring. Again, it is tempting to speculate that these changes might be indicative of prefrontal dysfunction. However, the socio-emotional environment provided by a female biparental family remains to be investigated in more detail, to assess whether it represents an "impoverished" or an overprotective or stressful environment.

DATA AVAILABILITY STATEMENT

The datasets generated for this study are available on request to the corresponding author.

ETHICS STATEMENT

The animal study was reviewed and approved by Ethics committee of Saxony-Anhalt, Germany.

AUTHOR CONTRIBUTIONS

TS conducted 3D analysis of stained neurons, statistical analysis, preparation of figures and was involved in writing parts of the mansucript. JB did brain preparations, guided histological staining, 3D analysis and statistics and wrote signifcant parts of the manuscript. KB led the project, planned the experimental design, guided analysis including statistics, wrote signficant parts of the manuscript and did final editing of the submitted draft.

FUNDING

This work was supported by German-Israeli Foundation for Scientific Research and Development.

ACKNOWLEDGMENTS

We would like to appreciate the expert technical assistance of Ute Kreher with the histological procedures and of Julia Heinzelmann with manuscript editing.

REFERENCES

Abraham, E., and Feldman, R. (2018). The neurobiology of human allomaternal care; implications for fathering, coparenting and children's social development. *Physiol. Behav.* 193, 25–34. doi: 10.1016/j.physbeh.2017.12.034

Bales, K. L., and Saltzman, W. (2016). Fathering in rodents: neurobiological substrates and consequences for offspring. *Horm. Behav.* 77, 249–259. doi: 10.1016/j.yhbeh.2015.05.021

Bambico, F. R., Lacoste, B., Hattan, P. R., and Gobbi, G. (2015). Father absence in the monogamous california mouse impairs social behavior and modifies dopamine and glutamate synapses in the medial prefrontal cortex. *Cereb. Cortex* 25, 1163–1175. doi: 10.1093/cercor/bht310

Baskerville, S. (2002). The politics of fatherhood. *Pol. Sci. Polit.* 35, 695–699. doi: 10.1017/S1049096502001191

Bester-Meredith, J. K., and Marler, C. A. (2003). Vasopressin and the transmission of paternal behavior across generations in mated, cross-fostered Peromyscus mice. *Behav. Neurosci.* 117, 455–463. doi: 10.1037/0735-7044.117.3.455

Birnie, A. K., Taylor, J. H., Cavanaugh, J., and French, J. A. (2013). Quality of maternal and paternal care predicts later stress reactivity in the cooperatively-breeding marmoset (*Callithrix geoffroyi*). *Psychoneuroendocrinology* 38, 3003–3014. doi: 10.1016/j.psyneuen.2013.08.011

Bock, J., and Braun, K. (1999a). Blockade of N-methyl-D-aspartate receptor activation suppresses learning-induced synaptic elimination. *Proc. Natl. Acad. Sci. U S A* 96, 2485–2490. doi: 10.1073/pnas.96.5.2485

Bock, J., and Braun, K. (1999b). Filial imprinting in domestic chicks is associated with spine pruning in the associative area, dorsocaudal neostriatum. *Eur. J. Neurosci.* 11, 2566–2570. doi: 10.1046/j.1460-9568.1999.00713.x

Bock, J., Breuer, S., Poeggel, G., and Braun, K. (2017). Early life stress induces attention-deficit hyperactivity disorder (ADHD)-like behavioral and brain metabolic dysfunctions: functional imaging of methylphenidate treatment in a novel rodent model. *Brain Struct. Funct.* 222, 765–780. doi: 10.1007/s00429-016-1244-7

Bock, J., Poeschel, J., Schindler, J., Börner, F., Shachar-Dadon, A., Ferdman, N., et al. (2016). Transgenerational sex-specific impact of preconception stress on the developmentof dendritic spines and dendritic length in the medial

prefrontal cortex. *Brain Struct. Funct.* 221, 855–863. doi: 10.1007/s00429-014-0940-4

Bock, J., Rether, K., Gröger, N., Xie, L., and Braun, K. (2014). Perinatal programming of emotional brain circuits: an integrative view from systems to molecules. *Front. Neurosci.* 8:11. doi: 10.3389/fnins.2014.00011

Braun, K., and Champagne, F. A. (2014). Paternal influences on offspring development: behavioural and epigenetic pathways. *J. Neuroendocrinol.* 26, 697–706. doi: 10.1111/jne.12174

Braun, K., and Poeggel, G. (2001). Recognition of mothers voice evokes metabolic activation in the medial prefrontal cortex and thalamus of Octodon degus pups. *Neuroscience* 103, 861–864. doi: 10.1016/s0306-4522(01)00074-4

Braun, S., and Scheich, H. (1997). Influence of experience on the representation of the 'mothering call' in frontoparietal and auditory cortex of pups of the rodent Octodon degus: FDG mapping. *J. Comp. Physiol. A* 181, 697–709. doi: 10.1007/s003590050151

Braun, K., Seidel, K., Holetschka, R., Groeger, N., and Poeggel, G. (2013). Paternal deprivation alters the development of catecholaminergic innervation in the prefrontal cortex and related limbic brain regions. *Brain Struct. Funct.* 218, 859–872. doi: 10.1007/s00429-012-0434-1

Braun, K., Seidel, K., Weigel, S., Roski, C., and Poeggel, G. (2011). Paternal deprivationalters region- and age-specific interneuron expression patterns in the biparental rodent, Octodon degus. *Cereb. Cortex* 21, 1532–1546. doi: 10.1093/cercor/bhq208

Bryan, G. K., and Riesen, A. H. (1989). Deprived somatosensory-motor experience in stumptailed monkey neocortex: dendritic spine density and dendritic branching of layer IIIB pyramidal cells. *J. Comp. Neurol.* 286, 208–217. doi: 10.1002/cne.902860206

Chugani, H. T., Behen, M. E., Muzik, O., Juhász, C., Nagy, F., and Chugani, D. C. (2001). Local brainfunctional activity following early deprivation: a study of postinstitutionalized Romanian orphans. *NeuroImage* 14, 1290–1301. doi: 10.1006/nimg.2001.0917

Colonnello, V., Iacobucci, P., Fuchs, T., Newberry, R. C., and Panksepp, J. (2011). Octodon degus. A useful animal model for social-affective neuroscience research: basic description of separation distress, social attachments and play. *Neurosci. Biobehav. Rev.* 35, 1854–1863. doi: 10.1016/j.neubiorev.2011.03.014

De Casper, A. J., and Fifer, W. P. (1980). Of human bonding: newborns prefer their mothers' voices. *Science* 208, 1174–1176. doi: 10.1126/science.7375928

Demuth, S., and Brown, S. L. (2004). Family structure, family processes and adolescent delinquency: the significance of parental absence versus parental gender. *J. Res. Crime Delinq.* 41, 58–81. doi: 10.1177/0022427803256236

Erhard, R., and Janig, H. (2003). *Folgen der Vaterentbehrung: Eine Literaturstudie.* Wien: BMSG.

Feldman, R. (2016). The neurobiology of mammalian parenting and the biosocial context of human caregiving. *Horm. Behav.* 77, 3–17. doi: 10.1016/j.yhbeh.2015.10.001

Feldman, R., Braun, K., and Champagne, F. A. (2019). The neural mechanisms and consequences of paternal caregiving. *Nat. Rev. Neurosci.* 20, 205–224. doi: 10.1038/s41583-019-0124-6

Feldman, M. L., and Peters, A. (1979). A technique for estimating total spine numbers on golgi-impregnated dendrites. *J. Comp. Neurol.* 188, 527–542. doi: 10.1002/cne.901880403

Fifer, W. P., and Moon, C. M. (1994). The role of mother's voice in the organization of brain function in the newborn. *Acta Paediatr. Suppl.* 397, 86–93. doi: 10.1111/j.1651-2227.1994.tb13270.x

Franz, M., Schmitz, N., Lieberz, K., and Schepank, H. (1999). Wenn der Vater fehlt. epidemiologische befunde zur bedeutung früher abwesenheit des vaters für die psychische gesundheit im späteren Leben/The missingfather. Epidemiological findings on the significance of early absence of the father for mental health in later life. *Z. Psychosom. Med. Psychother.* 45, 260–278. doi: 10.13109/zptm.1999.45.3.260

Frazier, C. R., Trainor, B. C., Cravens, C. J., Whitney, T. K., and Marler, C. A. (2006). Paternal behaviour influences development of aggression and vasopressin expression in male California mouse offspring. *Horm. Behav.* 50, 699–707. doi: 10.1016/j.yhbeh.2006.06.035

Fuchs, T., Iacobucci, P., MacKinnon, K. M., and Panksepp, J. (2010). Infant-mother recognition in asocial rodent (*Octodon degus*). *J. Comp. Psychol.* 124, 166–175. doi: 10.1037/a0018704

Garfield, C. F., and Isacco, A. (2006). Fathers and the well-child visit. *Pediatrics* 117, e637–e645. doi: 10.1542/peds.2005-1612

Glynn, L. M., and Baram, T. Z. (2019). The influence of unpredictable, fragmented parental signals on the developing brain. *Front. Neuroendocrinol.* 53:100736. doi: 10.1016/j.yfrne.2019.01.002

Hanson, M. A., and Gluckman, P. D. (2014). Early developmental conditioning of later health and disease: physiology or pathophysiology? *Physiol. Rev.* 94, 1027–1076. doi: 10.1152/physrev.00029.2013

Harper, C. C., and McLanahan, S. S. (2004). Father absence and youth incarceration. *J. Res. Adolesc.* 14, 369–397. doi: 10.1111/j.1532-7795.2004.00079.x

He, Z., Guo, Q., Yang, Y., Wang, L., Zhang, S., Yuan, W., et al. (2018). Pre-weaning paternal deprivation impairs social recognition and alters hippocampal neurogenesis and spine density in adult mandarin voles. *Neurobiol. Learn Mem.* 155, 452–462. doi: 10.1016/j.nlm.2018.09.006

Heindel, J. J., Balbus, J., Birnbaum, L., Brune-Drisse, M. N., Grandjean, P., Gray, K., et al. (2015). Developmental origins of health and disease: integrating environmental influences. *Endocrinology* 156, 3416–3421. doi: 10.1210/EN.2015-1394

Helmeke, C., Seidel, K., Poeggel, G., Bredy, T., Abraham, A., and Braun, K. (2009). Paternal deprivation during infancy results in dendrite- and time-specific changes of dendritic development and spine formation in the orbitofrontal cortex of the biparental rodent Octodon degus. *Neuroscience* 163, 790–798. doi: 10.1016/j.neuroscience.2009.07.008

Hiser, J., and Koenigs, M. (2018). The multifaceted role of the ventromedial prefrontal cortex in emotion, decision making, social cognition and psychopathology. *Biol. Psychiatry* 83, 638–647. doi: 10.1016/j.biopsych.2017.10.030

Horner, C. H., and Arbuthnott, E. (1991). Methods of estimation of spine density—are spines evenly distributed throughout the dendritic field? *J. Anat.* 177, 179–184.

Juby, H., and Farrington, D. P. (2001). Disentangling the link between disrupted families and delinquency sociodemography, ethnicity and risk behaviours. *Br. J. Criminol.* 41, 22–40. doi: 10.1093/bjc/41.1.22

Kindler, H., and Grossmann, K. (2004). "Vater-Kind-Bindung und die Rolle der Väter in den ersten Lebensjahren ihrer Kinder," in *Frühe Bindung. Entstehung und Entwicklung*, ed. L. Ahnert (München, Basel: Ernst Reinhard Verlag), 240–255.

Ko, J. (2017). Neuroanatomical substrates of rodent social behavior: the medial prefrontal cortex and its projection patterns. *Front. Neural. Circuits* 11:41. doi: 10.3389/fncir.2017.00041

Kohl, J., Autry, A. E., and Dulac, C. (2017). The neurobiology of parenting: a neural circuit perspective. *Bioessays* 39, 1–11. doi: 10.1002/bies.201600159

Kohl, J., Babayan, B. M., Rubinstein, N. D., Autry, A. E., Marin-Rodriguez, B., Kapoor, V., et al. (2018). Functional circuitarchitecture underlying parental behaviour. *Nature* 556, 326–331. doi: 10.1038/s41586-018-0027-0

Kumazawa-Manita, P. N., Hashikawa, P. T., and Iriki, D. A. (2018). The 3D stereotaxic brain atlas of the degu. *Brain Sci.* 231, 65–74.

Kumazawa-Manita, N., Katayama, M., Hashikawa, T., and Iriki, A. (2013). Three dimensional reconstruction of brain structures of the rodent Octodon degus: a brain atlas constructed by combining histological and magnetic resonance images. *Exp. Brain Res.* 231, 65–74. doi: 10.1007/s00221-013-3667-1

Maccari, S., Krugers, H. J., Morley-Fletcher, S., Szyf, M., and Brunton, P. J. (2014). The consequences of early-life adversity: neurobiological, behavioural and epigenetic adaptations. *J. Neuroendocrinol.* 26, 707–723. doi: 10.1111/jne.12175

Markham, J. A., and Greenough, W. T. (2004). Experience-driven brain plasticity: beyond the synapse. *Neuron Glia Biol.* 1, 351–363. doi: 10.1017/s1740925x05000219

McGraw, L. A., and Young, L. J. (2010). The prairie vole: an emerging model organism for understanding the social brain. *Trends Neurosci.* 33, 103–109. doi: 10.1016/j.tins.2009.11.006

Meaney, M. J. (2001). Maternal care, gene expression and the transmission of individual differences in stress reactivity across generations. *Annu. Rev. Neurosci.* 24, 1161–1192. doi: 10.1146/annurev.neuro.24.1.1161

O'Neill, R. (2002). Experiments in living: the fatherless family. *Civitas*. 9, 1–20. Available online at: https://fkce.wordpress.com/2002/09/01/4/.

Okanoya, K., Tokimoto, N., Kumazawa, N., Hihara, S., and Iriki, A. (2008). Tool-use training in a species of rodent: the emergence of an optimal motor strategy and functional understanding. *PLoS One* 3:e1860. doi: 10.1371/journal.pone.0001860

Ovtscharoff, W. Jr., Helmeke, C., and Braun, K. (2006). Lack of paternal care affects synapticdevelopment in the anterior cingulate cortex. *Brain Res.* 1116, 58–63. doi: 10.1016/j.brainres.2006.07.106

Paxinos, G., and Watson, C. (2004). *The Rat Brain in Stereotaxic Coordinates*. 5th ed. New York, NY: Elsevier.

Pinkernelle, J., Abraham, A., Seidel, K., and Braun, K. (2009). Paternal deprivation induces dendritic and synaptic changes and hemispheric asymmetry of pyramidal neurons in the somatosensory cortex. *Dev. Neurobiol.* 69, 663–673. doi: 10.1002/dneu.20726

Poeggel, G., and Braun, K. (1996). Early auditory filial learning in degus (Octodon degus): behavioral and autoradiographic studies. *Brain Res.* 743, 162–170. doi: 10.1016/s0006-8993(96)01039-6

Poeggel, G., Helmeke, C., Abraham, A., Schwabe, T., Friedrich, P., and Braun, K. (2003). Juvenile emotional experience alters synaptic composition in the rodent cortex, hippocampus and lateral amygdala. *Proc. Natl. Acad. Sci. U S A* 100, 16137–16142. doi: 10.1073/pnas.2434663100

Pohl, T. T., Young, L. J., and Bosch, O. J. (2019). Lost connections: oxytocin and theneural, physiological and behavioral consequences of disrupted relationships. *Int. J. Psychophysiol.* 136, 54–63. doi: 10.1016/j.ijpsycho.2017.12.011

Rosenzweig, M. R., and Bennett, E. L. (1996). Psychobiology of plasticity: effects of training and experience on brain and behavior. *Behav. Brain Res.* 78, 57–65. doi: 10.1016/0166-4328(95)00216-2

Saltzman, W., Harris, B. N., De Jong, T. R., Perea-Rodriguez, J. P., Horrell, N. D., Zhao, M., et al. (2017). Paternal care in biparental rodents: intra-and interindividual variation. *Integr. Comp. Biol.* 57, 589–602. doi: 10.1093/icb/icx047

Seidel, K., Poeggel, G., Holetschka, R., Helmeke, C., and Braun, K. (2011). Paternal deprivation affects the development of corticotrophin-releasing factor-expressing neurones in prefrontal cortex, amygdala and hippocampus of the biparental Octodon degus. *J. Neuroendocrinol.* 23, 1166–1176. doi: 10.1111/j.1365-2826.2011.02208.x

Sholl, D. A. (1953). Dendritic organization in the neurons of the visual and motor cortices of the cat. *J. Anat.* 87, 387–406.

Tabbaa, M., Lei, K., Liu, Y., and Wang, Z. (2017). Paternal deprivation affects social behaviors and neurochemical systems in the offspring of socially monogamous prairie voles. *Neuroscience* 343, 284–297. doi: 10.1016/j.neuroscience.2016.12.011

Wang, J., Tai, F., Yan, X., and Yu, P. (2012). Paternal deprivation alters play-fighting, serum corticosterone and the expression of hypothalamic vasopressin and oxytocin in juvenile male mandarin voles. *J. Comp. Physiol. A Neuroethol. Sens. Neural. Behav. Physiol.* 198, 787–796. doi: 10.1007/s00359-012-0748-8

Wilson, S. C. (1982). Contact-promoting behavior, social development and relationship with parents in sibling juvenile degus (*Octodon degus*). *Dev. Psychobiol.* 15, 257–268. doi: 10.1002/dev.420150309

Wright, J. W., and Kern, M. D. (1992). Stereotaxic atlas of the brain of Octodon degus. *J. Morphol.* 214, 299–320. doi: 10.1002/jmor.1052140306

Wu, R., Song, Z., Wang, S., Shui, L., Tai, F., Qiao, X., et al. (2014). Early paternal deprivation alters levels of hippocampal brain-derived neurotrophic factor and glucocorticoid receptor and serum corticosterone and adrenocorticotropin in a sexspecific way in socially monogamous mandarin voles. *Neuroendocrinology* 100, 119–128. doi: 10.1159/000366441

Yu, P., An, S., Tai, F., Zhang, X., He, F., Wang, J., et al. (2012). The effects of neonatal paternal deprivation on pair bonding, NAcc dopamine receptor mRNA expression and serum corticosterone in mandarin voles. *Horm. Behav.* 61, 669–677. doi: 10.1016/j.yhbeh.2012.02.028

Zhang, T. Y., Labonté, B., Wen, X. L., Turecki, G., and Meaney, M. J. (2013). Epigenetic mechanisms for the early environmental regulation of hippocampal glucocorticoid receptor gene expression in rodents and humans. *Neuropsychopharmacology* 38, 111–123. doi: 10.1038/npp.2012.149

Conflict of Interest: The authors declare that the research was conducted in the absence of any commercial or financial relationships that could be construed as a potential conflict of interest.

frontiers in Synaptic Neuroscience

MINI REVIEW
published: 10 September 2020
doi: 10.3389/fnsyn.2020.566615

Early-Occurring Dendritic Spines Alterations in Mouse Models of Alzheimer's Disease Inform on Primary Causes of Neurodegeneration

Martine Ammassari-Teule [1,2]*

[1]Institute of Biochemistry and Cell Biology, CNR-National Research Council, Rome, Italy, [2]Laboratory of Psychobiology, IRCCS Santa Lucia Foundation, Rome, Italy

The consensus that synaptic failure is the earliest cause of cognitive deterioration in Alzheimer's disease (AD) has initially led to investigate structural (dendritic spines) and physiological (LTP) synaptic dysfunctions in mouse models of AD with established cognitive alterations. The challenge is now to track down ultra-early alterations in spines to uncover causes rather than disease's symptoms. This review article pinpoints dysregulations of the postsynaptic density (PSD) protein network which alter the morphology and function of spines in pre- and early- symptomatic hAPP mouse models of AD, and, hence, inform on primary causes of neurodegeneration.

Keywords: Alzheimer's disease, presymptomatic stage, full-length APP, Aβ oligomers (Aβo), dendritic spines, synaptic proteins

OPEN ACCESS

Edited by:
Ka Wan Li,
Vrije Universiteit Amsterdam, Netherlands

Reviewed by:
Albert Giralt,
University of Barcelona, Spain
Hélène Marie,
Centre National de la Recherche Scientifique (CNRS), France

***Correspondence:**
Martine Ammassari-Teule
martine.teule@cnr.it

Received: *28 May 2020*
Accepted: *17 August 2020*
Published: *10 September 2020*

Citation:
Ammassari-Teule M (2020) Early-Occurring Dendritic Spines Alterations in Mouse Models of Alzheimer's Disease Inform on Primary Causes of Neurodegeneration. Front. Synaptic Neurosci. 12:566615. doi: 10.3389/fnsyn.2020.566615

INTRODUCTION

Re-arrangements of synaptic connectivity in neural circuits of memory allow individual experiences to be encoded, stored, and subsequently recalled. These re-arrangements occur at the level of dendritic spines (spines), the neuron's dendrites protrusions which host excitatory synapses and can change their number, volume, and shape in response to environmental stimuli. The morphological plasticity of spines is supported by the dynamic properties of their actin cytoskeleton. Close to the presynaptic active zone, the postsynaptic density (PSD) of spines contains receptors, cytoskeletal, scaffolding/adaptors proteins, and signaling molecules representative of multiple pathways which control synaptic activity by maintaining a physiological balance between the morphology and the function of spines (Lee et al., 2012). Changes in shape, therefore, affect the electrical properties of spines (Tønnesen and Nägerl, 2016), modify the amount of excitatory neurotransmission (Yuste et al., 2000), and alter the wiring diagram of memory circuits through a redistribution of synaptic weights in neuronal ensembles (Varga et al., 2011; Rochefort and Konnerth, 2012).

In Alzheimer's disease (AD), data showing that episodic memory is altered in the absence of massive neurodegeneration have established that synaptic failure is the earliest cause of cognitive deterioration (Selkoe, 2002). Hence, the search for alterations in the PSD protein network involved in structural (spines) and physiological (LTP) synaptic dysfunctions has become mainstream in the AD field (Tackenberg et al., 2009; Yu and Lu, 2012). Being mostly accessible in mouse models of the disease, these alterations

have been investigated in mice overexpressing mutant human genes—amyloid protein precursor (APP), Presenilin-1 (PS1), and microtubule-associated protein Tau known to cause clinical and neuropathological alterations in familiar forms of AD. The production of mutant mice bearing single or several transgenes that were expressed in distinct wild-type backgrounds has, however, generated a variety of phenotypes that differ in the onset, the progression and the severity of AD-like symptoms (Hsiao et al., 1996). Thus, a myriad of factors impacting on structural and functional synaptic plasticity have been identified in AD mice (Tu et al., 2014; Aoki and Sherpa, 2017) and patients (Gong and Lippa, 2010), but at different ages and in association with variable neurodegenerative burdens.

Although these investigations have put forward the disruptive role of a variety molecular and biological components that alter the functionality of spines—and are suitable to be targeted in a therapeutic perspective-, the current challenge is to uncover the mechanisms that initiate the earliest spine dysfunctions with the double objective of: (i) unveiling causes rather than disease's symptoms; and (ii) intervening to prevent rather than to contrast neurodegeneration (Llorens-Martin et al., 2014). Considering that the presence of circulating Aβ oligomers (Aβo) associates with the early signs synapto-toxicity (Lambert et al., 1998; Hsia et al., 1999; Mucke et al., 2000; Beckman et al., 2019), this review pinpoints dysregulations of the PSD protein network which disrupt the morphology and function of spines in early developing *in vitro* and *in vivo* human mutant APP models, and can inform on primary causes of neurodegeneration.

Aβ-INDUCED ALTERATION OF THE PSD NETWORK DISRUPTS DENDRITIC SPINES IN CULTURED NEURONS

Wild-Type Neurons Exposed to Aβo

Aβo selectively bind the postsynaptic component of excitatory synapses (Lacor et al., 2007; Renner et al., 2010; Cline et al., 2018), and exposure of wild-type neurons in culture to Aβo is sufficient to trigger *in vitro* "phenocopies" of AD spines pathology. For example, pyramidal neurons in rat hippocampal organotypic slices exposed to picomolar levels (∼100–300 pM) of soluble Aβo show a decrease in spine density and in the number of electrophysiologically active synapses in association with a reduction of NMDA receptor-mediated calcium influx. Of note, these effects are reverted by Aβ-specific antibodies, or by the small molecule scylloinositol (ASD 103) which prevents Aβ aggregation (Shankar et al., 2007). More recently, acute exposure to Aβo (100 nM) was found to increase phosphorylation of the cofilin-1 protein in the postsynaptic compartment and to favor its distribution in the Triton-insoluble fractions, with consequent stabilization of *F*-actin in spines, impairment of synaptic plasticity, and disruption of synaptic transmission due to the formation of cofilin-actin rods (Rush et al., 2018). Also, insertion of Aβ derived diffusible ligands (ADDL, 500 nM) in the medium of cultured mature cortical pyramidal neurons induces spine dysgenesis associated with depletion of kalirin-7, a key regulator of spines formation while overexpression of kalirin-7 prevents ADDL-induced spine degeneration (Xie et al., 2019). Data showing that synthetic and human-derived Aβo stimulates microglia proliferation at subneurotoxic nanomolar (250 nM) concentrations (Neniskyte et al., 2011) in wild-type neurons suggest that neuroinflammation plays an early role in Aβo-related neuronal subcellular alterations. Consistent with this view, hippocampal neurons in cultures exposed to Aβo in a microglia-conditioned medium show reduced levels of dendritic proteins Ac-TN and MAP2, postsynaptic proteins PSD95 and GRIP1, and presynaptic protein synaptophysin (Maezawa et al., 2011). In apparent contrast with these findings, *in vivo* time-lapse imaging of spines in organotypic hippocampal slices treated with micromolar (1 μM) concentrations of Aβo reveals an increase in the density of total dendritic spines due, however, to a rise of immature stubby spines with no head and neck differentiation preventing synaptic signal compartmentalization and therefore unlikely to enhance synaptic transmission (Ortiz-Sanz et al., 2020). Suggesting that the toxicity of Aβo is independent of its subcellular localization, overproduction of axonal or dendritic Aβo in rat cultured cortical neurons disrupts both synaptic density and plasticity (Wei et al., 2010). Aβo (10 μM) also impact scaffolding and cytoskeletal proteins in cortical neurons in culture. Specifically, a reduction in PSD-95 levels at glutamatergic synapses (Roselli et al., 2005), a disassembly of Homer1b and Shank1, two scaffold proteins that couple PSD-95 with ionotropic and metabotropic glutamate receptors (Roselli et al., 2009), and a significant reduction in the density and morphology of spines accompanied by decreased levels of the spine cytoskeletal protein drebrin (Lacor et al., 2007) have been reported.

Mutant hAPP Neurons

Compared to wild-type neurons exposed to Aβo, neurons from AD mice have the advantage to inform on the chronology of synaptic alterations whose severity varies according to: (i) the age and the neurodegenerative burden of the mouse model used for the preparation of neurons in culture; and (ii) the degree of maturation of cells, which depends on the number of days they are kept growing *in vitro* (DIV). For example, in cultured neurons from Tg2576 cortices and hippocampi prepared at embryonic days 16 and 18, the first synaptic alterations are detected on the postsynaptic side. Those consist in a synaptic reduction of PSD-95 and glutamate receptor subunit GluA1 levels observed at 12 DIV, which become more severe at 19 DIV since not only synaptic but total levels of PSD-95 and GluR1 are decreased and fewer spines, identified by PSD-95, spinophilin, drebrin, and *F*-actin staining are counted. Interestingly, 19 DIV is also the time point where the first presynaptic alteration, i.e., decreased levels of synaptophysin, is detected (Almeida et al., 2005). To better intercept *in vitro* developmental changes in spines, Penazzi et al. (2016) established a long term *ex vivo* model of hippocampal slices prepared from 7- or 14-day-old mice that were kept in culture for 15 or 20 days. Spine loss and progressive changes from mushroom- to stubby-shaped spines in CA1 hippocampal neurons were observed in all preparations, but these dysfunctions were considerably stronger in the P14/20 DIV condition. Of note, the changes

in spines observed in cultured neurons were fully consistent with those exhibited by the same mice at 3- 4- and 5-week of age. Confirming that the most severe alterations occur in the most mature AD neurons, primary cortical neurons prepared from postnatal day 1 APP/PS1 mice and fixed at DIV 10 and 16 revealed that while only the spine head diameters were reduced at DIV 10, head diameters, surface areas, and *F*-actin levels were reduced in spines measured at DIV16 (Kommaddi et al., 2018). Then, consistent with data showing that spine loss in AD patients and mice models occur through a pathway involving the calcium-dependent phosphatase calcineurin (CaN), neurons isolated in the vicinity of plaques and further exposed to soluble Aβo was found to activate CaN, which then activated the transcriptional factor nuclear factor of activated T cells (NFAT) involved in $Ca^{(2+)}$ dysregulation (Abdul et al., 2009). Remarkably, even in the absence of Aβo, the activation of CaN or NFAT pathways is sufficient to produce dystrophic neurites, dendritic simplification, and dendritic spine loss (Wu et al., 2010).

Aβ-INDUCED EARLY DISRUPTION OF PSD NETWORK AND SPINES IN RESTING CONDITIONS

Asymptomatic Stage

The earliest evidence of spine loss in a mouse model of AD is provided by Lanz et al. (2003) who reported a decrease in spines in Golgi-stained pyramidal neurons in the CA1 subfield of the hippocampus in 2-month-old PDAPP mice expressing the V717F hAPP mutation in a C57BL/6xDBA/2xSwiss-Webster background. Of note, the loss of spines was detected only at the age of 3 months in Tg2576 mice expressing the same mutation but in a C57BL6xSJL6 background. More recently, in a study aimed at investigating the time course of entorhinal cortex (EC) dysfunction in AD mice, we measured synaptic activity/plasticity and dendritic spines in 2- and 6-month-old hAPP bearing the FAD Swedish and Indiana APP mutations (Criscuolo et al., 2017). Field potentials recorded in EC superficial Layer II after stimulation of the same layer revealed that input-output curves and LTD were unaltered while LTP was absent in *2-month-old* mutants. Consistent with the LTP deficit, a massive increase in the number of immature thin spines lacking post-synaptic components was observed in the same layer. Interestingly, these synaptic defects were associated with a selective impairment in the EC-dependent novel object-place-context recognition task. At the age of 6 months, all electrophysiological parameters were altered and mice were impaired in all recognition memory tasks, including the simple reactivity to a novel object introduced at the same place and context of a previously explored object). By showing that the LTP deficit precedes impairments in basal transmission and LTD, but associates with spine loss, these *in vivo* observations confirm the aforementioned *in vitro* data (Almeida et al., 2005) that AD synaptic failure initiates by dysregulation of postsynaptic elements. Indeed, abnormalities in PSD cytoskeletal proteins contribute to early spine loss. For example, at the same age, hAPP mice show an enhancement of phosphorylated p38 MAPKinase, a key regulator of pro-inflammatory cytokines involved in multiple aspects of cell physiology including cytoskeleton remodeling (Cuenda and Rousseau, 2007). Even earlier, Kommaddi et al. (2018) report depolymerization of *F*-actin accompanied by increased globular-actin (G-actin) in *1-month-old* APPswe/PS1ΔE9 mice. Confirming the primary role of cytoskeletal, alterations in synaptic deterioration, the levels of the scaffold proteins PSD95 and homer1, and of the glutamate receptor subunit GluA1 are unaltered. Supporting the functional role of *F*-actin in spines, the impairment in contextual fear conditioning (CFC) recall shown by APP/PS1 mice at *2 months* of age was rescued by *in situ* injections of the actin-polymerizing agent jasplakinolide. Although no visualization and measurement of spines were carried out in this model, direct stochastic optical reconstruction microscopy (dSTORM) revealed that *F*-actin depolymerization strongly disrupts the nano-organization of radiating *F*-actin rods in spines imaged on cortical neuron dendrites. The disruptive effect of actin disassembly on the morphology and function of cortical synapses in 2-month-old mutants led the authors to conclude that *F*-actin depolymerization is causal and not consequential to spine disruption (Kommaddi et al., 2018).

Early Symptomatic Stage

Around 3 months of age, all mice bearing hAPP mutations alone or in association with PS1 and Tau mutations show elevated levels of soluble Aβo which significantly impact the structural and plastic properties of spines in key brain regions for cognition. Disruption of hippocampal circuits in 3-month-old APP_{ind} mutants due to synaptic protein alterations was first reported by Hsia et al. (1999). Although dendritic spines were not measured in this study, a deficit in synaptic transmission was associated with a reduction of synaptophysin in presynaptic terminals and in the number of microtubule-associated protein two-positive neurons in the CA1 region revealed that dysfunctions in the PSD protein network were already present in these young mutants. Remarkably, the addition of the Swedish transgene to the Indiana mutation increased synaptic transmission deficits. More recently, evidence has accumulated that 3-month-old hAPP mutants show a reduction in hippocampal and/or cortical spines in association with abnormal caspase-3 accumulation (D'Amelio et al., 2011), *F*-actin disassembly (Kommaddi et al., 2018), or upregulation of full-length APP translation (Borreca et al., 2020). Further support to the link between Aβ-induced alterations in the PSD network and disruption of synaptic plasticity comes from data which show that phosphorylation of the actin-binding protein cofilin-1 (pcof1) is increased in the postsynaptic enriched fraction of cortical synaptosomes of 3-month-old APP/PS1 mice. Complementary immunohistochemical investigations revealed that p-cof1 is increased in cortical spines which otherwise showed larger synaptic areas. The authors conclude that, as in cortical neurons in culture, Aβo-induced excessive stabilization of actin in spines which prevents their plastic remodeling in response to stimuli (Rush et al., 2018). At the same age, mice homozygous for the PS2APP transgene show an abnormal contribution of GluN2B NMDA receptors to hippocampal

synaptic plasticity compared to the wild-type mice (Hanson et al., 2015) while dynamics imaging of spines in the cerebral cortex of APPswe/PS1ΔE9 mice reveals an aberrant enhancement of spine turnover associated with a decrease in the number of persistent spines (Heiss et al., 2017). In the same mice, a reduction in dendritic calcium activity and in the size of spines is detected in the primary motor cortex during quiet resting but not during treadmill running which suggests some form of activity-dependent recovery specific to motor behavior (Bai et al., 2017). Then, consistent with the view that morphological alterations of spines trigger synaptic failure, Androuin et al. (2018) report that spines measured in 3-month-old APP/PS1 knock-in mice exhibit a reduction in length and an enlargement of necks before the diminution of synaptic density in the stratum radiatum layer of the hippocampus. Mathematical modeling of these data suggests that these morphological changes disrupt the electrical compartmentalization of spines and produce a selective diminution of postsynaptic potentials in spine heads required for LTP. This hypothesis is then confirmed experimentally by showing that LTP, but not basal transmission, is impaired in hippocampal slices from these mutant mice.

COGNITIVE ACTIVITY DISCLOSES OR ANTICIPATES OBSERVATION OF Aβ-INDUCED SPINE DISRUPTION

The paradox of studies aimed at investigating structural synaptic plasticity defects in AD mice is that despite data that show that activity-triggered plasticity relates directly to cognitive processing (Kasai et al., 2010), spines in AD mouse models have scarcely been examined under cognitive challenge. If memory requires changes in neuronal networks based on modifications in strength and number of synapses, better characterization of synaptic defects underlying memory dysfunction in AD mice are expected to emerge during or immediately after mice are asked to form memories. Because the state of activation of synapses affects Aβ homeostasis (Cirrito et al., 2005; Tampellini, 2015) which, in turn, increases Aβo secretion and depresses excitatory synaptic transmission, it is of primary importance determining which age cognitive activity-induced release of Aβo starts to impact synapses in hAPP mutants, and how brain circuits reorganize to contrast early synaptic dysfunctions.

APP 23 Mice Show Regular Hippocampal Spines at Rest but Form More Training-Induced Spines

Middei et al. (2010) provided the first evidence that training produces compensatory reshaping of memory circuits in a mouse model of AD. Seven-month-old APP23 mice trained in a water maze were found to travel a longer distance to find the submerged platform compared to wild-type mice. After the experiments, mice were sacrificed to evaluate the impact of spatial training on dendritic spines and synaptic plasticity in the hippocampus. Spine density did not differ between mutant mice and wild-type mice in the control cage and pseudo-training conditions. In the training condition, all mice showed a posttraining increase in spines which indicates that reactive plasticity was spared by the mutation. The increase in spines was, however, stronger in the mutant mice than in the wild-type mice. Synaptic plasticity measured in slices from pseudo-trained mice revealed no difference in LTP induction and maintenance between genotypes. In slices from trained mice, LTP was regularly induced in both genotypes but decayed more rapidly in the mutant mice. These findings reveal that hAPP circuits are unaltered in non-training conditions but undergo compensatory stronger remodeling in training conditions to sustain a less efficient, likely more effortful, cognitive performance. Thus, if more spines are formed in trained mutant mice to compensate for the disruptive effect of training-induced Aβo release at hippocampal synapses, it could be the decay in LTP maintenance depends on the training mobilization of more synapses which reduces the pool of synapses available for LTP.

Cognitive Activity Enhances Aβ Release in the Hippocampus of 2-Month-Old Tg2576 Mice and Prevents the Learning-Induced Formation of Spines

We previously reported that 2-month-old Tg2576 show intact density and morphology of hippocampal spines at rest, and regular CFC when returned 1 day after to the safety training context (D'Amelio et al., 2011). Measurements of spines in the CFC circuitry upon CFC recall reveal however that, differently from wild-type mice, Tg2576 mice do not show any increase in mushroom spines in the CA1 region of the hippocampus. Conversely, both wild-type and Tg2576 mice show an increase in mushroom spines in the BLA region of the amygdala, but the presence of an additional increase in BLA thin spines in Tg2576 mice indicates more substantial BLA rewiring in the mutant mice. Dot blot quantification of Aβlevels in each region 24 h after CFC encoding reveals that lack of CFC-induced hippocampal spines in the mutant mice can be ascribed to the selective vulnerability of their hippocampus to the activity-induced release of Aβo. Western blot analyses carried out using the N terminal-specific-anti Aβ antibody AD54D2, and the C terminal-specific anti-Aβ42 antibodies (clone 295F2) confirmed that the Aβ signal was selectively increased in the hippocampus, but not in the amygdala, in CFC-trained Tg2576 mice. Importantly, the observation that the hippocampal rise of Aβ42 returns to wild-type levels 48 h after the conditioning reveals its transitory nature as well as its suitability to be relaunched by further cognitive activity It is therefore likely that multiple transient episodes of Aβo release triggered every time presymptomatic mice face cognitive tasks can be the starting points of synaptic failure which aggravates over time.

Neuroinflammation Mediates Structural Plasticity Impairments in Preclinical APPswe/PS1δE9 Mice

Around 4/5 months of age, APPswe/PS1δE9 (δE9) mice exhibit amyloid plaques but do not manifest cognitive alterations

and, hence, can be considered as a preclinical model of AD. Using an *in vivo* two-photon microscopy, Zou et al. (2015) imaged spines in the sensory-motor cortex of δE9 mice at rest and found that, consistent with their normal cognitive state, these mice show a large number of intact spines far from the plaques zone. The same authors (Zou et al., 2016) reported however that, at the same age, these mice exhibit a strong deficit in experience-dependent structural plasticity. Specifically, they fail to increase in dendritic spine density following rearing in an enriched environment (EE) and to stabilize these newly formed connections over time. Because amyloid plaques are present at this age point, reduction of BACE1 activity obtained by crossing δE9 with BACE1-KO mice decreased the amyloid burden and restored EE-induced spine formation but did not improve spine stabilization. Differently, the anti-inflammatory drug pioglitazone or the interleukin-1 receptor antagonist IL-1 RA entirely rescued the formation and stabilization of spines suggesting that neuroinflammation phenomena, independent from those triggered by the presence of amyloid plaques, are present in cognitively intact mutants and strongly impair experience-dependent structural plasticity.

UPSTREAM TO Aβo: ROLE OF THE UPREGULATION OF FULL-LENGTH APP TRANSLATION IN AD ONSET

Close correlations between Aβo release, dysregulation of cytoskeletal proteins like *F*-actin, and disruption in shape, density, and plasticity of spines provide mechanistic interpretations for early synapse destabilization but also give insights into the primary causes of degeneration. In particular, if the formation of Aβo is consequential to pathogenic APP cleavage, the events that trigger the unbalance in favor of amyloid APP processing are likely to contribute to the disease onset. Among those, evidence that upstream to its abnormal proteolysis, full-length APP is overexpressed in familiar (Johnston et al., 1994; Vignini et al., 2013) and sporadic (Matsui et al., 2007) AD patients, and in their respective murine models (Howlett and Richardson, 2009) is getting an increased interest.

This point was early taken by Lanz et al. (2003) who underlined that the developmental effects of APP overexpression on the early loss of spines cannot be ruled out. Interestingly, a longitudinal evaluation of hAPPmRNA and APP levels in the Tg2576 hippocampus revealed that the messenger and the protein are maximally expressed in cognitively asymptomatic 1-month-old mutants (Borreca et al., 2016). This elevation associates with reduced expression of the Fragile-X Mental Retardation Protein (FMRP) and augmented expression of the heteronuclear Ribonucleoprotein C (hnRNP C), two RNA bindings proteins (RBPs) which, in healthy conditions, repress and increase APP translation and expression respectively. The recent observation that polysomal APP mRNA and protein signals associate with decreased levels of the phosphorylated form of initial translation factor eIF2α, a blocker of overall translation, in 1- and 3-month-old Tg2576 mice further indicates that abnormally increased translational mechanisms sustain presymptomatic upregulation of hAPP levels in this model. Confirming that upregulation of translation contributes to AD pathogenesis, pharmacological (salubrinal) restoration of proper translational control in early symptomatic 3-month-old Tg2576 mice reverts structural and functional alterations including spine loss and prevalent LTD at CA1 hippocampal synapses, downregulates their increased levels of the β-secretase enzyme BACE-1, one main determinant of amyloidogenic APP processing, and prevents the manifestation of cognitive alterations (Borreca et al., 2020). Consistent with these findings, compounds like MMP13 (Zhu et al., 2019), which regulates BACE-1 translation, or posiphen, which decreases the production of toxic Aβ by lowering APP translation, are effective in rescuing cognitive deficits in hAPP mutant mice (Lahiri et al., 2007) and sporadic AD patients (Teich et al., 2018). Together, these data suggest that the dysregulation of APP cleavage whose Aβo formation and spines deterioration are the earliest manifestations could largely depend on the abnormal amount of full-length APP to be cleaved at early stages of development.

CONCLUSION

The data presented in this short review show that structural and functional degradation of spines mediates the earliest signs of synaptic failure in hAPP mutants and that analyzing the molecular dysfunctions at the origin of spine alterations unveils primary causes of degeneration. Two points in the reported studies need, however, special consideration.

In the AD models examined, synaptic failure is detected as soon as circulating Aβo is present in their brains. Indeed, the causal link between synaptic failure and Aβo is supported by data showing that a majority of molecular dysfunctions which negatively impact dendritic spines in young hAPP mutants (e.g., kalirin-7 disruption) are also observed in wild-type neurons exposed to Aβo alone. Nevertheless, other neurotoxic peptides derived from APP processing like Carboxyl-terminal fragments (Lauritzen et al., 2019), the AICD-amyloid precursor protein intracellular domain (Konietzko, 2012) or the secreted APP ectodomain- sAPPα and (Ishida et al., 1997) which impact synaptic plasticity and are increasingly detected in early AD patients (Perneczky et al., 2013, 2014) could also be involved. Moreover, hAPP mutations in the reported studies were often associated with PS1 mutations suggesting a role for this peptide independent from the facilitation it exerts on APP processing (Thinakaran, 1999).

Of particular relevance among the reviewed data is the observation that cognitively challenged AD mice show synaptic alterations that are undetectable in resting conditions. *In vitro* evidence that neuronal activity increases the formation and release of Aβ peptides in hippocampal neurons overexpressing APP which then shows impairment in excitatory synaptic transmission (Kamenetz et al., 2003) provides a plausible explanatory framework. However, *in vivo* evidence (Pignataro et al., 2019) that cognitive activity enhances Aβ release

in the hippocampus of 2-month-old Tg2576 mice and prevents the learning-induced formation of spines in this region indicates that contrary to the beneficial effect of diffuse EE-related sensorial/social stimulation on cognition, focused cognitive activity increases Aβ load in regions supporting high cognitive functions which accelerates the cognitive decline. This aspect should be carefully considered in designing cognitive stimulation protocols aimed at preventing cognitive deterioration at the onset of mild cognitive impairments.

AUTHOR CONTRIBUTIONS

The author confirms being the sole contributor of this work and has approved it for publication.

FUNDING

This work was supported by the National Research Council of Italy (AGESPAN Project to MA-T) and IRCCS Santa Lucia Foundation.

REFERENCES

Abdul, H. M., Sama, M. A., Furman, J. L., Mathis, D. M., Beckett, T. L., Weidner, A. M., et al. (2009). Cognitive decline in Alzheimer's disease associated with selective changes in the calcineuro/NFAT signaling. *J. Neurosci.* 29, 12957–12969. doi: 10.1523/JNEUROSCI.1064-09.2009

Almeida, C. G., Tampellini, D., Takahashi, R. H., Greengard, P., Lin, M. T., Snyder, E. M., et al. (2005). Beta-amyloid accumulation in APP mutant neurons reduces PSD-95 and GluR1 in synapses. *Neurobiol. Dis.* 20, 187–198. doi: 10.1016/j.nbd.2005.02.008

Androuin, A., Potier, B., Nägerl, U. V., Cattaert, D., Danglot, L., Thierry, M., et al. (2018). Evidence for altered dendritic spine compartmentalization in Alzheimer's disease and functional effects in a mouse model. *Acta Neuropathol.* 135, 839–854. doi: 10.1007/s00401-018-1847-6

Aoki, C., and Sherpa, A. D. (2017). Making of a synapse: recurrent roles of drebrin a at excitatory synapses throughout life. *Adv. Exp. Med. Biol.* 1006, 119–139. doi: 10.1007/978-4-431-56550-5_8

Bai, Y., Li, M., Zhou, Y., Ma, L., Qiao, Q., Hu, W., et al. (2017). Abnormal dendritic calcium activity and synaptic depotentiation occurs early in a mouse model of Alzheimer's disease. *Mol. Neurodegener.* 12:86. doi: 10.1186/s13024-017-0228-2

Beckman, D., Ott, S., Donis-Cox, K., Janssen, W. G., Bliss-Moreau, E., Rudebeck, P. H., et al. (2019). Oligomeric Aβ in the monkey brain impacts synaptic integrity and induces accelerated cortical aging. *Proc. Natl. Acad. Sci. U S A* 116, 26239–26246. doi: 10.1021/jacs.7b12124.s001

Borreca, A., Gironi, K., Amadoro, G., and Ammassari-Teule, M. (2016). Opposite dysregulation of fragile-X mental retardation protein and heteronuclear C ribonucleoprotein protenin associates with enhanced APP translation in Alzheimer disease. *Mol. Neurobiol.* 53, 3227–3323. doi: 10.1007/s12035-015-9229-8

Borreca, A., Valeri, F., De Luca, M., Ernst, L., Russo, A., Nobili, A., et al. (2020). Transient upregulation of translational efficiency in podromal and early symptomatic Tg2576 mice contributes to Aβ pathology. *Neurobiol. Dis.* 139:104787. doi: 10.1016/j.nbd.2020.104787

Cirrito, J. R., Yamada, K. A., Finn, M. B., Sloviter, R. S., Bales, K. R., May, P. C., et al. (2005). Synaptic activity regulates interstitial fluid amyloid-beta levels *in vivo*. *Neuron* 48, 913–922. doi: 10.1016/j.neuron.2005.10.028

Cline, E. N., Bicca, M. A., Viola, K. L., and Klein, W. L. (2018). The amyloid-β oligomer hypothesis: beginning of the third decade. *J. Alzheimer's Dis.* 64, S567–S610. doi: 10.3233/JAD-179941

Criscuolo, C., Fontebasso, V., Middei, S., Stazi, M., Ammassari-Teule, M., Yan, S. S., et al. (2017). Entorhinal cortex dysfunction can be rescued by inhibition of microglial RAGE in an Alzheimer's disease mouse model. *Sci. Rep.* 7:42370. doi: 10.1038/srep42370

Cuenda, A., and Rousseau, S. (2007). p38 MAP-kinases pathway regulation, funciton and role in human diseases. *Biochem. Biophys. Acta* 1773, 1358–1375. doi: 10.1016/j.bbamcr.2007.03.010

D'Amelio, M., Cavallucci, V., Middei, S., Marchetti, C., Pacioni, S., Ferri, A., et al. (2011). Casapse-3 triggers early synaptic dysfunction in a mouse model of Alzheimer disease. *Nat. Neurosci.* 14, 69–76. doi: 10.1038/nn.2709

Gong, Y., and Lippa, C. F. (2010). Review: disruption of the postsynaptic density in Alzheimer's disease and other neurodegenerative dementia. *Am. J. Alzheimers Dis. Other Dem.* 25, 547–555. doi: 10.1177/1533317510382893

Hanson, J. E., Pare, J.-F., Deng, L., Smith, Y., and Zhou, Q. (2015). Altered GluN2B NMDA receptor function and synaptic plasticity during early pathology in the PS2APP mouse model of Alzheimer's disease. *Neurobiol. Dis.* 74, 254–262. doi: 10.1016/j.nbd.2014.11.017

Heiss, J. K., Barrett, J., Yu, Z., Haas, L. T., Kostylev, M. A., and Strittmatter, S. M. (2017). Early activation of experience-independent dendritic spine turnover in a mouse model of Alzheimer is disease. *Cereb. Cortex.* 27, 3660–3674. doi: 10.1093/cercor/bhw188

Howlett, D. R., and Richardson, J. C. (2009). The pathology of APP transgenic mice: a model of Alzheimer's disease or simply overexpression of APP? *Histol. Histopathol.* 24, 83–100. doi: 10.14670/HH-24.83

Hsia, A. Y., Masliah, E., McColongue, L., Yu, G. Q., Tatsuno, G., Hu, K., et al. (1999). Plaque-independent disruption of neural circuits in Alzheimer's disease mouse models. *Proc. Natl. Acad. Sci. U S A* 96, 3228–3233. doi: 10.1073/pnas.96.6.3228

Hsiao, K., Chapman, P., Nilsen, S., Eckman, C., Harigaya, Y., and Younkin, S. (1996). Correlative memory deficits, abeta elevation and amyloid plaques in transgenic mice. *Science* 274, 99–102. doi: 10.1126/science.274.5284.99

Ishida, A., Furukawa, F., Keller, J. N., and Mattson, M. P. (1997). Secreted form of beta-amyloid precursor protein shifts the frequency dependency for induction of LTD and enhances LTP in hippocampal slices. *Neuroreport* 8, 2133–2137. doi: 10.1097/00001756-199707070-00009

Johnston, J. A., Cowburn, R. F., Norgren, S., Wiehager, B., Venizelos, N., Winblad, B., et al. (1994). Increased beta-amyloid release and levels of amyloid precursor protein (APP) in fibroblast cell lines from family members with the swedish Alzheimer's disease APP670/671 mutation. *FENS Lett.* 354, 274–278. doi: 10.1016/0014-5793(94)01137-0

Kamenetz, F., Tomita, T., Hsieh, H., Seabrook, G., Borchelt, D., Iwatsubo, T., et al. (2003). APP processing and synaptic function. *Neuron* 37, 925–937. doi: 10.1016/s0896-6273(03)00124-7

Kasai, H., Fukuda, M., Watanabe, S., Hayashi-Takagi, A., and Noguchi, J. (2010). Structural dynamics of dendritic spines in memory and cognition. *Trends Neurosci.* 33, 121–129. doi: 10.1016/j.tins.2010.01.001

Kommaddi, R. P., Das, D., Karunakaran, S., Nanguneri S. Bapat, D., Ray A. Shaw, E., Bennett, D. A., et al. (2018). Aβ mediates F-actin disassemby in dendritic spines leading to cognitive deficits in Alzheimer's disease. *J. Neurosci.* 38, 1085–1099. doi: 10.1523/JNEUROSCI.2127-17.2017

Konietzko, U. (2012). AICD nuclear signaling and its possible contribution to Alzheimer's disease. *Curr. Alzheimer Res.* 9, 200–216. doi: 10.2174/156720512799361673

Lacor, P. N., Buniel, M. C., Furlow, P. W., Clemente, A. S., Velasco, P. T., Wood, M., et al. (2007). Aβ oligomer-induced aberrations in synapse composition, shape and density provide a molecular basis for loss of connectivity in Alzheimer's disease. *J. Neurosci.* 27, 796–807. doi: 10.1523/jneurosci.3501-06.2007

Lahiri, D. K., Chen, D., Maloney, B., Holloway, H. W., Yu, Q. S., Utsuki, T., et al. (2007). The experimental Alzheimer's disease drug posiphen [(+)-phenserine] lowers amyloid-beta peptide levels in cell culture and mice. *J. Pharmacol. Exp. Ther.* 320, 386–396. doi: 10.1124/jpet.106.112102

Lambert, J. C., Pasquier, F., Cottel, D., Frigard, B., Amouyel, P., and Charter-Harlin, M. C. (1998). A new polymorphism in the APOE promoter associated with risk of developing Alzheimer's disease. *Hum. Mol. Genet.* 7, 533–540. doi: 10.1093/hmg/7.3.533

Lanz, T. A., Carter, D. B., and Merchant, K. M. (2003). Dendritic spine loss in the hippocampus of young PDAPP and Tg2576 mice and its prevention by the ApoE2 genotype. *Neurobiol. Dis.* 13, 246–253. doi: 10.1016/s0969-9961(03)00079-2

Lauritzen, I., Pardossi-Piquard, R., Bourgeois, A., Bécot, A., and Checler, F. (2019). Does intraneuronal accumulation of carboxyl-terminal fragments of the amyloid protein precursor trigger early neurotoxicity in Alzheimer's disease? *Curr. Alzheimer Res.* 16, 453–457. doi: 10.2174/1567205016666190325092841

Lee, K. F. H., Soares, C., and Beique, J. C. (2012). Examining form and function of dendritic spines. *Neural Plast.* 2012:704103. doi: 10.1155/2012/704103

Llorens-Martin, M., Blazquez-Llorca, L., Benavidess-Piccione, R., Rabano, A., Hernandez, F., Avila, J., et al. (2014). Selective alterations of neurons and circuits related to early memory loss in Alzheimer's disease. *Front. Neuroanat.* 8:38. doi: 10.3389/fnana.2014.00038

Maezawa, I., Zimin, P. I., Wulff, H., and Jin, L. W. (2011). Amyloid-beta protein oligomers at low nanomolar concentrations activate microglia and induce microglial neurotoxicity. *J. Biol. Chem.* 286, 3693–3706. doi: 10.1074/jbc.m110.135244

Matsui, T., Ingelsson, M., Fukumoto, H., Ramasamy, K., Kowa, H., Frosch, M. P., et al. (2007). Expression of APP pathway mRNAs and proteins in Alzheimer's disease. *Brain Res.* 1161, 116–123. doi: 10.1016/j.brainres.2007.05.050

Middei, S., Roberto, A., Berretta, N., Panico, M. B., Lista, S., Bernardi, G., et al. (2010). Learning discloses abnormal structural and functional plasticity at hippocampal synapses in the APP23 mouse model of Alzheimer's disease. *Learn. Mem.* 17, 236–240. doi: 10.1101/lm.1748310

Mucke, L., Masliah, E., Yu, G. Q., Mallory, M., Rockenstein, E. M., Tatsuno, G., et al. (2000). High-level neuronal expression of abeta 1-42 in wild-type human amyloid protein precursor transgenic mice: synaptotoxicity without plaque formation. *J. Neurosci.* 20, 4050–4058. doi: 10.1523/jneurosci.20-11-04050.2000

Neniskyte, U., Neher, J. J., and Brown, G. C. (2011). Neuronal death induced by nanomolar amyloid β is mediated by primary phagocytosis od neurons by microglia. *J. Biol. Chem.* 286, 39904–39913. doi: 10.1074/jbc.M111.267583

Ortiz-Sanz, C., Gamindo-Blasco, A., Valero, J., Batoka, L., Brandt, R., Zugaza, J. L., et al. (2020). Early effects of Aβ oligomers on dendritic spine dynamics and arborization in hippocampal neurons. *Front. Synaptic Neurosci.* 12:2. doi: 10.3389/fnsyn.2020.00002

Penazzi, L., Tackenberg, C., Ghon, A., Golovyahskina, N., Niewidok, B., Selle, K., et al. (2016). Aβ-mediated spine changes in the hippocampus are microtubule-dependent and can be reversed by a subnanomolar concentration of the microtubule-stabilizing agent epothilone D. *Neuropharmacology* 105, 84–95. doi: 10.1016/j.neuropharm.2016.01.002

Perneczky, R., Alexopoulos, P., and Kurz, A. (2014). Soluble amyloid precursor proteins and secretases as Alzheimer's disease biomarkers. *Trends Mol. Med.* 20, 8–15. doi: 10.1016/j.molmed.2013.10.001

Perneczky, R., Guo, L. H., Kagerbauer, S. M., Werle, L., Kurz, A., Martine, J., et al. (2013). Soluble amyloid precursor protein β as blood-based biomarker of Alzheimer disease. *Transl. Psychiatry* 3:e227. doi: 10.1038/tp.2013.11

Pignataro, A., Meli, G., Pagano, R., Fontebasso, V., Battistella, R., Conforto, G., et al. (2019). Activity-induced amyloid β oligomers drive compensatory synaptic rearrangements in brain circuits controlling memory of presymptomatic Alzheimer's disease mice. *Biol. Psychiatry* 86, 185–195. doi: 10.1016/j.biopsych.2018.10.018

Renner, M., Lacor, P. N., Velasco, P. T., Xu, J., Contractor, A., Klein, W. L., et al. (2010). Deleterious effects of amyloid beta oligomers activity as an extracellular scaffold mGluR5. *Neuron* 66, 739–754. doi: 10.1016/j.neuron.2010.04.029

Rochefort, N., and Konnerth, A. (2012). Dendritic spines: from structures to *in vivo* function. *EMBO Rep.* 13, 699–708. doi: 10.1038/embor.2012.102

Roselli, F., Hutzler, P., Wegerich, Y., Livrea, P., and Almeida, O. F. X. (2009). Disassembly of shank and homer synaptic clusters is driven by soluble beta-amyloid$_{(1-40)}$ through divergent NMADAR-dependent pathways. *PLoS One* 4:e6011. doi: 10.1371/journal.pone.0006011

Roselli, F., Tirard, M., Lu, J., Hutzler, P., Lamberti, P., Livrea, P., et al. (2005). Soluble beta-amyloid$_{1-40}$ induces NMDA-dependent degradation of postsynaptic density-95 at glutamatergic synapses. *J. Neurosci.* 25, 11061–11070. doi: 10.1523/jneurosci.3034-05.2005

Rush, T., Martinez-Hernandez, J., Dollmeyer, M., Frandemiche, M. L., Borel, E., Boisseau, S., et al. (2018). Synaptotoxicity in Alzheimer's disease involved a dysregulation of actin cytoskeleton dynamics through cofilin-1 phosphorylation. *J. Neurosci.* 38, 10349–10361. doi: 10.1523/JNEUROSCI.1409-18.2018

Selkoe, D. J. (2002). Alzheimer's disease is a synaptic failure. *Science* 298, 789–791. doi: 10.1126/science.1074069

Shankar, G. M., Bloodgood, B. L., Townsend, M., Walsh, D. M., Selkoe, D. J., and Sabatini, B. L. (2007). Natural oligomers of the Alzheimer amyloid-beta protein induce reversible synapse loss by modulating an NMDA-type glutamate receptor-dependent signaling pathway. *J. Neurosci.* 27, 2866–2875. doi: 10.1523/JNEUROSCI.4970-06.2007

Tackenberg, C., Ghori, A., and Brandt, R. (2009). Thin, stubby or mushroom: spine pathology in Alzheimer's disease. *Curr. Alzheimer Res.* 6, 261–268. doi: 10.2174/156720509788486554

Tampellini, D. (2015). Synaptic activity and Alzheimer's disease: a critical update. *Front. Neurosci.* 9:423. doi: 10.3389/fnins.2015.00423

Teich, A. F., Sharma, E., Barnwell, E., Zhang, H., Staniszewski, A., Utsuki, T., et al. (2018). Translational inhibition of APP by posiphen: efficacy, pharmacodynamics and pharmacokinetics in the APP/PS1 mouse. *Alzheimers Dement.* 4, 37–45. doi: 10.1016/j.trci.2017.12.001

Thinakaran, G. (1999). The role of presenilins in Alzheimer's disease. *J. Clin. Invest.* 104, 1321–1327. doi: 10.1172/JCI8728

Tønnesen, U., and Nägerl, U. V. (2016). Dendritic spines as tunable regulators of synaptic signals. *Front. Psychiatry* 7:101. doi: 10.3389/fpsyt.2016.00101

Tu, S., Okamoto, S., Lipton, S. A., and Xu, H. (2014). Oligomeric Aβ-induced synaptic dysfunction in Alzheimer's disease. *Mol. Neurodegener.* 9:48. doi: 10.1186/1750-1326-9-48

Varga, Z., Jia, H., Sakmann, B., and Konnerth, A. (2011). Dendritic coding of multiple sensory inputs in single cortical neurons *in vivo*. *Proc. Natl. Acad. Sci. U S A* 108, 15420–15425. doi: 10.1073/pnas.1112355108

Vignini, A., Morganti, S., Salvolini, E., Sartini, D., Luzzi, S., Fiorini, R., et al. (2013). Amyloid precursor protein expression is enhanced in human platelets from subjects with Alzheimer's disease and frontotemporal lobe degeneration: a real-time PCR study. *Exp. Gerontol.* 48, 1505–1518. doi: 10.1016/j.exger.2013.10.008

Wei, W., Nguyen, L. N., Kessels, H. W., Hagiwara, H., Sisodia, S., and Malinow, R. (2010). Amyloid beta from axons and dendrites reduces local spine number and plasticity. *Nat. Neurosci.* 12, 190–196. doi: 10.1038/nn.2476

Wu, H. Y., Hudry, E., Hashimoto, T., Kuchibhotla, K., Rozkalne, A., Fan, Z., et al. (2010). Amyloid beta induces the morphological neurodegenerative triad of spine loss, dendrite semplification and neuritic dystrophies through calcineurin activation. *J. Neurosci.* 30, 2636–2649. doi: 10.1523/jneurosci.4456-09.2010

Xie, Z., Shapiro, L. P., Cahill, M. E., Russel, T. A., Lacor, P. N., Klein, W. L., et al. (2019). Kalirin-7 prevents dendritic spine dysgenesis induced by amyloid beta-derived oligomers. *Eur. J. Neurosci.* 49, 1091–1101. doi: 10.1111/ejn.14311

Yu, W., and Lu, B. (2012). Synapses and dendrtic spines as pathogenic targets in Alzheimer's disease. *Neural Plast.* 2012:247150. doi: 10.1155/2012/247150

Yuste, R., Majewska, A., and Holthoff, K. (2000). From form to function: calcium compartmentalization in dendritic spines. *Nat. Neurosci.* 3, 653–659. doi: 10.1038/76609

Zhu, B. L., Long, Y., Luo, W., Yan, Z., Lai, Y. J., Zhao, L. G., et al. (2019). MMP13 inhibition rescues cognitive decline in Alzheimer transgenic mice *via* BACE1 regulation. *Brain* 142, 176–192. doi: 10.1093/brain/awy305

Zou, C., Montagna, E., Shi, Y., Peters, F., Blazquez-Llorca, L., Shi, S., et al. (2015). Intraneuronal APP and extracellular Aβ independently cause dendritic spine pathology in transgenic mouse models of Alzheimer's disease. *Acta Neuropathol.* 129, 909–920. doi: 10.1007/s00401-015-1421-4

Zou, C., Shi, Y., Ohli, J., Schuller, U., Dorostkar, A. A., and Herms, J. (2016). Neuroinflammation impairs adaptive structural plasticity of dendritic spines in a preclinical model of Alzheimer's disease. *Acta Neuropathol.* 131, 235–246. doi: 10.1007/s00401-015-1527-8

Conflict of Interest: The author declares that the research was conducted in the absence of any commercial or financial relationships that could be construed as a potential conflict of interest.

frontiers in Synaptic Neuroscience

MINI REVIEW
published: 30 September 2020
doi: 10.3389/fnsyn.2020.00031

Dendritic Spines Shape Analysis—Classification or Clusterization? Perspective

Ekaterina Pchitskaya[1]* *and Ilya Bezprozvanny*[1,2]*

[1]*Laboratory of Molecular Neurodegeneration, Institute of Biomedical Systems and Biotechnology, Peter the Great St. Petersburg Polytechnic University, St. Petersburg, Russia,* [2]*Department of Physiology, UT Southwestern Medical Center at Dallas, Dallas, TX, United States*

Dendritic spines are small protrusions from the dendrite membrane, where contact with neighboring axons is formed in order to receive synaptic input. Changes in size, shape, and density of synaptic spines are associated with learning and memory, and observed after drug abuse in a variety of neurodegenerative, neurodevelopmental, and psychiatric disorders. Due to the preeminent importance of synaptic spines, there have been major efforts into developing techniques that enable visualization and analysis of dendritic spines in cultured neurons, in fixed slices and in intact brain tissue. The classification of synaptic spines into predefined morphological groups is a standard approach in neuroscience research, where spines are divided into fixed categories such as thin, mushroom, and stubby subclasses. This study examines accumulated evidence that supports the existence of dendritic spine shapes as a continuum rather than separated classes. Using new approaches and software tools we reflect on complex dendritic spine shapes, positing that understanding of their highly dynamic nature is required to perform analysis of their morphology. The study discusses and compares recently developed algorithms that rely on clusterization rather than classification, therefore enabling new levels of spine shape analysis. We reason that improved methods of analysis may help to investigate a link between dendritic spine shape and its function, facilitating future studies of learning and memory as well as studies of brain disorders.

Keywords: dendritic spines, neuronal morphology, mushroom spine, thin spine, stubby spine, classification, clusterization

OPEN ACCESS

Edited by:
Carlo Sala,
Institute of Neuroscience (CNR), Italy

Reviewed by:
Maurizio Giustetto,
University of Turin, Italy
Katharine R. Smith,
University of Colorado Denver, United States

***Correspondence:**
Ekaterina Pchitskaya
katrincreative@yandex.ru
Ilya Bezprozvanny
ilya.bezprozvanny@utsouthwestern.edu

Received: *28 April 2020*
Accepted: *02 July 2020*
Published: *30 September 2020*

Citation:
Pchitskaya E and Bezprozvanny I (2020) Dendritic Spines Shape Analysis—Classification or Clusterization? Perspective. Front. Synaptic Neurosci. 12:31. doi: 10.3389/fnsyn.2020.00031

INTRODUCTION

Dendritic spines are tiny protrusions from dendrites, which form functional contacts with neighboring axons of other neurons (Smith et al., 2014). Dendritic spines are very plastic and their size and shape are constantly changing in response to neuronal activity. Complex machinery composed of various signaling molecules and cascades maintains the unique structure and function of dendritic spines (Yasuda, 2017; Nakahata and Yasuda, 2018). Dendritic spine shape is controlled by the actin cytoskeleton. A characteristic feature of excitatory spines is a postsynaptic density (PSD), which is visible on electron microphotographs. PSD consist of densely packed ion channels, receptors, and kinases/phosphatases anchored by scaffolding proteins. Learning and memory formation processes are tightly linked to remodeling or elimination of

existing dendritic spines and formation of new ones, which enables modulation of information transfer efficiency between neurons (Yang et al., 2014; Segal, 2017; Chidambaram et al., 2019; Stein and Zito, 2019). For example, motor learning induces rapid growth of new dendritic spines at mice contralateral motor cortex neurons, and subsequent elimination of spines existing before training, so the overall spine density is relatively constant (Xu et al., 2009). For all these reasons, dendritic spines are believed to serve as sites for memory formation and storage, initiating memory consolidation through mechanisms of potentiation and depression of synaptic activity (Zhou et al., 2004; Bourne and Harris, 2007; Kasai et al., 2010; Bailey et al., 2015).

Changes in dendritic spines were detected after being subject to various stimuli, including drug administration (Barrientos et al., 2018), hypoxia (Saraceno et al., 2012), environmental changes (Ashokan et al., 2018), neurodevelopmental (Nishiyama, 2019), neurodegenerative (Herms and Dorostkar, 2016) and psychiatric diseases (Penzes et al., 2011) and many others. Neurodegenerative disorders are characterized by synapse loss and dendritic spine abnormalities in the brain region associated with the disease. For example, Alzheimer's disease is known to be accompanied by dendritic spine shrinkage and elimination in the hippocampal and cortexes areas, which is proposed to start before any clinical evidence of the disease, like cognitive decline and memory dysfunction, manifests (Tackenberg et al., 2009; Boros et al., 2017). Genetic neurodegenerative disorder Huntington's disease is characterized by synapse loss in the striatal brain region, which is linked with progressive movement discoordination (Nithianantharajah and Hannan, 2013). In contrast, autism spectrum disorders are characterized by a significant increase in spine density on various brain areas, including frontal, temporal, and parietal lobes and lateral nucleus of the amygdala (Nishiyama, 2019). Compared with healthy subjects, patients with Fragile X syndrome have elevated numbers of dendritic protrusions in the cingulate, temporal, and visual cortex with prevalence of immature one (Bagni and Zukin, 2019; Nishiyama, 2019). The balance between spine appearance, maturation, elimination, and plasticity is critical for proper brain function. Methods for analyzing and understanding the morphology of dendritic spines are critically important for many fields of neuroscience. In this mini-review article, we discuss recent developments, approaches, and software tools that facilitate analysis of complex dendritic spine morphology on microscopic images obtained from cultured neurons, fixed brain slices, and intact brain tissue.

DENDRITIC SPINES SHAPE CLASSIFICATION AND ITS LIMITATIONS

A synapse is a zone of specialized contact between two neurons, serving to transmit information from cell to cell. Most synapses are formed between the axonal bouton and the dendritic spine, which is a specialized protrusion from the dendritic membrane. Dendritic spines come in a variety of shapes and sizes, differing greatly across brain areas, cell types, and animal species (Ghani et al., 2017). During structural analysis dendritic spines are traditionally grouped into four fixed classes according to their morphological features reflecting head and neck properties: mushroom, thin, stubby, and filopodia (**Figure 1**). Mushroom spines have a large head and a small neck, separating them from a dendrite. They form strong synaptic connections, have the longest lifetime, and therefore are thought to be sites of long-term memory storage (Hayashi and Majewska, 2005; Bourne and Harris, 2007). Thin spines have a structure similar to the mushroom spines, but their head is smaller relative to the neck. They are more dynamic than mushroom spines and believed to be "learning spines," responsible for forming new memories during the synaptic plasticity process, accompanied by head enlargement (Hayashi and Majewska, 2005; Bourne and Harris, 2007). Stubby spines typically do not have a neck. They are known to be the predominant type in the early stages of postnatal development but are also found in small amounts in adulthood, where they are likely formed due to the disappearance of mushroom spines (Hering and Sheng, 2001). Filopodia are long, thin dendritic membrane protrusions without a clear head, commonly observed in developing neurons. These spines may also be found in mature neurons, but under specific conditions, for example, induction of plasticity after different types of brain injury (Yoshihara et al., 2009). Compared to other types of dendritic spines, filopodia are very mobile and flexible structures with a short lifetime. On electron micrographs, filopodia in most cases do not have PSD and the neighboring axonal terminal contain only a few synaptic vesicles, indicating that they are not likely to form functional synapses. Because of this, filopodia are usually excluded from spine counts during synaptic density calculation (Berry and Nedivi, 2017). There are also additional spine shape classes which have been named by different research groups such as branched and cup-shaped spines (Maiti et al., 2015), but they are not widely used in the field.

Classification of spines into the mushroom, thin, and stubby was initially performed manually, but this is a very labor-intensive process that is prone to subjective errors. Multiple segmentation and classification algorithms were developed to automatize this process, making it faster, easier, and with minimal bias introduced by an experimenter. Classification is performed using a decision tree based on the estimation of several key parameters, such as the size of the spine head, and the ratio of head to the neck, are the most popular approaches, implemented in a variety of software packages available for free and commercially (Koh et al., 2002; Rodriguez et al., 2008; Son et al., 2011; Swanger et al., 2011; Risher et al., 2014; Basu et al., 2016, 2018; Dickstein et al., 2016). Alternative approaches were developed, based on semi-supervised learning (Shi et al., 2014) and classification in the likelihood ratio space using shape and appearance features characterizing dendritic spine morphology (Ghani et al., 2017).

Despite its wide use, the classification approach described above has serious limitations. The transition between mushroom, thin and stubby spine subtypes occurs abruptly in the classification, but in reality, there is a continuum of spines shapes and sizes (Yuste and Bonhoeffer, 2004; Berry and Nedivi, 2017). This statement is supported by research data about spine morphology organization, examining live and fixed brain tissue

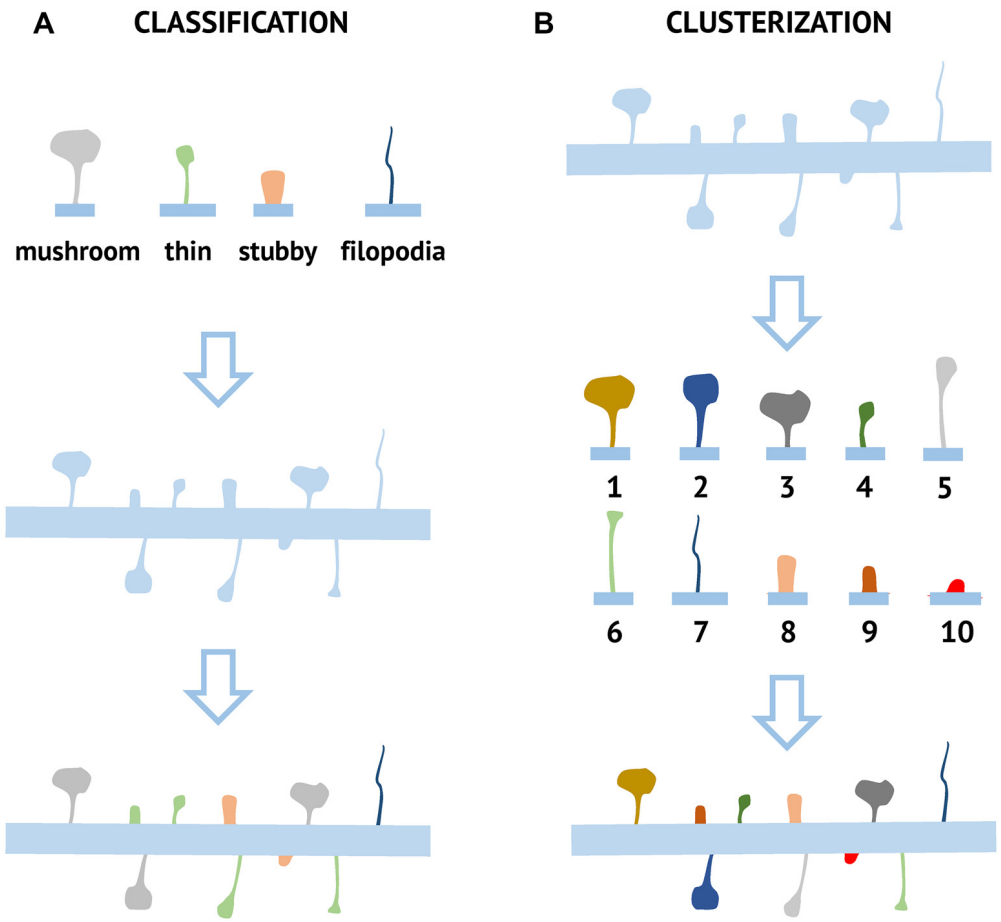

FIGURE 1 | Comparison of classification and clusterization pipelines used for the analysis of dendritic spine morphology. For classification approach **(A)** several possible morphological spine types (mushroom, stubby, thin, and filopodia) are defined based on pre-determined criteria. Each spine is then assigned to one of these classes based on numerical morphological criteria. For the clusterization approach **(B)**, spines are grouped into clusters based on their common morphological features. Ten different clusters (1–10) are shown as an example, but the number of different clusters and parameters used for clusterization depends on the particular algorithm and dataset.

(Wallace and Bear, 2004; Arellano et al., 2007; Tonnesen et al., 2014; Loewenstein et al., 2015). A study that focused on the morphology of neurons in layers II and III of a mouse visual cortex discovered that a continuous distribution rather than several discrete peaks were observed for each morphological parameter (Arellano et al., 2007). Distribution of dendritic spine length and head diameter in neurons of cortical layer III was also characterized by unimodal distribution (Wallace and Bear, 2004). No evidence of the existence of defined spine types was obtained in another study performed in the neocortex (Loewenstein et al., 2015). A study of the correlation between spine shape and compartmentalization of synapses indicated a great diversity in spine morphology, which was not consistent with standard classification systems (Tonnesen et al., 2014). Advances in live imaging make it possible to analyze the shape of a particular dendritic spine for a prolonged time, which revealed unique plasticity properties. Even stable, persistent spines are changing continuously in their orientation and shape, which also argue the pros existence of the shape continuum (Berry and Nedivi, 2017).

Analysis of spine morphology is also limited by the resolution limit of light microscopy. The size of dendritic spines usually does not exceed 1,000 nm for its largest dimension in the head, while the sizes of other parts are much smaller. For confocal microscopy resolution, the limit is estimated as half of the excitation wavelength, which is approximately 200–300 nm. For two-photon microscopy, the resolution is even lower due to the longer excitation wavelength used in these experiments. Furthermore, resolution along the z-axis is even lower than in the xy-plane in confocal and 2-photon imaging experiments. Low resolution leads to erroneous measurements of spine shapes, which leads to erroneous dendritic spine classification. For example, spine neck width is believed to be the key factor influencing dendritic spine compartmentalization and efficiency of signal transduction (Tonnesen et al., 2014). However, visualization of such small structures can only be done with

super-resolution imaging, which provides much more detailed information about spine shapes than standard light microscopic methods. Super-resolution imaging studies suggest that stubby spines are significantly over-represented in literature, which is the consequence of the low resolution of the neck, as it is small (Tonnesen et al., 2014).

Improvement of dendritic spine visualization methods is an important part of the unbiased assessment of their morphology. Due to the lack of clear boundaries between different spine classes, the same brain sample may yield different ratios of mushroom, thin, and stubby spines, depending on the criteria used to separate these classes from each other, meaning analyses are often biased and poorly reproducible. An attempt to fit the continuous distribution of spine shapes and sizes into pre-defined and rigid categories can result in multiple sources and potential errors. For example, thin and mushroom spines are two classical spine subtypes that have a very similar shape and the only critical parameter by which they can be distinguished is the head size. The head size is proportional to the area of PSD, the number of receptors at postsynapse, and synaptic strength (Kharazia and Weinberg, 1999; Takumi et al., 1999; Ganeshina et al., 2004; Arellano et al., 2007). On another hand, the length and width of the spine neck are related to the magnitude of postsynaptic potential (Tonnesen et al., 2014). The morphology of synapses varies depending on the strength of synaptic contact. Changes in synaptic strength during long-term potentiation and long-term depression are associated, respectively, with enlargement or shrinkage of the spine head (Yuste and Bonhoeffer, 2001; Holtmaat and Svoboda, 2009). During this process, it has been suggested that there is an interconversion between the thin and mushroom spine at a given synapse, however, it is not possible to subjectively define this point because of the continuum of spine sizes and shapes.

An additional source of error is related to the structure of the morphological data. Because imaging data are collected across different neurons from primary cultures or animal species of different sexes, it leads to the generation of a multi-level data structure. Recently published research speculates that using conventional statistical methods for working with such types of data, may lead to the generation of erroneous conclusions, and mixed-effects models have been proposed to correct this (Paternoster et al., 2018).

NON-CLASSIFICATION APPROACHES TO DENDRITIC SPINE SHAPES ANALYSIS

The analysis could be more precise and reliable by considering a continuum of spine shapes and forms and there are potential solutions for these classification problems. It has been proposed that reliance on objectively defined morphological parameters, rather than on classification into subjective shape-based groups, may help to solve some of these problems (Mancuso et al., 2013).

One widely used non-classification approach is the direct measurement of key morphological descriptors. A comparison of classification and direct morphometric measurement accuracy during dendritic spine morphology assessment has demonstrated that the second approach is much more sensitive (Ruszczycki et al., 2012). However, the direct morphometric measurement approach does not provide information about spine shape, which is important for biological function. For example, the measurement of spine head size works well for thin and mushroom spines, where it is well correlated with synaptic strength and PSD area (Kharazia and Weinberg, 1999; Takumi et al., 1999; Ganeshina et al., 2004; Arellano et al., 2007), but in filopodia and stubby type spines the head is not clearly defined and therefore not a key parameter in defining its morphology.

A newly emerging approach is a clusterization of spines according to similarities in their shape. This "clusterization" approach aims to automatically group spines into similar structural classes based on selected algorithms and without *a priori* input (**Figure 1**), meaning the results of clusterization are defined by data structure. The spine is presented as a set of values of parameters reflecting its morphology, starting from obvious such as neck and head size to a more complex geometrical parameters that may include a combination of several measurements. The algorithm assesses similarities between spines based on the value of selected parameters and performs clusterization. In this approach principal component analysis (PCA) is used to reduce data dimensionality before clusterization (**Figure 2**).

The first practical implementation of the clustering approach was published (Ghani et al., 2016) a few years after its initial suggestion (Mancuso et al., 2013; **Table 1**). A histogram of oriented gradients (HOG), disjunctive normal shape models (DNSM), morphological features, intensity profile based features, or their combination were used to quantitatively describe dendritic spine shapes. HOG is a feature descriptor used in object recognition and computer vision (Dalal and Triggs, 2005). The input image is divided into small connected parts where gradient direction is counted, visualized as an arrowhead, pointing at discrete angle 0, 30, 60, 90, etc. Later these parts are combined to a larger one and a histogram of obtained gradients is built that describes the analyzed object. DNSM represent a shape as a union of convex polytopes, which are constructed by intersections of half-spaces (Mesadi et al., 2015). Intensity profile based features are built after examination of intensities profile in the regions where the dendritic spine neck is expected to be located (between the head and a dendrite; Erdil et al., 2015). The analysis was performed on 2D maximum intensity projections (**Figure 3B**) from a 3D stack of two-photon microscopic images due to the non-sufficient resolution along the z-axis. Processing of data was generated with the help of morphological descriptors or their combination by x-means, clustering algorithm results to generate 4 distinct dendritic spines clusters. In all cases at least one of these clusters could not be clearly defined as mushroom, thin, or study spines. Authors concluded that their findings support the idea of existence of intermediate spine shapes. Later, the combination of DNSM and HOG morphological features was used to perform dendritic spine classification with help of a kernel density estimation (KDE) based framework, which enabled analysis of spine shape classes separability in the likelihood ratio space (Ghani et al., 2017).

Another group published an unsupervised construction of the spine shape taxonomy in the same year (Bokota et al., 2016;

TABLE 1 | Summary of non-classification approaches to dendritic spines shapes analysis.

No	Year	Reference	Sample	Microscopy	Spines form representation (Figure 3)	Preprocessing and feature extraction approach	Number of features	Software (+ provided, – not provided)	Morphological features analysis approach	Software availability
1	2016	Ghani et al. (2017)	7–10 day old mouse brain slices neurons (region not specified)	Two-photon	2D projection from image series	Histogram of oriented gradients (HOG), disjunctive normal shape models (DNSM), morphological features, intensity profile based features or their combination	Varying, from 12 for morphological to 346 for DNSM features	Custom (–)	X-means clustering, number of clusters selected automatically using the Bayesian information criterion (BIC; =4)	NA
2	2016	Bokota et al. (2016)	19–21 days *in vitro* hippocampal neurons	Confocal	2D projection from image series	The most often used morphological features according to literature data	11 (reduced to 6)	Custom (–)	C-means clustering (=10), average-linkage hierarchical clustering (=10), data dimensionality reduction by 2D principal component analysis (PCA)	UR
3	2018	Luengo-Sanchez et al. (2018)	layer III pyramidal neurons of the human cingulate cortex	Confocal	3D triangular surface mesh Multiresolution Reeb graph	Surface of a spine is modeled by 7 segments, which are presented as linked to each other ellipses. From 54 parameters used to describe dendritic spines, 36 reflect ellipses geometry and position and 18 describe more complex features, such as spine growth direction	54	Imaris for segmentation ($), custom software for feature extraction (+)	Clustering by probabilistic model with Gaussian finite mixtures, number of clusters selected automatically using the Bayesian information criterion (BIC; =6)	FA
4	2019	Kashiwagi et al. (2019)	18–22 days *in vitro* hippocampal neurons	SIM	3D triangular surface mesh	Segmentation of spines by multilevel thresholding based on Otsu's method following geodesic active contour, combination of morphological features and high geometric features	10 (reduced to 5)	Custom (+)	Division into mushroom and non-mushroom spines using SVM classifier, mapping the trajectories of individual spines shape transitions in the feature space, data dimensionality reduction by 3D principal component analysis (PCA)	FA
5	2019	Choi et al. (2019)	18–22 days *in vitro* hippocampal neurons	SIM	3D triangular surface mesh	Processing as in No4 with addition of 5 more features reflecting spines head and neck size	10	DXplorer (–)	K-means clustering, coordinate plot, radar plot and 2D scatter plot with t-Distributed Stochastic Neighbor Embedding	NA
6	2019	Driscoll et al. (2019)	CLARITY-cleared mouse brain neurons (region not specified)	LSM		Machine-learning based supervised spines detection	n/d	u-shape3D software (+)	Unsupervised hierarchical clustering (=9), data dimensionality deduction by 2D principal component analysis (PCA)	NA

Software availability—NA, not available; UR, available upon request; FA, freely available.

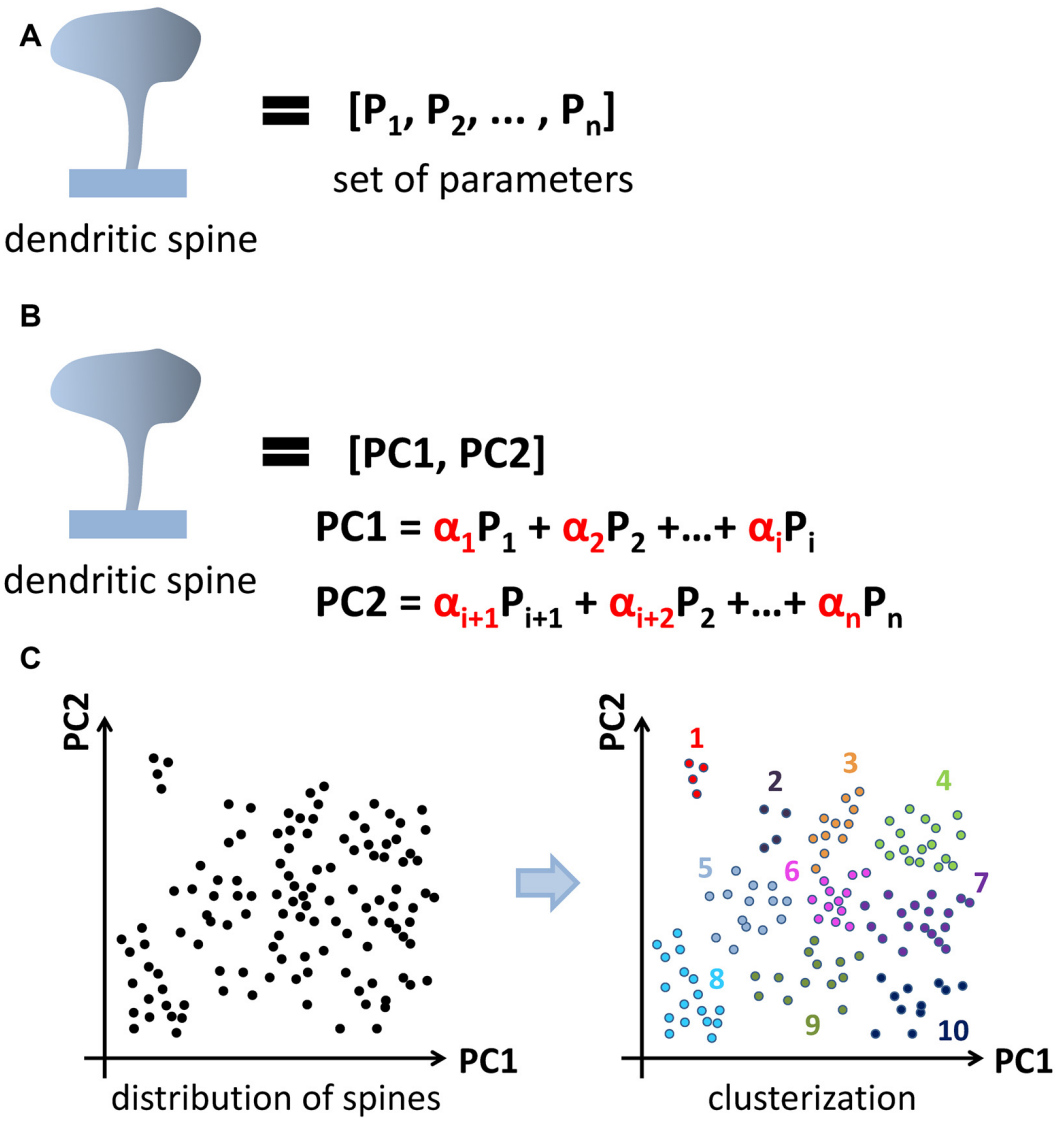

FIGURE 2 | Application of principal component analysis (PCA) method to dendritic spine clusterization. Spine shape is characterized by a set of parameters **(A)**. PCA method is used to reduce data dimensionality before clusterization. Newly generated parameters called principal components composed from initial one and form an orthonormal basis **(B)**. After PCA dataset in new coordinates is subjected to clusterization **(C)**. Cluster shape and content depend on the clusterization method used (k-means, c-means, hierarchical, et cetera).

Table 1). As a first step in the analysis, 11 features that have been most often used in previous publications were extracted from 2D projections of confocal image stacks (**Figure 3B**). Furthermore, the PCA method was applied to reduce the data dimensionality. Two components were generated, representing a linear combination of six features from 11 initially selected, while five others were neglected due to their relative insignificance. This provides a 2D (or 3D) orthogonal basis, where each spine can be presented as a point at the intersection of corresponding values of two generated components. In this research, dendritic spines in the control group and after chemical LTP induction were compared at two time points with 10 min difference. Only 300 pairs of dendritic spines with the closest meanings of selected parameters were used for further analysis. The authors reasoned that such dataset normalization was due to the initial high diversity of the spine population. Clusterization was performed for spines from both groups at two time points together to build shape taxonomy. Two well-established algorithms, c-means and average-linkage hierarchical representing crisp and fuzzy types of clustering were used. In each case, 11 clusters were formed, but their shape and content were different. Clusters vary greatly from small peripheral to overcrowded, while some clusters were well represented and separated from each other.

To analyze changes in dendritic spine morphology over time, the authors generated a transition shape model, which calculated the probability of dendritic spine transition from one taxonomic unit to another, visually presented as a transition graph. The statistical difference between the resulting models for the control and cLTP groups were analyzed with bootstrap-based statistical tests. The statistics depended only on the changes of distribution, demonstrating the differences between models build with c-means clustering, while models build with hierarchical clustering showed significant difference with statistics comparing the transition of spines between shapes. No statistically relevant differences were found between models when transitions between clusters were compared rather than the whole model, probably because of the little number of analyzed spines. The authors concluded that the clustering algorithm greatly influences the result, and therefore should be selected carefully, considering the properties of the data and experiment design. This study is the only study published so far, where different clustering algorithms were compared using the same dataset. This study was also the first that compared the control and experimental group of dendritic spines in terms of clusters.

More recently, spines from two 40 and 85 year old individuals, layer III pyramidal neurons in the cingulate cortex reconstructed in 3D were subjected to clusterization (Luengo-Sanchez et al., 2018; **Table 1**). Before clusterization, detached or fragmented spines, due to the diffraction limit of confocal microscopy spines, were repaired by semi-supervised mesh processing algorithms, while spines with extreme features were excluded from the data set. To characterize the spines, the surface was divided into regions according to a multiresolution Reeb graph. In total, seven segments, which are presented as ellipses linked to each other, were generated to mimic the geometry of a spine, and their major geometrical aspects such as length, width, size or curvature were used to generate 36 spines morphology parameters (**Figure 3C**). In order to create a more precise and sophisticated spine model with an additional 18 features, such as spine growth direction, were also used. To get a more in-depth insight into the nature of generated clusters the most representative feature classification rules, based on the RIPPER algorithm, were generated for each cluster, with each spine was attributed to its most probable cluster. However, the authors established that a single rule cannot be used to characterize all the spines within a cluster, and suggested that each cluster should be defined by one, two, or three observable features.

A cluster consisting of short stubby-like spines was the most homogeneous example, while a cluster with long spines with relatively big heads has the highest variability within a cluster. Stubby-like spines were also clearly separated from other spine classes (Bokota et al., 2016). The authors compared the number of spines in each cluster for apical and basal dendrites, and the dependence of spine shapes on distance from the soma and age of subjects. Statistical analysis showed that cluster distribution significantly differs for all investigated cases. A more precise comparison revealed that only some clusters have valuable differences depending on dendritic compartment, age or combination of both, providing the new information of the relationship between spine shape and function. Basal dendrites displayed smaller stubby-like spines, while apical dendrites have more relatively medium and large spines with a distinct head. Individuals younger than 40 tended to have more small spines, while those over 80 years had more big spines. Since small spines are believed to be a «learning spines», serving as sites where new memories are generated, the authors concluded, that younger subjects have more capabilities of learning, which requires spine plasticity. In addition, the research group evaluated an algorithm generating simulated spines for each cluster using as a basis of 54 morphological features. This simulation reveals the possibility of building a computational model of a pyramidal neuron, which can be used to study neuronal plasticity.

New horizons in the computational analyses of the morphological features of dendritic spines have been created by the application of high-resolution microscopy. Structural illumination microscopy (SIM) enables precise visualization of dendritic spines and measurements of their nanoscale morphological features (Smith et al., 2014). Key morphological descriptors measured on images obtained by SIM are comparable in resolution to electron microscopy. At the same time, SIM provides an ability to analyze many more spines than EM and can also be applied to the analysis of live neurons. SIM microscopy is also able to provide one more meaningful morphological feature, a concave surface: the place where the synaptic junction is thought to be formed. The dynamics of concave surface contacts may define correspondingly dynamic, stable, and degrading synaptic contacts, providing more insight into the potential link between synaptic structure and function.

A method of measuring the nanoscale surface geometry of synaptic spines from SIM images was recently developed (Kashiwagi et al., 2019; **Table 1**). For the segmentation of spines on SIM images, the combination of Otsu's multi-level thresholding algorithm with geodesic active contours showed the best result. After that, a polygonal mesh was build basing on spine voxel representation using the marching cube algorithm (**Figure 3D**). Totally 10 morphological features were extracted from 1,335 dendritic spines, including basic shape features such as length or volume, and more complex parameters obtained by discrete differential-geometry operators such as convex hull volume and open angle. We noticed that the morphological features of large spines could be also measured on neuronal images obtained with high-resolution confocal microscopy with narrow confocal aperture (0.5 AU). Further processing with PCA led to the generation of three components composed of five morphological features (length, volume, convex hull ratio, coefficient of variation in distance, and open angle) covering 93% of data variance.

When analyzing the shapes of spines distributed in 3D feature space, the authors noticed that spines exhibited a continuum of morphologies, supporting the idea that the classification into thin, mushroom, or stubby spines does not reflect the presence of discrete subclasses. The authors also noted that spines with a clearly identifiable head are located close to each other. An SVM classifier with a nonlinear kernel trained on the manually labeled dataset was used to divide spines into mushroom-shaped and non-mushroom. Analysis of spine

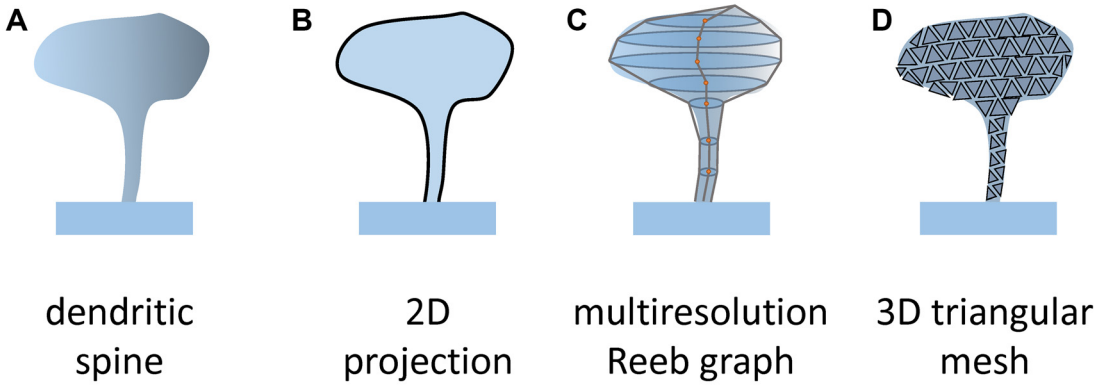

FIGURE 3 | Methods of spines segmentation. To assess numerical values of parameters describing spines shape **(A)** it is necessary to define object boundary. In 2D projection, spines are presented as flat objects (**B**; Ghani et al., 2016; Bokota et al., 2016). In 3D it was proposed to present the spine surface as a set of ellipses along the spine centerline that are connected (**C**; Luengo-Sanchez et al., 2018; Choi et al., 2019) or a triangle mesh (**D**; Kashiwagi et al., 2019). Such a presentation enables us to extract more complex parameters reflecting the constructed model of the spine.

shapes in a kinase-dead allele of Ca^{2+}/calmodulin-dependent protein kinase IIα (CaMKIIαK42R/K42R) knock-in mouse was performed using this approach and it was discovered that the mushroom shaped spines have reduced volume in mutant mice when compared to the control. In contrast, the volume was not changed in non-mushroom spines but their length was significantly elevated in mutant mice samples.

The data obtained during longitudinal SIM imaging of dendritic spine dynamics *in vivo* were also analyzed by the clustering approach. A trajectory was built in 3D feature space, reflecting the changes of spine shape from these data. Interestingly, spines in different parts of feature space showed different patterns of behavior, which enable us to divide them into three groups. The first group predominantly consists of small mushroom spines having short trajectories without an orientation preference, the second group consists of large mushroom spines that moved bidirectionally along the axis, corresponding to medium/thin and large/round shape features, and the third group was composed of non-mushroom spines with highly variable trajectories. The authors concluded that these three groups of spines overlapped in the feature space, and their distribution did not support the existence of distinct shape classes.

In 2019 a new software DXplorer was developed. It enables interactive three-dimensional analysis of dendritic spines morphology (Choi et al., 2019; **Table 1**). In DXplorer 3D rendering of spines displayed together with the parallel coordinate plot, radar plot, and 2D scatter plot with t-Distributed Stochastic Neighbor Embedding generated in agreement with their high dimensional features. This work is an extension of earlier work (Kashiwagi et al., 2019) and similar methods for the preparation of samples and data acquisition were used in both studies. The authors noticed that using only five morphological features (Kashiwagi et al., 2019) is not enough to distinguish all spines, especially the spines that belong to different types, because spine head and neck dimensions are not included. For example, these features have very close values for some mushroom and stubby spines, and therefore it is impossible to discriminate between them. To overcome this issue five more parameters were added: maximum head diameter (hMax), minimum head diameter (hMin), maximum neck diameter (nMax), minimum neck diameter (nMin), and HNR, which is the ratio of head to the neck (hMax/nMax). To find similar 3D phenotypes, users can group spines with similar shapes through interactive selection using the feature and similarity plot. In addition, the similarity plot panel can be used to divide the spines using the k-means clustering algorithm into a certain number of clusters, which are larger than groups formed in 2D feature space using t-Distributed Stochastic Neighbor Embedding method. Analysis of classification accuracy in 2D by rendering the classified spines in 3D by expert neuroscientists showed that 2D image-based classification had an error rate of 44.27% in identifying spines shapes. The errors occurred most often when stubby spines were labeled as thin spines in 2D projection. This experiment demonstrated that 2D image-based classification has a very high error rate, and therefore analysis in 3D is required to characterize spine shapes correctly.

The application of light sheet microscopy (LSM) enables the collection of morphological information from an intact brain or a large portion of it without physical separation. In a recent application of this technology, a cleared-tissue axially swept light-sheet microscopy (ctASLM; Chakraborty et al., 2019) was used to collect imaging data using mouse brain precleared with PEGASOS method. The dendritic protrusions on these images were analyzed with u-shape3D free available software (Driscoll et al., 2019). As a result, nine dendritic spine clusters with similar shapes were generated after unsupervised hierarchical clustering based on morphological measures, such as the ratio of the spine neck area to the spine surface area. The distribution of obtained classes is shown in the 2D feature space generated by PCA. The development of spine clusterization approaches based on LSM data is a very promising future direction of this research.

CONCLUDING REMARKS

The examples discussed above support the conclusion that the dendritic spine clusterization approach reflects a continuum of spine shapes and sizes much better than classification into predefined groups. The application of the clusterization approach enables more precise analysis and reveals qualitatively new information about synaptic spines. All of the groups discussed above concluded that continuous morphological variables rather than pre-defined spine classes should be used to describe spines morphologies. The clustering approach aims to identify and group objects with similar shapes, with different shape classes determined by the structure of the data. Different clustering algorithms give different results on the same dataset, so clusters vary in shape and content, which may greatly influence the interpretation of these data. Future research will be needed to compare existing methods and identify optimal approaches to clusterization (**Table 1**). These algorithms should offer maximal discrimination of clusters that facilitate subsequent analysis and identification of the differences between control and experimental groups. It is also possible that a new and superior clusterization algorithm will be developed for this purpose in the future.

As discussed above, there is no consensus on which spine shape descriptors should be used as input for the clusterization procedure. Taking into account the results of the approaches discussed here, we propose that this set of parameters should include not only obvious morphological metrics such as spine head diameter, spine area, and volume but also complex geometrical features that enable a more sophisticated description of complex dendritic spines shapes. Proper statistical procedures for comparing clustered spine data from control and experimental groups need to be developed in the future.

Another important issue is the biological interpretation of clusterization data. In the classification approach putative biological functions of "mushroom," "thin," and "stubby" spines have been extensively discussed. Further research will be needed to relate the complex shapes of a particular cluster of spines to its physiological role.

Despite all these challenges, this emerging approach to the analysis of dendritic spine shapes opens a new and powerful trend in neuroscience research. The availability of high quality, free, and robust software is critical for these ideas to become reality. Once developed, such tools will greatly facilitate the investigation of dendritic spines, including function, structure, plasticity, and pathology. Providing datasets, distributives, and source code by developers is an essential step to speed up this process and to open the way to further improvement and adaptation of these methods.

AUTHOR CONTRIBUTIONS

The manuscript was drafted and revised for intellectual content by EP and IB, with material support from IB. All authors contributed to the article and approved the submitted version.

FUNDING

This work was supported by the Academic Excellence Project 5-100 from the Peter the Great St. Petersburg Polytechnic University (IB) and National Institutes of Health grants R01AG055577 and R01NS056224 (IB). EP is a holder of the Russian Presidential Stipend SP-1929.2018.4. IB is the Carl J. and Hortense M. Thomsen Professor in Alzheimer's Disease Research.

REFERENCES

Arellano, J. I., Benavides-Piccione, R., Defelipe, J., and Yuste, R. (2007). Ultrastructure of dendritic spines: correlation between synaptic and spine morphologies. *Front. Neurosci.* 1, 131–143. doi: 10.3389/neuro.01.1.1.010.2007

Ashokan, A., Lim, J. W. H., Hang, N., and Mitra, R. (2018). Complex housing causes a robust increase in dendritic complexity and spine density of medial prefrontal cortical neurons. *Sci. Rep.* 8:7308. doi: 10.1038/s41598-018-25399-4

Bagni, C., and Zukin, R. S. (2019). A synaptic perspective of fragile X syndrome and autism spectrum disorders. *Neuron* 101, 1070–1088. doi: 10.1016/j.neuron.2019.02.041

Bailey, C. H., Kandel, E. R., and Harris, K. M. (2015). Structural components of synaptic plasticity and memory consolidation. *Cold Spring Harb. Perspect. Biol.* 7:a021758. doi: 10.1101/cshperspect.a021758

Barrientos, C., Knowland, D., Wu, M. M. J., Lilascharoen, V., Huang, K. W., Malenka, R. C., et al. (2018). Cocaine-induced structural plasticity in input regions to distinct cell types in nucleus accumbens. *Biol. Psychiatry* 84, 893–904. doi: 10.1016/j.biopsych.2018.04.019

Basu, S., Plewczynski, D., Saha, S., Roszkowska, M., Magnowska, M., Baczynska, E., et al. (2016). 2dSpAn: semiautomated 2-d segmentation, classification and analysis of hippocampal dendritic spine plasticity. *Bioinformatics* 32, 2490–2498. doi: 10.1093/bioinformatics/btw172

Basu, S., Saha, P. K., Roszkowska, M., Magnowska, M., Baczynska, E., Das, N., et al. (2018). Quantitative 3-D morphometric analysis of individual dendritic spines. *Sci. Rep.* 8:3545. doi: 10.1038/s41598-018-35164-2

Berry, K. P., and Nedivi, E. (2017). Spine dynamics: are they all the same? *Neuron* 96, 43–55. doi: 10.1016/j.neuron.2017.08.008

Bokota, G., Magnowska, M., Kusmierczyk, T., Lukasik, M., Roszkowska, M., and Plewczynski, D. (2016). Computational approach to dendritic spine taxonomy and shape transition analysis. *Front. Comput. Neurosci.* 10:140. doi: 10.3389/fncom.2016.00140

Boros, B. D., Greathouse, K. M., Gentry, E. G., Curtis, K. A., Birchall, E. L., Gearing, M., et al. (2017). Dendritic spines provide cognitive resilience against Alzheimer's disease. *Ann. Neurol.* 82, 602–614. doi: 10.1002/ana.25049

Bourne, J., and Harris, K. M. (2007). Do thin spines learn to be mushroom spines that remember? *Curr. Opin. Neurobiol.* 17, 381–386. doi: 10.1016/j.conb.2007.04.009

Chakraborty, T., Driscoll, M., Jeffery, E., Murphy, M., Roudot, P., Chang, B.-J., et al. (2019). Light-sheet microscopy of cleared tissues with isotropic, subcellular resolution. *Nat. Methods* 16, 1109–1113. doi: 10.1038/s41592-019-0615-4

Chidambaram, S. B., Rathipriya, A. G., Bolla, S. R., Bhat, A., Ray, B., Mahalakshmi, A. M., et al. (2019). Dendritic spines: revisiting the physiological role. *Prog. Neuropsychopharmacol. Biol. Psychiatry* 92, 161–193. doi: 10.1016/j.pnpbp.2019.01.005

Choi, J., Lee, S.-E., Cho, E., Kashiwagi, Y., Okabe, S., Chang, S., et al. (2019). "Interactive dendritic spine analysis based on 3D morphological features," in *2019 IEEE Visualization Conference (VIS)*, (Vancouver, BC: IEEE).

Dalal, N., and Triggs, B. (2005). "Histograms of oriented gradients for human detection," in *2005 IEEE Computer Society Conference on Computer Vision and Pattern Recognition (CVPR'05)*, San Diego, CA, USA, 886–893.

Dickstein, D. L., Dickstein, D. R., Janssen, W. G., Hof, P. R., Glaser, J. R., Rodriguez, A., et al. (2016). Automatic dendritic spine quantification from confocal data with neurolucida 360. *Curr. Protoc. Neurosci.* 77, 1.27.1–1.27.21. doi: 10.1002/cpns.16

Driscoll, M., Welf, E., Jamieson, A., Dean, K., Isogai, T., Fiolka, R., et al. (2019). Robust and automated detection of subcellular morphological motifs in 3D microscopy images. *Nat. Methods* 16, 1037–1044. doi: 10.1038/s41592-019-0539-z

Erdil, E., Argunsah, A. O., Tasdizen, T., Unay, D., and Cetin, M. (2015). "A joint classification and segmentation approach for dendritic spine segmentation in 2-photon microscopy images," in *2015 IEEE 12th International Symposium on Biomedical Imaging (ISBI)*, New York, NY, USA, 797–800.

Ganeshina, O., Berry, R. W., Petralia, R. S., Nicholson, D. A., and Geinisman, Y. (2004). Differences in the expression of AMPA and NMDA receptors between axospinous perforated and nonperforated synapses are related to the configuration and size of postsynaptic densities. *J. Comp. Neurol.* 468, 86–95. doi: 10.1002/cne.10950

Ghani, M. U., Erdil, E., Kanik, S. D., Argunsah, A. Ö., Hobbiss, A. F., Israely, I., et al. (2016). *Dendritic Spine Shape Analysis: A Clustering Perspective*. Cham: Springer International Publishing, 256–273.

Ghani, M. U., Mesadi, F., Kanik, S. D., Argunsah, A. O., Hobbiss, A. F., Israely, I., et al. (2017). Dendritic spine classification using shape and appearance features based on two-photon microscopy. *J. Neurosci. Methods* 279, 13–21. doi: 10.1016/j.jneumeth.2016.12.006

Hayashi, Y., and Majewska, A. K. (2005). Dendritic spine geometry: functional implication and regulation. *Neuron* 46, 529–532. doi: 10.1016/j.neuron.2005.05.006

Hering, H., and Sheng, M. (2001). Dentritic spines: structure, dynamics and regulation. *Nat. Rev. Neurosci.* 2, 880–888. doi: 10.1038/35104061

Herms, J., and Dorostkar, M. M. (2016). Dendritic spine pathology in neurodegenerative diseases. *Annu. Rev. Pathol.* 11, 221–250. doi: 10.1146/annurev-pathol-012615-044216

Holtmaat, A., and Svoboda, K. (2009). Experience-dependent structural synaptic plasticity in the mammalian brain. *Nat. Rev. Neurosci.* 10, 647–658. doi: 10.1038/nrn2699

Kasai, H., Hayama, T., Ishikawa, M., Watanabe, S., Yagishita, S., and Noguchi, J. (2010). Learning rules and persistence of dendritic spines. *Eur. J. Neurosci.* 32, 241–249. doi: 10.1111/j.1460-9568.2010.07344.x

Kashiwagi, Y., Higashi, T., Obashi, K., Sato, Y., Komiyama, N. H., Grant, S. G. N., et al. (2019). Computational geometry analysis of dendritic spines by structured illumination microscopy. *Nat. Commun.* 10:1285. doi: 10.1038/s41467-019-09337-0

Kharazia, V. N., and Weinberg, R. J. (1999). Immunogold localization of AMPA and NMDA receptors in somatic sensory cortex of albino rat. *J. Comp. Neurol.* 412, 292–302. doi: 10.1002/(sici)1096-9861(19990920)412:2<292::aid-cne8>3.0.co;2-g

Koh, I. Y. Y., Lindquist, W. B., Zito, K., Nimchinsky, E. A., and Svoboda, K. (2002). An image analysis algorithm for dendritic spines. *Neural Comput.* 14, 1283–1310. doi: 10.1162/089976602753712945

Loewenstein, Y., Yanover, U., and Rumpel, S. (2015). Predicting the dynamics of network connectivity in the neocortex. *J. Neurosci.* 35, 12535–12544. doi: 10.1523/jneurosci.2917-14.2015

Luengo-Sanchez, S., Fernaud-Espinosa, I., Bielza, C., Benavides-Piccione, R., Larrañaga, P., and DeFelipe, J. (2018). 3D morphology-based clustering and simulation of human pyramidal cell dendritic spines. *PLoS Comput. Biol.* 14(6):e1006221. doi: 10.1371/journal.pcbi.1006221

Maiti, P., Manna, J., Ilavazhagan, G., Rossignol, J., and Dunbar, G. L. (2015). Molecular regulation of dendritic spine dynamics and their potential impact on synaptic plasticity and neurological diseases. *Neurosci. Biobehav. Rev.* 59, 208–237. doi: 10.1016/j.neubiorev.2015.09.020

Mancuso, J. J., Chen, Y., Li, X., Xue, Z., and Wong, S. T. (2013). Methods of dendritic spine detection: from Golgi to high-resolution optical imaging. *Neuroscience* 251, 129–140. doi: 10.1016/j.neuroscience.2012.04.010

Mesadi, F., Cetin, M., and Tasdizen, T. (2015). *Disjunctive Normal Shape and Appearance Priors with Applications to Image Segmentation*. Cham: Springer International Publishing, 703–710.

Nakahata, Y., and Yasuda, R. (2018). Plasticity of spine structure: local signaling, translation and cytoskeletal reorganization. *Front. Synaptic Neurosci.* 10:29. doi: 10.3389/fnsyn.2018.00029

Nishiyama, J. (2019). Plasticity of dendritic spines: molecular function and dysfunction in neurodevelopmental disorders. *Psychiatry Clin. Neurosci.* 73, 541–550. doi: 10.1111/pcn.12899

Nithianantharajah, J., and Hannan, A. J. (2013). Dysregulation of synaptic proteins, dendritic spine abnormalities and pathological plasticity of synapses as experience-dependent mediators of cognitive and psychiatric symptoms in Huntington's disease. *Neuroscience* 251, 66–74. doi: 10.1016/j.neuroscience.2012.05.043

Paternoster, V., Rajkumar, A. P., Nyengaard, J. R., Børglum, A. D., Grove, J., and Christensen, J. H. (2018). The importance of data structure in statistical analysis of dendritic spine morphology. *J. Neurosci. Methods* 296, 93–98. doi: 10.1016/j.jneumeth.2017.12.022

Penzes, P., Cahill, M. E., Jones, K. A., VanLeeuwen, J.-E., and Woolfrey, K. M. (2011). Dendritic spine pathology in neuropsychiatric disorders. *Nat. Neurosci.* 14, 285–293. doi: 10.1038/nn.2741

Risher, C., Ustunkaya, T., Alvarado, J., and Eroglu, C. (2014). Rapid golgi analysis method for efficient and unbiased classification of dendritic spines. *PLoS One* 9:e107591. doi: 10.1371/journal.pone.0107591

Rodriguez, A., Ehlenberger, D. B., Dickstein, D. L., Hof, P. R., and Wearne, S. L. (2008). Automated three-dimensional detection and shape classification of dendritic spines from fluorescence microscopy images. *PLoS One* 3:e1997. doi: 10.1371/journal.pone.0001997

Ruszczycki, B., Szepesi, Z., Wilczynski, G. M., Bijata, M., Kalita, K., Kaczmarek, L., et al. (2012). Sampling issues in quantitative analysis of dendritic spines morphology. *BMC Bioinformatics* 13:213. doi: 10.1186/1471-2105-13-213

Saraceno, G. E., Castilla, R., Barreto, G. E., Gonzalez, J., Kölliker-Frers, R. A., and Capani, F. (2012). Hippocampal dendritic spines modifications induced by perinatal asphyxia. *Neural Plast.* 2012:873532. doi: 10.1155/2012/873532

Segal, M. (2017). Dendritic spines: morphological building blocks of memory. *Neurobiol. Learn. Mem.* 138, 3–9. doi: 10.1016/j.nlm.2016.06.007

Shi, P., Huang, Y., and Hong, J. (2014). Automated three-dimensional reconstruction and morphological analysis of dendritic spines based on semi-supervised learning. *Biomed. Opt. Express* 5, 1541–1553. doi: 10.1364/boe.5.001541

Smith, K. R., Kopeikina, K. J., Fawcett-Patel, J. M., Leaderbrand, K., Gao, R., Schürmann, B., et al. (2014). Psychiatric risk factor ANK3/ankyrin-G nanodomains regulate the structure and function of glutamatergic synapses. *Neuron* 84, 399–415. doi: 10.1016/j.neuron.2014.10.010

Son, J., Song, S., Lee, S., Chang, S., and Kim, M. (2011). Morphological change tracking of dendritic spines based on structural features. *J. Microscopy* 241, 261–272. doi: 10.1111/j.1365-2818.2010.03427.x

Stein, I. S., and Zito, K. (2019). Dendritic spine elimination: molecular mechanisms and implications. *Neuroscientist* 25, 27–47. doi: 10.1177/1073858418769644

Swanger, S. A., Yao, X., Gross, C., and Bassell, G. J. (2011). Automated 4D analysis of dendritic spine morphology: applications to stimulus-induced spine remodeling and pharmacological rescue in a disease model. *Mol. Brain* 4:38. doi: 10.1186/1756-6606-4-38

Tackenberg, C., Ghori, A., and Brandt, R. (2009). Thin, stubby or mushroom: spine pathology in Alzheimer's disease. *Curr. Alzheimer Res.* 6, 261–268. doi: 10.2174/156720509788486554

Takumi, Y., Ramirez-Leon, V., Laake, P., Rinvik, E., and Ottersen, O. P. (1999). Different modes of expression of AMPA and NMDA receptors in hippocampal synapses. *Nat. Neurosci.* 2, 618–624. doi: 10.1038/10172

Tonnesen, J., Katona, G., Rozsa, B., and Nagerl, U. V. (2014). Spine neck plasticity regulates compartmentalization of synapses. *Nat. Neurosci.* 17, 678–685. doi: 10.1038/nn.3682

Wallace, W., and Bear, M. F. (2004). A morphological correlate of synaptic scaling in visual cortex. *J. Neurosci.* 24, 6928–6938. doi: 10.1523/jneurosci.1110-04.2004

Xu, T., Yu, X., Perlik, A. J., Tobin, W. F., Zweig, J. A., Tennant, K., et al. (2009). Rapid formation and selective stabilization of synapses for enduring motor memories. *Nature* 462, 915–919. doi: 10.1038/nature08389

Yang, G., Lai, C. S., Cichon, J., Ma, L., Li, W., and Gan, W. B. (2014). Sleep promotes branch-specific formation of dendritic spines after learning. *Science* 344, 1173–1178. doi: 10.1126/science.1249098

Yasuda, R. (2017). Biophysics of biochemical signaling in dendritic spines: implications in synaptic plasticity. *Biophys. J.* 113, 2152–2159. doi: 10.1016/j.bpj.2017.07.029

Yoshihara, Y., De Roo, M., and Muller, D. (2009). Dendritic spine formation and stabilization. *Curr. Opin. Neurobiol.* 19, 146–153. doi: 10.1016/j.conb.2009.05.013

Yuste, R., and Bonhoeffer, T. (2001). Morphological changes in dendritic spines associated with long-term synaptic plasticity. *Annu. Rev. Neurosci.* 24, 1071–1089. doi: 10.1146/annurev.neuro.24.1.1071

Yuste, R., and Bonhoeffer, T. (2004). Genesis of dendritic spines: insights from ultrastructural and imaging studies. *Nat. Rev. Neurosci.* 5, 24–34. doi: 10.1038/nrn1300

Zhou, Q., Homma, K. J., and Poo, M. M. (2004). Shrinkage of dendritic spines associated with long-term depression of hippocampal synapses. *Neuron* 44, 749–757. doi: 10.1016/j.neuron.2004.11.011

Conflict of Interest: The authors declare that the research was conducted in the absence of any commercial or financial relationships that could be construed as a potential conflict of interest.

frontiers in Synaptic Neuroscience

BRIEF RESEARCH REPORT
published: 16 November 2020
doi: 10.3389/fnsyn.2020.551691

Local Postsynaptic Signaling on Slow Time Scales in Reciprocal Olfactory Bulb Granule Cell Spines Matches Asynchronous Release

*Tiffany Ona Jodar[1,2†], Vanessa Lage-Rupprecht[1,3†], Nixon M. Abraham[4], Christine R. Rose[5] and Veronica Egger[1]**

[1] Regensburg University, Regensburg, Germany, [2] Institut D'Investigacions Biomèdiques, Barcelona, Spain, [3] Fraunhofer Institute for Algorithms and Scientific Computing, St. Augustin, Germany, [4] Indian Institute of Science Education and Research, Pune, India, [5] Heinrich Heine University Duesseldorf, Düsseldorf, Germany

In the vertebrate olfactory bulb (OB), axonless granule cells (GC) mediate self- and lateral inhibitory interactions between mitral/tufted cells via reciprocal dendrodendritic synapses. Locally triggered release of GABA from the large reciprocal GC spines occurs on both fast and slow time scales, possibly enabling parallel processing during olfactory perception. Here we investigate local mechanisms for asynchronous spine output. To reveal the temporal and spatial characteristics of postsynaptic ion transients, we imaged spine and adjacent dendrite Ca^{2+}- and Na^{+}-signals with minimal exogenous buffering by the respective fluorescent indicator dyes upon two-photon uncaging of DNI-glutamate in OB slices from juvenile rats. Both postsynaptic fluorescence signals decayed slowly, with average half durations in the spine head of $t_{1/2\_}\Delta[Ca^{2+}]_i$ ~500 ms and $t_{1/2\_}\Delta[Na^{+}]_i$ ~1,000 ms. We also analyzed the kinetics of already existing data of postsynaptic spine Ca^{2+}-signals in response to glomerular stimulation in OB slices from adult mice, either WT or animals with partial GC glutamate receptor deletions (NMDAR: GluN1 subunit; AMPAR: GluA2 subunit). In a large subset of spines the fluorescence signal had a protracted rise time (average time to peak ~400 ms, range 20 to >1,000 ms). This slow rise was independent of Ca^{2+} entry via NMDARs, since similarly slow signals occurred in ΔGluN1 GCs. Additional Ca^{2+} entry in ΔGluA2 GCs (with AMPARs rendered Ca^{2+}-permeable), however, resulted in larger ΔF/Fs that rose yet more slowly. Thus GC spines appear to dispose of several local mechanisms to promote asynchronous GABA release, which are reflected in the time course of mitral/tufted cell recurrent inhibition.

Keywords: olfactory bulb, granule cell, two-photon (2P) uncaging, two-photon sodium imaging, two-photon calcium imaging, asynchronous release, reciprocal synapse, recurrent inhibition

OPEN ACCESS

Edited by:
Carlo Sala,
Italian National Research Council, Italy

Reviewed by:
Claudia Lodovichi,
Italian National Research Council, Italy
Eric Hanse,
University of Gothenburg, Sweden

***Correspondence:**
Veronica Egger
Veronica.Egger@ur.de

†These authors share first authorship

Received: *14 April 2020*
Accepted: *19 October 2020*
Published: *16 November 2020*

Citation:
Ona Jodar T, Lage-Rupprecht V, Abraham NM, Rose CR and Egger V (2020) Local Postsynaptic Signaling on Slow Time Scales in Reciprocal Olfactory Bulb Granule Cell Spines Matches Asynchronous Release. Front. Synaptic Neurosci. 12:551691. doi: 10.3389/fnsyn.2020.551691

INTRODUCTION

In the vertebrate olfactory bulb (OB), the lateral dendrites of the principal mitral and tufted cells are interconnected via local GABAergic interneurons. The most abundant class of these local neurons, the axonless granule cells (GC), mediate self- and lateral inhibitory interactions between mitral/tufted cells via reciprocal dendrodendritic synapses that on the GC dendrite are housed in large spines (Shepherd, 2004). These reciprocal synapses have been directly demonstrated to play

a role in odor discrimination and learning (Abraham et al., 2010; Gschwend et al., 2015). Moreover, they are also critically involved in generating bulbar γ-oscillations (Rall and Shepherd, 1968; Nusser et al., 2001; Lagier et al., 2004), which are thought to contribute to odor coding via synchronization and gating of mitral cell output (e.g., Buonviso et al., 2003; Fukunaga et al., 2014; Osinski and Kay, 2016).

Recordings of dendrodendritic inhibition of mitral cells have revealed that recurrent inhibition happens as a barrage of IPSCs (Isaacson and Strowbridge, 1998; Schoppa et al., 1998). Within this barrage, early IPSCs will occur with a very short latency (below 10 ms), but recurrent activity takes several hundreds of milliseconds to subside. While this long tail of recurrent inhibition is unlikely to directly contribute to odor discrimination itself (Uchida and Mainen, 2003; Abraham et al., 2004, 2010), it may well play a role in learning and memory formation (Gschwend et al., 2015; see section "Discussion").

The underlying asynchronous release is at least to a major extent due to processing in GCs, since asynchronous responses were demonstrated following flash photolysis of Ca^{2+} in mitral cell lateral dendrites (Chen et al., 2000). Moreover, while the massive release of glutamate during the commonly used protocol for mitral cell excitation (20–50 ms depolarization in the voltage-clamp mode) might result in activation of slow release pathways not accessible to unitary transmission, we have shown recently, that local, unitary-like two-photon uncaging of glutamate (TPU) can still cause prolonged release of GABA within a time window of up to 500 ms post uncaging (Lage-Rupprecht et al., 2020).

As to possible mechanisms for late output, unitary EPSPs evoked by spontaneous mitral/tufted cell input or local TPU are mediated by both AMPA and NMDA receptors, and decaying with a time constant <50 ms (as recorded at the GC soma, Bywalez et al., 2015). Thus slower actions downstream of ionotropic receptors would be required to trigger cascades that result in asynchronous release events beyond 100 ms. A number of global mechanisms has been proposed to promote asynchronous release from GC spines. These include a delay of global GC action potentials (AP) due to the prominent I_A current (Schoppa and Westbrook, 1999; Kapoor and Urban, 2006), and a prolonged Ca^{2+} entry due to synaptic activation of a non-specific cation current I_{CAN}, possibly in coincidence with global APs (Hall and Delaney, 2002; Egger, 2008; Stroh et al., 2012).

Since as in other synapses reciprocal release of GABA is Ca^{2+}-dependent (Isaacson and Strowbridge, 1998), how could spine Ca^{2+} signals mediate asynchronous release? To answer this question, we explored several potential local mechanisms that might be involved in slow spine Ca^{2+} signaling and thus are directly related to the biophysical properties of individual spines.

While the endogenous Ca^{2+} buffering capacity κ_E in GC spines is not unusually high (∼120) and thus cannot explain lingering Ca^{2+}, the Ca^{2+} extrusion from the spine cytosol is sluggish (rate γ ∼500 s^{-1} at RT), which might support asynchronous output (Egger and Stroh, 2009).

As to postsynaptic spine Ca^{2+} signals upon glomerular mitral cell stimulation (100 μM OGB-1, Egger et al., 2005), responses in juvenile rat GC spines are robust, with an average amplitude of ∼40% ΔF/F, and rise within ∼80 ms. Their decay kinetics are slower than those of backpropagating AP-mediated transients, with a clearly bimodal distribution of durations. While ∼2/3 of spine signals decayed by half within ∼600 ms, the remaining 1/3 decayed very slowly, with half durations beyond 1.5 s. Identical signal properties including the fraction of "slow spines" are observed in response to TPU of glutamate (Bywalez et al., 2015). This unitary postsynaptic Ca^{2+} entry is mainly mediated by NMDA receptors, with additional contributions by low- and high voltage activated Ca^{2+} channels and Ca^{2+}-induced Ca^{2+} release (CICR; Egger et al., 2005). Relief from the Mg^{2+} block is provided via a local AP ("spine spike," Bywalez et al., 2015), while native GC AMPA receptors are not Ca^{2+}-permeable (Jardemark et al., 1997; Egger et al., 2005).

However, these previous recordings of synaptic fluorescence transients were all performed with the Ca^{2+} indicator dye OGB-1 (100 μM, K_d = 200 nM). Therefore transients are substantially buffered and do not reflect true kinetics of Ca^{2+} signals (Egger and Stroh, 2009), even though their observed decay times seem to fit well with the time scale of asynchronous release. Thus here we asked whether synaptic signals are indeed slow, also in comparison to AP-mediated transients, by using a low-affinity Ca^{2+} dye.

Moreover, we had observed earlier on that the triggering of long-lasting depolarizations in the wake of synaptically evoked GC APs required both NMDA receptor activation and opening of voltage-gated Na^+ channels (Na_v; observed in both juvenile rats and adult mice) and that these long-lasting depolarizations were carried by TRPC1/4 heteromeric channels (Egger, 2008; Stroh et al., 2012). Since we know by now that local postsynaptic inputs can trigger "spine spikes" within the spine head (Bywalez et al., 2015), we hypothesized that already local synaptic signals might involve a long-lasting cationic inward current I_{CAN} (via TRPCs or otherwise). To this end, we combined Na^+ imaging based on the dye SBFI (Rose et al., 1999; Ona-Jodar et al., 2017) with TPU of glutamate.

Finally, we noticed that in spite of similar endogenous Ca^{2+} dynamics and similar amplitudes of spontaneous and evoked synaptic transients in adult mouse and juvenile rat GCs (Egger et al., 2005; unpublished observations Egger and Stroh, Egger and Stroh, 2009; Abraham et al., 2010), postsynaptic Ca^{2+} signals in adult mouse GCs were yet slower with regard to their rise time (original data set from Abraham et al., 2010, in which kinetics had not been analyzed quantitatively). This study had revealed a correlation between behavioral performance in a go/no-go odor discrimination task, and modifications of postsynaptic ΔCa^{2+} into the majority of GC spines via viral transfection, across three sample groups: (1) WT mice, (2) mice with a deletion of the GluA2 AMPAR subunit (ΔGluA2; increased Ca^{2+} entry) which resulted in faster discrimination and thus a gain of function, and (3) mice with a deletion of the NR1 NMDAR subunit (ΔGluN1, i.e., reduced Ca^{2+} entry), which resulted in slowed discrimination, i.e., a loss of function. Here we provide a quantitative analysis of the kinetics of the respective Ca^{2+} signals and the response probability and use the genetic pharmacology provided by the viral knockdown to infer possible mechanisms for the slow rise.

In summary, here we aim to unravel the pyhsiological time courses of postsynaptic Ca^{2+} and Na^+ signals in juvenile rat

GCs in order to investigate their overlap with the previously established time course of asynchronous release. Moreover, we describe an additional potential source of delayed release from adult mouse GC spines.

METHODS

Juvenile Rat Experiments: Preparation, Electrophysiology

Sagittal OB brain slices (thickness 300 μm) were prepared in artificial cerebrospinal fluid (ACSF, composition see below) following procedures in accordance with the rules laid down by the EC Council Directive (86/89/ECC) and German animal welfare legislation. Slices were incubated a water bath at 33°C for 30 min and then kept at room temperature (22°C) until recordings were performed.

The extracellular ACSF was bubbled with carbogen and contained (in mM): 125 NaCl, 26 $NaHCO_3$, 1.25 NaH_2PO_4, 20 glucose, 2.5 KCl, 1 $MgCl_2$, and 2 $CaCl_2$. Whole cell current clamp recordings were performed at room temperature (22 °C) and granule cells were held near their resting potential of −80 mV. Granule cells were filled with an internal solution containing the following substances (in mM): 130 K-Methylsulfate, 10 HEPES, 4 $MgCl_2$, 2 ascorbic acid, 10 phosphocreatine-di-tris-salt, 2.5 Na_2ATP, 0.4 NaGTP, and 1 mM SBFI (Na^+-binding benzofuran isophthalate, Teflabs, Austin, TX, United States and Molecular Probes, Eugene, OR, United States) or 0.1 OGB-6F (Ca^{2+} indicator, Thermo Fisher Scientific, Waltham, MA, United States). The patch pipette resistance varied between 6 and 7 MΩ.

Juvenile Rat Experiments: Combined Two-Photon Imaging and Uncaging

For Na^+ imaging experiments, electrophysiology and imaging were performed as in Ona-Jodar et al. (2017), and for Ca^{2+} imaging experiments as in Bywalez et al. (2015). Uncaging is also described in detail in Bywalez et al. (2015). Imaging and uncaging were performed on a Femto-2D-uncage microscope (Femtonics, Budapest, Hungary). Two tunable, Verdi-pumped Ti:Sa lasers (Chameleon Ultra I and II respectively, Coherent, Santa Clara, CA, United States) were used in parallel. The first laser was set either to 840 nm for excitation of OGB-6F or to 800 nm for excitation of SBFI in GC spines and dendrites, and the second laser was set to 750 nm for uncaging of caged glutamate. The two laser lines were directly coupled into the pathway of the microscope with a polarization cube (PBS102, Thorlabs Inc., Newton, NJ, United States) and two motorized mirrors. As caged compound we used DNI-caged glutamate (DNI; Femtonics). DNI was used at 1 mM in a closed perfusion circuit with a total volume of 12 ml. Caged compounds were washed in for at least 10 min before starting measurements. The uncaging laser was switched using an electro-optical modulator (Pockels cell model 350-80, Conoptics, Danbury, CT, United States).

Na^+ and Ca^{2+} signals were imaged in line scanning mode with a temporal resolution of ∼1 ms. The scan position was checked and readjusted if necessary before each measurement to account for drift.

Adult Mouse GC Ca^{2+} Imaging (Data From Abraham et al., 2010)

The experiments in adult mice are described in Abraham et al. (2010); the new analyses presented here are based on the very same data set. Briefly (see Abraham et al., 2010, for details), GC-specific deletion of GluA2 AMPAR subunit and GluN1 NMDAR subunit had been achieved by viral expression of Cre recombinase in mice with conditional alleles of GluA2 and GluN1. To restrict the deletion to GCs we had injected rAAV Cre only in the anterior portion with respect to the center of the dorsal OB surface. OB slices had been prepared after an incubation time of at least 2 weeks. GluA2- and GluN1-depleted GCs had been identified by somatic fluorescence arising from co-expression of Cre recombinase and Kusabira orange (Tang et al., 2009). Mitral/tufted cells had been activated via glomerular extracellular stimulation, and responding GC spines had been searched for with two-photon Ca^{2+} imaging in GCs patched below the stimulated glomerulus that had responded to glomerular stimulation with a detectable EPSP (see also **Figure 3A**).

Data Analysis and Statistics

Imaging data were analyzed with custom written macros in Igor Pro (Wavemetrics, Lake Oswego, OR, United States), as described previously (Egger et al., 2003, 2005). All imaging signals (OGB-6, OGB-1, SBFI) were analyzed in terms of $\Delta F/F = (F(t) - F_0)/F_0$. Rise times were measured between 20 and 80% of the absolute maximal ΔF/F amplitude, and half durations $t_{1/2}$ reflect the period from this maximal amplitude to the half-maximal amplitude. SBFI ΔF/F signals were converted into absolute concentration changes $\Delta[Na^+]_i$ according to the previously established calibration on the same system: for non-saturating signals a 10% change in fluorescence emission of SBFI corresponds to a change of 22.3 mM in $[Na^+]_i$ (Ona-Jodar et al., 2017). The response probability is an estimate of the release probability and was calculated as the ratio of detected responses to the total number N of stimulations (average $N = 14 \pm 5$ in WT).

Statistical comparisons were made with non-parametric tests (Wilcoxon test for paired and Mann-Whitney test for unpaired data sets). Comparisons between WT GC responses and the ΔGluA2 and ΔGluN1 GC groups were made via pairwise Mann-Whitney tests with Bonferroni correction. Frequency distributions of parameters were compared with the Kolmogorov-Smirnov test. Mean values are given ± SD.

RESULTS

Time Course of Synaptic Spine Ca^{2+} Signals With Minimal Exogenous Buffering

To investigate the local mechanisms underlying the asynchronous component of reciprocal GABA release, we

aimed to detect local postsynaptic Ca^{2+} signaling in GC spines with as little exogenous buffering as possible, since sluggish extrusion of Ca^{2+} might also contribute to delayed release (Egger and Stroh, 2009). The low-affinity dye OGB-6F ($K_d \approx 8$ μM, Tran et al., 2018) was used at a concentration of 100 μM, where the kinetics of OGB-6F fluorescence transients in response to single somatic APs $(\Delta F/F)_{sAP}$ are identical to the kinetics determined by extrapolation of measurements with varying concentrations of OGB-1 ($K_d \approx 0.2$ μM) to zero added buffer (Egger and Stroh, 2009).

TPU of DNI with similar parameters as in Bywalez et al. (2015; **Figure 1A**) evoked Ca^{2+} transients $(\Delta F/F)_{TPU}$ in juvenile rat GC spine heads (postnatal days PND11-19), with a mean amplitude of 24 ± 9%, a mean rise time of 55 ± 32 ms and a mean half duration $t_{1/2}$ of 445 ± 225 ms (n = 11 spines, **Figures 1B,C**). These transients were strictly localized to the spine head (mean $(\Delta F/F)_{TPU}$ amplitude in adjacent dendritic shaft 2 ± 1%, ratio vs. spine head 0.09 ± 0.03). While $t_{1/2}$ was difficult to analyze in some of the individual spine responses because of noise, the averaged transient yielded a $t_{1/2}$ of ∼550 ms, substantially slower than the half-duration of AP-mediated transients recorded in a subset of these spines (n = 8, $t_{1/2}$ of averaged ΔF/F ∼100 ms, **Figure 1B** bottom). The influence of buffering on the rise time should be less pronounced since the latter mostly reflects the duration of Ca^{2+} entry into the cytoplasm. Indeed, the set of rise times is statistically not different from a previous TPU data set using also DNI and OGB-1 (rise time 76 ± 57 ms, median 60 ms, n = 42, P = 0.19, Mann-Whitney test; data from Bywalez et al., 2015).

Time Course of Synaptic Spine Na^+ Signals With Minimal Added Exogenous Buffering

Postsynaptic Na^+ signals could report the activity of the Ca^{2+}-impermeable GC AMPARs and of spine Na_Vs and TRPC1/4 in a more direct way than Ca^{2+} signals and thus yield additional information on the state of the locally activated GC spine. We performed two-photon Na^+ imaging using SBFI at a concentration of 1 mM. This is far below both the Na^+ concentration of 15 mM in the internal solution and the apparent K_D of SBFI, so the degree of introduced buffering is negligible (Mondragão et al., 2016; **Figure 2**).

The ensuing Na^+ signals following TPU of glutamate at individual spine heads with similar parameters as in the OGB-6F experiments had a mean amplitude of $-(\Delta F/F)_{TPU}$ = 4.9 ± 1.4% in the spine head of juvenile rat GCs (PND 11–18). They were localized to the spine head to some extent but mostly also detectable in the adjacent dendritic shaft (mean amplitude ratio dendrite/spine 0.56 ± 0.38 of spine signal; P < 0.001 vs. spine signal amplitude; n = 13 spines in 11 GCs). Conversion of the spine signal amplitude to absolute changes in $[Na^+]_i$ (Rose et al., 1999; Ona-Jodar et al., 2017) yielded a mean increase $\Delta[Na^+]_i$ by ∼10 mM. The average rise time was 250 ± 130 ms and the half duration $t_{1/2}$ = 890 ± 770 ms in the spines, including frequently observed plateau-like phases. Individual $(\Delta F/F)_{TPU}$ signals in dendritic shafts were usually too noisy for kinetic analysis.

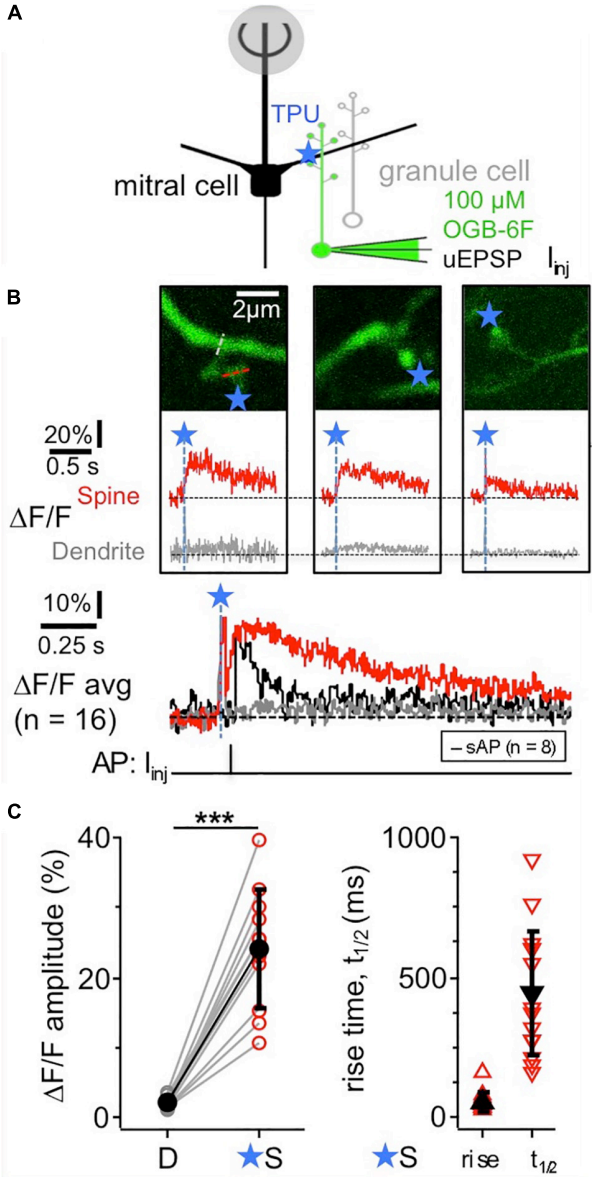

FIGURE 1 | TPU-evoked Ca^{2+} entry into juvenile rat GC spines with low exogenous buffering. Imaging of TPU-evoked Ca^{2+} transients within GC spines with low exogenous buffering (100 μM OGB-6F). **(A)** Scheme of experiment: whole cell recording from GC (filled with dye via pipette) and TPU at spine head. The pipette was also used for brief current injections to evoke somatic APs (sAP). **(B)** Top: two-photon scans (z-projections) of three representative examples of individual spines filled with OBG-6F. Blue stars denote uncaging locations. Red and gray dotted line indicate line scan positions. Middle: respective averaged fluorescence transients $(\Delta F/F)_{TPU}$ that were collected from line scans across the spine heads above (S, red) and the adjacent dendrite at the base of the spine neck (D, gray). Blue dashed lines and star: time point of uncaging. Bottom: $(\Delta F/F)_{TPU}$ transients averaged across experiments (Ca^{2+} imaging: n = 11 spines) with the same time axis, spine response in red and dendrite response in gray. The black trace in the Ca^{2+} imaging graph represents the averaged response $(\Delta F/F)_{AP}$ to a backpropagating somatically evoked AP (recorded in n = 8 of the 11 spines). **(C)** Cumulative plots of $(\Delta F/F)_{TPU}$ amplitudes in dendrite and spine pairs (highly significantly different: P < 0.001, Wilcoxon test), and of rise times and half durations $t_{1/2}$ of $(\Delta F/F)_{TPU}$ within the spine heads (mostly not detectable in the dendrites).

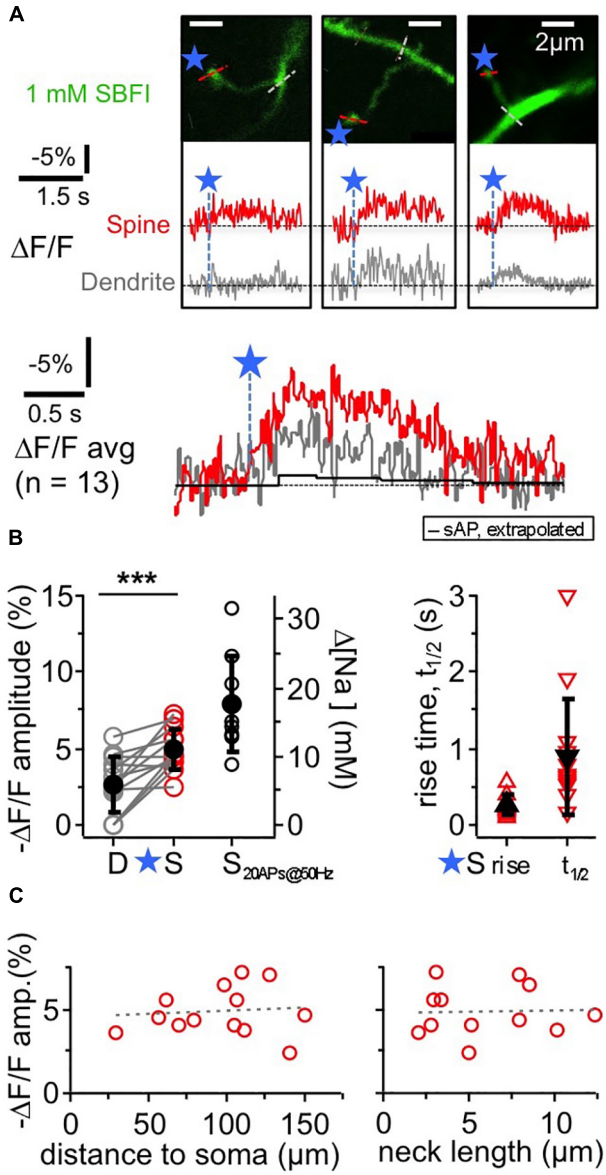

FIGURE 2 | TPU-evoked Na^+ entry into juvenile rat GC spines. Imaging of TPU-evoked Na^+ transients within GC spines with low exogenous buffering (1 mM SBFI). Experimental setup as in **Figure 1A**. **(A)** See also **Figure 1B**. Top: two-photon z-stacks of three representative examples of individual spines filled with SBFI. Blue stars denote uncaging locations. Red and gray dotted line indicate line scan positions for the leftmost spine. Middle: respective averaged fluorescence transients $(\Delta F/F)_{TPU}$ within the above spines (S, red) and within the adjacent dendrite (at the base of the spine neck, D, gray). Bottom: $(\Delta F/F)_{TPU}$ transients averaged across experiments (n = 13 spines) with the same time axis, spine response in red and dendrite response in gray. Note the similar time course of the dendritic response. Black trace: extrapolated response $(\Delta F/F)_{AP}$ to a single backpropagating somatically evoked AP (from mean response to 20 APs at 50 Hz, see **(B)** Amplitude $(\Delta F/F)_{AP} \approx -0.4\%$, $t_{1/2} \approx 1.7$ s). **(B)** Cumulative plots. Left panel: $(\Delta F/F)_{TPU}$ amplitudes in dendrite and spine pairs (highly significantly different, $P < 0.001$, Wilcoxon test) and $(\Delta F/F)_{50Hz}$ amplitudes in response to a 50 Hz train of 20 APs in a subset of the same spine heads (n = 9). Right axis: changes in $[Na^+]_i$ concentration (calibration from Ona-Jodar et al., 2017). Right panel: half

(Continued)

FIGURE 2 | Continued

durations $t_{1/2}$ of $(\Delta F/F)_{TPU}$ within the spine heads ($t_{1/2}$ could not be measured in most dendritic transients because of noise). **(C)** $(\Delta F/F)_{TPU}$ spine amplitudes vs. distance of the spine to the soma and spine neck length (means 99 ± 35 µm and 5.9 ± 3.3 µm respectively, n = 12). Dashed lines: linear fit. No significant correlations.

As for TPU-evoked Ca^{2+} transients (Bywalez et al., 2015), there were no significant correlations between spine $(\Delta F/F)_{TPU}$ amplitudes and distance to soma or spine neck length (**Figure 2C**), and also no correlation between the amplitude ratio of spine/dendrite and spine neck length (not shown).

Again, we averaged data across all spine/dendrite pairs (**Figure 2A** bottom). The averaged spine signal showed an initial plateau-like phase of ∼600 ms, and the averaged dendrite signal mirrored the kinetics of the spine signal, which is expected because of the fast diffusion of Na^+ into the dendrite (Mondragão et al., 2016). Still, these TPU-evoked Na^+ signals are very slow in view of the overall fast diffusion of Na^+ and also compared to recent data from synaptic Na^+ signals in hippocampal pyramidal neuron spines (their $t_{1/2}$ ∼20 ms; Miyazaki and Ross, 2017), and therefore are best explained by a persistent influx of Na^+ (see section "Discussion"). The TPU-evoked spine Na^+ signals are also very large as compared to the Na^+ influx induced by single backpropagating APs. The latter was on the order of 0.4 mM (as extrapolated from train stimulation of a subset of the same spines with 20 APs at 50 Hz: $(\Delta F/F)_{50Hz} = -7.9 \pm 3.1\%$ $n = 9$, **Figure 2B**; see Figure 5 in Ona-Jodar et al. (2017) for train responses).

From these experiments we conclude that the time course of asynchronous components of GABA release triggered by unitary activation (Lage-Rupprecht et al., 2020) matches well with substantial and prolonged elevation of postsynaptic Na^+ and Ca^{2+} concentrations in the GC spine. Late release therefore might result from local processing following unitary inputs to the reciprocal spine (see section "Discussion").

Postsynaptic GC Spine Ca^{2+} Signals in Adult Mice

As shown above, both postsynaptic Ca^{2+} and Na^+ signaling in juvenile rat GC spines is likely to persist for several 100 ms. Moreover, we noticed that in spite of similar endogenous Ca^{2+} dynamics (with regard to both buffering capacity and extrusion: Egger and Stroh, 2009), postsynaptic spine Ca^{2+} transients in adult mice evolved yet more sluggishly. Here we analyzed the kinetics and response probability of postsynaptic GC spine Ca^{2+} signals in response to glomerular stimulation from an earlier data set that was recorded with two-photon fluorescence imaging in acute bulb slices from WT animals or from animals with partial GC GluN1 or GluA2 deletions via viral transfection (PND 36–66; dye 100 µM OGB-1; Abraham et al., 2010).

Postsynaptic Ca^{2+} transients in WT adult mouse GC spines were also strictly localized to spine heads and occurred with a rather low probability upon glomerular stimulation, even though compound EPSPs were readily recorded at the soma (see **Figure 3B**), rendering the set of recorded individual responses rather small (estimated response probability P_r 0.10 ± 0.06,

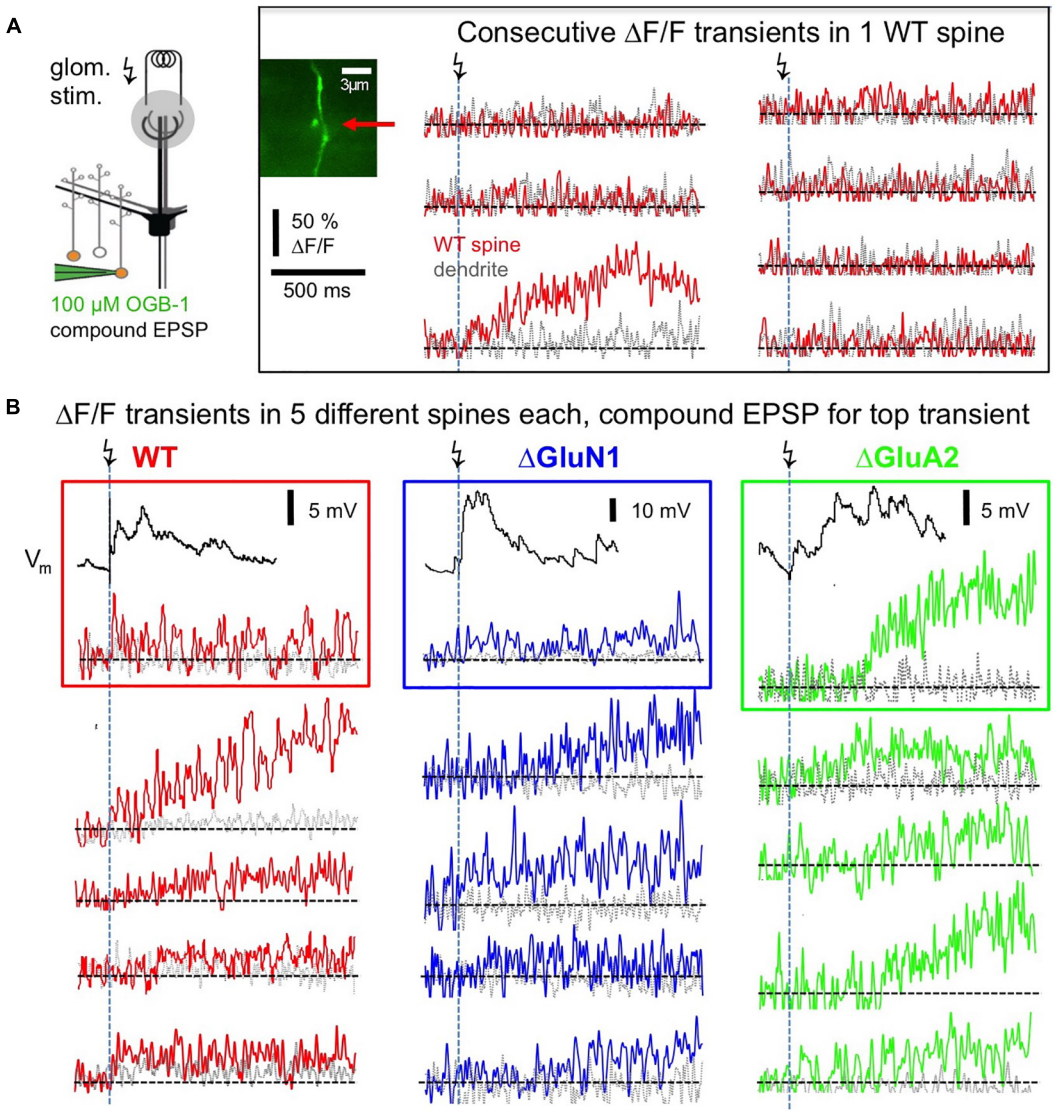

FIGURE 3 | Postsynaptic responses in adult WT, ΔGluA2 and ΔGluN1 GC spines. **(A)** Left: Scheme of experiment (modified from Abraham et al., 2010, their **Figure 2**). Electrical glomerular stimulation and whole-cell recording of the resulting compound EPSP from a GC, including two-photon imaging of a responding spine and its adjacent dendritic shaft. Genetically modified GCs (ΔGluA2 and ΔGluN1) were identified by the expression of the fluorescent construct Kusabira-Orange. Middle: scan of a WT spine and dendrite. Right: line scans through the spine and dendrite during consecutive glomerular stimulations. Only one response occurred (3rd trace), that shows a slowly evolving Ca^{2+} transient confined to the spine head. **(B)** Single responses from other spines, with each trace imaged in a different spine. Same scales for ΔF/F and time as in **(A)**. Top transients with their associated compound EPSP recordings. Left (red): WT GCs. Middle (blue): ΔGluN1 GCs. Right (green): ΔGluA2 GCs. Note the larger size and yet slower evolution compared to WT and ΔGluN1.

n = 13 spines; **Figures 3A**, **4A–C**, see section "Methods"). While some responses rose rather quickly (e.g., top left response in **Figure 3B**, distribution in **Figures 4B,C**), in most cases the peak amplitude of these $(\Delta F/F)_{syn}$ signals occurred several 100 ms later (average time to peak (TTP) 420 ± 440 ms, beginning with 20 ms, n = 14 events; 2 events with peak beyond scan time of 1,000 ms; if these are included with the end of scan as peak time: TTP_{min} = 540 ± 510 ms). TTP was uncorrelated to peak amplitude (r = 0.32, P = 0.11, n = 14). Such slowly rising signals were never observed in the adjacent dendrite. We also recorded responses to single backpropagating APs $(\Delta F/F)_{sAP}$ in 9 of the 13 spines, with mean rise times of 15 ± 4 ms (see also Stroh et al., 2012).

This slow rise was unrelated to Ca^{2+} entry via NMDARs, since similarly slow signals occurred in ΔGluN1 GC spines with reduced Ca^{2+} entry (**Figures 3B**, **4A–C**; ΔGluN1 TTP 580 ± 260 ms, beginning with 200 ms, n = 13 events; 4 events with peak beyond scan, TTP_{min} = 740 ± 350 ms; no significant difference to WT TTP_{min}: Kolmogorov-Smirnov test P = 0.09). The probability to observe such events in ΔGluN1 GCs (P_r = 0.18 ± 0.15, n = 7 spines) was also not significantly different from WT.

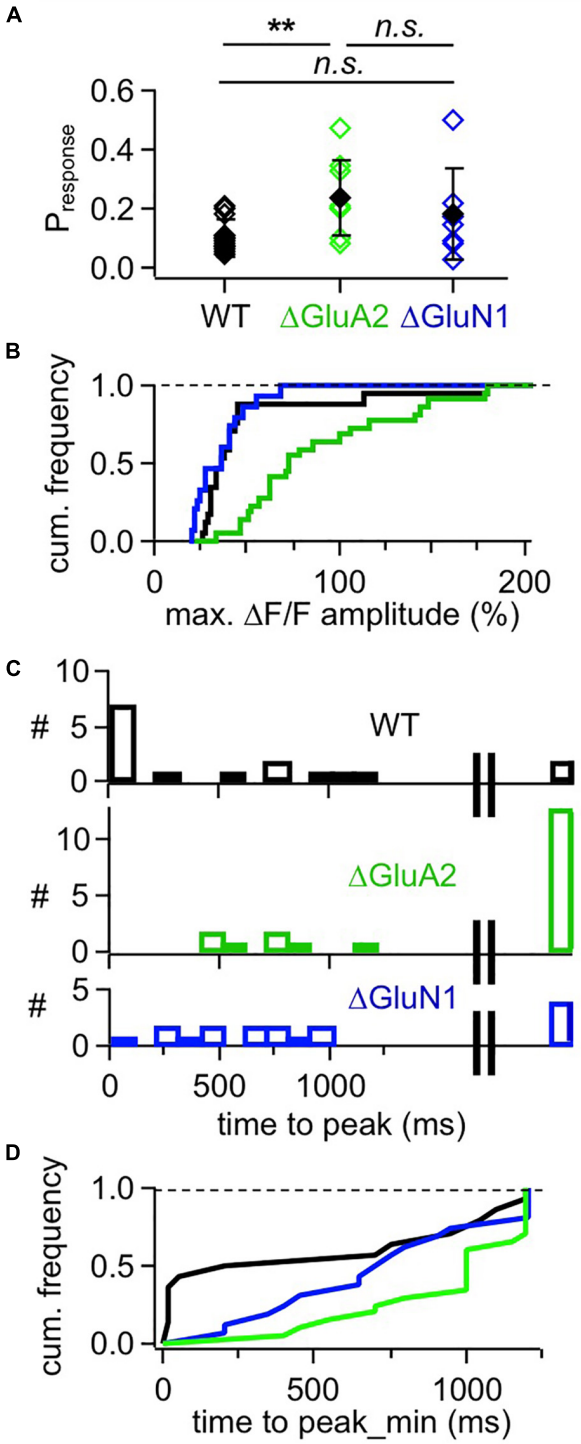

FIGURE 4 | Cumulative analyses of responses in adult mouse WT, ΔGluA2 and ΔGluN1 GCs. **(A)** Estimated likelihood of observing a $(\Delta F/F)_{syn}$ response upon glomerular stimulation ("response probability," calculated as number of responses divided by number of stimulations). Pairwise comparison (Mann-Whitney test) and Bonferroni: P_r WT vs. ΔGluA2: $P = 0.0018$, ΔGluA2 vs. ΔGluN1: $P = 0.42$, WT vs. ΔGluN1: $P = 0.51$. **(B)** Frequency distribution of $(\Delta F/F)_{syn}$ response amplitudes for the three GC groups. WT is different from ΔGluA2, but not from ΔGluN1 ($P < 0.001$ and $P = 0.16$, Kolmogorov-Smirnov). **(C)** Distributions of $(\Delta F/F)_{syn}$ response time to peak for the three GC groups. The rightmost bar shows the responses where the peak might not yet have been reached within the scanning time window (up to 1,200 ms post stimulation). **(D)** Frequency distribution of $(\Delta F/F)_{syn}$ response time to peak for the three GC groups, with peaks possibly beyond scan window set to 1,200 ms (minimal time to peak). WT is different from ΔGluA2, but not from ΔGluN1 ($P = 0.02$ and $P = 0.09$, Kolmogorov-Smirnov test).

Additional Ca^{2+} entry due to GluA2 deletion, however, resulted in larger ΔF/Fs that rose even more slowly than in WT spines (**Figures 3B**, **4A–C**; ΔGluA2 TTP 680 ± 250 ms, beginning with 400 ms, $n = 7$ events; 13 events with peak beyond scan; all events: $TTP_{min} = 960 \pm 270$ ms: Kolmogorov-Smirnov test $P < 0.02$ vs. WT). The probability of such events was significantly higher than in WT ($P_r = 0.24 \pm 0.13$, $n = 8$ spines, $P = 0.006$), possibly due to their improved detectability because of larger ΔF/F amplitudes. Such a slow evolution in postsynaptic Ca^{2+} should also be reflected in the strength and time course of reciprocal GABA release. Indeed, it was shown previously in recordings of mitral cell hyperpolarizing potentials following a train of 20 APs at 50 Hz (a stimulation that efficiently activates reciprocal release from GCs; Figure 4 in Abraham et al., 2010), that ΔGluA2 resulted in a significantly stronger and almost two times longer mitral cell recurrent inhibition compared to WT. The relevant time scales match our time to peak data including the late peaks of $(\Delta F/F)_{syn}$ reported above (ΔGluA2: half duration $t_{1/2}$ ~1,150 ms; WT: $t_{1/2}$ ~600 ms). Conversely, ΔGluN1 did not exert a significant influence on the duration of recurrent inhibition and only a mild reduction on its amplitude, in line with the lack of a significant effect on TTP of $(\Delta F/F)_{syn}$ described above (Supplementary Information in Abraham et al., 2010).

DISCUSSION

Relation Between Ca^{2+} and Na^{+} Transients in the GC Spine Head and Asynchronous Release

Asynchronous release—i.e., release that happens later than the fast coupling of HVA presynaptic Ca^{2+} currents to the release machinery (e.g., Kaeser and Regehr, 2014)—is a phenomenon known from many central synapses. It is often observed at repetitively stimulated synapses (Wen et al., 2013), which would also hold true for the classical dendrodendritic inhibition protocol, where voltage-clamped mitral cells are being depolarized for 20–50 ms and thus ongoing release of glutamate from mitral cells is likely to happen over dozens of ms and subsequent asynchronous release of GABA has been documented by many groups (see section "Introduction"). Thus it is at first surprising that local, unitary-like stimulation of GC spines by TPU would suffice to elicit asynchronous release, which we have recently documented (Lage-Rupprecht et al., 2020). However, the temporal extent of this asynchronous release was shorter

than in the classical dendrodendritic inhibition experiments (maximal extent of ∼500 ms vs. >1 s) and therefore there might be additional mechanisms involved whenever GCs are activated more strongly.

The NMDAR-mediated Ca^{2+} current into juvenile rat GC spines is expected to recede within less than 200 ms (e.g., Hestrin et al., 1990; Egger et al., 2005). It is thus on its own unlikely to mediate substantial asynchronous release far beyond the first 100 ms, even though the slow extrusion of Ca^{2+} from the cytoplasm may contribute to delayed release (Egger and Stroh, 2009). To further unravel signaling downstream of the NMDAR and Na_v activation during the local spine spike, we investigated the time course of postsynaptic Na^+ and Ca^{2+} elevations with minimal exogenous buffering. Both ion species showed prolonged elevations for durations well compatible with asynchronous output.

Previously, somatic AP-mediated and postsynaptic Ca^{2+} transients recorded with 100 μM OGB-1 were observed to decay with roughly equal half durations of 600 ms (except for the subpopulation of "slow spines" featuring transients with $t_{1/2} > 1.5$ s, which made up one third; Egger et al., 2005; Bywalez et al., 2015). Whereas here TPU-evoked transients were always substantially longer than AP-evoked transients in the same spine, on the order of 500 vs. 100 ms, dissociating physiological postsynaptic Ca^{2+} dynamics from exogenous buffer effects. Interestingly, "slow spines" were not observed here, also not in an additional set of $n = 12$ spine responses that was excluded from the analysis because of inadvertently longer uncaging intervals. This observation might be explained by the existence of a Ca^{2+}-dependent extrusion mechanism, that is activated only by high levels of $[Ca^{2+}]_i$ which are buffered away in the presence of 100 μM OGB-1 (such as Ca^{2+}-ATPases, Na^+/Ca^{2+} exchangers or mitochondrial Ca^{2+} uniporters, e.g., Sabatini et al., 2002; Chamberland et al., 2019).

In particular, there was a substantial and long-lasting postsynaptic elevation of Na^+. This detected $\Delta[Na^+]_i$ is ∼20-fold higher than what could be extrapolated for a single backpropagating GC AP from responses to train stimulation (∼10 vs. ∼0.4 mM, see **Figure 2A**). Thus there must be substantial postsynaptic Na^+ entry on top of local Na_v activation, in line with earlier reports of Na^+ signals in response to suprathreshold synaptic stimulation in hippocampal pyramidal neurons (Rose and Konnerth, 2001). In GC spines, the average time course of $\Delta[Na^+]_i$ showed a plateau-like phase of >500 ms, very much unlike recent observations of single synaptic Na^+ transients in spines of hippocampal pyramidal neurons which decayed within 20 ms—but were of a similar magnitude (∼5 mM; Miyazaki and Ross, 2017). While the slow decay of the GC spine $\Delta[Na^+]_i$ might be explained to some extent by the diffusive barrier provided by the high neck resistance (predicted as ≥1 GΩ, Bywalez et al., 2015), the origin of the $[Na^+]_i$ plateau requires a persistent Na^+ entry that outlasts AMPAR/NMDAR activation. It thus might indeed be related to extended local TRPC1/4 activation downstream of NMDAR activation, since there was no global plateau current in ΔGluN1 GCs (Stroh et al., 2012).

Alternatively or in addition, the $[Na^+]_i$ plateau might correspond to a local UP state, i.e., a local plateau potential [which are known to occur in dendrites of e.g., prefrontal pyramidal cells or striatal spiny neurons (Milojkovic et al., 2005; Plotkin et al., 2011)] in the GC spine which could cause TRPC1/4 activation and thus ongoing local influx of Ca^{2+} sufficient to trigger recurrent release. This influx should also happen close to the release machinery, since buffering of GC Ca^{2+} by EGTA had no effect on asynchronous release (Isaacson, 2001). Such local UP states or plateau potentials might not be evident in GC somatic membrane potential recordings due to substantial filtering by the large spine neck resistance, even though preliminary simulations of UP states in GC spines show that such plateaus would undergo considerably less filtering that spine spikes because of their slow kinetics (Aghvami and Egger, unpublished observations). So far, evidence for plateau-like states within GC spines could not be gathered from our somatic current clamp recordings; spine recordings with advanced voltage-sensitive dyes would be required to further elucidate this issue. Increased $[Na^+]_i$ within the observed regime might also provide positive feedback to NMDARs via an upregulation of NMDAR Ca^{2+} currents by the Src kinase (Yu et al., 1997; Yu and Salter, 1998) and thus cause persistent Ca^{2+} and Na^+ entry. Further experiments are required to unravel such interactions.

The large size of $\Delta[Na^+]_i$ amplitudes in the adjacent dendrite is unexpected, since Na^+ diffusion from the spine into the dendrite should result in a substantial drop in concentration (e.g., Miyazaki and Ross, 2017) and GC spine necks are particularly long (∼6 μm in our sample, **Figure 2C**). Possible explanations for this observation include the large volume of GC spine heads (similar radius as the dendrite, Egger and Stroh, 2009), weak Na^+ extrusion from the spine head and neck, or that the source of the synaptically triggered persistent Na^+ entry mechanism postulated above is present and activated also within the dendritic shaft. In any case, dendritic Na_v channels (e.g., Egger et al., 2003; Nunes and Kuner, 2018) are unlikely to contribute to this signal since we have shown previously that the postsynaptic spine depolarization undergoes strong attenuation and thus both dendritic Na_v and Ca_v channels will not become activated (Bywalez et al., 2015)—unless several spines receive coincident inputs (Müller and Egger, 2020).

Postsynaptic Ca^{2+} Signals in Adult Mouse vs. Juvenile Rat

Endogenous Ca^{2+} buffering and extrusion, postsynaptic ΔCa^{2+} amplitudes and synaptic AP-evoked Ca^{2+} signals and long-lasting depolarizations are similar in adult mouse GCs as in juvenile rat GCs (Egger et al., 2005; Egger, 2008; Egger and Stroh, 2009; Abraham et al., 2010; Stroh et al., 2012). However, a more detailed analysis of the synaptic responses showed also two striking differences. First, we observed a strongly reduced release probability P_r (0.1 vs. 0.5). This effect might be due to maturation of the bulbar network, since in rats the strength of dendrodendritic inhibition was reported to decline steeply between PND15 and PND20 (Dietz et al., 2011). While this P_r value is no more than an estimate due to the small number of recorded responses and substantial noise in some experiments, we observed similar values also for recordings from ΔGluN1

and ΔGluA2 GCs, with the slight increase for ΔGluA2 possibly explained by the improved detectability of signals in these cells.

Second, yet more strikingly, we observed a broad variability in signal onset and rise. In all three types of GCs, there was a subset of signals with an apparently delayed onset and a very slow evolution within hundreds of milliseconds up to seconds. These features were unchanged between WT and ΔGluN1, so NMDARs are not required to generate such responses. Rather, the ΔGluA2 GCs showed an increased fraction of such slow signals, indicating that Ca^{2+}-permeable AMPARs can also feed into this mechanism. This effect could be mediated perhaps by enhancing postsynaptic Ca^{2+} induced Ca^{2+} release (CICR) that we have previously shown to also occur in rat GC spines (Egger et al., 2005). Such a Ca^{2+}-dependent mechanism might also be supported by slow extrusion (Egger and Stroh, 2009). Together with the current observations these data are consistent with voltage-gated Ca^{2+} channels or Ca^{2+}-permeable AMPARs triggering CICR, rather than NMDARs, as was also observed in other neuron types (e.g., Chávez et al., 2006; Plotkin et al., 2013). In any case, the respective mechanism is also likely to undergo developmental upregulation since a delayed and extended postsynaptic Ca^{2+} rise was not observed in young rat GC spines. In adult mice, somatic GC Ca^{2+} responses to odorants were also reported to show a high variability with regard to onset and rise (Wienisch and Murthy, 2016).

Intriguingly, apparently slowly rising signals in GC spines may also be of presynaptic origin, e.g., due to late firing of principal neurons in response to glomerular stimulation (Kapoor and Urban, 2006; Gire et al., 2012; Giridhar and Urban, 2012). In our experiments, this source might also contribute in the wake of glomerular stimulation; a correlation with late EPSPs is difficult to test because of the high spontaneous activity and low number of responses in our recordings. However, such delayed presynaptic activity is probably not a main source of slowly rising signals in our data set, since an enhancement of presynaptic signal contributions specifically in ΔGluA2 GCs appears rather unlikely.

As already implied by this possibility of delayed presynaptic inputs, slow signals in OB networks are not restricted to GC-mediated recurrent inhibition; representations of olfactory stimuli in general are known to evolve over long time scales of hundreds to thousands of ms (Friedrich and Laurent, 2001; Uchida and Mainen, 2003; Abraham et al., 2004, 2010; Rinberg et al., 2006; Gschwend et al., 2015). Aside from the original notion that these time scales are required for decorrelation of principal neuron activity, persistent representations might also be involved in the formation of odor after-images (Patterson et al., 2013).

With regard to further functions of slow signals, they are at first glance unlikely to play a direct role during odor discrimination or background segregation, since these discriminations usually occur within considerably less than 500 ms, even for difficult mixtures and/or many components (Abraham et al., 2004, 2010; Kepecs et al., 2005; Rokni et al., 2014; Bhattacharjee et al., 2019). Rather, slow signals may be involved in learning and plasticity, also during learning of the mixture discrimination task (Abraham et al., 2004, 2010; Gschwend et al., 2015).

Aberrant slow signals due to pathological changes (extended or reduced asynchronous release) would thus be expected to disrupt plasticity induction. Indeed, several pathologies such as Alzheimer's disease have been associated with enhanced asynchronous release (reviewed in Kaeser and Regehr, 2014), for example at the neuromuscular junction, and interestingly also for fast-spiking interneurons in epileptic foci in both human and rat (Jiang et al., 2012). However, so far no loss of function has been observed for the ΔGluA2 modification. Pathological or other modulations of asynchronous release from granule cells might also influence both slow and fast network oscillations, i.e., the respiration coupled θ and probably more importantly γ rhythm that GCs have been associated with (e.g., Fukunaga et al., 2014). Such interactions between asynchronous release and rhythmic activity have been demonstrated in other GABAergic interneurons, including hippocampal cholecystokinin-positive basket interneurons that are crucially involved in generation of the hippocampal theta rhythm (e.g., Hefft and Jonas, 2005), and in cortical parvalbumin-positive GABAergic neurons that power γ oscillations (e.g., Traub et al., 1998). Interestingly, increased asynchronous release of GABA might reduce the ability of these PV+ neurons to sustain γ and has been proposed as one possible mechanism for uncoupling in schizophrenia (Volman et al., 2011).

In conclusion, we find that several mechanisms such as delayed and slowly evolving excitation, slow removal of Ca^{2+} and perhaps extended local postsynaptic depolarization as indicated by the persistent elevation of Na^{+} may feed into asynchronous GC spine output. Since on the other hand there is also a fast, synchronous component of reciprocal release (Halabisky et al., 2000; Lage-Rupprecht et al., 2020), GC spines are obviously capable of parallel processing on multiple time scales, a property that appears to be further refined with maturation.

DATA AVAILABILITY STATEMENT

The raw data supporting the conclusions of this article will be made available by the authors, without undue reservation.

ETHICS STATEMENT

Ethical review and approval was not required for the animal study because according to German animal welfare legislation, our experiments in acute brain slices of rats and mice are classified as *in vitro* and do not require the approval of an ethics committee. We are, however, monitored and certified by the authorities with regard to animal handling and the preparation process, which involves anesthesia and decapitation.

AUTHOR CONTRIBUTIONS

Rat granule cell Ca^{2+} imaging was performed by VL-R, rat granule cell Na^{+} imaging by TOJ, mouse viral injections by NA

and mouse granule cell Ca^{2+} imaging by VE. VL-R, TOJ, and VE analyzed the data. VE, NA, and CR designed the research. VE wrote the manuscript. All authors except for TOJ contributed to editing the manuscript.

FUNDING

This study was funded by the BMBF (German Ministry of Education and Research, FKZ 01GQ1502; VE) with additional equipment funding by DFG-SFB 870 (Deutsche Froschungsgemeinsschaft, EG135/5-1) and GSN-LMU. Regensburg University Library provided the open access publication fees.

ACKNOWLEDGMENTS

We wish to thank A. Pietryga-Krieger for expert technical assistance, Dr. N. Gerkau (Heinrich Heine University Düsseldorf) for initial help with Na^{+} imaging, and B. Rozsa for DNI-glutamate.

REFERENCES

Abraham, N. M., Egger, V., Shimshek, D. R., Renden, R., Fukunaga, I., Sprengel, R., et al. (2010). Synaptic inhibition in the olfactory bulb accelerates odor discrimination in mice. *Neuron* 65, 399–411. doi: 10.1016/j.neuron.2010.01.009

Abraham, N. M., Spors, H., Carleton, A., Margrie, T. W., Kuner, T., and Schaefer, A. T. (2004). Maintaining accuracy at the expense of speed: stimulus similarity defines odor discrimination time in mice. *Neuron* 44, 865–876. doi: 10.1016/s0896-6273(04)00753-6

Bhattacharjee, A. S., Konakamchi, S., Turaev, D., Vincis, R., Nunes, D., Dingankar, A. A., et al. (2019). Similarity and strength of glomerular odor representations define a neural metric of sniff- invariant discrimination time. *Cell Rep.* 28, 2966–2978.e2965.

Buonviso, N., Amat, C., Litaudon, P., Roux, S., Royet, J.-P., Farget, V., et al. (2003). Rhythm sequence through the olfactory bulb layers during the time window of a respiratory cycle. *EJN* 17, 1811–1819. doi: 10.1046/j.1460-9568.2003.02619.x

Bywalez, W. G., Patirniche, D., Rupprecht, V., Stemmler, M., Herz, A. V. M., Pálfi, D., et al. (2015). Local postsynaptic voltage-gated sodium channel activation in dendritic spines of olfactory bulb granule cells. *Neuron* 85, 590–601. doi: 10.1016/j.neuron.2014.12.051

Chamberland, S., Moratalla, A. Z., and Topolnik, L. (2019). Calcium extrusion mechanisms in dendrites of mouse hippocampal CA1 inhibitory interneurons. *Cell Calcium* 77, 49–57. doi: 10.1016/j.ceca.2018.12.002

Chávez, A. E., Singer, J. H., and Diamond, J. S. (2006). Fast neurotransmitter release triggered by Ca influx through AMPA-type glutamate receptors. *Nature* 443, 705–708. doi: 10.1038/nature05123

Chen, W. R., Xiong, W., and Shepherd, G. M. (2000). Analysis of relations between NMDA receptors and GABA release at olfactory bulb reciprocal synapses. *Neuron* 25, 625–633. doi: 10.1016/s0896-6273(00)81065-x

Dietz, S. B., Markopoulos, F., and Murthy, V. N. (2011). Postnatal development of dendrodendritic inhibition in the Mammalian olfactory bulb. *Front. Cell Neurosci.* 5:10.

Egger, V. (2008). Synaptic sodium spikes trigger long-lasting depolarizations and slow calcium entry in rat olfactory bulb granule cells. *EJN* 27, 2066–2075. doi: 10.1111/j.1460-9568.2008.06170.x

Egger, V., and Stroh, O. (2009). Calcium buffering in rodent olfactory bulb granule cells and mitral cells. *J. Physiol.* 587, 4467–4479. doi: 10.1113/jphysiol.2009.174540

Egger, V., Svoboda, K., and Mainen, Z. F. (2003). Mechanisms of lateral inhibition in the olfactory bulb: efficiency and modulation of spike-evoked calcium influx into granule cells. *J. Neurosci.* 23, 7551–7558. doi: 10.1523/jneurosci.23-20-07551.2003

Egger, V., Svoboda, K., and Mainen, Z. F. (2005). Dendrodendritic synaptic signals in olfactory bulb granule cells: local spine boost and global low-threshold spike. *J. Neurosci.* 25, 3521–3530. doi: 10.1523/jneurosci.4746-04.2005

Friedrich, R. W., and Laurent, G. (2001). Dynamic optimization of odor representations by slow temporal patterning of mitral cell activity. *Science* 291, 889–894. doi: 10.1126/science.291.5505.889

Fukunaga, I., Herb, J. T., Kollo, M., Boyden, E. S., and Schaefer, A. T. (2014). Independent control of gamma and theta activity by distinct interneuron networks in the olfactory bulb. *Nat. Neurosci.* 17, 1208–1216. doi: 10.1038/nn.3760

Gire, D. H., Franks, K. M., Zak, J. D., Tanaka, K. F., Whitesell, J. D., Mulligan, A. A., et al. (2012). Mitral cells in the olfactory bulb are mainly excited through a multistep signaling path. *J. Neurosci.* 32, 2964–2975. doi: 10.1523/jneurosci.5580-11.2012

Giridhar, S., and Urban, N. N. (2012). Mechanisms and benefits of granule cell latency coding in the mouse olfactory bulb. *Front. Neural Circ.* 6:40–40.

Gschwend, O., Abraham, N. M., Lagier, S., Begnaud, F., Rodriguez, I., and Carleton, A. (2015). Neuronal pattern separation in the olfactory bulb improves odor discrimination learning. *Nat. Neurosc.* 18, 1474–1482. doi: 10.1038/nn.4089

Halabisky, B., Friedman, D., Radojicic, M., and Strowbridge, B. W. (2000). Calcium influx through NMDA receptors directly evokes GABA release in olfactory bulb granule cells. *J. Neurosci.* 20, 5124–5134. doi: 10.1523/jneurosci.20-13-05124.2000

Hall, B. J., and Delaney, K. R. (2002). Contribution of a calcium-activated non-specific conductance to NMDA receptor-mediated synaptic potentials in granule cells of the frog olfactory bulb. *J. Physiol.* 543, 819–834. doi: 10.1113/jphysiol.2002.024638

Hefft, S., and Jonas, P. (2005). Asynchronous GABA release generates long-lasting inhibition at a hippocampal interneuron–principal neuron synapse. *Nat. Neurosc.* 8, 1319–1328. doi: 10.1038/nn1542

Hestrin, S., Sah, P., and Nicoll, R. A. (1990). Mechanisms generating the time course of dual component excitatory synaptic currents recorded in hippocampal slices. *Neuron* 5, 247–253. doi: 10.1016/0896-6273(90)90162-9

Isaacson, J. S. (2001). Mechanisms governing dendritic gamma-aminobutyric acid (GABA) release in the rat olfactory bulb. *Proc. Natl. Acad. Sci. U.S.A.* 98, 337–342. doi: 10.1073/pnas.021445798

Isaacson, J. S., and Strowbridge, B. W. (1998). Olfactory reciprocal synapses: dendritic signaling in the CNS. *Neuron* 20, 749–761. doi: 10.1016/s0896-6273(00)81013-2

Jardemark, K., Nilsson, M., Muyderman, H., and Jacobson, I. (1997). Ca2+ ion permeability properties of (R,S) alpha-amino-3-hydroxy-5-methyl-4-isoxazolepropionate (AMPA) receptors in isolated interneurons from the olfactory bulb of the rat. *J. Neurophysiol.* 77, 702–708. doi: 10.1152/jn.1997.77.2.702

Jiang, M., Zhu, J., Liu, Y., Yang, M., Tian, C., Jiang, S., et al. (2012). Enhancement of asynchronous release from fast-spiking interneuron in human and rat epileptic neocortex. *PLoS Biol.* 10:e1001324. doi: 10.1371/journal.pbio.1001324

Kaeser, P. S., and Regehr, W. G. (2014). Molecular mechanisms for synchronous, asynchronous, and spontaneous neurotransmitter release. *Ann. Rev. Physiol.* 76, 333–363. doi: 10.1146/annurev-physiol-021113-170338

Kapoor, V., and Urban, N. N. (2006). Glomerulus-specific, long-latency activity in the olfactory bulb granule cell network. *J. Neurosci.* 26, 11709–11719. doi: 10.1523/jneurosci.3371-06.2006

Kepecs, A., Uchida, N., and Mainen, Z. F. (2005). The sniff as a unit of olfactory processing. *Chem. Sens.* 31, 167–179. doi: 10.1093/chemse/bjj016

Lage-Rupprecht, V., Zhou, L., Bianchini, G., Aghvami, S. S., Rózsa, B., Sassoé-Pognetto, M., et al. (2020). Presynaptic NMDA receptors cooperate with local action potentials to implement activity-dependent GABA release from the reciprocal olfactory bulb granule cell spine. *bioRxiv* [Preprint]. 440198.

Lagier, S., Carleton, A., and Lledo, P.-M. (2004). Interplay between local GABAergic interneurons and relay neurons generates gamma oscillations in the rat olfactory bulb. *J. Neurosci.* 24, 4382–4392. doi: 10.1523/jneurosci.5570-03.2004

Milojkovic, B. A., Radojicic, M. S., and Antic, S. D. (2005). A strict correlation between dendritic and somatic plateau depolarization in the rat prefrontal cortex pyramidal neurons. *J. Neurosci.* 25, 3940–3951. doi: 10.1523/jneurosci.5314-04.2005

Miyazaki, K., and Ross, W. N. (2017). Sodium dynamics in pyramidal neuron dendritic spines: synaptically evoked entry predominantly through AMPA Receptors and removal by diffusion. *J. Neurosc.* 37, 9964–9976. doi: 10.1523/jneurosci.1758-17.2017

Mondragão, M. A., Schmidt, H., Kleinhans, C., Langer, J., Kafitz, K. W., and Rose, C. R. (2016). Extrusion versus diffusion: mechanisms for recovery from sodium loads in mouse CA1 pyramidal neurons. *J. Physiol.* 594, 5507–5527. doi: 10.1113/jp272431

Müller, M., and Egger, V. (2020). Dendritic integration in olfactory bulb granule cells: threshold for lateral inhibition and role of active conductances upon simultaneous activation. *PLoS Biol.* doi: 10.1371/journal.pbio.3000873

Nunes, D., and Kuner, T. (2018). Axonal sodium channel NaV1.2 drives granule cell dendritic GABA release and rapid odor discrimination. *PLoS Biol.* 16:e2003816. doi: 10.1371/journal.pbio.2003816

Nusser, Z., Kay, L. M., Laurent, G., Homanics, G. E., and Mody, I. (2001). Disruption of GABAA receptors on GABAergic interneurons leads to increased oscillatory power in the olfactory bulb network. *J. Neurophysiol.* 86, 2823–2833. doi: 10.1152/jn.2001.86.6.2823

Ona-Jodar, T., Gerkau, N. J., Sara Aghvami, S., Rose, C. R., and Egger, V. (2017). Two-photon Na(+) imaging reports somatically evoked action potentials in rat olfactory bulb mitral and granule cell neurites. *Front. Cell Neurosci.* 11:50.

Osinski, B. L., and Kay, L. M. (2016). Granule cell excitability regulates gamma and beta oscillations in a model of the olfactory bulb dendrodendritic microcircuit. *J. Neurophysiol.* 116, 522–539. doi: 10.1152/jn.00988.2015

Patterson, M. A., Lagier, S., and Carleton, A. (2013). Odor representations in the olfactory bulb evolve after the first breath and persist as an odor afterimage. *Proc. Natl. Acad. Sci. U.S.A.* 110, E3340–E3349.

Plotkin, J. L., Day, M., and Surmeier, D. J. (2011). Synaptically driven state transitions in distal dendrites of striatal spiny neurons. *Nat. Neurosci.* 14, 881–888. doi: 10.1038/nn.2848

Plotkin, J. L., Shen, W., Rafalovich, I., Sebel, L. E., Day, M., Chan, C. S., et al. (2013). Regulation of dendritic calcium release in striatal spiny projection neurons. *J. Neurophysiol.* 110, 2325–2336. doi: 10.1152/jn.00422.2013

Rall, W., and Shepherd, G. M. (1968). Theoretical reconstruction of field potentials and dendrodendritic synaptic interactions in olfactory bulb. *J. Neurophysiol.* 31, 884–915. doi: 10.1152/jn.1968.31.6.884

Rinberg, D., Koulakov, A., and Gelperin, A. (2006). Sparse odor coding in awake behaving mice. *J. Neurosci.* 26, 8857–8865. doi: 10.1523/jneurosci.0884-06.2006

Rokni, D., Hemmelder, V., Kapoor, V., and Murthy, V. N. (2014). An olfactory cocktail party: figure-ground segregation of odorants in rodents. *Nat. Neurosc.* 17, 1225–1232. doi: 10.1038/nn.3775

Rose, C. R., and Konnerth, A. (2001). NMDA receptor-mediated Na+ signals in spines and dendrites. *J. Neurosci.* 21, 4207–4214. doi: 10.1523/jneurosci.21-12-04207.2001

Rose, C. R., Kovalchuk, Y., Eilers, J., and Konnerth, A. (1999). Two-photon Na+ imaging in spines and fine dendrites of central neurons. *Pflügers Archiv.* 439, 201–207. doi: 10.1007/s004249900123

Sabatini, B., Oertner, T. G., and Svoboda, K. (2002). The life cycle of Ca2+ ions in dendritic spines. *Neuron* 33, 439–452. doi: 10.1016/s0896-6273(02)00573-1

Schoppa, N. E., Kinzie, J. M., Sahara, Y., Segerson, T. P., and Westbrook, G. L. (1998). Dendrodendritic inhibition in the olfactory bulb is driven by NMDA receptors. *J. Neurosci.* 18, 6790–6802. doi: 10.1523/jneurosci.18-17-06790.1998

Schoppa, N. E., and Westbrook, G. L. (1999). Regulation of synaptic timing in the olfactory bulb by an A-type potassium current. *Nat. Neurosci.* 2, 1106–1113. doi: 10.1038/16033

Shepherd, G. M. (2004). *Olfactory Bulb. The Synaptic Organization of the Brain*. Oxford: Oxford University Press.

Stroh, O., Freichel, M., Kretz, O., Birnbaumer, L., Hartmann, J., and Egger, V. (2012). NMDA receptor-dependent synaptic activation of TRPC channels in olfactory bulb granule cells. *J. Neurosci.* 32, 5737–5746. doi: 10.1523/jneurosci.3753-11.2012

Tang, W., Ehrlich, I., Wolff, S. B., Michalski, A. M., Wolfl, S., Hasan, M. T., et al. (2009). Faithful expression of multiple proteins via 2A-peptide self- processing: a versatile and reliable method for manipulating brain circuits. *J. Neurosci.* 29, 8621–8629. doi: 10.1523/jneurosci.0359-09.2009

Tran, V., Park, M. C. H., and Stricker, C. (2018). An improved measurement of the Ca(2+)- binding affinity of fluorescent Ca(2+) indicators. *Cell Calcium* 71, 86–94. doi: 10.1016/j.ceca.2018.01.001

Traub, R. D., Spruston, N., Soltesz, I., Konnerth, A., Whittington, M. A., and Jefferys, G. R. (1998). Gamma-frequency oscillations: a neuronal population phenomenon, regulated by synaptic and intrinsic cellular processes, and inducing synaptic plasticity. *Prog. Neurobiol.* 55, 563–575. doi: 10.1016/s0301-0082(98)00020-3

Uchida, N., and Mainen, Z. F. (2003). Speed and accuracy of olfactory discrimination in the rat. *Nat. Neurosci.* 6, 1224–1229. doi: 10.1038/nn1142

Volman, V., Behrens, M. M., and Sejnowski, T. J. (2011). Downregulation of parvalbumin at cortical GABA synapses reduces network gamma oscillatory activity. *J. Neurosci.* 31, 18137–18148. doi: 10.1523/jneurosci.3041-11.2011

Wen, H., Hubbard, J. M., Rakela, B., Linhoff, M. W., Mandel, G., and Brehm, P. (2013). Synchronous and asynchronous modes of synaptic transmission utilize different calcium sources. *eLife* 2:e01206.

Wienisch, M., and Murthy, V. N. (2016). Population imaging at subcellular resolution supports specific and local inhibition by granule cells in the olfactory bulb. *Sci. Rep.* 6:29308. doi: 10.1038/srep29308

Yu, X.-M., Askalan, R., Keil, G. J., and Salter, M. W. (1997). NMDA channel regulation by channel-associated protein tyrosine kinase src. *Science* 275:674. doi: 10.1126/science.275.5300.674

Yu, X.-M., and Salter, M. W. (1998). Gain control of NMDA-receptor currents by intracellular sodium. *Nature* 396, 469–474. doi: 10.1038/24877

Conflict of Interest: The authors declare that the research was conducted in the absence of any commercial or financial relationships that could be construed as a potential conflict of interest.

frontiers in Synaptic Neuroscience

ORIGINAL RESEARCH
published: 05 January 2021
doi: 10.3389/fnsyn.2020.573714

Calcium Sensors STIM1 and STIM2 Regulate Different Calcium Functions in Cultured Hippocampal Neurons

Liliya Kushnireva[1,2], *Eduard Korkotian*[1,2]* *and Menahem Segal*[1]*

[1]Department of Neurobiology, The Weizmann Institute, Rehovot, Israel, [2]Faculty of Biology, Perm State University, Perm, Russia

There are growing indications for the involvement of calcium stores in the plastic properties of neurons and particularly in dendritic spines of central neurons. The store-operated calcium entry (SOCE) channels are assumed to be activated by the calcium sensor stromal interaction molecule (STIM) which leads to activation of its associated Orai channel. There are two STIM species, and the differential role of the two in SOCE is not entirely clear. In the present study, we were able to distinguish between transfected STIM1, which is more mobile primarily in young neurons, and STIM2 which is less mobile and more prominent in older neurons in culture. STIM1 mobility is associated with spontaneous calcium sparks, local transient rise in cytosolic $[Ca^{2+}]_i$, and in the formation and elongation of dendritic filopodia/spines. In contrast, STIM2 is associated with older neurons, where it is mobile and moves into dendritic spines primarily when cytosolic $[Ca^{2+}]_i$ levels are reduced, apparently to activate resident Orai channels. These results highlight a role for STIM1 in the regulation of $[Ca^{2+}]_i$ fluctuations associated with the *formation* of dendritic spines or filopodia in the developing neuron, whereas STIM2 is associated with the *maintenance* of calcium entry into stores in the adult neuron.

Keywords: dendritic spines, filopodia, store operated channels, STIM, hippocampal culture, cytosolic calcium, calcium stores

OPEN ACCESS

Edited by:
P. Jesper Sjöström, McGill University, Canada

Reviewed by:
Ilya Bezprozvanny, University of Texas Southwestern Medical Center, United States
Antoine de Chevigny, INSERM U901 Institut de Neurobiologie de la Méditerranée, France

***Correspondence:**
Eduard Korkotian
eduard.korkotian@weizmann.ac.il
Menahem Segal
menahem.segal@weizmann.ac.il

Received: *17 June 2020*
Accepted: *07 December 2020*
Published: *05 January 2021*

Citation:
Kushnireva L, Korkotian E and Segal M (2021) Calcium Sensors STIM1 and STIM2 Regulate Different Calcium Functions in Cultured Hippocampal Neurons. Front. Synaptic Neurosci. 12:573714. doi: 10.3389/fnsyn.2020.573714

INTRODUCTION

Calcium stores assume a critical role in the handling of cytosolic calcium concentration ($[Ca^{2+}]_i$) in neurons and non-neuronal cells alike (Verkhratsky, 2005; Zalk et al., 2007). The main intracellular calcium-accumulating organelle is the endoplasmic reticulum (ER). Release of calcium from ER is important for cases, where the influx of calcium ions from the extracellular space is not sufficient to raise $[Ca^{2+}]_i$, to levels needed to activate calcium-dependent protein phosphorylation, or in cases where there are no sufficient calcium channels on the plasma membrane such as in juvenile neurons. Depletion of calcium from the ER stores is sensed by stromal interaction molecule (STIM). It clusters near the depleted store, relocates to the plasma membrane, where it interacts with Orai1 voltage-independent calcium channel, to allow calcium influx into the stores, to refill them (Bogeski et al., 2012; Segal and Korkotian, 2014; Kraft, 2015). The interaction of stores/STIM/Orai complex was studied extensively in non-neuronal cells, and its malfunction has been implicated in immunological diseases (Feske et al., 2006). Compared to the vast literature on STIM/Orai functions in non-excitable cells, much less is known about their role in central neurons. STIM and Orai are localized in brain

tissue (Skibinska-Kijek et al., 2009; Segal and Korkotian, 2016), and STIM1/Orai1 can be converted from a dispersed to a punctate form upon depletion of calcium stores with thapsigargin (Klejman et al., 2009). They are important in the regulation of growth cone motility (Mitchell et al., 2012), in the regulation of voltage-gated calcium channels (Park et al., 2010), and in detrimental effects of chronic epilepsy (Steinbeck et al., 2011) and oxidative stress (Henke et al., 2013). Earlier work ascribed a role for store-operated calcium entry (SOCE) also in synaptic plasticity, in that SOCE antagonists reduce long-term potentiation in hippocampal neurons (Baba et al., 2003). The recent association of septins (Tada et al., 2007; Sharma et al., 2013) with SOCE is intriguing indeed, as septins have been found in dendritic spines of central neurons (Xie et al., 2007) and may provide a link between dendritic spines and calcium stores. Another peptide that regulates the activity of STIM1 is NEUROD2 (Guner et al., 2017) which is found in cortical neurons and attests to the importance of STIM1 in the regulation of stored calcium. In earlier studies, we explored the role of Orai1 in dendritic spine growth and plasticity (Korkotian et al., 2017; Tshuva et al., 2017) to suggest that Orai1 is critically involved in intracellular calcium regulation, specifically in dendritic spines. The present study focuses on STIMs. There are two species of STIM in central neurons, STIM1 and STIM2, and their possible differential roles in calcium stores are not entirely clear. While studies associate STIM1 with Orai1 (e.g.,Skibinska-Kijek et al., 2009; Pavez et al., 2019), there are indications that STIM2 is the dominant species in hippocampal neurons (Sun et al., 2014; Zhang et al., 2015). We were able to detect both STIM1&2 in cultured neurons (Korkotian et al., 2017), but possibly in different neuronal compartments and/or developmental stages of the neurons. In the present study, we focus on the dynamics of both STIMs concerning intracellular calcium regulation. Our results indicate that unlike STIM2, STIM1 predominates in young cells; it is highly mobile within dendrites and has a potential role in causing an influx of calcium through apparent calcium sparks (Ross, 2015) and in the formation and growth of filopodia, as suggested before for growth cones (Mitchell et al., 2012; Pavez et al., 2019). STIM2, on the other hand, is active in the more mature neurons, where it is mobilized in response to a reduction of ambient $[Ca^{2+}]_i$ and moves into dendritic spines.

MATERIALS AND METHODS

Cultures

Animal handling was as per the guidelines of the Institutional Animal Care and Use Committee of the Weizmann Institute and with the Israeli National guidelines on animal care. Cultures were prepared as detailed elsewhere (Korkotian et al., 2017). Briefly, E18–19 rat embryos were removed from pregnant decapitated mother's womb under sterile conditions. The hippocampi were dissected free and placed in a chilled (4°C), oxygenated Leibovitz L15 medium (Gibco) enriched with 30 mM glucose and gentamicin (Sigma, 20 μg/ml), and mechanically dissociated. About 10^5 cells in 1 ml medium were plated on 13 mm circular glass coverslips in each well of a 24 well plate. Cells were left to grow in the incubator at 37°C, 5% CO_2.

Neurons were transfected at 6–7 days *in vitro* (DIV) with EBFP2 or EGFP (to image cell morphology), and STIM1-mCherry or STIM2-YFP using lipofectamine 2000 and were used for imaging at 10–20 DIV.

Immunostaining

Cover glasses bearing transfected primary hippocampal cells were washed briefly with a standard extracellular solution. Cultures were then fixed with 4% paraformaldehyde in 0.1 M phosphate-buffered saline (PBS, pH 7.4) for 20 min, and washed thereafter with PBS thoroughly. Cultures were incubated for 1 h with 10% normal horse serum (NHS) in 0.1% Triton X-100 containing PBS and subsequently incubated for 24 h at 4°C with the specific antibodies. Anti STIM1 (Santa Cruz, rabbit IgG, 1:200) and anti STIM2 (goat polyclonal IgG, Santa Cruz, 1:200) were combined in different testing conditions. Cultures were incubated for 1 h with Alexa 568-labeled or Alexa 633-labeled anti-goat or anti-mouse secondary antibody (Molecular Probes, Eugene, OR, USA; 1:200, in PBS). Coverslips were rinsed, transferred onto glass slides, and mounted for visualization on a Zeiss upright LSM 880 (which allows simultaneous visualization of four fluorophores) with an anti-fading mounting medium. In all cases, secondary and tertiary dendritic segments were visualized. It should be noted that although STIM1 (**Figures 1A,D**) and STIM2 (**Figures 1B,E**) share some structural homology, they were physically located in distinctly different cellular compartments, indicating that their antibodies express low cross-reactivity (**Figures 1C,F**). Confocal image stacks were used for 3D reconstructions using Zeiss software. Figures were prepared using Photoshop CS4 graphics software (Adobe, San Jose, CA, USA).

Live Cell Imaging

Cultures were placed in the imaging chamber, on the stage of the confocal microscope using a 40× water immersion objective (1.0 NA) and imaged at a rate of 10–20 frames/s. No photo-bleaching was detected under these conditions. Standard recording medium contained (in mM); NaCl 129, KCl 4, $MgCl_2$ 1, $CaCl_2$ 2, glucose 10, HEPES 10, pH was adjusted to 7.4 with NaOH and osmolality to 320 mOsm with sucrose. Cultures were incubated with Fluo-2AM or Calcium Orange AM (CO; 2 μM, Invitrogen) for 1 h at room temperature to image variations in $[Ca^{2+}]_i$ resulting from spontaneous network activity or changes associated with STIM1 or STIM2. Imaging of cell morphology (blue, imaged at 405 nm), calcium variations (488 nm or 543 nm), and STIM1/2 (514/543 nm) were made with the appropriate wavelengths. Images were taken in the fast scan mode of the Zeiss 880 confocal microscope, using a two-track setting, in which first the 488 nm illumination was applied alone, and then a combination of 405 and 543 nm was used. This setting minimizes the cross-talk between different dyes and still allows the fast scan necessary for calcium imaging. Pinhole size was adjusted to about 2 μm. All measurements were conducted with identical laser parameters for all groups (e.g., intensity, optical section, duration of exposure, and spatial resolution).

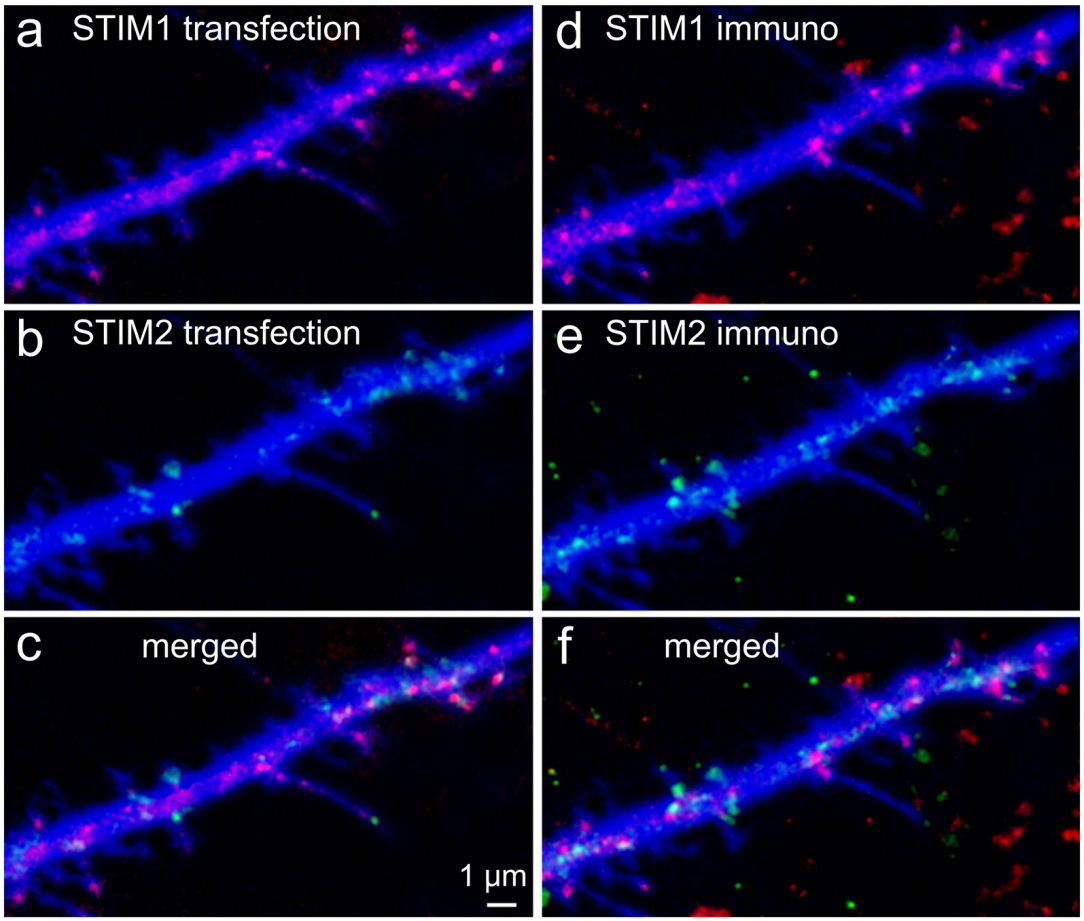

FIGURE 1 | Colocalization of transfected stromal interaction molecule 1 (STIM1) or STIM2 with native STIMs identified by immunocytochemistry. Cells were transfected at 7 days *in vitro* (DIV) and fixed in PFA at 10 DIV. Secondary antibodies were Cy2 anti-rabbit and Cy5 anti-goat. Lasers and channels were distributed as follows: BFP (cell morphology marker) 405 nm (blue), Cy2 (STIM1, anti-rabbit) 458 nm, STIM2 + YFP 514 nm, STIM1 + mCherry 543 nm, Cy5 (STIM2, anti-goat) 633 nm. Overall, in the figure, STIM1 is shown in red and STIM2 in green. 3D-reconstructed Z-stacks, slow, high-resolution imaging mode, separate imaging tracks, and the GASP detector of Zeiss 880 were used for best dye/staining separation. Partial overlap of the transfected species with the immunocytochemically detected species was clear for STIM1 (**A,D**, respectively) and was different from those of STIM2 **(B,E)**. It should be noted that some transfected STIM1&2 puncta **(A)** were not detected in the immunostaining for STIM1&2 **(D)**, probably because the antibody detects fewer puncta in the fixed tissue, unlike the transfected species that is imaged in-toto. This can be seen in the merged images **(C,F)**.

The immunostained cells were carefully examined and all cases of overlapping of two or more cells were discarded. Only well-identified cells and their segments were analyzed. In each randomly selected segment of 50 μm in length, all present protrusions were identified and counted (without preselection). They were expected to be fewer in the younger segments than in the older ones. The analysis was carried out in optical sections with a thickness of 0.8 μm. The total number of fragments with protrusions was taken as 100%. Then the similar short areas without any processes were distinguished. We tried to keep their number equal to the number of fragments with processes. This was also taken as 100%. After that, each of the dendritic fragments (with or without a process), was carefully examined for the presence of STIM1 or STIM2 puncta. The number of positive cases was expressed as a percentage of the total. The reliability of the assay was ensured by randomly selected cells/segments, careful optical sectioning, and high-quality immunostaining.

Statistical Analysis

Fluorescent intensity was measured using ImageJ (NIH, USA) and the MATLAB (R2010b, USA)-based line-scan acquisition program. Measurements were made in a double-blind procedure (in some cases even with three independent observers) to assure unbiased observations. Dendritic protrusions were categorized either as spines, consisting of a clear head, usually larger than 0.5 μm in diameter and a short neck, or filopodia, long protrusions which are devoid of a discernable head. Dendritic spines that were used for calcium imaging were identified in the BFP-transfected neurons and analyzed independently of the measurements of calcium transients in these same spines. Statistical comparisons were made using

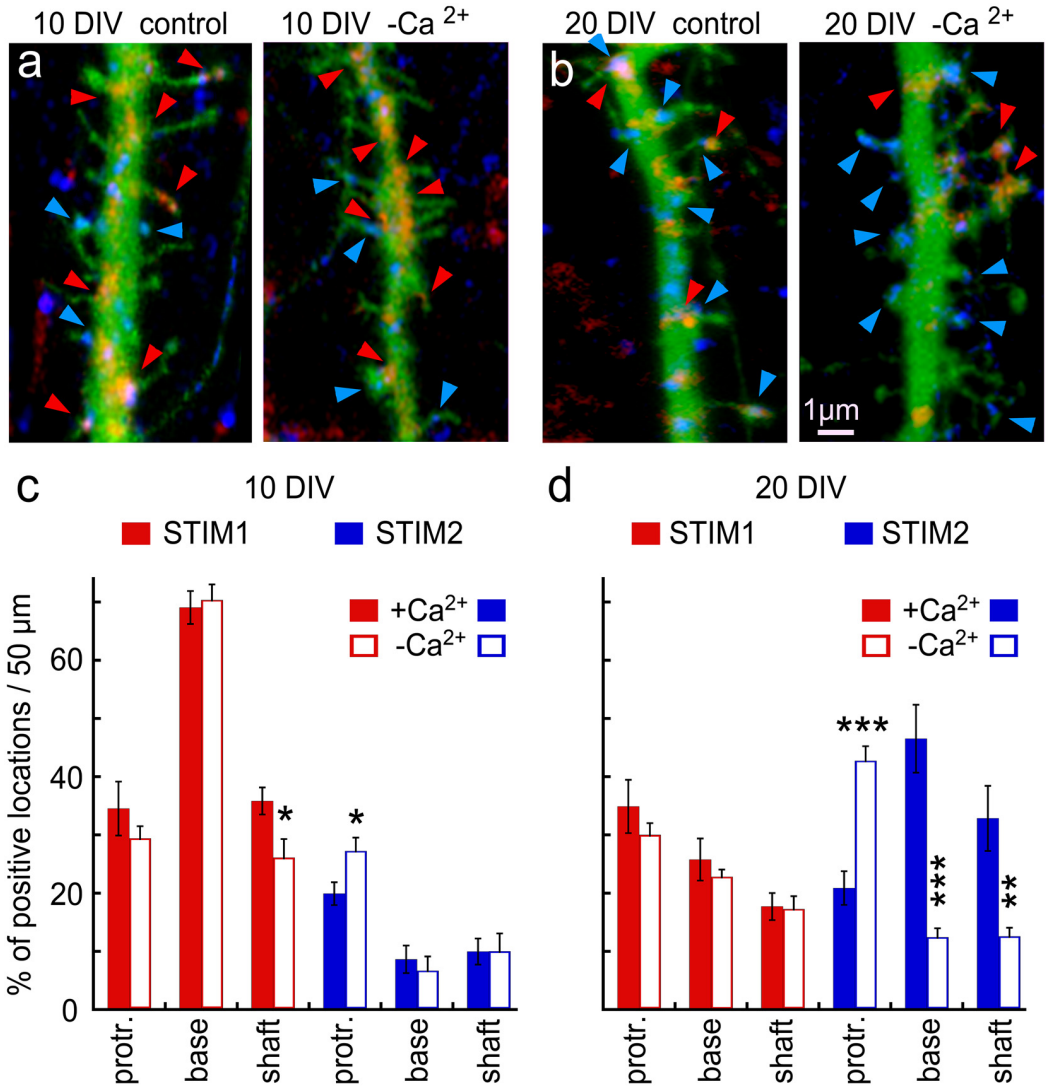

FIGURE 2 | Immunohistochemical localization of STIM1&2 in cultured hippocampal neurons with and without extracellular calcium. **(A,B)** Sample dendrites were taken from 10- to 20-day-old cultures and stained for STIM1(red) and STIM2 (blue) in cells transfected with EGFP (green) to visualize morphology in the presence and absence of extracellular calcium. It is apparent that the 10-day-old culture contains more STIM1 than STIM2 puncta, and the opposite is seen in the 20-day-old neuron. Under the calcium-free condition, STIM2 flows into protrusions in young and, especially, old culture. **(C)** Bar graphs quantification of the results illustrated on the left. The difference between STIM1 and 2 in 10 DIV in both conditions is highly significant (control conditions: $n = 10$ dendrites from five cells for each group, ANOVA $p < 0.0001$; in calcium-free medium: $n = 10$ dendrites from five cells for each group, ANOVA $p < 0.0001$). **(D)** Bar graphs quantification of the results illustrated on the right. The difference between STIM1 and 2 in 20 DIV in both conditions is highly significant (control conditions: $n = 10$ dendrites from five cells for each group, ANOVA $p < 0.0002$; in calcium-free medium: $n = 10$ dendrites from five cells for each group, ANOVA $p < 0.0001$). *Significant, $0.05 > p > 0.01$; **very significant, $0.01 > p > 0.001$; ***highly significant, $p < 0.001$.

t-tests or ANOVA, as the case requires, using MATLAB and KaleidaGraph software.

RESULTS

Since others and we have identified both STIM1 and STIM2 in hippocampal neurons, we explored the possibility that they are located at different neuronal compartments or possibly that they are expressed at different developmental ages and geared for different functions. Indeed, there was a striking age-dependent difference in presence of STIM1&2 in dendritic protrusions (filopodia and spines), such that STIM1 was more prevalent in the 10 days *in vitro* cells (10 DIV), compared to STIM2 (**Figure 2**), and the other way around for the 20 DIV neurons. This indicates that STIM1 may have a role in neuronal development and synapse formation, unlike STIM2, which may function in the maintenance and regulation of store-operated currents in the adult neurons.

To further explore the role of STIM1 in the formation of dendritic protrusions, we time-lapse imaged at high-resolution

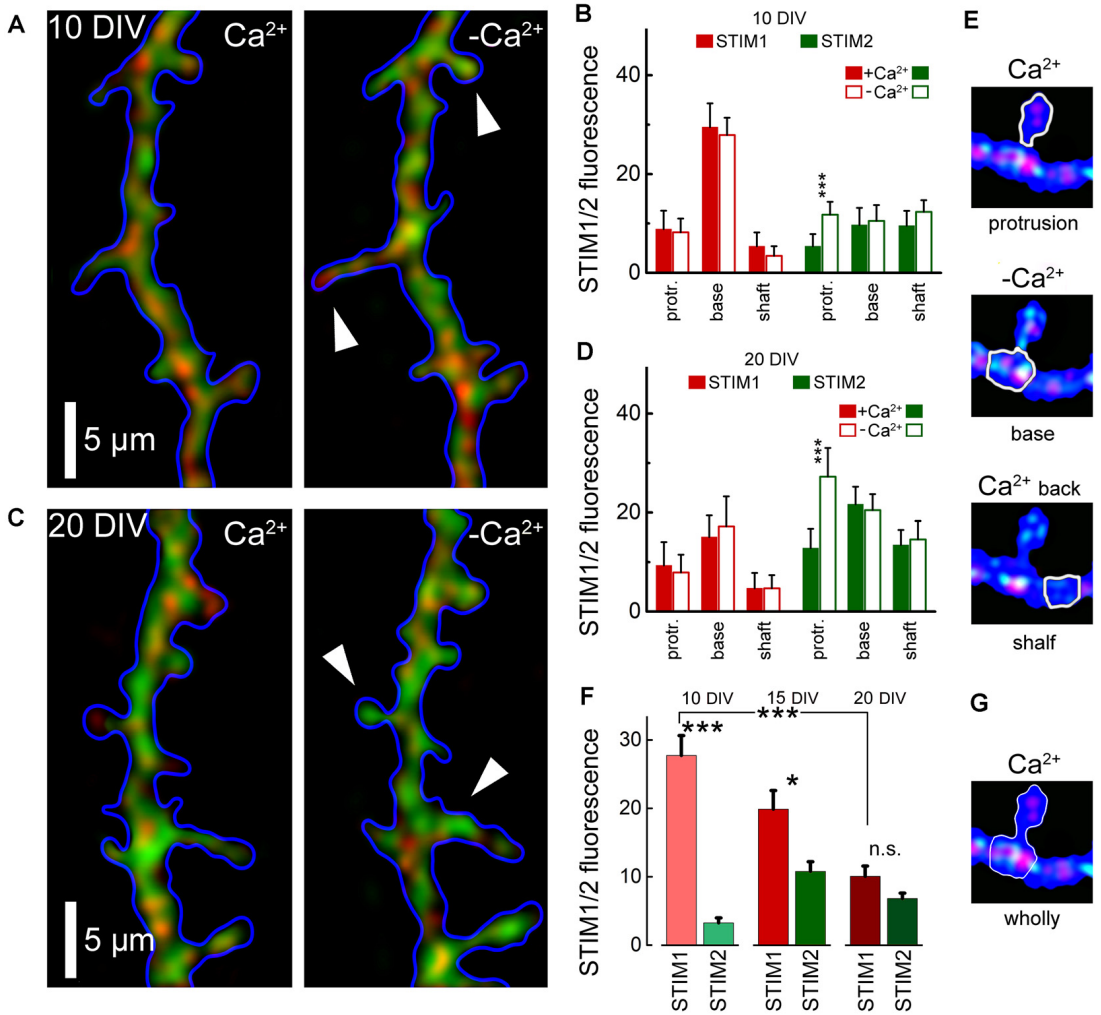

FIGURE 3 | Averaged STIM 1&2 fluorescence in protrusion, base, and shaft dendrites, in normal medium (2 mM Ca) and 15 min after incubation with a calcium-free medium. **(A)** STIM1 (red) and 2 (green) fluorescence in cell incubated with and without calcium, 10 DIV. **(B)** Bar graphs: averaged fluorescence minus background for in each group, 10 DIV. The difference between STIM1 and 2 in the base in both conditions and the difference between STIM2 with and without calcium in protrusion is highly significant (n = 10 dendrites from six cells for each group, ANOVA $p < 0.001$). **(C)** STIM1 (red) and 2 (green) fluorescence in a medium with and without calcium, 20 DIV. **(D)** Bar graphs: averaged fluorescence minus background for in each group, 20 DIV. The difference between STIM1 and 2 in the base in both conditions is not significant, but the difference between STIM2 with and without calcium in protrusion is highly significant (n = 8 dendrites from four cells for each group, ANOVA $p < 0.001$). **(E)** An example of the moving of STIM1/2 puncta in a protrusion (spine) in medium with and without calcium and after the return of calcium back to normal. White arrows mark protrusions in which the influx of STIM2 in a calcium-free medium is most noticeable (**A,C**, right panels). **(F)** STIM1 and STIM2 fluorescence at the base with protrusions (filopodia or spines) with background subtracted, at 10 DIV, 15, and 20 DIV. DIV 10: 34 protrusions; DIV 15: 30; DIV 20: 35 protrusions. **(G)** An example fluorescence calculation of STIM1/2 puncta at the base with protrusions (spine) for **(F)**. *Significant, $0.05 > p > 0.01$; ***highly significant, $p < 0.001$; n.s., not significant, $p \geq 0.05$.

dendrites of cultured neurons at 10 and 20 DIV (**Figure 2**). At a younger age, the dendrites are motile and new protrusions, spines, and filopodia emerge and disappear. Comparing two time-points, with and without Ca^{2+} (after 15 min) of the same dendrites, we found that new filopodia at 10 DIV, are endowed with STIM1 puncta (**Figures 2A,C**). This was not the case for dendritic spines, which are much less motile compared with filopodia, and are less associated with STIM1 in the more mature neurons (**Figures 2B,D**). The age-dependent difference between STIM1 and 2 was seen clearly in the live tissue, not subject to fixation (**Figure 3**), clearly indicating that this disparity is genuine and that only STIM2 responds to a reduction in ambient $[Ca^{2+}]_o$.

The association of STIM1 with the morphological changes in the host neuron was studied using time-lapse imaging of dendritic segments in the presence of STIM1 puncta (**Figure 4**). The young neurons are far more dynamic than the older ones, and new filopodia and spines can be formed and eliminated within 15 min of imaging. In the intermediate aged neurons (15 DIV) both filopodia and novel spines can

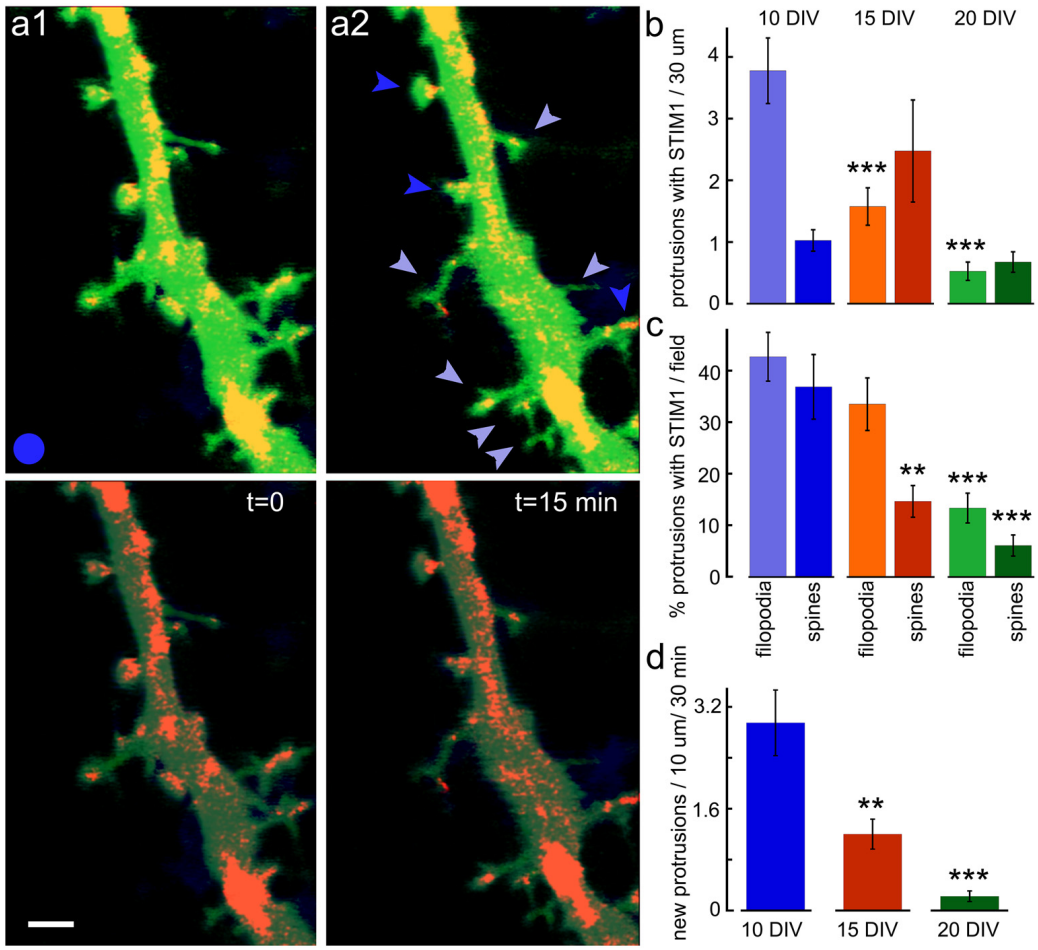

FIGURE 4 | New protrusions are associated with STIM1. **(A1)** Puncta are shown at two time-points; t = 0 and **(A2)** t = 15 min. Top images are EGFP (green, for morphology) and STIM1-mCherry (red) merged. Bottom panels show the same fields with EGFP dimmed. Scale bar = 2 μm. **(B)** The overall ratio of STIM1-containing protrusions in 10, 15, and 20 DIV is shown in absolute values. The total number of protrusions per standard field (filopodia and spine-like structures) are shown for all three ages (n = 40 fields for each age). **(C)** The normalized proportion of STIM1-positive protrusions as a percent of the total number of protrusions per field. **(D)** The appearance of new protrusions, associated with STIM1 puncta for DIV 10, 15, and 20 in the standard field per 30 min is summarized. **Very significant, 0.01 > p > 0.001; ***highly significant, p < 0.001.

be formed within 15 min of observations, and far fewer protrusions are seen in the 20 DIV cells. In all cases, the majority of novel protrusions are associated with the presence of STIM1 puncta.

In earlier experiments, we found that STIM1 puncta are mobile along the dendrites, and occasionally enter dendritic spines and filopodia. We now explored the possible association of STIM1 mobility with local fluctuation of ambient $[Ca^{2+}]_i$. To examine this, we followed STIM1 puncta using time-lapse photography to find that they move along dendrites at a slow rate (**Figure 5A**). Simultaneous measurement of ambient $[Ca^{2+}]_i$ clearly indicates that passage of STIM1 puncta in the field of view is associated with a transient local rise of $[Ca^{2+}]_i$. This local rise follows by 5–10 s the entry of STIM1 puncta into the field of view (**Figures 5B1–3**). Such local rise of $[Ca^{2+}]_i$ is different from that produced by a large synchronized, back-propagating action-potential or a transient local synaptic spike (**Figures 5G,H**) which has a fast rise time, less than 0.5 s to peak and fast decay, but is not related to STIM1 motility. This change is local and is not seen in regions adjacent to the traveling STIM puncta (**Figures 5C–F**). The smaller the size of the STIM1 puncta, the more motile it is (**Figure 5I**).

To clarify the distinction between local and generalize calcium transients even further, and to examine the role of synaptic activity and network-related formation of dendritic spines and filopodia, we compared STIM-associated calcium transients in control and tetrodotoxin (TTX)-treated cultures, where network activity is aborted. Surprisingly, there were a significantly larger number of STIM1-associated calcium transients, as well as the formation of short-lived filopodia in presence of TTX compared to control (**Figure 6**). The morphological results, showing that TTX triggers elongation of spines are similar to previous

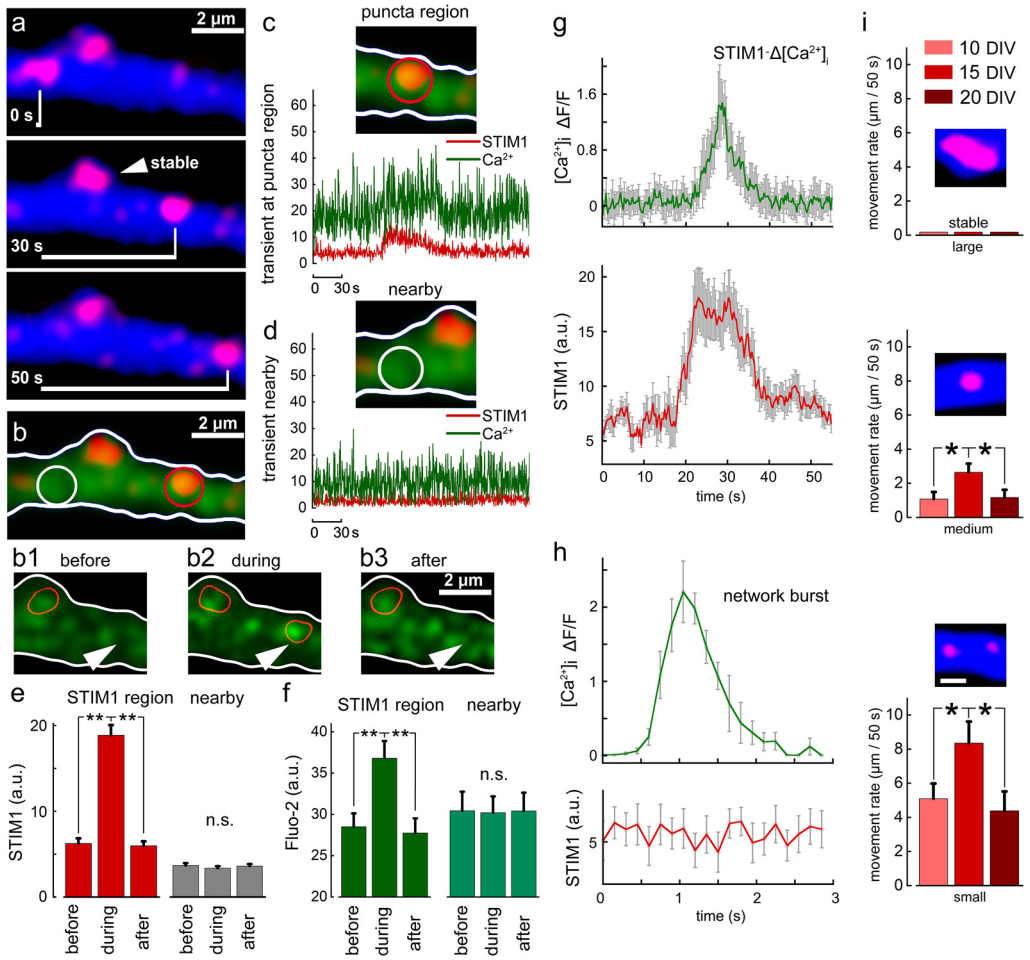

FIGURE 5 | Motility of STIM1 puncta along a dendrite and their association with a transient rise of $[Ca^{2+}]_i$. **(A)** Three images of a dendritic segment containing one stable STIM1 puncta, and a mobile one moving from left to right. **(B)** Fluo2 sensor shows calcium transients. Panels **(B1–3)** show calcium transient in the area, marked with an arrowhead. The current location of the mobile STIM1 punctum is marked with a red contour. The second red contour corresponds to the stable STIM1 punctum. **(C)** When punctum is present at the red location on the right a calcium transient can be detected. **(D)** In an adjacent location, neither puncta nor calcium transient is seen. Averaged data, $n = 10$ regions from different cells and different cultures. Three time points are taken: right before the entrance of puncta into the selected region (before) in the presence of puncta within the region of interest (during) and right after the puncta left the region (after). Simultaneously, measurements from a randomly selected nearby region were made (nearby). STIM1 for these time points (**E**, red). Nearby region (**E**, gray). Calcium for these time points (**F**, dark green). Calcium measurements from a nearby region (**F**, light green). **(G)** Time course of change in $[Ca^{2+}]_i$ fluorescence at the STIM1 puncta (top, green) and the STIM1 fluorescence (red, low trace) of 10 dendrites. Note that STIM1 fluorescence precedes the rise of $[Ca^{2+}]_i$ and is sustained after the calcium change subsided. **(H)** A fast synapse-evoked $[Ca^{2+}]_i$ rise that is not associated with a change in STIM fluorescence. Note the much faster time course of change in the synaptic event compared to the change seen above. **(I)** Movement rates (µm/50 s of three sizes of STIM1 puncta (large: >2 µm, medium: 1–2 µm and small: <1 µm), at three age groups, 10, 15 and 20 DIV. Small puncta move faster than medium and large ones at all age groups ($p < 0.05$). The faster movement rate is observed at 15 DIV compared to 10 and 20 DIVs for both medium and small-sized STIM1 puncta (medium: $n = 27$, 19 and 17 for 10, 15 and 20 DIV, respectively, $F = 3.58$, $p < 0.05$; small: $n = 27$, 14 and 8, $F = 3.02$, $p < 0.05$). *Significant, $0.05 > p > 0.01$; **very significant, $0.01 > p > 0.001$; n.s., not significant, $p \geq 0.05$.

observations on the acute effects of TTX on the formation of spinules (Verbich et al., 2016).

A direct comparison between STIMs relations to ambient $[Ca^{2+}]_i$ variations at different ages was made for both STIM1 and STIM2 (**Figure 7**). In all cases, comparisons were made with adjacent regions on the dendrites, not endowed with a STIM2 puncta (**Figure 7D**). There was no correlation between movements of STIM2 puncta along the dendrite and changes in ambient $[Ca^{2+}]_i$ (**Figure 7C**), unlike the case with STIM1 (**Figure 7G**). In general, STIM2 puncta have much lower motility than STIM1 puncta (**Figure 7H**), or are generally stable (84% of all STIM2 puncta are stable, $n = 30$; representative puncta from six cells, DIV 20). During the formation of new filopodia at DIV 10, STIM2 puncta were not associated with newly formed protrusions (**Figure 7J**).

Finally, since in earlier studies we and others have proposed that STIM2 is the store calcium sensor, we now compared the response of STIM1 and STIM2 to a reduction in ambient calcium, which has been shown to cause depletion of store calcium. Under

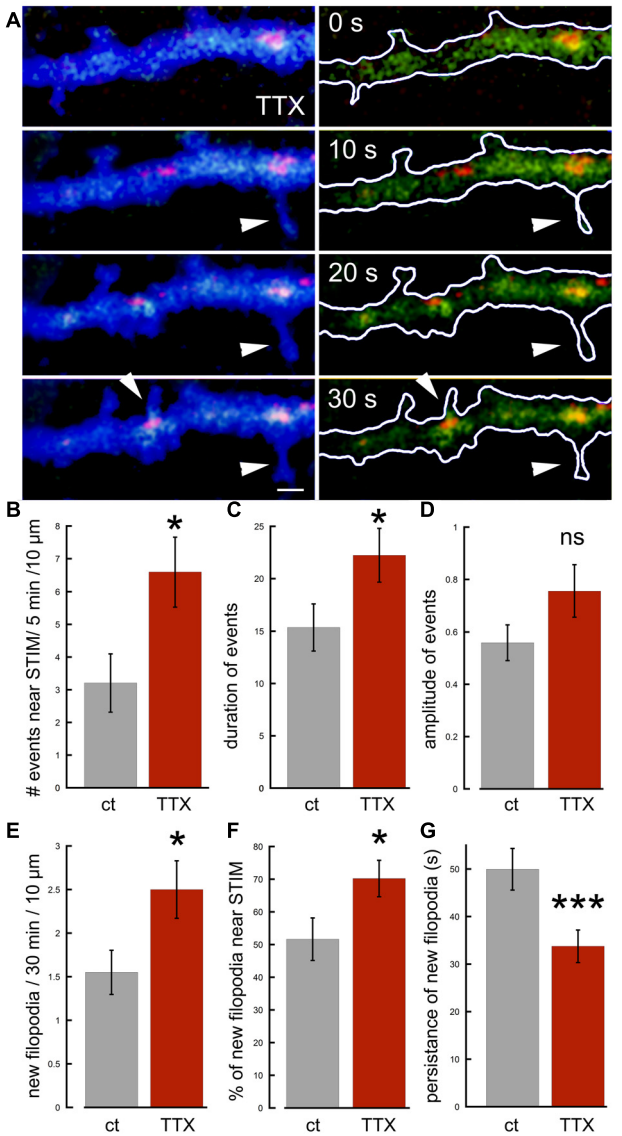

FIGURE 6 | Effects of tetrodotoxin (TTX) on STIM1-associated calcium transients and the formation of nascent filopodia. **(A)** Sample illustration of a dendrite at four time-points, 10 s apart, from top to bottom, showing calcium transients (green), associated with STIM1 puncta (red) in EBFP-transfected neuron (blue), recorded in TTX. Some calcium transients in the dendrite are associated with filopodia outgrowth (arrowheads). **(B)** The number of calcium transients during 5 min per standard segment is measured in control and TTX (n = 20 fields, seven cells for each). **(C)** Averaged duration of events (n = 40 events, 20 fields for each) scale = secs. **(D)** Averaged amplitude of events (n = 40 events, 20 fields for each). **(E)** All related to filopodia outgrowth: new filopodia per 30 min per standard segment, associated with STIM1 puncta and calcium transients (n = 40 fields, seven cells for each). **(F)** Percent of new filopodia associated with STIM1, of total new filopodia per standard field (n = 40 fields). **(G)** Averaged persistence of new filopodia in time (seconds; n = 55 protrusions for each). *Significant, $0.05 > p > 0.01$; ***highly significant, $p < 0.001$; n.s., not significant, $p \geq 0.05$.

these conditions, we expect to detect the movement of STIM molecules to regions in the cytosol across from membranous Orai1. Strikingly, while STIM1 puncta did not change position across 15 min of calcium deprivation (**Figure 3**), STIM2 appeared to move significantly into filopodia/spines (**Figures 3A,C**, right panels). Hence, it is likely that this movement is associated with the triggering of calcium influx following its deprivation.

Finally, the nature of the changes in calcium concentration in relation to STIM1 movement was studied by careful localization of the fluorescent puncta with local calcium variations in the same and adjacent regions of the dendrite (**Figure 8**). Strikingly, the entry of STIM to the region of interest was accompanied by an increase in spontaneous calcium bursts, akin to those described before as calcium sparks (Ross, 2015). These events were larger than random noise and were seen only in presence of STIM puncta in the region of interest. While the present results do not indicate the mechanism by which STIM1 causes a calcium spark, previous studies suggested such mechanisms (Ross, 2015; Dittmer et al., 2017), and further experiments are required to clarify this possibility in our cultured neurons.

These studies indicate that STIM1, but not STIM2, is associated with local dynamics of $[Ca^{2+}]_i$ and the formation of novel filopodia. Since filopodia are found predominantly in young neurons, whereas they are converted or replaced by stable spines in older neurons, we compared STIM1- associated filopodia and mature dendritic spines in 1- and 2-week-old cultures (**Figure 3**). As predicted, STIM1 was associated with filopodia but less with spines in the young cultures, but this distinction was not seen in the older neurons, where STIM2 plays a role in calcium influx, primarily in calcium- starved neurons. This indicates that STIM1 may have a pivotal role in the formation of filopodia in the young cells. This is a logical extension of the assumption that STIM1 may be important especially when there are sparse synaptic connections and little ambient fluctuations of $[Ca^{2+}]_i$ that is produced in mature spines by afferent activity. In contrast, STIM2 is assumed to underlie the mechanism that is responsible for the influx of calcium when the stored calcium is low, especially in the mature neurons.

DISCUSSION

STIM1&2 have been shown to play an important role in the regulation of SOCE channels in neuronal and non-neuronal cells. In peripheral (e.g., muscle) cells that are not endowed with a rich diversity of voltage and ligand-gated calcium channels, the ability to regulate $[Ca^{2+}]_i$, and in parallel, $[Ca^{2+}]$ in ER stores is dependent on SOCE channels and the role of voltage-insensitive calcium channel Orai1 is rather critical. The regulation of voltage/ligand-insensitive channels is pretty complicated and demands the presence of a sensor for the estimation of the possible depletion of the calcium stores, and a message to activate the Orai1 channels. This is subserved by the STIM proteins, which in turn, are regulated by septins (Xie et al., 2007; Palty et al., 2012). In neurons, there are two main STIM proteins, STIM1&2, and it was debated which is the dominant form of STIM and what cellular function is it associated with. Our current results suggest that STIM1 is prevalent in young cells where it is associated with calcium influx and formation of filopodia, whereas STIM2 is associated with

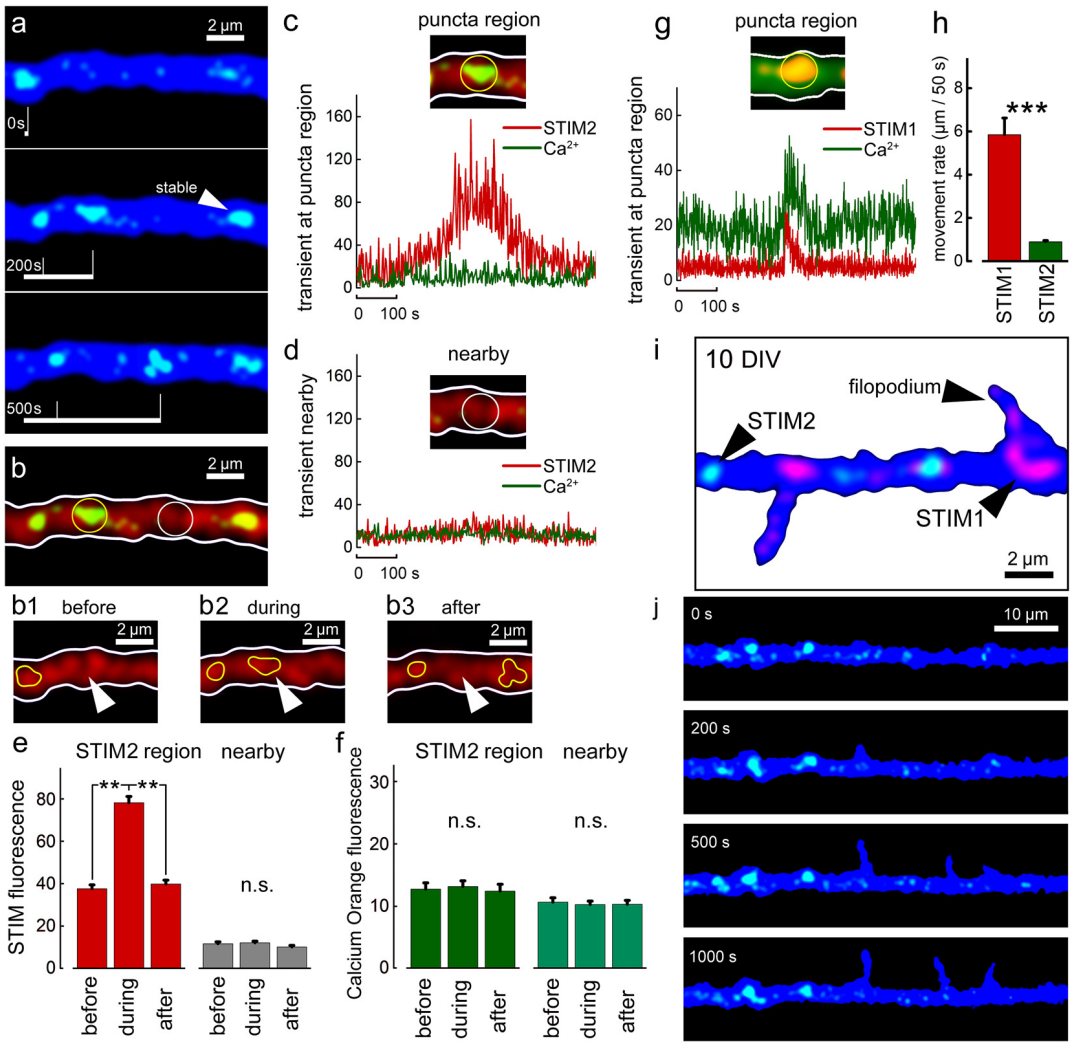

FIGURE 7 | STIM2-YFP puncta movement in relation to $[Ca^{2+}]_i$ transients. **(A)** Sample illustration of stable and mobile STIM2-YFP (green) puncta over 500 s, DIV 10. Cell morphology marked with EBFP (blue). Overall number of motile/stable puncta per segments of 50 µm: DIV 10: 0.4 ± 0.2/3.3 ± 0.4 (nine cells, $n = 14$ segments); DIV 15: 0.5 ± 0.4/3.4 ± 0.4 (six cells, $n = 13$ segments); DIV 20: 0.9 ± 0.3/4.3 ± 0.2 (six cells, $n = 10$ segments). **(B)** Same dendritic segment with Calcium Orange (CO) fluorescence (red). Two regions are marked with yellow and white circles: with punctum and nearby regions, respectively. Panels **(B1–3)** show the region marked with arrowhead before, during, and after the entrance of the STIM2 punctum (yellow contour). Stable punctum contour is shown on the left. **(C)** Corresponding graph demonstrating the change in STIM2 (red) and CO (green) fluorescence over time inside the marked region. **(D)** A nearby region without STIM2 and the corresponding traces. **(E)** Averaged mobile STIM2 fluorescence before, during, and after the entrance into the region of interest (left, red columns) and in the nearby region (gray). All for DIV 10. $n = 6$ paired region, five cells. **(F)** CO fluorescence for same times and regions as in **(E)**. **(G)** Sample STIM1 puncta fluorescence over time inside the marked region for comparison vs. STIM2: a calcium transient can be detected (Fluo-2, green trace). **(H)** Averaged rate of motility per 50 s, DIV 15, regardless of size puncta, STIM1: 5.9 µm ± 0.8, $n = 27$ representative motile puncta from nine cells; STIM2: 0.9 µm ± 0.1, $n = 20$ representative motile puncta from eight cells. Note that the motility of STIM2 puncta is much lower that of STIM1, difference highly significant, $t = 6.39$, $p < 0.001$. **(I)** Example of a cell at 10 DIV, co-transfected with STIM1 (red) and STIM2 (green). EBFP for cell morphology (blue). **(J)** Example of filopodia spontaneous outgrowth at DIV 10, over 1,000 s in STIM2 transfected neuron (green). Note the lack of association of the growth with STIM2. **Very significant, $0.01 > p > 0.001$; ***highly significant, $p < 0.001$; n.s., not significant, $p \geq 0.05$.

the more mature neuron, and is associated with SOCE, following calcium starvation.

Our previous results associated STIM2 with Orai1 in the *mature* cultured hippocampal neurons (Korkotian et al., 2017). We were also able to link Orai1 with synaptic plasticity (Tshuva et al., 2017). Assuming that our current results also involve the functioning of Orai1 channels, these results indicate that the STIM1/2-Orai1 coupling is likely to be involved in the early stages of neuronal development and the formation of functional networks.

STIM1 and STIM2 are very similar single transmembrane proteins, and both are calcium-sensors. In the current studies, we indicate that they do not share the same morphological location within the neurons and possibly their functions. This assertion

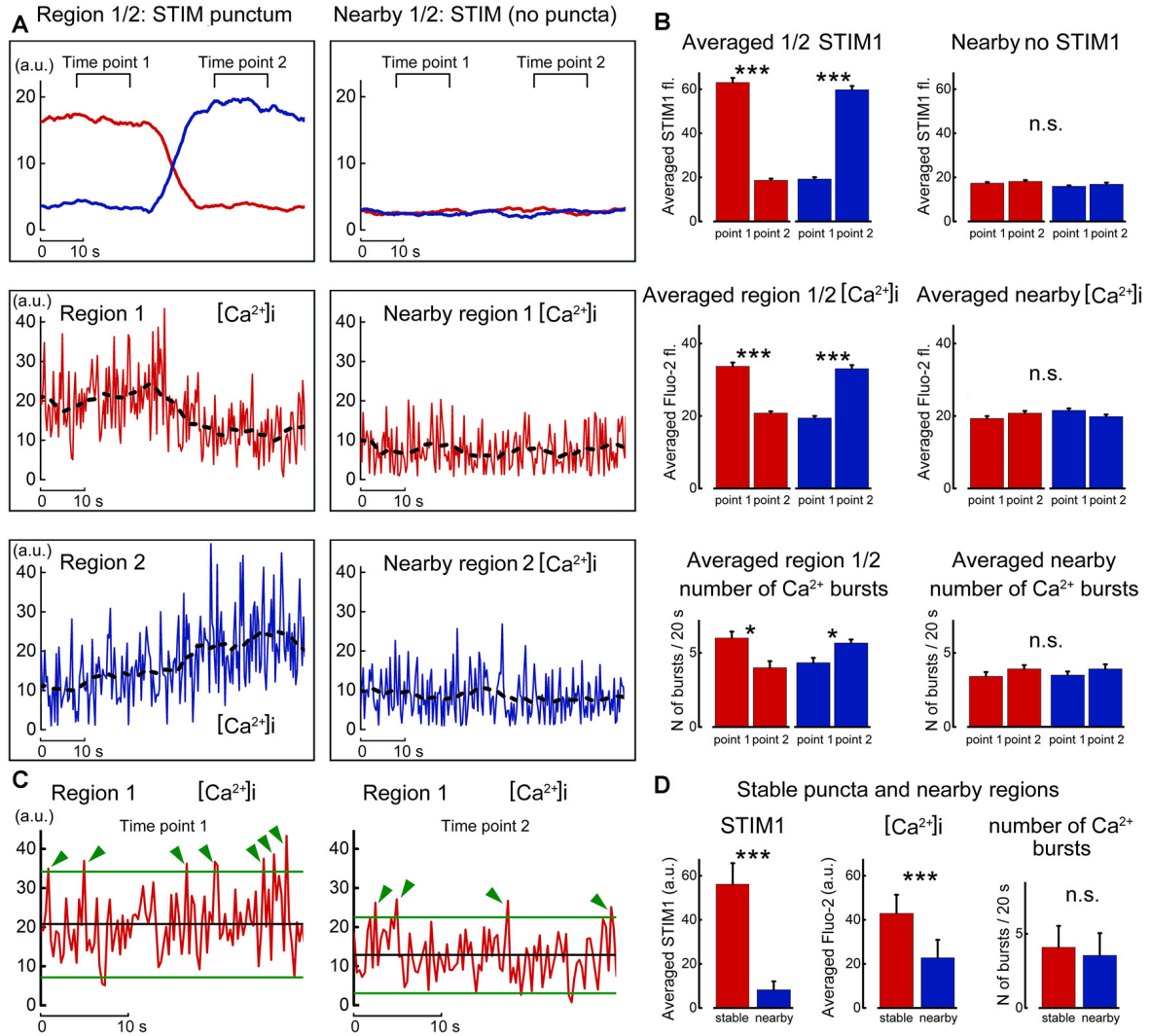

FIGURE 8 | Motility of STIM1 punctum is correlated with local calcium sparks. **(A)** Movement of a STIM1 punctum from region 1 to region 2 (top left, as in **Figure 6**) and by comparison to an adjacent region, where no STIM1 puncta are detected (top right). Below, calcium fluctuations in the corresponding region 1 and nearby quiet region, and calcium fluctuation in region 2 to where the STIM1 punctum moved. **(B)** Averaged fluorescence of STIM1 and corresponding Fluo2 fluorescence in the two positions where STIM1 was detected. **(C)** Expanded traces taken from region#1 in the presence (left) and absence (right) of STIM1 punctum. Two lines are drawn at 2 SD from the mean, and deviations of the calcium fluorescence line above the regions are marked with green arrows. **(D)** Average fluorescence of STIM1 and Ca^{2+} level in regions of stable puncta and nearby region in 10 s; the number of Ca^{2+} bursts in 20 s, $n = 9$ cells, DIV 15. *Significant, $0.05 > p > 0.01$; ***highly significant, $p < 0.001$; n.s., not significant, $p \geq 0.05$.

is confirmed by comparing the immunolocalization of the two proteins (e.g., **Figure 1**), as well as their transfected species. The overlap between the transfected STIMs and their native species indicates that the respective transfected STIMs assume the same functions as the native ones, justifying their use for the analysis of the native STIMs.

We (Fishbein and Segal, 2007) and others (Verbich et al., 2016) have shown that synaptic activity is crucial for the maintenance and stability of neuronal morphology, such that blockade of activity causes the disappearance of dendritic spines and formation and elongation of filopodia. In the present study, we explored this further to find that blockade of activity using TTX can cause STIM-associated increase in spontaneous calcium transients and elongation of nascent filopodia. These observations highlight the role of synapse-independent transient calcium events triggered by STIM1 that are implicit in the functional maturation of dendritic filopodia, akin to what has been described in growth cones (Mitchell et al., 2012; Pavez et al., 2019).

The current results propose that STIM1 is more effective in young cells, that it is more effective in non-active neurons, and that it is associated with filopodia, the immature organelle, more than with dendritic spines, the more stable appendages of the dendrite of a pyramidal neuron. STIM1 puncta are more mobile, and when they move along dendrites, they are associated with the formation of local calcium transients. This is in sharp contrast

with STIM2, which appear later in life, are less punctate, and are much less mobile. Thus, the two STIM species are likely to be associated with different functions in the developing and mature neurons, although both are linked to the Orai channel. Thus, two molecules of the same family can be distributed in different cellular compartments, and assume similar roles at different ages of the parent neuron. A hint to such disparity in age/function is in our recent publication (Korkotian et al., 2017) on STIM1/2/Orai localization; when cytosolic calcium is reduced in adult cultured neurons, STIM2 has a much higher tendency to become associated with Orai channels than STIM1. Taken together with our current results, these observations indicate that STIM2 may have a dynamic role, as suggested before, to sense a reduction in store-calcium and move to the plasma membrane to activate Orai to allow an influx of calcium into the store. In contrast, STIM1 may be less tuned to changes in store-calcium but will allow calcium influx in relation to the formation of novel filopodia, as suggested for growth cones (Pavez et al., 2019). The contribution of each molecule species to the ongoing $[Ca^{2+}]_i$ regulation needs further exploration.

The comparison between $[Ca^{2+}]_i$ evoked by synaptic activity and by apparent activation of the STIM1/Orai coupling is interesting indeed. The synaptically-evoked rise in $[Ca^{2+}]_i$ is rather large, but rise time and decay are much faster than STIM1 associated $[Ca^{2+}]_i$ rise. Both types of changes are estimated by the same high-affinity calcium sensor, Fluo-2AM, and so the difference in kinetics can be attributed to a different affinity of the sensor. The slower kinetics of the STIM1-evoked $[Ca^{2+}]_i$ reflects the lower magnitude of change, and the need to accumulate a significant amount of calcium to allow activation of calcium-dependent kinases, which will lead eventually to synaptic growth and plasticity.

The functional importance of the STIM/Orai complex has been studied in relation to its possible involvement in neurodegenerative Alzheimer's disease (AD). Both STIM2 (Sun et al., 2014; Zhang et al., 2015) and STIM1 (Zeiger et al., 2013) have been implicated in the regulation of amyloid-beta peptide, which has been shown to accumulate in AD (Zeiger et al., 2013), and have been shown to regulate the formation of dendritic spines in a mouse model of AD (Sun et al., 2014; Zhang et al., 2015). Since our results indicate that the two STIM species can reside side by side, at different ages and cellular locations, possibly a deficient STIM1 peptide may alter properties of SOCE channels, and consequently their involvement in the regulation of calcium stores in AD. However, our studies are conducted in very young neurons, compared to the human case and the mouse model, and so the proposal that STIMs are involved in the generation of AD needs further experimentation to explore this link further and to propose channels for the restoration of calcium deficiency in this disease.

DATA AVAILABILITY STATEMENT

The raw data supporting the conclusions of this article will be made available by the authors, without undue reservation.

ETHICS STATEMENT

The animal study was reviewed and approved and this study was carried out in accordance with the recommendations of the IACUC committee of the Weizmann Institute, which is adhered to the Israeli law for handling of research animals. The protocol was approved by the IACUC committee of the Weizmann Institute.

AUTHOR CONTRIBUTIONS

EK and MS designed the experiments. EK and LK conducted the experiments and analyzed the data. EK, LK, and MS wrote the manuscript. All authors contributed to the article and approved the submitted version.

FUNDING

This research was supported by Israel Science Foundation grant 623/14.

REFERENCES

Baba, A., Yasui, T., Fujisawa, S., Yamada, R. X., Yamada, M. K., Nishiyama, N., et al. (2003). Activity-evoked capacitative Ca^{2+} entry: implications in synaptic plasticity. *J. Neurosci.* 23, 7737–7741. doi: 10.1523/JNEUROSCI.23-21-07737.2003

Bogeski, I., Kilch, T., and Niemeyer, B. A. (2012). ROS and SOCE: recent advances and controversies in the regulation of STIM and Orai. *J. Physiol.* 590, 4193–4200. doi: 10.1113/jphysiol.2012.230565

Dittmer, P. J., Wild, A. R., Dell'Acqua, M. L., and Sather, W. A. (2017). STIM1 Ca^{2+} sensor control of L-type Ca^{2+} channel-dependent dendritic spine structural plasticity and nuclear signaling. *Cell Rep.* 19, 321–334. doi: 10.1016/j.celrep.2017.03.056

Feske, S., Gwack, Y., Prakriya, M., Srikanth, S., Puppel, S. H., Tanasa, B., et al. (2006). A mutation in Orai1 causes immune deficiency by abrogating CRAC channel function. *Nature* 441, 179–185. doi: 10.1038/nature04702

Fishbein, I., and Segal, M. (2007). Miniature synaptic currents become neurotoxic to chronically silenced neurons. *Cereb. Cortex* 17, 1292–1306. doi: 10.1093/cercor/bhl037

Guner, G., Guzelsoy, G., Isleyen, F. S., Sahin, G. S., Akkaya, C., Bayam, E., et al. (2017). NEUROD2 regulates Stim1 expression and store-operated calcium entry in cortical neurons. *eNeuro* 4:ENEURO.0255-16.2017. doi: 10.1523/ENEURO.0255-16.2017

Henke, N., Albrecht, P., Bouchachia, I., Ryazantseva, M., Knoll, K., Lewerenz, J., et al. (2013). The plasma membrane channel ORAI1 mediates detrimental calcium influx caused by endogenous oxidative stress. *Cell Death Dis.* 4:e470. doi: 10.1038/cddis.2012.216

Klejman, M. E., Gruszczynska-Biegala, J., Skibinska-Kijek, A., Wisniewska, M. B., Misztal, K., Blazejczyk, M., et al. (2009). Expression of STIM1 in brain and puncta-like co-localization of STIM1 and ORAI1 upon depletion of Ca^{2+} store in neurons. *Neurochem. Int.* 54, 49–55doi: 10.1016/j.neuint.2008.10.005

Korkotian, E., Oni-Biton, E., and Segal, M. (2017). The role of the store-operated calcium entry channel Orai1 in cultured rat hippocampal synapse formation and plasticity. *J. Physiol.* 595, 125–140. doi: 10.1113/JP272645

Kraft, R. (2015). STIM and ORAI proteins in the nervous system. *Channels* 9, 245–252. doi: 10.1080/19336950.2015.1071747

Mitchell, C. B., Gasperini, R. J., Small, D. H., and Foa, L. (2012). STIM1 is necessary for store-operated calcium entry in turning growth cones. *J. Neurochem.* 122, 1155–1166. doi: 10.1111/j.1471-4159.2012.07840.x

Palty, R., Raveh, A., Kaminsky, I., Meller, R., and Reuveny, E. (2012). SARAF inactivates the store operated calcium entry machinery to prevent excess calcium refilling. *Cell* 149, 425–438. doi: 10.1016/j.cell.2012.01.055

Park, C. Y., Shcheglovitov, A., and Dolmetsch, R. (2010). The CRAC channel activator STIM1 binds and inhibits L-type voltage-gated calcium channels. *Science* 330, 101–105. doi: 10.1126/science.1191027

Pavez, M., Thompson, A. C., Arnott, H. J., Mitchell, C. B., D'Atri, I., Don, E. K., et al. (2019). STIM1 is required for remodeling of the endoplasmic reticulum and microtubule cytoskeleton in steering growth cones. *J. Neurosci.* 39, 5095–5114. doi: 10.1523/JNEUROSCI.2496-18.2019

Ross, W. N. (2015). Understanding calcium waves and sparks in central neurons. *Nat. Rev. Neurosci.* 13, 157–168. doi: 10.1038/nrn3168

Segal, M., and Korkotian, E. (2014). Endoplasmic reticulum calcium stores in dendritic spines. *Front. Neuroanat.* 8:64. doi: 10.3389/fnana.2014.00064

Segal, M., and Korkotian, E. (2016). Roles of calcium stores and store-operated channels in plasticity of dendritic spines. *Neuroscientist* 22, 477–485. doi: 10.1177/1073858415613277

Sharma, S., Quintana, A., Findlay, G. M., Mettlen, M., Baust, B., Jain, M., et al. (2013). An siRNA screen for NFAT activation identifies septins as coordinators of store-operated Ca^{2+} entry. *Nature* 499, 238–242. doi: 10.1038/nature12229

Skibinska-Kijek, A., Wisniewska, M. B., Gruszczynska-Biegala, J., Methner, A., and Kuznicki, J. (2009). Immunolocalization of STIM1 in the mouse brain. *Acta Neurobiol. Exp.* 69, 413–428.

Steinbeck, J. A., Henke, N., Opatz, J., Gruszczynska-Biegala, J., Schneider, L., Theiss, S., et al. (2011). Store-operated calcium entry modulates neuronal network activity in a model of chronic epilepsy. *Exp. Neurol.* 232, 185–194. doi: 10.1016/j.expneurol.2011.08.022

Sun, S., Zhang, H., Liu, J., Popugaeva, E., Xu, N.-J., Feske, S., et al. (2014). Reduced synaptic STIM2 expression and impaired store-operated calcium entry cause destabilization of mature spines in mutant presenilin mice. *Neuron* 82, 79–93. doi: 10.1016/j.neuron.2014.02.019

Tada, T., Simonetta, A., Batterton, M., Kinoshita, M., Edbauer, D., and Sheng, M. (2007). Role of Septin cytoskeleton in spine morphogenesis and dendrite development in neurons. *Curr. Biol.* 17, 1752–1758. doi: 10.1016/j.cub.2007.09.039

Tshuva, R. Y., Korkotian, E., and Segal, M. (2017). ORAI1-dependent synaptic plasticity in rat hippocampal neurons. *Neurobiol. Learn. Mem.* 140, 1–10. doi: 10.1016/j.nlm.2016.12.024

Verbich, D., Becker, D., Vlachos, A., Mundel, P., Deller, T., and Anne McKinney, R. (2016). Rewiring neuronal microcircuits of the brain *via* spine head protrusions—a role for synaptopodin and intracellular calcium stores. *Acta Neuropathol. Commun.* 4:38. doi: 10.1186/s40478-016-0311-x

Verkhratsky, A. (2005). Physiology and pathophysiology of the calcium store in the endoplasmic reticulum of neurons. *Physiol. Rev.* 85, 201–279. doi: 10.1152/physrev.00004.2004

Xie, Y., Vessey, J. P., Konecna, A., Dahm, R., Macchi, P., and Kiebler, M. A. (2007). The GTP-binding protein Septin 7 is critical for dendrite branching and dendritic-spine morphology. *Curr. Biol.* 17, 1746–1751. doi: 10.1016/j.cub.2007.08.042

Zalk, R., Lehnart, S. E., and Marks, A. R. (2007). Modulation of the ryanodine receptor and intracellular calcium. *Annu Rev Biochem.* 76, 367–385. doi: 10.1146/annurev.biochem.76.053105.094237

Zeiger, W., Vetrivel, K. S., Buggia-Prévot, V., Nguyen, P. D., Wagner, S. L., Villereal, M. L., et al. (2013). Ca^{2+} influx through store-operated Ca^{2+} channels reduces Alzheimer disease β-amyloid peptide secretion. *J. Biol. Chem.* 288, 26955–26966. doi: 10.1074/jbc.M113.473355

Zhang, H., Wu, L., Pchitskaya, E., Zakharova, O., Saito, T., Saido, T., et al. (2015). Neuronal store-operated calcium entry and mushroom spine loss in amyloid precursor protein knock-in mouse model of Alzheimer's disease. *J. Neurosci.* 35, 13275–13286. doi: 10.1523/JNEUROSCI.1034-15.2015

Conflict of Interest: The authors declare that the research was conducted in the absence of any commercial or financial relationships that could be construed as a potential conflict of interest.

Advantages of publishing in Frontiers

OPEN ACCESS
Articles are free to read for greatest visibility and readership

FAST PUBLICATION
Around 90 days from submission to decision

HIGH QUALITY PEER-REVIEW
Rigorous, collaborative, and constructive peer-review

TRANSPARENT PEER-REVIEW
Editors and reviewers acknowledged by name on published articles

Frontiers
Avenue du Tribunal-Fédéral 34
1005 Lausanne | Switzerland

Visit us: www.frontiersin.org
Contact us: frontiersin.org/about/contact

REPRODUCIBILITY OF RESEARCH
Support open data and methods to enhance research reproducibility

DIGITAL PUBLISHING
Articles designed for optimal readership across devices

FOLLOW US
@frontiersin

IMPACT METRICS
Advanced article metrics track visibility across digital media

EXTENSIVE PROMOTION
Marketing and promotion of impactful research

LOOP RESEARCH NETWORK
Our network increases your article's readership